Universitat Autònoma de Barcelona

Artificial Neural Networks in the Wastewater Industry
From Conventional to Data-based Industrial Control

Ivan Pisa Dacosta

Universitat Autònoma
de Barcelona

Department of Telecommunications and Systems Engineering

Artificial Neural Networks in the Wastewater Industry

From Conventional to Data-based Industrial Control

Ph.D. Thesis in Electronic and Telecommunication Engineering

by

Ivan Pisa Dacosta

Thesis Advisors:
Dr. Antoni Morell Pérez, Dr. José López Vicario and Prof. Ramon Vilanova Arbós
Escola d'Enginyeria
Universitat Autònoma de Barcelona (UAB)

June, 2022

II

To my beloved parents, sister and nieces

"No great mind has ever existed without a touch of madness."

- Aristotle

Abstract

The incursion of the Industry 4.0 has motivated the adoption of data-driven methodologies in industrial environments. From the development of new soft-sensors to the adoption of predictive maintenance processes, this paradigm is changing the way as industries are conceived. Moreover, the interconnectivity proposed by the fifth generation communication systems (5G) introduces the exchange of huge amounts of information, not only between machines and humans, but also among industrial systems. Nevertheless, the management of industries still depend on the adoption of the always reliable conventional controllers. For that reason, this thesis main aim is to provide an insight on the application of Deep Learning methodologies, and especially Artificial Neural Networks (ANN), for the operation of a critical industrial infrastructure, a Wastewater Treatment Plant (WWTP).

First, ANNs are considered to support conventional controllers in the difficult task of managing effluent pollutant limits violations. To achieve this, ANNs are considered to implement an ANN-based soft-sensor able to predict the effluent concentrations. Then, predictions are fed into conventional controllers so as to let them actuate beforehand. This fact provides a much better control performance since nearly all the effluent violations are avoided.

Next, the adoption of ANNs as tools implementing control structures is addressed. Instead of using conventional controllers supported by these tools, the whole controller is implemented by ANNs performing all the tasks, from the data preprocessing to the estimation of the control actuation. Such controllers are able to offer a superior performance regarding the behaviour of conventional structures. But, the important point is that this can be achieved only considering input and output measurements of the process under control. Notwithstanding, the fact of relying on data can induce a bad management of the industrial environment if non-idealities are introduced in the control structure. For that reason, the adoption of ANN is also proposed to correct such non-idealities and therefore, avoid mismanagement issues. This is performed by means of Denoising Autoencoders (DAE) able to clean the noise-corrupted measurements and by ANNs correcting the delays introduced in the control systems.

Finally, the adoption of Transfer Learning (TL) techniques to design new ANN-based controllers as well as the development of a metric measuring their transferability are addressed in the last part of this thesis. The main aim is to determine the transfer suitability of ANN-based control structures derived in a source environment to transfer them into a target domain. Thus, the control structures of the new environment can be obtained without resorting to the design and development of controllers from scratch. This not only entails the reduction of the control design process complexity, but also lead to the development of a highly scalable control design approach.

Acknowledgements

Here we go again, another stage completed, a new accomplishment. Nevertheless, this has not been possible without the sustain and the help provided by those who have made this stage little bit easier. I want to deeply thank my three directors for their motivation and involvement towards this thesis. First, I would like to express my deepest gratitude to my tutor, and somehow, my colleague Dr. José López Vicario, for his patience, his advises and his tireless support. Thank you for trusting in me for the very beginning. Also, to Dr. Antoni Morell Pérez, for involving me in the world of Artificial Intelligence and for our hours of conversations. I will not forget our running and cycling sessions. To Dr. Ramon Vilanova Arbós, for making this thesis a reality. Thanks a lot for your dedication and experience. Also, for the travels we have done together. This PhD thesis would not be performed without their support. All this worth this acknowledgement. I also want to make this acknowledge extensible to the ASAC and WIN groups, which have been there whenever I have needed. It is also extensible to the Department of Telecommunications and Systems Engineering, especially for Susana and Chari, fun and tireless in their work. Also, to La Secretaria d'Universitats i recerca del Departament d'Empresa i Coneixement de la Generalitat de Catalunya for its financial support through its FI grant.

I cannot forget about the closest people which have been next to me during this journey. My office mate Guillem who has been sharing lots of moments and experiences in the closest desk. Edith, who has been a supporting point form the first day. Patri, Dani, Eloi, Lluís, Carlos, Pere, Edward, Elvis, Pedro, Jordi and Victor, who have been there to share moments, laughs and huge amounts of coffee. Martí and Dani my loyal partners of our combat sessions. A special mention needs to be done to Noemí. She has been suffering me without complaining of anything. Your advice and your encouragement have been a fundamental part of these last months. Eight months together are more than enough to see that such a partner cannot be found elsewhere, I hope this will be infinitely increasing and of course, blessed SAF! Then, I cannot forget of my friends, Silvia, Meritxell, Uri, Adri, Sara, Christian, Ainhoa and Andrea, you are part of this work.

This acknowledgment cannot be concluded without showing my eternal gratitude to all my family: Alfonso, Ana, Noelia, Germán, Sara and Lucía. For sure that this thesis would have not been possible without you.

Ivan Pisa Dacosta,
June 2022

Contents

List of Figures

List of Tables

Acronyms

ANN	Artificial Neural Network
ASM1	Activated Slude Model No.1
ASM2	Activated Sludge Model No.2
ASM2d	Activated Sludge Model No.2d
ASM3	Activated Sludge Model No.3
ASS-NHRS	ANN-based Soft-Sensor $S_{NH,e}$ Reduction Scenario
ASS-NTRS	ANN-based Soft-Sensor $S_{Ntot,e}$ Reduction Scenario
ASS-PRS	ANN-based Soft-Sensor Pollutant Reduction Scenario
AWGN	Additive White Gaussian Noise
BOD$_5$	Biological Oxygen Demand
BSM1	Benchmark Simulation Model No.1
BSM1-LT	Benchmark Simulation Model No.1 Long-Term
BSM2	Benchmark Simulation Model No.2
COD	Chemical Oxygen Demand
DAE	Denoising Autoencoder
DC	Default BSM2 Control strategy
DCPS-NH	$S_{NH,e}$ DC Prediction Structure
DCPS-NT	$S_{Ntot,e}$ DC Prediction Structure
DO	Dissolved Oxygen
DO ANN-based PI	Dissolved Oxygen ANN-based PI
DO Control Loop	Dissolved Oxygen Control Loop
DO→NO ANN-based PI	Dissolved Oxygen to Nitrate-nitrogen transferred ANN-based PI
DPPDT	Double Pole Plus Dead-Time
DS	Default Scenario
ECAPS	Effluent Concentration and Alarm Prediction System
EQI	Effluent Quality Index
ETFE	Empirical Transfer Function Estimation

FFNN	Feed-forward Neural Network
FLC	Fuzzy Logic Controller
FOPDT	First Order Plus Dead-Time
FT	Fine-tuning
FTDO ANN-based PI	Fine-tuned Dissolved Oxygen ANN-based PI
HC	Hierarchical Control Strategy
HCPS-NH	$S_{NH,e}$ HC Prediction Structure
HCPS-NT	$S_{Ntot,e}$ HC Prediction Structure
HS	Hierarchical Scenario
IAE	Integral of the Absolute Error
IMC	Internal Model Controller
IoT	Internet of Things
ISE	Integral of the Squared Error
IWA	International Water Association (IWA)
$\boldsymbol{J(\theta)}$	Cost function
$\boldsymbol{K_{La,x}}$	Oxygen transfer coefficient of xth reactor tank
LSTM	Long Short-Term Memory Cell
MAPE	Mean Average Percentage Error
MDS	Multidimensional Scaling
$\boldsymbol{ME}$	Mixing Energy
$\boldsymbol{MET_{prod}}$	Methane Production
MI	Mutual Information
MLP	Multilayer Perceptron
MPC	Model Predictive Controller
MSE	Mean Squared Error
NKj	Kjeldahl nitrogen
NO Control Loop	Nitrate-nitrogen Control Loop
NO ANN-based PI	Nitrate-nitrogen ANN-based PI
NO Control Loop	Nitrate-nitrogen Control Loop
NO→DO ANN-based PI	Nitrate-nitrogen to Dissolved Oxygen transferred ANN-based PI
OCI	Overall Cost Index
OL	Open Loop Configuration
OLPS-NH	$S_{NH,e}$ OL Prediction Structure
OLPS-NT	$S_{Ntot,e}$ OL Prediction Structure
PCA	Principal Components Analysis

PI	Proportional Integral Controller
PID	Proportional Integral Derivative Controller
PH	Prediction Horizon
Q_a	Internal recycle flow rate
Q_{bypass}	Bypass flow rate
Q_{do}	Dewatering unit overflow rate
Q_e	Effluent flow rate
Q_{in}	Influent flow rate
Q_{po}	Primary overflow rate
Q_{pu}	Primary clarifier underflow rate
Q_r	External recycle flow rate
Q_{tu}	Thickener underflow flow rate
Q_w	Wastage flow rate
Q_x	Flow rate of the xth biological reactor tank
R^2	Determination Coefficient
ReLU	Rectified Linear Uniform activation function
RMSE	Root Mean Squared Error
RNN	Recurrent Neural Network
SGD	Stochastic Gradient Descent
S_{NH}	Ammonium and ammonia nitrogen concentration
$S_{NH,e}$	Ammonium and ammonia nitrogen concentration in the effluent
$S_{NH,po}$	Ammonium and ammonia nitrogen concentration in the primary clarifier output
$S_{NO,x}$	Nitrite and nitrate nitrogen in the xth reactor tank
$S_{Ntot,e}$	Total nitrogen in the effluent
SOPDT	Second Order Plus Dead-Time
$S_{O,x}$	Dissolved oxygen in the x-th reactor tank
t_a	Actuation delay
T_{as}	Environmental temperature
t_d	Sensor delay
$t_{f_{BSM1}}$	Final time of BSM1 simulation
$t_{f_{BSM2}}$	Final time of BSM2 simulation
$t_{i_{BSM1}}$	Initial time of BSM1 simulation
$t_{i_{BSM2}}$	Initial time of BSM2 simulation
TL	Transfer Learning
t_r	Response time

t_s	Sampling time
TSM	Transfer Suitability Metric
T_{SS}	Total Suspended Solids
t_{time}	Training time
WL	Window Length
WWTP	Wastewater Treatment Plant
5G	Fifth Generation

Chapter 1

Introduction

1.1 Motivation

Industrial environments are one of the scenarios where the evolution of humanity and technology are more noticeable. Industry can be seen as an indicator of the productive and economical muscle of different territories. In most of the countries, those regions showing a powerful industrial environment are the ones with the most prosperous future in terms of employment, development, and profits. Notwithstanding, these facts are not new at all. Historically, industrial environments have been the scenarios where the highest changes have been produced over time. Starting with the first industrial expansion, or the Industry 1.0, better known as the Industrial Revolution in the 1784, factories were mechanised thanks to the power of steam and water. This entailed a huge evolution in the manufacturing process, especially in the fabric's domain. Later, in the 1870, it was the turn of the Industry 2.0 expansion, where the appearance of the assembly line and the evolution of energy towards the electrical power motivated the change of industry to the mass production era. The production of fabrics and consumption elements were less complex while their productive costs were reduced. Moreover, industrial systems became more complex and that was translated in the need of industrial control structures. It was not before the 1922 when the first mathematical description of the Proportional Integral Derivative controllers (PIDs) was performed. By the ends of the sixties, the complete automated factories, which adopted lots of control laws, became more than a fairy tale, they were a reality. The evolution of the electronics as well as the development of computers and Information Technologies (IT) led to the third industrial expansion (Industry 3.0). This evolution arose as the transformation of the industrial sector towards the consumption industry. In addition, this evolution has also motivated the era of the globalisation, where the industrial production became more disseminated around the world than it had been before. Nowadays, however, the industry is experiencing a new transformation, the 4th industrial revolution better known as Industry 4.0, which has arisen as the revolution of the interconnected industry.

This new revolution is driven by, among others, the emergence of data-based systems and networks devoted to digitalising industrial scenarios. New technological trends such as the Cyber-physical Systems (CPS), cloud-computing, data analytic systems or virtualization technologies, are some of the key players of this new industrial paradigm [Ust17]. In that sense, the Industry 4.0 should be understood as the ecosystem and interconnectivity of the previously mentioned systems rather than their individual behaviour. Figure 1.1 depicts the idea behind the Industry 4.0 paradigm, where an interconnected industry can be understood as the adoption of such systems. Notice that the common point among the different systems involved in the Industry 4.0 is that they need to exchange massive amounts of information to assure the correct behaviour of the industrial environment. In addition, if the development of the Internet of Things (IoT) solutions is also considered, one can observe that the number of industrial measurements and available data is increasing exponentially. Thus, it can be said that the industry is also heading towards the big data era. This fact motivates the appearance of new industrial trends which will transform the industries not only in a digitalised scenario, but also in a self-management environment [Wol17]. Their main idea is to gather and store industrial data to generate as much value as possible from them. The appearance of predictive maintenance tasks, the adoption of data-driven methods in industrial environments or the design and implementation of data-based soft-sensors are some use-cases of big data in the Industry 4.0 paradigm. Thereby, the adoption of these latest trends opens a new path to develop innovative technologies and methodologies which not only support the industry management, but also provide a wide range of possibilities.

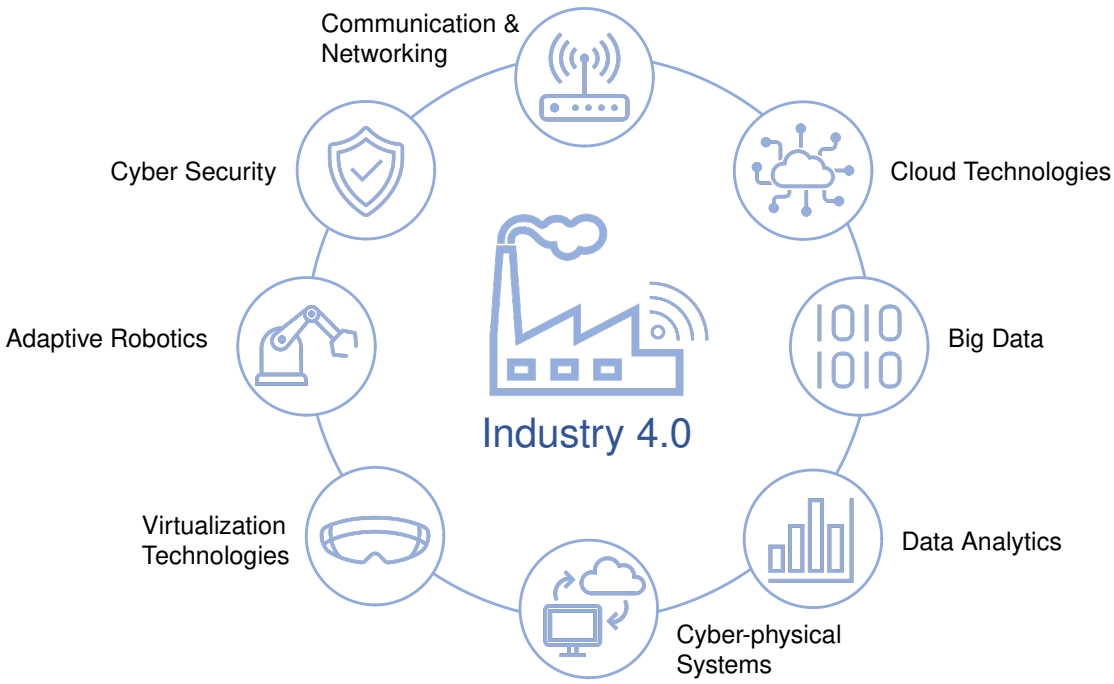

Figure 1.1: Involved systems and technologies in the Industry 4.0 paradigm.

When talking about big data in industry one must also refer to Deep Learning (DL), an important allied which is the motivator of most of the new industrial trends focused on the use of data. Inside the DL domain, the development and adoption of Artificial Neural Networks (ANNs), which consist in intelligent systems able to adapt from experience and generalise its solutions to unknown scenarios [DS17, Chapter 1]. Their adoption has arisen the interest of the research community during the last years as a result of their ability to correctly perform either classification or regression tasks. This is achieved by means of learning the intrinsic linear and non-linear relationships between the input and output data of the process being modelled. Their main characteristic is that there is no need to know these relationships if input and output measurements of the process being modelled are available. This will be performed by the same ANN. In that sense, their adoption has been disseminated among a great number of applications, for instance, as image and pattern recognition tools [DS17, Section 5.4]. More complex networks, such as Recurrent Neural Networks (RNNs), have been considered in predictive text and natural language processing applications [Goo16, Chapter 12]. All this has paved the way to apply ANNs for more purposes which go beyond the pattern recognition and language-based applications.

It is in the industrial field where the appearance of the Industry 4.0 and the available number of industrial measurements make the ANNs an element to take into consideration. Their abilities to model non-linear relationships have motivated their use in different kind of tasks such as:

- Predictive maintenance and anomaly detection: Predictive maintenance is particularly useful in assembly lines to predict which part of the line and when it will be about to fail. This is of most importance for those industries which cannot stop their activity: being able to predict when an element is going to fail gives enough time to perform the required maintenance without stopping the industrial activity. Anomaly detection is as important as predictive maintenance. In assembly lines, it is considered to determine those products or pieces which are not passing the quality criteria. This gives the operator a very useful information. The mix of both, predictive maintenance and anomaly detection, is one of the current uses of ANNs at industrial domains [Coo19, Han20].
- Development of soft-sensors: Soft-sensors are considered to forecasting measurements of harsh industrial environments where conventional sensors are neither suitable, nor feasible [Sou16]. Some of these environments consist in petrochemical industries [Ran13], sewage systems [Zha18b, Zha18c] or water management facilities [Ben07, Can16, Man17, Con18].

Nevertheless, there are more tasks where ANNs can make the difference. For instance, to extract features from industrial measurements or to implement data-based controllers among others. In the first case, ANNs are considered to obtain features which cannot be determined at a first sight. Therefore, industrial operators are provided with extra information that helps them to take decisions related to the industrial environment. On the other hand, the implementation of data-based controllers entails a reduction of the industrial control design complexity, which sometimes is crucial depending on the environment to control. In that sense, Wastewater Treatment Plants (WWTPs), which are industrial scenarios devoted

to cleaning and treating the urban and industrial residual waters, are one of the industrial environments where the application of ANNs could be of utmost interest. The WWTPs behaviour relies on highly complex and non-linear biological and biochemical processes [Hen87, Hen00]. Processes which are suitable to be modelled by ANNs. In addition, WWTPs are also known to be industries prone to generate pollutant and harmful products for the aquatic life in the cleaning processes of residual waters. In a world where the environmental pollution is a critical issue, it is important to reduce the industrial pollutant products. Hence, most of the control approaches considered in the WWTPs are devoted to mitigating the effects of these components at the same time they try to maintain the required operational conditions to let the biological and biochemical processes actuate in a proper manner [Yan95]. In that sense, most industrial controllers applied in the WWTP scenarios consist in conventional strategies such as the Proportional Integral (PI) controllers [Ale08, Ger14, Nop10, Bar18], Model Predictive Controllers (MPCs) [She08], Fuzzy Logic controllers (FL) or mixes of them [San15b, San16, Rev17]. Their control performance has corroborated their adoption in the management of WWTPs. But the emergence of ANNs could change the landscape. Recently, the ANNs potential has motivated their adoption in the industrial control domain due to their ability in the prediction and classification tasks. This motivate their adoption as a previous stage for industrial controller which can benefit from the information provided by ANNs. Notwithstanding, their deployment can go beyond this point. For that reason, the aim of this thesis is to provide an assessment of different applications of ANNs in the industrial control domain, especially in WWTPs. Therefore, the needs and prominent issues related to conventional control structures will be detected and ANN-based solutions proposed so as to tackle them.

1.1.1 Industrial Control Enhancement

Conventional structures have been widely considered in industrial environments. They offer a good enough control performance, but, on some occasions, their actuations are counterproductive under an environmental and economical point of view. Moreover, an actuation provided by a control structure can degrade control actuations on other process units of the plant. For instance, in the WWTP domain, the actuations over the oxygen control loop are counterproductive with respect to the actuation over the nitrogen control. In that sense, the classification and prediction performance provided by ANNs have motivated their adoption as tools to support the conventional industrial controllers [Fos16]. However, their use-cases have not been completely assessed. There are some aspects regarding the topology of industrial measurements as well as the control enhancement objective that needs to be tackled. As a result, the first research questions regarding the application of ANNs in such situations have arisen:

- **Research Question 1:** *What kind of preprocessing is required by the industrial measurements?*
- **Research Question 2:** *Are ANNs capable of supporting conventional controllers and improve their control and environmental performance?*

1.1.2 Industrial Control Complexity and Scalability

Industrial scenarios are characterised by performing highly complex operations which most of the times require an industrial controller to be correctly designed and tuned. In addition, the appearance of the Industry 4.0 and the increasingly automatization of industries are showing and exponential growth in the adoption of control strategies. Strategies which most of the time are not formed by simple PID or MPCs controllers but considering mixes and hierarchical structures [San15b]. Moreover, not all the controllers can be adopted since some of them could become unstable in certain industrial scenarios. This entails a reduction on the scalability of control strategies as well as a deep knowledge of the process under control. In that sense, ANNs power is such that they could be considered to alleviate these issues. Recently, some research on the application of ANNs as part of the control structures such as ANN-based FLC have motivated their adoption as the main control tool [Han18a]. Besides, their adoption could provide an increment of the scalability of control structures since ANNs only require input and output measurements of the process under control. Consequently, new research questions on the adoption of ANNs as the main control structure of industrial environments need to be answered:

- ◎ **Research Question 3:** *Can ANNs act as industrial controllers?*
- ◎ **Research Question 4:** *Are ANN-based controllers stable?*
- ◎ **Research Question 5:** *Are ANN-based controllers scalable?*

1.1.3 Control Strategies Transferability

The adoption of ANNs as new data-based controllers can open a new path in the design and implementation of new control approaches. Their capability of generalisation makes them a suitable tool to implement different control strategies which could be adopted in multiple control loops. This will be translated in an exponential growth of the industrial control scalability since a unique structure can not only be managing more than one control loop in one domain, but also in other industrial environments. However, ANNs have some drawbacks. They have to be designed and trained in order to achieve a good performance in the tasks for which they have been trained for. This process can become a high time consuming and difficult task to perform [Ami20]. For that reason, Transfer Learning (TL) solutions have arisen as the solution to these problems: transfer the knowledge of the ANN from a source domain to a target one can alleviate the design issues as well as it can increase the scalability of the ANN-based control solutions. Nevertheless, TL cannot be applied carelessly in critic scenarios such as petrochemistry or WWTP environments. Therefore, some research questions arise because of these issues:

- ◎ **Research Question 6:** *Can an ANN-based control solution be transferred?*
- ◎ **Research Question 7:** *Can the transfer suitability be measured?*

As it is observed, ANNs have arisen as a really powerful ally in the industrial control domain, but their adoption is still in their infancy. Therefore, this thesis aims to fill this gap. To achieve this, this thesis will try to give an answer to each one of the aforementioned research inquiries at the same time the prominent issues of conventional controllers and the application of ANNs in the industrial control domain are tackled. More precisely, ANN-based solutions are proposed at three different stages. At the first stage, ANNs will be considered to implement a soft sensor able to measure the effluent concentrations of a WWTP. Its main objective consists in improving the control and environmental performance of conventional controllers. These ANNs will be designed and trained considering industrial measurements which most of the times are unbalanced or present a data scarcity issue. Then, ANNs will be adopted in the implementation of an ANN-based controller able to maintain certain concentrations of the ANNs at the given set-points. Its stability as well as the correction needed to avoid the non-idealities of the measurements will be also assessed. Last but not least, the possibility of transferring the ANN-based solutions between different industrial control domains as well as the option of measuring the transfer suitability will be analysed.

1.2 Objectives

The three general objectives of this thesis are focused on giving an answer to the research questions that have arisen due to the application of ANNs in the industrial control domain.

- **Research Objective I**: *Improve the control and environmental performance of currently adopted conventional approaches.*

  This objective is aligned with the Research Questions 1 and 2, which arise with the adoption of ANNs as supportive tools for conventional controllers. To fulfil it, an ANN-based soft sensor showing a good prediction performance has to be obtained. Since its purpose is to support conventional controllers, the ANN-based soft sensor will be deployed over a WWTP scenario being managed by MPC and FLC conventional controllers. Besides, it aims to determine those moments when a control actuation is required. In that manner, the reduction of the control operational costs is sought.

- **Research Objective II:** *Implement a stable ANN-based controller*

  Taking the Research Questions 3, 4, and 5 into account, this objective is devoted to designing and implementing an industrial controller based on input and output measurements of a WWTP scenario. Its main aim is to manage and maintain the operability of WWTPs. Moreover, the stability of the controller and its correct behaviour with non-ideal measurements must be assured if its adoption as the unique control approach of a WWTP scenario is desired.

◎ **Research Objective III:** *Analyse the suitability of transferring ANN-based controllers.*

The third objective is aligned with the fulfilment of the Research Questions 6 and 7. The adoption of a unique ANN-based control structure of a WWTP environment will be evaluated. Moreover, the suitability of transferring the control knowledge among different control loops and scenarios will be assessed as well. Besides, a new measurement approach will be defined to shed some light in the field of TL.

1.3 Thesis Outline

The thesis consists in seven different chapters whose main objective is to tackle the issues of conventional control structures by means of Deep Learning approaches. In such a context, the thesis is divided in three blocks depending on their purpose: (i) Chapters 1 and 3 introduce and place the thesis with respect to the current state-of-art, (ii) Chapters 4, 5, 6 and 7, which depict the contents of the research performed during the realisation of this thesis, and (iii) Chapter 8, which concludes the document. In that sense, Chapter 4, 5, 6 and 7 main aim is to determine the principal issues that must be tackled if the adoption of ANN-based solutions in the management of industrial scenarios is desired. Moreover, an analysis of the most relevant works in the literature and the research contributions performed in this thesis will be discussed along these chapters.

Figure 1.2 depicts the roadmap of this thesis. As it is observed, the main contributions of the thesis can be split into four connected stages. More precisely, the first stage is focused on the problems and solutions that arise as a consequence of the adoption of ANN-based solution to support conventional controllers managing WWTP scenarios. The second and third stages are devoted to analysing and studying the adoption of ANNs as industrial controllers rather than supportive mechanisms. Finally, the last stage aims to analyse the transferability and suitability of the ANN-based controllers into new control environments. Taking all this into account, the outline of the thesis is as follows:

Chapter 1 introduces and places the thesis in the research line of the industrial control domain, especially, in the application of ANN-based solutions in the management of WWTPs. The motivation of the thesis as well as the sought objectives are presented here. Moreover, a brief analysis of the published research works in which this thesis is based on is also performed in this chapter.

Chapter 2 describes the main concepts regarding the ANN approaches considered in this thesis. Section 2.1 describes the two main architectures adopted: (i) the Multilayer Perceptron, and (ii) the Long Short-Term Memory cells. Their training process as well as their regularisation and evaluation are described in Section 2.2. Finally, a brief introduction to Transfer Learning techniques are shown in Section 2.3.

Chapter 3 is devoted to describing and analysing the background on the industrial control of WWTPs. There are a huge variety of topologies and architectures of WWTPs, from the ones

overseeing the reduction of the nitrogen-derived components of residual urban waters to the ones aiming to reduce not only the nitrogen but also the phosphorus components. In order to ensure generalisation, and replicability of the proposed contributions, this thesis bases its results on the Benchmark Simulation Model No.1 (BSM1) and No.2 (BSM2) [Cop02, Ger14]. Besides, brief analyses of the soft-sensing as well as the conventional control approaches that are being applied by the research community, especially, the PI, MPC, FLC and IMC controllers, are provided in Sections 3.2 and 3.3, respectively.

Chapter 4 discusses the research contributions performed in the adoption of ANNs as a support for conventional controllers. Thereby, it is aligned with Research Objective I. In this chapter two principal ANN-based solutions are presented to support the conventional controllers: (i) an

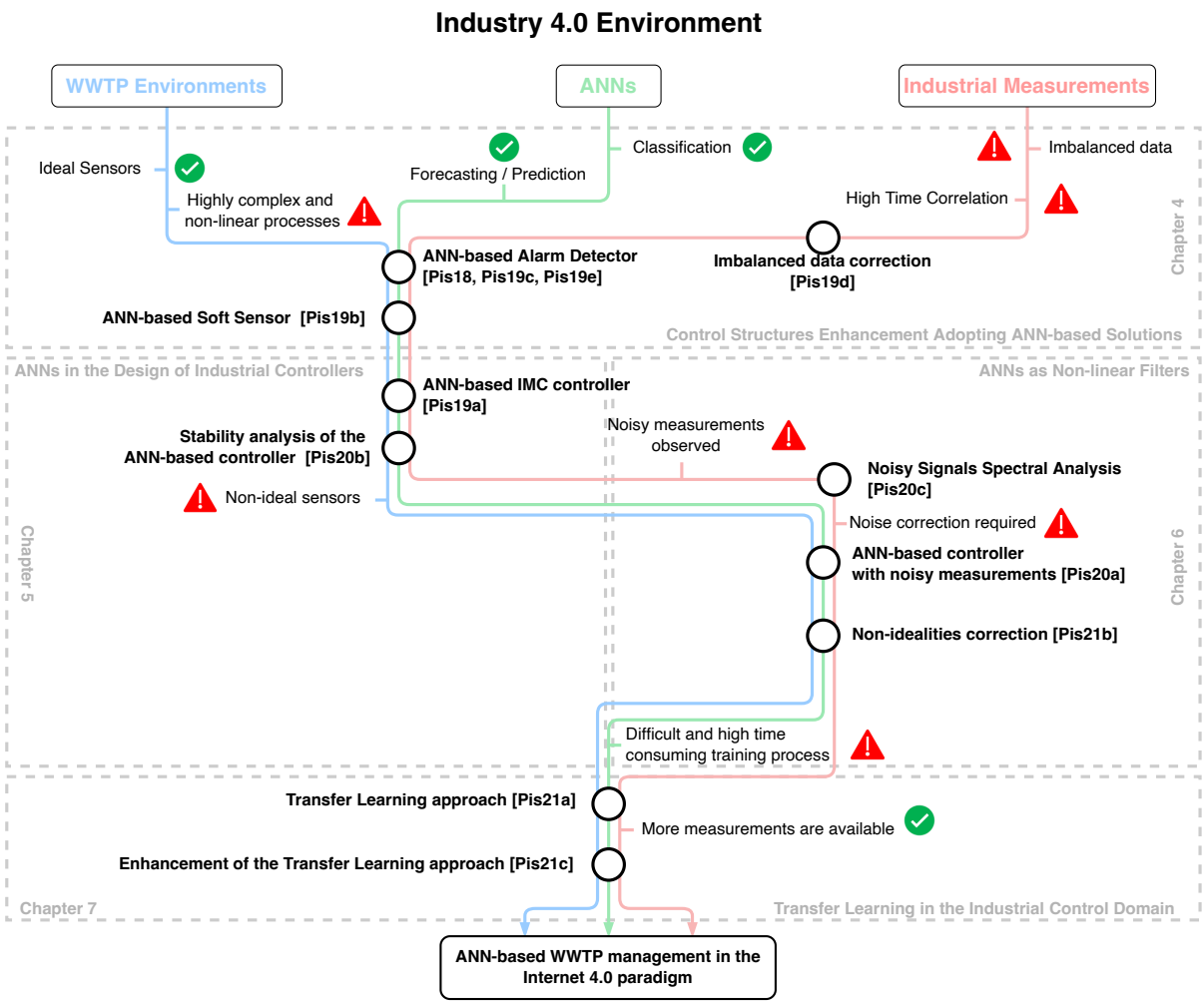

Figure 1.2: Thesis roadmap. The chapters of the thesis and the publications in which they are based on are shown here. As it is observed, the prominent issues that must be tackled when applying ANNs in the industrial control domain are depicted. Research contributions per chapter have also been highlighted in bold to clearly point to the most important contributions of this thesis. Finally, warnings stand for issues that need to be tackled and ticks for features and events easing the deployment of ANNs.

ANN-based Alarm Detector, and (ii) an ANN-based Control Selector. The former is in charge of determining the amount of pollutant components that the WWTP will generate as a consequence of its behaviour. Section 4.1 shows the related work attaining the development of soft-sensors. Then, Section 4.2 analyses the structure of the proposed alarm detector and its performance. Moreover, this alarm detector sets the basis of the ANN-based Control Selector, whose main aim is to determine the control structure to apply at each moment and as a result of the predicted WWTP effluent values. Its behaviour, structure, and performance in contrast to conventional structures is analysed in Section 4.3. This chapter is based on the work presented in [Pis19b, Pis19c] as journal articles, in [Pis18, Pis19d] as conference papers and [Pis19e] as a conference paper published as a book chapter.

Chapter 5 is aligned with Research Objective II. Its main aim is to show and discuss the application of ANNs as industrial controllers. For that purpose, an ANN-based PI as well as an Internal Model Controller (IMC) structure, which completely relies on ANNs, have been designed to manage the default control loops of the BSM1 scenario. As a controller being designed from scratch, the ANN-based IMC stability is thoroughly analysed to ensure its correct behaviour along time. Section 5.1 shows the related work attaining the development of ANN-based controllers. The structure of the ANN-based PI as well as its prediction and control performance are assessed in Section 5.2. Then, the internal structure of the ANN-based IMC, its performance and its stability are shown in Section 5.3. This chapter is based on the research contributions presented in [Pis19a, Pis20b, Pis20c, Pis21d] as conference papers and in [Pis20a, Pis21c] as journal articles.

Chapter 6 is also aligned with Research Objective II. The main purpose of this chapter is to assess the adoption of ANNs as elements correcting the effects of non-idealities introduced in the control structures. In that sense, a Data-based Control Enhancement Processing Approach devoted to firstly denoising the noise-corrupted measurements and secondly to correct the effects related to the delays. Since ANN-based controllers rely on the data considered in their training process, they are prone to suffering whenever ideal measurements are not available. For that reason, the adoption of the Data-based Control Enhancement Processing Approach is considered here so as to improve the ANN-based PI and ANN-based IMC control performance. The description and behaviour of the Data-based Control Enhancement Processing approach is shown in Section 6.2. Section 6.3 is devoted to showing the behaviour of the ANN-based PI when it is precedented by the Data-based Control Enhancement Processing approach. In Section 6.4 the behaviour of the ANN-based IMC as well as its stability is assessed once the incoming measures are denoised by the Denoising stage of the proposed system. Finally, Section 6.5 concludes the chapter. This chapter is based on the research contributions presented in [Pis19a, Pis20c, Pis20b] as conference papers and part of the work presented in [Pis20a, Pis21c] as journal articles.

Chapter 7, which is aligned with Research Objective III, analyses and discusses the transferability of ANN-based controllers in domains for which they have not been trained for. In order to perform

this analysis, the ANN-based controllers obtained in Chapter 5 will be transferred between the WWTP most important control loops just to determine if the control performance is maintained or not. Section 7.1 shows the related work attaining transfer learning approaches in industrial scenarios. Information related to the transferability of the ANN-based controller and results of the performed analyses are shown in Section 7.2. Not only this, the performance of the ANN-based controller can be even improved when it is transferred. A fine-tuning (FT) process can be performed whenever the ANN-based controller is not performing well enough. Section 7.2.3 is devoted to analysing the effects of the FT process in the complete control structure when it is applied over the WWTP environment. Finally, WWTP can be considered as critic infrastructure that need to be correctly managed. For that reason, the control performance of a transferred ANN-based controller must be computed a priori just in case it is not able to manage the plant. Section 7.3 follows this line and shows a new transfer suitability measuring approach to determine if an ANN-based controller can be transferred or not. This chapter summarises the works presented in [Pis21c] as a journal article and in [Pis21a] as a conference publication. Moreover, an extra contribution has been submitted to ETFA 2022 [Pis22].

Chapter 8 depicts the most important conclusions attained in the course of this thesis. Future lines of research are as well identified and provided in this chapter.

1.4 Research Contributions

The results that have been obtained during the realisation of this thesis have been published as 13 research contributions in the form of five journal articles, seven conference publications and one book chapter. Table 1.1 shows the most important metrics of the research works published as journal articles. For each contribution, the quartile (Q) in the field of engineering and the impact factor (IF) of the journal are provided accordingly to the JCR Clarivate and FECYT journal analyses. Metrics which are not yet available are denoted with N/A. In addition, the number of citations accordingly to Scopus database is also given. Table 1.2 depicts the seven works published as conference papers. In this table, the number of citations are given accordingly to Scopus database with the exception of [Pis18], whose number of citations are provided by Google Scholar. Finally, Table 1.3 provides information about the research contributions published as a book chapter.

Table 1.1: Analysis of the contributions presented in journal articles. Most important parameters of the articles [Pis19b, Pis19c, Pis20a, Pis21b, Pis21c] are shown.

Title	Journal	Q	IF	Citations	Year
ANN-Based Soft Sensor to Predict Effluent Violations in Wastewater Treatment Plants	Sensors	Q1	3.275	39	2019
LSTM-Based Wastewater Treatment Plants Operation Strategies for Effluent Quality Improvement	IEEE Access	Q1	3.745	12	2019
Denoising Autoencoders and LSTM-Based Artificial Neural Networks Data Processing for Its Application to Internal Model Control in Industrial Environments — The Wastewater Treatment Plant Control Case	Sensors	Q1	3.576	8	2020
Industrial Control under Non-Ideal Measurements: Data-Based Signal Processing as an Alternative to Controller Retuning	Sensors	Q1	3.576	1	2021
Transfer Learning in Wastewater Treatment Plant Control Design: From Conventional to Long Short-Term Memory-Based Controllers	Sensors	Q1	3.576	0	2021

Table 1.2: Analysis of the contributions presented in conference publications. Most important parameters of the publications [Pis18,Pis19a,Pis19d,Pis20b,Pis20c,Pis21a,Pis21d] are shown. * denotes the citations retrieved by Google Scholar database.

Title	Conference	Cites	Year
A Recurrent Neural Network for Wastewater Treatment Plant effluents' prediction	XXXIX Jornadas de Automática	9*	2018
Data preprocessing for ANN-based industrial time-series forecasting with imbalanced data	27th European Signal Processing Conference (EUSIPCO)	2	2019
ANN-based Internal Model Control strategy applied in the WWTP industry	24th IEEE International Conference on Emerging Technologies and Factory Automation (ETFA)	5	2019
LSTM-based IMC approach applied in Wastewater Treatment Plants: performance and stability analysis	21st IFAC World Congress	2	2020
Noisy Signals in Wastewater Treatment Plants data-driven control: Spectral Analysis approach for the design of ANN-IMC controllers	IEEE Conference on Industrial Cyberphysical Systems (ICPS)	3	2020
LSTM based Plug-and-Play controller for Dissolved Oxygen Control in Wastewater Treatment	IWA Digital World Water Congress (IWA DWWC2021)	0	2021
Transfer Learning Approach for the Design of Basic Control Loops in Wastewater Treatment Plants	26th IEEE International Conference on Emerging Technologies and Factory Automation (ETFA)	1	2021

Table 1.3: Analysis of the contribution [Pis19e] presented in a conference and published as a book chapter.

Chapter Title	Book Title	Publisher	Cites
Artificial Neural Networks Application to Support Plant Operation in the Wastewater Industry	Technological Innovation for Industry and Service Systems	Springer: Cham	2

Chapter 2

Brief Introduction to ANN Approaches

In this thesis ANNs are considered due to their ability in modelling non-linear and highly complex systems [DS17, Chapter 1]. They have arisen as a suitable tool able to perform different tasks such as classification, pattern recognition, system identification, speech and language processing, and control of systems [DS17, Section 1.1.3]. Their power has motivated their adoption in several industrial scenarios such as the WWTP environments to implement different kinds of soft-sensors or even to support conventional controllers. For that reason, before assessing these implementations in the WWTP domain, a brief overview of ANNs is provided in this chapter. Its main aim is to provide the reader with an overview of the different ANN-based approaches considered in this thesis. First, the main ANNs topologies are presented, especially the Multilayer Perceptron Networks and the Long Short-Term Memory cells. Then, their training process and the most common evaluation approaches are presented. Finally, a brief introduction to the Transfer Learning concept is provided.

2.1 ANN Architectures

ANNs general architecture consists in a set of layers formed by neurons whose main objective is to modify the incoming measurements and transform them into output ones following a learnt model. The main point is that this model is obtained by means of an iterative process where the different interconnections among neurons, known as weights, are adapted to replicate the real process that the ANN is modelling.

Generally, the ANNs architecture is determined by the number of layers and the kind of interconnection between their nodes. For instance, structures forwarding the information in cascade consider three different types of layers:

- **Input layer**: it is in charge of receiving the incoming data and pass them to the next layer. Normally the amount of neurons is equal to the number of input data.

- **Hidden layer**: it is in charge of gathering the data coming from the input layer and modify them following the learnt model. The number of hidden layers as well as the number of neurons per hidden layer are arbitrary and decided by the designer.
- **Output layer**: it is in charge of gathering the data coming from the hidden layers and adapt them to the final purpose of the ANN. The number of neurons in the output layer equals to the number of outputs required.

Each layer is also characterised by the activation function it implements. There are different types of functions, however, the ones considered in this thesis correspond to those usually adopted to perform regression tasks, i.e., the Hyperbolic Tangent (*tanh*),

$$tanh(x) = \frac{e^x - e^{-x}}{e^x + e^{-x}} \tag{2.1}$$

the Linear, $f(x) = x$, and its Rectified Linear Uniform (ReLU) function,

$$ReLU(x) = \begin{cases} 0 & x < 0 \\ x & x \geq 0 \end{cases} \tag{2.2}$$

and the sigmoid,

$$\sigma(x) = \frac{1}{1 + e^{-x}} \,. \tag{2.3}$$

Their main aim is to modify the output of each layer according to its purpose. Moreover, the activation function considered in the output layer determines the purpose of the whole ANN. If it performs regression tasks, the linear activation function must be considered. On the other hand, if classification purposes are desired instead, $\sigma(x)$ or its vectorised version, the softmax function, must be adopted [DS17, Section 1.3.2]. It is computed as:

$$\sigma(\mathbf{x})_i = \frac{e^{x_i}}{\sum_{j=1}^{N} e^{x_j}} \tag{2.4}$$

where x_i denotes each element in $\mathbf{x}$.

Two types of ANNs are considered in terms of the interconnections between the neurons of the ANN's layers: the Feed-forward Neural Network (FFNN) and the RNN:

- **FFNNs**: ANNs wherein interconnections feed-forward the information in cascade, i.e, through the input layer to the output layer. One of the most important and well-known architecture corresponds to the Multilayer Perceptron (MLP) [DS17, Chapter 5].

- **RNNs**: ANNs wherein interconnections can pass the information either in cascade, or backwards. Its highest drawback, known as the vanishing and exploding gradients, is alleviated with gated RNN, especially with the Long Short-Term Memory (LSTM) cells [Goo16, Section 10.10].

2.1.1 Multilayer Perceptron Networks

MLP networks consist in the concatenation of different hidden layers between the ANN's input and output. The interconnections between the neurons of subsequent layers are forward without going backwards. To better understand their behaviour, let's consider the MLP net shown in Figure 2.1. It depicts a MLP net with the input, the output, and one hidden layer.

The network considers N input measurements $\mathbf{x} = [x_1, x_2, \cdots, x_{N-1}, x_N]^T$, $\mathbf{x} \in \mathbb{R}^{N\times 1}$, which will be modified according to the learnt model through the hidden and output layers. Thus, if the net considers an output layer with M outputs, $\widehat{\mathbf{y}} = [\widehat{y}_1, \widehat{y}_2, \cdots, \widehat{y}_{M-1}, \widehat{y}_M]$, $\widehat{y} \in \mathbb{R}^{M\times 1}$ and L hidden neurons in the hidden layer, the behaviour of the MLP will be computed as

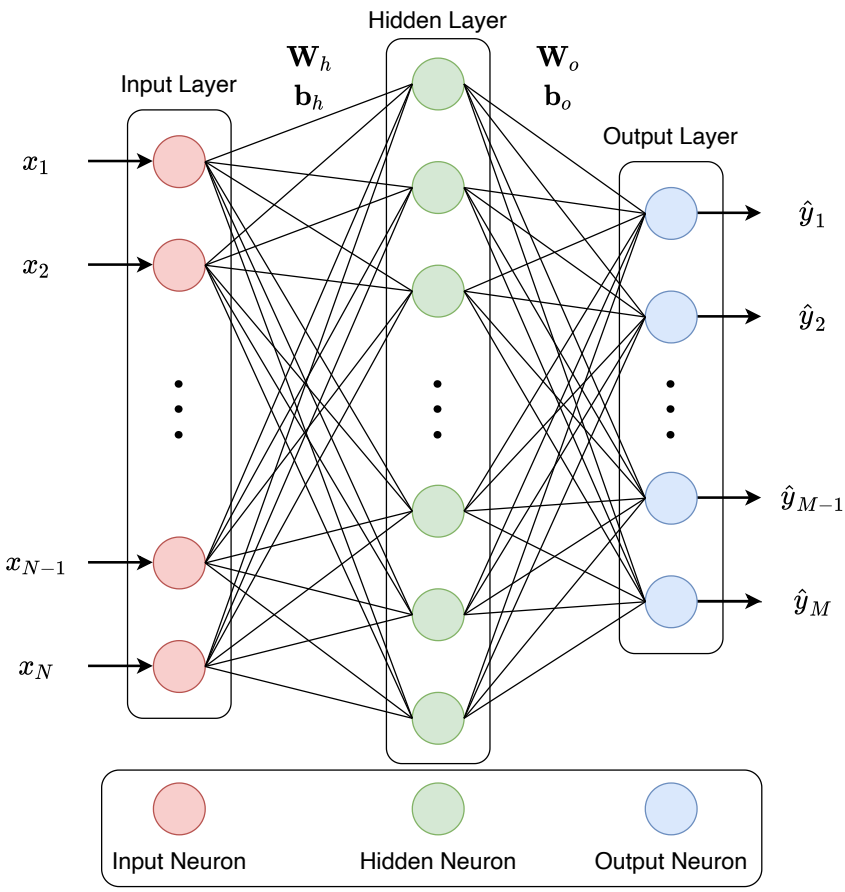

Figure 2.1: MLP architecture.

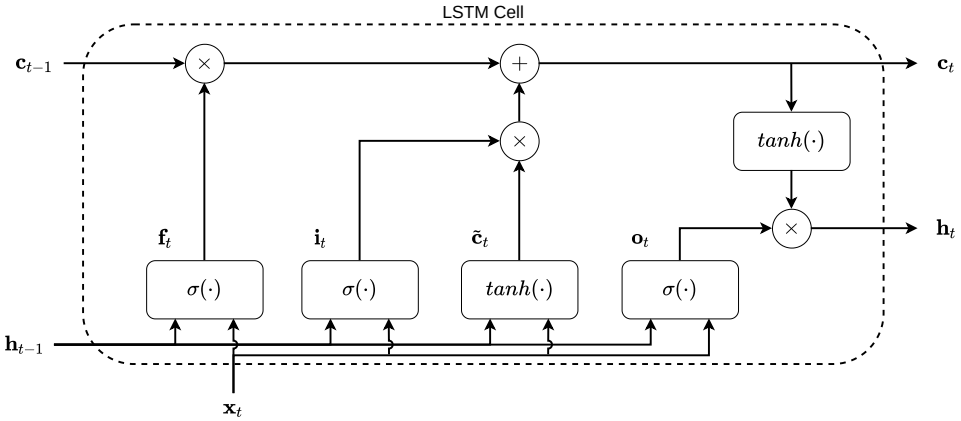

Figure 2.2: LSTM cell architecture.

$$\mathbf{h} = f\left(\mathbf{W}_h^T \cdot \mathbf{x} + \mathbf{b}_h\right) \tag{2.5}$$

where $\mathbf{W}_h \in \mathbb{R}^{N \times L}$ represents the weights matrix of the interconnections between the input and hidden layers, $\mathbf{b}_h \in \mathbb{R}^{L \times 1}$ to the biases, and $f(\cdot)$ to the considered activation function. ReLU activation functions are usually considered as the activation between input to hidden and hidden to hidden layers. $\mathbf{h} \in \mathbb{R}^{L \times 1}$ denotes the output of the hidden layer. Then, $\mathbf{h}$ is modified in the output layer as

$$\widehat{\mathbf{y}} = f\left(\mathbf{W}_o^T \cdot \mathbf{h} + \mathbf{b}_o\right) \tag{2.6}$$

where $\mathbf{W}_o \in \mathbb{R}^{L \times M}$ represents the weights matrix of the interconnections between the hidden and output layers, $\mathbf{b}_o \in \mathbb{R}^{M \times 1}$ the output layer biases, and $f(\cdot)$ its activation function. Since in this thesis only regression tasks are considered, the usual output activation function corresponds to the linear function.

2.1.2 Long Short-Term Memory Cells

The main point of LSTM cells is that they are recurrent networks able to intrinsically consider information about past events in the prediction of future ones [Goo16, Section 10.10]. The particularity of LSTM is that they have arisen as a solution to the well-known exploding and vanishing issues of RNN. Moreover, their good performance in the modelling of time-series and time-dependent values, such as speeches or texts, makes the LSTM cells a suitable structure to deal with industrial measurements [Wan18, Gre17]. Figure 2.2 depicts the internal structure of a LSTM cell. It considers three inputs: (i) the current input data ($\mathbf{x}_t$), the previous state ($\mathbf{c}_{t-1}$), and the previous output ($\mathbf{h}_{t-1}$). The outputs of the LSTM cell correspond to the actual output ($\mathbf{h}_t$) and its inner state cell ($\mathbf{c}_t$), respectively. In terms of the internal structure, LSTM cells consider three different gates: (i) the input ($\mathbf{i}_t$), (ii) the forget ($\mathbf{f}_t$) and (iii) the output ($\mathbf{o}_t$) gates. They are devoted to processing the inputs and to obtaining the desired predictions.

The input gate corresponds to a sigmoid layer in charge of determining the information which will modify $\mathbf{c}_{t-1}$ as a function of $\mathbf{x}_t$ and $\mathbf{h_{t-1}}$. Its outputs are computed as:

$$\mathbf{i}_t = \sigma(\mathbf{W}_i^T \mathbf{x}_t + \mathbf{U}_i^T \mathbf{h}_{t-1} + \mathbf{b}_i). \tag{2.7}$$

The forget gate determines the information of the inner cell state that needs to be reset:

$$\mathbf{f}_t = \sigma(\mathbf{W}_f^T \mathbf{x}_t + \mathbf{U}_f^T \mathbf{h}_{t-1} + \mathbf{b}_f). \tag{2.8}$$

Then, new candidates to substitute the inner cell state ($\tilde{c}_t$) are computed by a *tanh* layer. It considers the input data as well as the previous LSTM output:

$$\tilde{\mathbf{c}}_t = tanh(\mathbf{W}_c^T \mathbf{x}_t + \mathbf{U}_c^T \mathbf{h}_{t-1} + \mathbf{b}_c). \tag{2.9}$$

The output gate computes the output candidates of the LSTM cell as:

$$\mathbf{o}_t = \sigma(\mathbf{W}_o^T \mathbf{x}_t + \mathbf{U}_o^T \mathbf{h}_{t-1} + \mathbf{b}_o). \tag{2.10}$$

Finally, the output and the inner cell state are computed as a combination of the gates outputs:

$$\begin{aligned} \mathbf{c}_t &= \mathbf{f}_t \circ \mathbf{c}_{t-1} + \mathbf{i}_t \circ \tilde{\mathbf{c}}_{t-1} \\ \mathbf{h}_t &= \mathbf{o}_t \circ tanh(\mathbf{c_t}) \end{aligned} \tag{2.11}$$

where $\circ$ denotes the Hadamar or element-wise product of matrices and vectors. Notice that $\mathbf{W}_{i,f,c,o} \in \mathbb{R}^{N_i \times N_g}$, and $\mathbf{U}_{i,f,c,o} \in \mathbb{R}^{N_g \times N_g}$ are the weights of the different gates modifying $\mathbf{x}_t$ and $\mathbf{h}_{t-1}$, respectively. $\mathbf{b}_{i,f,c,o} \in \mathbb{R}^{N_g \times 1}$ are their biases. N_g and N_i are the number of hidden units per gate and the number of inputs, respectively.

2.2 Training Process

Before adopting the ANNs for their final purposes, they have to be trained. In the training process, the weights and biases are determined by means of an iterative process. Its main objective is to suit a model considering the available data. Three different training processes are defined [DS17, Section 2.3]:

- **Supervised training**: in this process the ANN is provided with pairs of input and output measurements of the model to suit. The weights are determined to replicate the output values given the input ones.

- **Unsupervised training**: in this process the ANN is only provided with input measurements. The main aim of unsupervised training is to obtain features of the given dataset and therefore, extract the knowledge from these features.

- **Reinforcement Learning**: it corresponds to a variant of the supervised training. ANNs, and therefore its weights, are trained by means of interacting with the environment where they are placed.

2.2.1 Training & Regularisation

The key point of the iterative process is that weights and biases ($\boldsymbol{\theta}$) are adapted to minimise a cost function ($J(\boldsymbol{\theta})$). This function reflects the ANN desired behaviour. For instance, ANNs devoted to performing classification tasks are usually trained considering supervised training options and the cross-entropy cost function. On the other hand, the Mean Squared Error (MSE) cost function is adopted for regression purposes [Goo16, Section 6.2]:

$$J(\boldsymbol{\theta}) = \frac{1}{N_p} \sum_{i=1}^{N_p} (\mathbf{y}_i - \widehat{\mathbf{y}}_i)^2 \tag{2.12}$$

where $\mathbf{y_i}$ and $\widehat{\mathbf{y}}_i$ are the original and the predicted data, and N_p the number of predictions, respectively. In order to optimise the cost function, standard optimization techniques such as Gradient Descent (SGD) based optimisers as well as the Back Propagation (BP) and Back Propagation Through Time (BPTT) algorithm are considered [Goo16, Sections 6.5 and 8.3.1]. BP and BPTT compute the gradient of the cost function by means of passing back the information from the cost function through the ANN structure. SGD consists in the adoption of the cost function's negative gradient to point towards its global minimum. The gradient contains all the partial derivatives of $J(\boldsymbol{\theta})$ with respect to the provided inputs $\mathbf{x}$. Thus, at each step the SGD adapts the weights and biases to obtain new values able to closer point to the global minimum of $J(\boldsymbol{\theta})$:

$$\boldsymbol{\theta}_{t+1} = \boldsymbol{\theta}_t - \epsilon \nabla_{\boldsymbol{\theta}} J(\boldsymbol{\theta}_t) \tag{2.13}$$

where $\nabla_{\boldsymbol{\theta}} J(\boldsymbol{\theta}_t)$ denotes the cost function's gradient provided the actual weights and biases $\boldsymbol{\theta}_t$. ϵ corresponds to the learning rate, an ANN hyperparameter determining the step of the gradient. It is also highly related to the ANN training time, since the lower the ϵ, the lower the gradient step and the larger the time to reach the global minimum. This also entails that SGD can get stuck in a local minimum. Otherwise, large ϵ values can lead the SGD to never converge.

Based on the SGD, there exist other optimisation algorithms speeding-up the ANN training process. This is the case of Momentum, which is in charge of accumulating an exponentially decay of the moving average of past gradients. Later, it continues moving towards their direction [Goo16, Section 8.3.2].

Moreover, RMSprop and Adam algorithms have arisen to facilitate the ANN training process not only enabling the adaption of the learning rate, but also the SGD acceleration [Goo16, Section 8.5]. Focusing on Adam algorithm, it consists in a variant of RMSprop and momentum. At each step time, it estimates the first and second order moments of the gradient. Then, these values are considered to determine the updated set of weights and biases of the ANN structure. The final set corresponds to:

$$\boldsymbol{\theta}^* = \arg\min_{\theta} J(\boldsymbol{\theta}) \tag{2.14}$$

Nevertheless, nothing can be done if measurements are not available. In that sense, huge numbers of measurements are required to properly train the ANNs and obtain a generalised model. To achieve this the available dataset must be split into three subsets:

- **Training dataset**: set of measurements considered in the training process. Weights and biases of the ANNs are determined with this subset.
- **Validation dataset**: set of measurements considered to test the performance of the ANN while its model is being fitted with the training dataset.
- **Test dataset**: set of measurements considered to evaluate the ANN final model performance.

Generally, the amount of the training data is chosen to be placed between a 60 and a 90% of the whole dataset. The remaining percentage is equally distributed to generate the validation and test sets. Since test dataset is not considered in the training of the ANN model, it will allow the ANN designers to compare the performance of the different structures with the same data. This entails a high dependence on the data and samples entering in the training and test datasets [DS17, Section 5.1.1]. For that reason, K-Fold cross-validation method has been considered to alleviate this dependence.

The main idea of K-Fold is to split the whole training dataset in K subsets where K-1 are considered to train the ANN structure while the remaining one is devoted to validating purposes. Thus, as many training processes as folds are performed. The overall ANN performance is computed as the average of the K different individual performance along the K different training processes [DS17, Section 5.1.1]. In that manner, a good fit of the ANN model, a good performance, and a high generalisation of the model can be achieved [Ber12, Ber18]. Figure 2.3 shows a schematic of K-Fold cross-validation process.

2.2.2 Regularisation

Despite the power of ANNs, they have their own drawbacks. Related to the amount of data and generalisation of ANN structures, overfitting is considered one of the most important issues of the ANNs. It is committed when the ANN structure is memorising the input / output pairs of data rather than generalising. Hence, an overfitted model would present a perfect performance when dealing with measurements

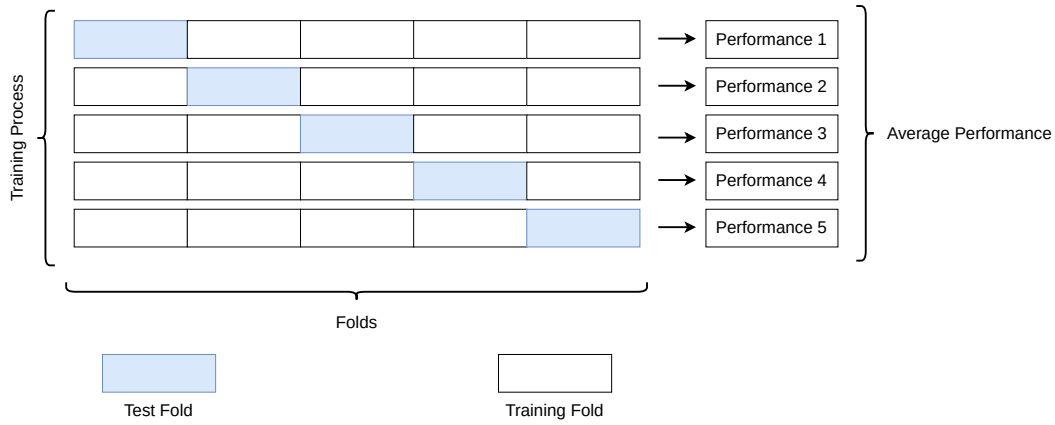

Figure 2.3: K-Fold process. Notice that the average of the different training processes (Performance 1 to 5) is considered as the overall ANN performance.

from the training dataset whereas it would behave very badly when facing measurements from the test dataset. For that reason, regularisation techniques must be applied to limit the memorisation capacities of the model. They avoid the specialisation of the model with respect some points of the dataset at the expense of learning only the intrinsic pattern of data. In other words, forcing the ANN to correctly generalise.

There exist different regularisation techniques such as penalties applied to the norm of certain parameters of the cost function, dataset augmentation, noise robustness, or the stop of the training process before committing overfitting [Goo16, Chapter 7]. Among all the regularisation techniques, this thesis mainly considers two: (i) the L2 Parameter regularisation, and (ii) the early stopping. L2 Parameter regularisation adds an extra penalty to the cost function driving the closest weights to the origin,

$$J_{reg}(\boldsymbol{\theta}) = J(\boldsymbol{\theta}) + \lambda\Omega(\boldsymbol{\theta}) = J(\boldsymbol{\theta}) + \frac{\lambda}{2}\left\|\boldsymbol{\theta}\right\|_2^2 . \tag{2.15}$$

where $\Omega(\boldsymbol{\theta})$ corresponds to the L2 regularisation parameter, λ to its regularisation value, and $J_{reg}(\boldsymbol{\theta})$ to the regularised cost function [Goo16, Section 7.1.1]. Hence, the memorisation of the input-output pairs of measurements will become a harder task and consequently, the appearance of overfitting avoided.

On the other hand, early stopping does not correspond to a regularisation technique as such. It is related to the training process since it does not directly affect the cost function. Instead, early stopping finishes the training process before overfitting is produced. This is performed when the ANN performance for the current epoch starts to drop when the validation dataset is considered whilst it is still improving for the training dataset. It is worth mentioning here that an epoch corresponds to a complete pass through the complete training dataset. One epoch may include several iterations depending on the training batch size. Thus, to properly apply this technique, a patience parameter must be given. It equals to the maximum number of epochs allowing a difference in the tendency between the validation and training performance.

2.2.3 Evaluation Metrics

Depending on the ANNs purpose, different evaluation metrics are defined. Classification oriented ANNs are generally evaluated by means of the F Score, the accuracy, the recall, and the precision metrics, among others [Che18]. These metrics show the classification performance of the given inputs and their predictions into different classes. Nevertheless, these metrics do not make sense in regression tasks. Regression metrics must measure the degree of difference between the forecasted values and the original ones. The closer the prediction with respect to the original value, the better the performance. For that reason, such a kind of metrics will be considered here since this thesis relies on regression-oriented ANNs. They consist in:

- **Root Mean Squared Error (RMSE)**: RMSE computes the similarity between predicted values and provided labels or original measurements. As an aggregated metric, it does not tell how large or small are the errors with respect to the original measurements. RMSE is computed as follows:

$$\text{RMSE} = \sqrt{\frac{1}{N_p}\sum_{i=1}^{N_p}\left(\mathbf{y}_i - \widehat{\mathbf{y}}_i\right)^2} \tag{2.16}$$

- **Mean Average Percentage Error (MAPE)**: MAPE is considered to give a sense of the error's magnitude. It computes the percentage of error committed with respect to the original value. Thus, complementing RMSE with MAPE values provides a vision of the magnitude of errors. MAPE is computed as:

$$\text{MAPE} = \frac{1}{N_p}\sum_{i=1}^{N_p}\left|\frac{\mathbf{y}_i - \widehat{\mathbf{y}}_i}{\mathbf{y_i}}\right| \tag{2.17}$$

- **Determination coefficient** $\left(R^2\right)$: R^2 is adopted to compute the ability of the ANN to follow the tendencies of the original measurements. The higher the R^2, the higher the correlation between the original and predicted measurements [Isl12]. This metric is computed as:

$$R^2 = 1 - \frac{\sum_{i=1}^{N_p}\left(\mathbf{y}_i - \widehat{\mathbf{y}}_i\right)^2}{\sum_{i=1}^{N_p}\left(\mathbf{y}_i - \bar{\mathbf{y}}\right)^2} \tag{2.18}$$

  where $\bar{\mathbf{y}}$ stands for the mean values of $\mathbf{y}$.

2.3 An overview of Transfer Learning

The main objective of Transfer Learning (TL) is to adopt the knowledge of an ANN properly trained in a source domain to later transfer it into a target domain. TL has been commonly used for designing and implementing image classifiers among others [Zhu21]. One clear example is shown in [Sar18, Chapter 6], where the Inception ANN, a general-purpose ANN-based image classifier, is adopted to develop a dog breed classifier. It is implemented considering the Inception classifier but, substituting its last layer by three new convolutional layers connected to the output of the penultimate one. Then, these layers are retrained in a fine-tuning process devoted to adapting the behaviour of the ANN to its ultimate purpose. Therefore, the dog breed classification performance will be derived from the Inception classification one and the fine-tuned structure [Sar18, Chapter 6]. This shows that TL techniques can be considered not only to obtain ANN models performing well in a source model, but also to speed up their designing process. The knowledge of the source model is shared with the target one [Sar18, Chapter 4].

TL techniques can be categorised into three classes as a function of the data availability in the source and target domains [Sar18, Chapter 4] [Cur21]:

- **Inductive Transfer Learning**: in inductive transfer learning, the source and target domains do not show data scarcity problems. Therefore, the transfer model can be designed and firstly trained in the source domain and then fine-tuned in the target domain in order to adapt its behaviour to its final application.
- **Transductive Transfer Learning**: Transductive transfer learning is characterised by the necessity of retraining the transferred model every time a new set of labelled data is available in the target domain. This is motivated by the fact that at the first moment, the target domain has no labelled data.
- **Unsupervised Transfer Learning**: Unsupervised transfer learning is characterised by the fact that there is no available data neither in the source domain, nor in the target one. Thus, this technique is mainly focused on solving unsupervised tasks like dimensionality reduction.

Chapter 3

An Overview of the Industrial Control of Wastewater Treatment Plants

This chapter provides the reader with an overview of the WWTP scenarios as well as their industrial control. First it introduces the WWTP scenarios on which this thesis is based on: the BSM1 and BSM2 frameworks whose main aim is to reproduce the behaviour of a general purpose WWTP. Then, it describes the BSM1 layout, its default PI control approach, its simulation protocol, and the considered evaluation criteria. Later, BSM2, the extension of BSM1 covering the sludge treatment, is presented. There, the description of the BSM2 layout, its default control strategies, its simulation protocol, and its evaluation criteria are provided. Finally, the current situation of the industrial control in the WWTP domain, especially in terms of the sensing and control approaches, is assessed.

3.1 Wastewater Treatment Plant Scenarios

Industrial scenarios have been characterised along the years by the highly complex and non-linear process they carried out, especially, since their automation. Most of these processes require operational conditions which must be maintained over the time. For instance, the temperature in the pasteurization processes or the angular speed of hard drive disks. In that sense, industrial control has arisen as one of the key actors achieving and managing these required conditions. Otherwise, the correct behaviour of the industrial scenario cannot be assured [Oga10, Chapter 1].

One of the critical scenarios where the industrial control is of utmost importance corresponds to the WWTP facilities. They are focused on treating the residual incoming urban waters and spilling a clean version of them into the receiving waters. They seek to reduce the amounts of Biochemical Oxygen Demand (BOD_5), Chemical Oxygen Demand (COD), the Total Suspended Solids (T_{SS}), and the phosphorus and nitrogen derived components such as the ammonium ($S_{NH,e}$) and the total nitrogen ($S_{Ntot,e}$) in the effluent. Levels which are not harmful for the aquatic ecosystems are sought. This is achieved by

means of performing highly complex and non-linear biochemical and biological processes whose main objective is to perform the nitrification and denitrification tasks [HS93, Yan95]. These have been modelled mathematically by the International Water Association (IWA) and collected in the Activated Sludge Models. The Activated Sludge Model No.1 (ASM1) depicts the processes performed to reduce the nitrogen derived pollutants. It has been extended by the Activated Sludge Model No.2 (ASM2), whose main aim is to describe not only the nitrogen pollutant reduction process, but also the phosphorus one. Moreover, ASM1 has been also updated with the Activated Sludge Model No.2d (ASM2d), which improves the denitrification process. Finally, the appearance of the next generation ASM models has motivated the development of the Activated Sludge Model No.3 (ASM3) [Hen00]. Besides, the IWA Task Group on Benchmarking of Control Strategies and the COST actions 682 and 624 proposed the adoption of the Benchmark Simulation Models, which have been widely adopted by the research community [Ger14]. The three most known are the BSM1, the Benchmark Simulation No.1 Long-Term (BSM1-LT) and the BSM2. Their main aim is to offer generality, easy comparison, and replicability of results. For that reason, these three benchmarks have become of high interest since most of the control structures to be deployed over a real WWTP scenario can be tested over them. This is crucial in those scenarios, like the WWTPs, where their productivity and processes cannot be neither uncontrolled nor stopped. In that sense, this thesis will consider two of these frameworks, the BSM1 and BSM2. The former is devoted to modelling the behaviour of a general purpose WWTP, however, it only contemplates the pollutant reduction process [Ger14, Section 3.1]. This is solved by means of BSM2, which in addition to the water line, implements the sludge processing [Ger14, Section 3.3].

3.1.1 Benchmark Simulation Model No.1

BSM1 models and replicates the behaviour of a general purpose WWTP devoted to reducing the nitrogen derived pollutant concentrations in the incoming residual urban waters [Cop02]. In order to offer generality, easy comparison, and replication of results, it implements its own layout with its default control approaches, simulation protocol, and evaluation criteria [Cop02].

Plant Layout

The WWTP plant considered by the BSM1 framework consists in a set of five biological tanks and a settler, all of them interconnected in series (see Figure 3.1). The tanks are modelled according to ASM1 and consequently, they are devoted to properly perform the nitrification and denitrification chemical and biochemical processes [HS93]. For that reason, the first two BSM1 tanks are anoxic, i.e., they work with a lack of oxygen. They are in charge of performing the denitrification process where the nitrate components of residual urban waters are transformed into nitrogen components. On the other hand, the three remaining tanks, are in charge of the nitrification process, where the ammonia (S_{NH}) concentrations are transformed into nitrates. Since this process needs oxygen to perform the chemical reactions, the three

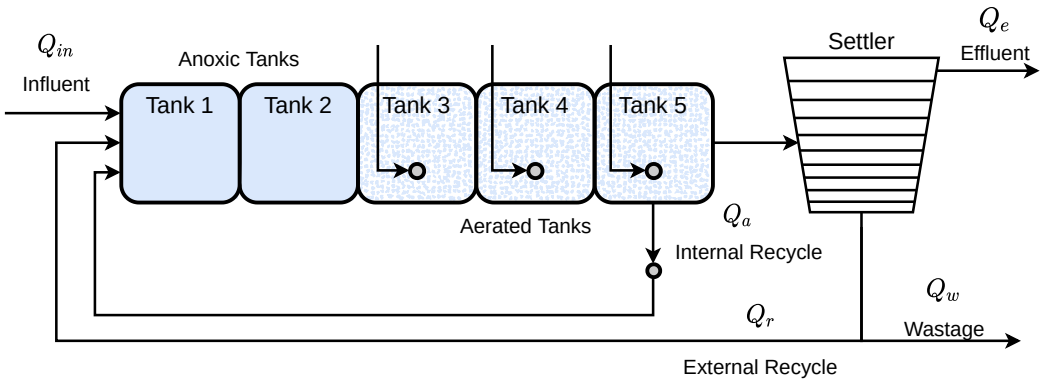

Figure 3.1: Benchmark Simulation Model No.1 layout.

last tanks of BSM1 are aerated [Cop02, Chapter 2].

In terms of their volume, each anoxic tank has a total volume of 1000 m^3 whereas each aerated one can process a volume of 1333 m^3. This entails that the biological reactors have a total capacity of 6000 m^3. This capacity is also shown by the settler which is modelled in ten different layers following the Takács model [Tak91]. The sixth layer starting from the bottom is the feed layer while the tenth layer is the one in charge of spilling the clarified water, i.e., the effluent flow rate (Q_e), into the receiving waters, usually rivers. The first layer, i.e., the one placed in the deepest part of the settler, is in charge of the wastage flow rate (Q_w), which equals to a flow rate of 385 $\mathrm{g/m}^3$. Besides, BSM1 considers two recycle flow rates: (i) the internal flow rate (Q_a), and (ii) the external recycle flow rate (Q_r). The internal flow goes from the last tank to the input of the WWTP. The external goes from the first layer of the settler to the input of the plant. The WWTP plant has been designed to manage an average influent flow rate (Q_{in}) of 18446 $\mathrm{m}^3/\mathrm{day}$ and an average Chemical Oxygen Demand (COD) of 300 $\mathrm{g/m}^3$.

Taking also into consideration the total volume of the BSM1 plant, 12000 m^3, one can compute the total retention time of the BSM1 model, which equals to 14.4h [Cop02, Section 2]. It defines the amount of time that water lasts inside the plant. These measurements entail that BSM1 models a medium scale WWTP with a population equivalent of approximately 58000 [Der20].

Default Control Approaches

BSM1 also implements its own default control approach which consists in two Proportional Integral controllers (PIs). Both PIs also consider the adoption of an anti-windup structure which avoids overshooting problems [Ale08]. They are focused on maintaining the dissolved oxygen concentration in the fifth tank ($S_{O,5}$) and the nitrate-nitrogen concentration in the second one ($S_{NO,2}$) at the set-points of 2 mg/L and 1 mg/L, respectively (see Figure 3.2).

The PI managing the $S_{O,5}$ modifies the oxygen transfer coefficient of the fifth tank ($K_{La,5}$) to modify the amount of oxygen in it. Physically, its actuation signal, $K_{La,5}(t)$, is related to the aperture of the

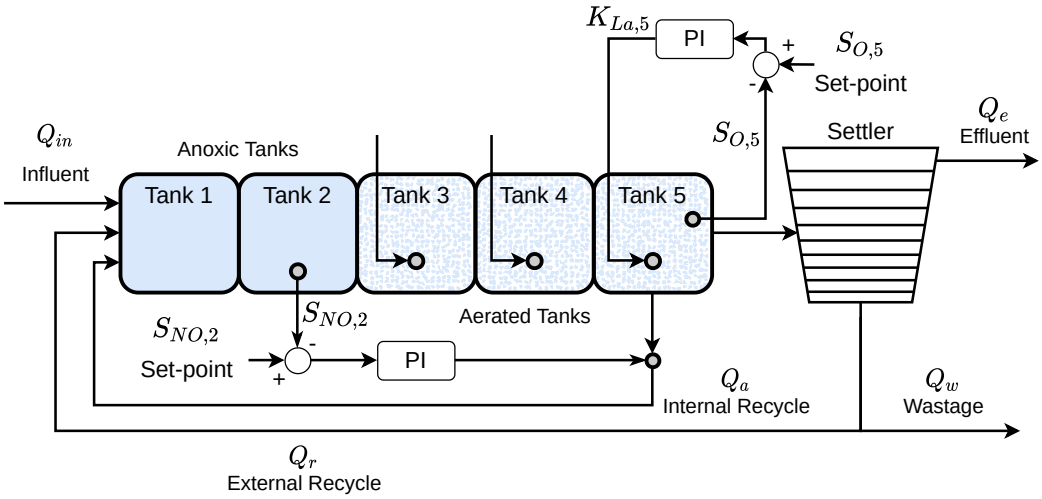

Figure 3.2: BSM1 default control strategy.

aeration valve of the fifth reactor tank. Hence, the larger the $K_{La,5}$, the higher the aeration of the tank. In that sense, $K_{La,5}(t)$ is computed by the PI according to the given set-point and the control signal, the measured $S_{O,5}(t)$. Thus, its value, when the anti-windup is not considered, is provided given the following expression:

$$K_{La,5}(s) = K_{S_{O,5}} \left[1 + \frac{1}{T_{i_{S_{O,5}}} \cdot s} \right] e_{S_{O,5}}(s) = 25 \left[1 + \frac{1}{1 \cdot 10^{-3} \cdot s} \right] e_{S_{O,5}}(s) \tag{3.1}$$

where $K_{S_{O,5}}$ corresponds to the gain of the PI controller, $T_{i_{S_{O,5}}}$ to its integral time and $e_{S_{O,5}}(s)$ to the error between the measured $S_{O,5}$ and its desired set-point. The default values of the PI parameters are: 25 and $1 \cdot 10^{-3}$ days for the $K_{S_{O,5}}$ and the $T_{i_{S_{O,5}}}$, respectively.

In terms of the $S_{NO,2}$ control loop, its PI manages the controlled signal, the $S_{NO,2}$ concentration, by means of manipulating the Q_a, its actuation signal. Therefore, it computes the aperture of the internal recycle flow rate as a function of the error between the measured $S_{NO,2}(t)$ and its set-point:

$$Q_a(s) = K_{Q_a} \left[1 + \frac{1}{T_{i_{Q_a}} \cdot s} \right] e_{S_{NO,2}}(s) = 10000 \left[1 + \frac{1}{0.0150 \cdot s} \right] e_{S_{NO,2}}(s) \tag{3.2}$$

where K_{Q_a} corresponds to the gain of the PI controller and $T_{i_{Q_a}}$ to its integral time. These parameters by default equal to 10000 and 0.0150 days, respectively. Besides, $e_{S_{NO,2}}$ equals to the error between the measured $S_{NO,2}$ and the given set-point, which usually equals to 1 mg/L.

Simulation Protocol

Since one of the BSM1 aims is to offer easy replication of results, it implements its own simulation protocol. Hence, new control strategies can be compared under the same circumstances following the

same criteria. To achieve this BSM1 considers two types of influent profiles: (i) a constant influent which shows the same concentrations along time, and (ii) three weather influents which vary according to the weather they are describing, all of them with a sampling interval of 15 minutes.

Before performing any analysis, the BSM1 model must be initialised to take the WWTP plant to its steady-state stage. This is performed by means of simulating a 100-day closed-loop configuration considering the constant influent profile without non-idealities in the measurements [Ale08, Section 3]. After this, the desired weather simulation can be carried out whenever it is precedented by a 14-day simulation of the dry-weather influent. In that sense, the dry, rainy, and stormy weathers are characterised by the rain and storm episodes they show:

- Dry weather: a 14-day influent profile showing neither rainy nor stormy episodes.

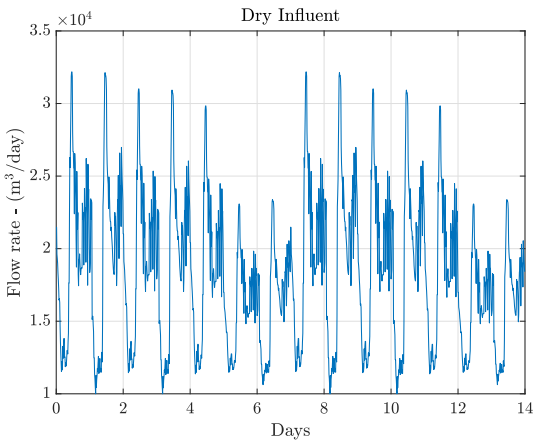

(a) Dry weather

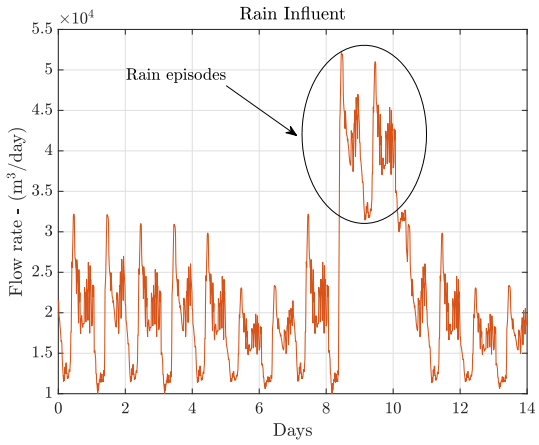

(b) Rainy weather

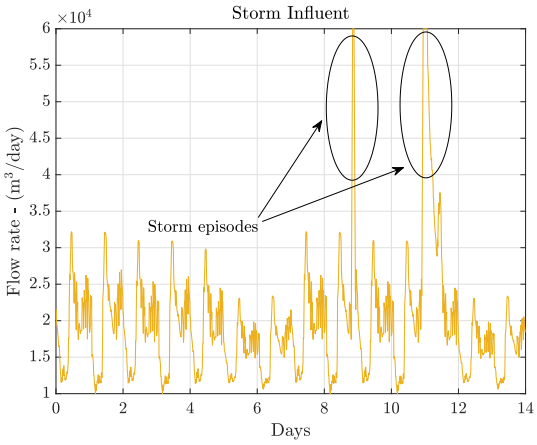

(c) Stormy weather

Figure 3.3: BSM1 weather influent profiles.

- Rainy weather profile: a 14-day influent profile showing two long rainy events from the 9th to the 10th day of the simulation (see Figure 3.3b).

- Stormy weather profile: a 14-day influent profile showing a heavy rain event at the 8th and 11th day of the simulation (see Figure 3.3c).

Since BSM1 also implements its own set of sensors, two types of simulations can be performed: (i) an ideal simulation, and (ii) a simulation where non-ideal sensors and actuators are considered. The former consists in the simulation of the BSM1 model when ideal sensors are adopted. The latter, instead, considers the non-idealities of the BSM1 sensors to perform a simulation where the WWTP performance reflects the noise and delay effects.

BSM1 sensors consider an Additive White Gaussian Noise (AWGN) model, i.e., a white zero mean and unit variance Gaussian noise. Moreover, each BSM1 sensor considers its own noise level, which is defined as the 2.5% of the maximum sensed value. Its objective is to multiply the unit variance of the AWGN distribution [Cop02, Section 7]. A and B_0 sensor classes are recommended for most of the concentration considered in the BSM1 management. They are characterised by their response time as well as by offering continuous measurements [Cop02, Table 11]. Class A sensors response time (t_r) equals to 1 minute while class B_0 sensors t_r equals to 10 minutes.

The effects introduced by sensors with non-idealities are defined by their respective transfer functions, $G_A(s)$ for the A class sensor and $G_{B_0}(s)$ for the B_0 class.

$$G_A(s) = \frac{1}{(1+\tau \cdot s)^2} \qquad G_{B_0}(s) = \frac{1}{(1+\tau \cdot s)^8} \tag{3.3}$$

where τ equals to the time constant of the transfer functions. Its value is set according to the sensor class: $t_r/3.89$ and $t_r/11.7724$ for the A and B_0 class, respectively [Cop02, Section 7].

BSM1 model will be considered in Chapters 5, 6 and 7. Among the 15 available measurements of the BSM1 model, only those which are related to the $S_{NO,2}$ and $S_{O,5}$ control strategies are considered. They correspond to the $S_{NO,2}$, the Q_a, the $K_{La,5}$, and the $S_{O,5}$. Besides, in Section 6.3, the dissolved oxygen ($S_{O,4}$), the nitrate nitrogen ($S_{NO,4}$), the ammonium ($S_{NH,4}$), the flow rate (Q_4), and the Total Suspended Solids ($T_{SS,4}$) at the fourth biological tank will be considered. The Total Suspended Solids concentration in the input ($T_{SS,in}$) is also taken into account. Among all these variables, it is noteworthy to mention that $K_{La,5}$ is not a concentration value. As it has been previously stated it corresponds to the actuation signal of the $S_{O,5}$ PI actuator which has a delay equal to four minutes. Table 3.1 shows the range of values that each sensor and actuator can measure as well as their class and delays.

Table 3.1: Parameters of the BSM1 sensors. Notice that the non-idealities of the different sensors are present in this table. Only those considered in this thesis are shown.

Measurement	Class of Sensor	Range of values	Introduced Delay
$K_{La,5}$	-	$0 - 360$ day^{-1}	4 minutes
Q_4	A	$0 - 100000$ m^3/day	1 minutes
Q_a	A	$0 - 100000$ m^3/day	1 minutes
$S_{NH,4}$	B_0	$0 - 20$ mg N/L	10 minutes
$S_{NO,2}$	B_0	$0 - 20$ mg N/L	10 minutes
$S_{NO,4}$	B_0	$0 - 20$ mg N/L	10 minutes
$S_{O,4}$	A	$0 - 10$ mg O/L	1 minute
$S_{O,5}$	A	$0 - 10$ mg O/L	1 minute
$T_{SS,4}$	A	$0 - 10000$ g SS/m^3	1 minute
$T_{SS,in}$	A	$0 - 1000$ g SS/m^3	1 minute

Evaluation Criteria

In order to offer easy comparison of results, BSM1 defines its own evaluation criteria. After performing the desired simulation, a set of measurements are obtained from the different sensors and actuators. These reflect the behaviour of the WWTP plant showing the effects not only of the biological and biochemical processes but also the effects of the control strategies. Only the measurements from the 7th day to the 14th day of the desired weather profile are considered in the evaluation criteria.

The BSM1 evaluation criteria consider two kind of evaluation metrics: (i) the loop level, and (ii) the plant operation metrics. The formers are devoted to assessing the control performance at the control loop level. This performance is measured by means of the Integral of the Absolute Error (IAE) and the Integral of the Squared Error (ISE) between the desired set-points and the concentrations measured in the WWTP plant.

$$\text{IAE} = \int_{t_{i_{BSM1}}}^{t_{f_{BSM1}}} |r_x(t) - y_x(t)|\, dt \tag{3.4}$$

$$\text{ISE} = \int_{t_{i_{BSM1}}}^{t_{f_{BSM1}}} (r_x(t) - y_x(t))^2\, dt \tag{3.5}$$

where $r_x(t)$ and $y_x(t)$ denote the given set-point and the measured value of the concentration for which IAE and ISE are being assessed. $t_{i_{BSM1}}$ and $t_{f_{BSM1}}$ stand for the initial and final day of the measurements considered in the BSM1 evaluation criteria, i.e., $t_{i_{BSM1}}$ = 7th day and $t_{f_{BSM1}}$ = 14th day. In that sense, IAE gives the same importance to all kind of errors whilst ISE penalises more the highest ones. Thereby, control performances showing low IAE and ISE values are desired.

On the other hand, the plant operation performance metrics aim is to measure how well are the control strategies performing. This performance is assessed in terms of the number of violations, the

Table 3.2: BSM1 concentration limits in the effluent.

Concentration	Limits
S_{Ntot}	18 g $\mathrm{N/m^3}$
COD	100 g $\mathrm{COD/m^3}$
S_{NH}	4 g $\mathrm{N/m^3}$
$T_{SS,e}$	30 g $\mathrm{SS/m^3}$
BOD_5	10 g $\mathrm{BOD/m^3}$

Effluent Quality Index (EQI) measured in Kg · pollution units · day^{-1} and the Overall Cost Index (OCI), which is dimensionless. Since WWTP industries are devoted to reducing the pollutant components of residual urban waters, some limits of pollutant concentrations in the effluent are established. For instance, regulations have been adopted by the European Union governments to assure that WWTPs are respecting the pollutant limits and therefore, they are not polluting the natural water resources [Eur91]. If they are exceeded, WWTPs will be prone to be sued. In fact, the violations of the effluents are given not only in terms of the number of violations, but also in terms of the percentage of time they are exceeded. The effluent concentrations that are measured consist in the total nitrogen in the effluent ($S_{Ntot,e}$), the COD, the $S_{NH,e}$, the $T_{SS,e}$ and the BOD_5. Notice that $S_{Ntot,e}$ is measured as the sum of S_{NO} and Kjeldahl nitrogen (NKj), which at the same time corresponds to the sum of organic nitrogen and S_{NH}. The limits that apply to these measurements are observed in Table 3.2.

Being related to the fines to be paid by WWTPs exceeding the effluent limits, EQI measures the global quality of the effluent. It is measured as the sum of the different compounds of the WWTP effluent averaged over a period of 7 days, from the 7th day to the 14th one.

$$\begin{aligned} EQI = \frac{1}{1000 \cdot T} \int_{t_{i_{BSM1}}}^{t_{f_{BSM1}}} & (B_{TSS} \cdot T_{SS}(t) + B_{COD} \cdot COD(t) + \\ & + B_{NKj} \cdot NKj(t) + B_{S_{NO}} \cdot S_{NO}(t) + B_{BOD_5} \cdot BOD_5(t)) \cdot Q_e(t) dt \end{aligned} \tag{3.6}$$

where B_{TSS}, B_{COD}, B_{NKj}, $B_{S_{NO}}$, and B_{BOD_5} are weighting factors. They are equal to 2, 1, 30, 10, and 2, respectively [Cop02, Section 6].

OCI measures the costs related to the operation of the WWTP. Thus, the lower the OCI, the lower the costs. It is computed as the sum of the different energy consumption and disposal generations.

$$OCI = AE + PE + 5 \cdot SP + 3 \cdot EC + ME \tag{3.7}$$

The energies and consumptions that intervene into the OCI are the Aeration Energy (AE) which is computed as

$$AE = \frac{S_O^{sat}}{T \cdot 1.8 \cdot 1000} \int_{t_{i_{BSM1}}}^{t_{f_{BSM1}}} \sum_{i=1}^{5} V_i \cdot K_{La,i}(t) dt, \tag{3.8}$$

where S_O^{sat} corresponds to the saturation concentration of the dissolved oxygen, which equals to 8 mg/L, and T to the observation time, which equals to 7 days for the case of BSM1. Then, V_i equals to the volume of the different biological tanks. The following two terms correspond to the Pumping Energy (PE) and the Sludge Production (SP). PE is related to the energy consumed by the pumps arranging the different tanks while SP is related to the quantity of sludge to be disposed. In BSM1 they are computed as

$$PE = \frac{1}{T} \int_{t_{i_{BSM1}}}^{t_{f_{BSM1}}} \left(0.004 \cdot Q_{in}(t) + 0.008 \cdot Q_a(t) + 0.05 \cdot Q_w(t)\right) dt. \tag{3.9}$$

and

$$\begin{aligned} SP = \frac{1}{T} \cdot \Bigg(& T_{SS,a}(t_{f_{BSM1}}) - T_{SS,a}(t_{i_{BSM1}}) + \\ & + T_{SS,s}(t_{f_{BSM1}}) - T_{SS,s}(t_{i_{BSM1}}) + \int_{t_{i_{BSM1}}}^{t_{f_{BSM1}}} T_{SS_w} \cdot Q_w \cdot dt \Bigg) \end{aligned} \tag{3.10}$$

where $T_{SS,a}$, $T_{SS,s}$ and $T_{SS,w}$ are the total suspended solids in the reactors, the settler, and the ones to be disposed, respectively. Finally, the consumption of the External Carbon (EC) and the Mixing Energy (ME) are also considered. EC defines the amount of external carbon added in the different tanks so as to ease the nitrification and denitrification processes. Thus, EC is computed as

$$EC = \frac{COD_{EC}}{T \cdot 1000} \int_{t_{i_{BSM1}}}^{t_{f_{BSM1}}} \left(\sum_{i=1}^{i=n} q_{EC,i} \right) dt \tag{3.11}$$

where $q_{EC,i}$ is the external carbon flow rate entering in the biological tanks. Finally, COD_{EC} corresponds to the concentration of the biodegradable substrate in the external carbon source. Its value equals to 400 g $\mathrm{COD/m^3}$. ME defines the energy consumed in the mixing process of the anoxic tanks to avoid settling. This energy is computed as a function of the tank volume as

$$ME = \frac{24}{T} \int_{t_{i_{BSM1}}}^{t_{f_{BSM1}}} \sum_{i=1}^{n=5} (0.005 \cdot V_i) \cdot dt \tag{3.12}$$

for those tanks whose K_{La} is lower than 20 days^{-1}. Otherwise, $ME = 0$.

3.1.2 Benchmark Simulation Model No.2

BSM2 framework consists in an extension of the BSM1 model. Not only does it model the biological treatment of the wastewater, but also the sludge processing. BSM2 also implements its own layout with its default control approaches, a simulation protocol, and the evaluation criteria to offer generality, easy comparison, and replication of results [Ger14, Section 3.3].

Plant Layout

BSM2 implements two different lines, the water, and the sludge treatment one. The former is in charge of the biological and biochemical treatment of the wastewater, and it is governed by the ASM1 model while the latter is in charge of performing the sludge treatment. Figure 3.4 depicts the BSM2 model. Notice that its water line is equivalent to the BSM1 model (see Subsection 3.1.1). Hence, its layout is the same as in BSM1 despite some differences in the volumes.

The water line consists in five interconnected biological reactor tanks and two clarifiers, the primary and the secondary. The primary clarifier has a total volume of 900 m^3 with an underflow of 147.6 $\mathrm{m}^3/\mathrm{day}$. Its overflow rate ($Q_{po}$) is the flow rate feeding the biological reactor tanks. Each anoxic tank now has a volume of 1500 m^3 while each aerated tank has a volume of 3000 m^3. This entails that the biological reactors have a total volume of 12000 m^3, the double with respect to the standard BSM1.

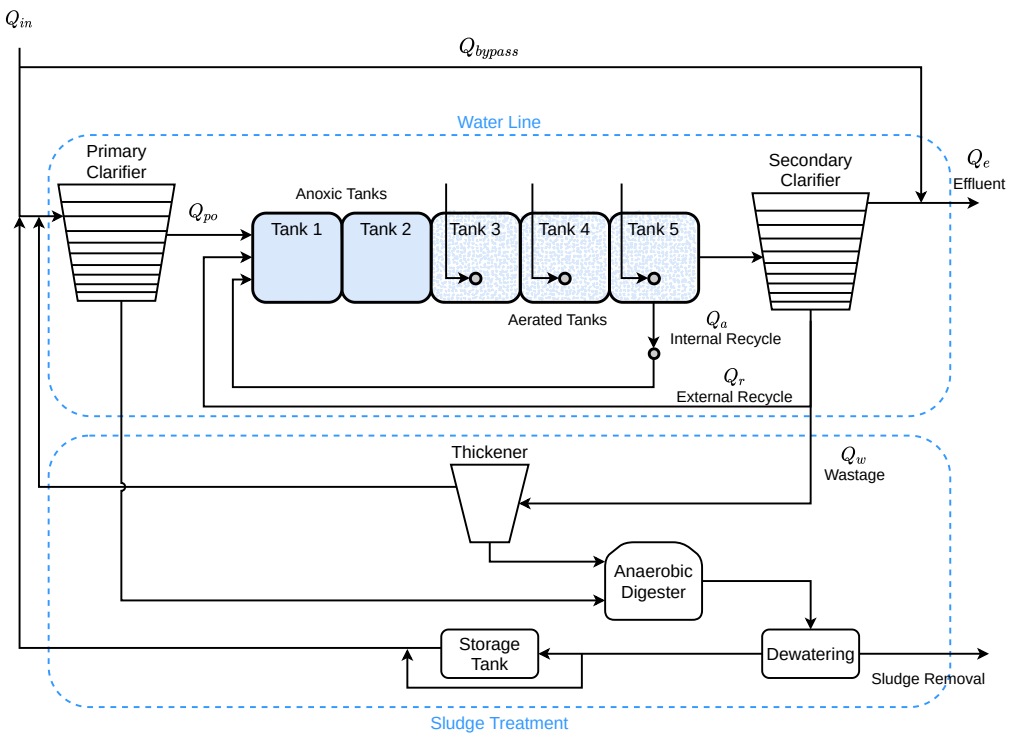

Figure 3.4: Benchmark Simulation Model No.2 layout.

The secondary clarifier has a total volume of 6000 m^3 and its feeding point is placed in the same point as the BSM1 one, i.e., in the sixth layer from the bottom [Ger14, Section 3.3]. BSM2 water line also includes two recirculation flows, the Q_a and the Q_r, which equal to 61944 $\mathrm{m}^3/\mathrm{day}$ and 20648 $\mathrm{m}^3/\mathrm{day}$, respectively. Considering an average influent flow rate of 20648.36 $\mathrm{m}^3/\mathrm{day}$ and an average COD in the influent of 592.53 mg/L, BSM2 water line has an average hydraulic retention time of 14 hours. All this yields to a population equivalent of 80000 [Saa14]. It also implements a bypass flow rate (Q_{bypass}) which directly spills the incoming wastewater in the receiving waters when the WWTP is full of capacity.

The sludge treatment line is the new add-on that BSM2 provides. It is in charge of the management and processing of the sludge disposals coming from the two clarifiers of the water line. The sludge treatment line is composed of the thickener, the anaerobic digester, the dewatering, and storage tank modules. The thickener and dewatering modules have no volume since they consist in ideal point separators. The thickener underflow equals to 30.9 $\mathrm{m}^3/\mathrm{day}$. The dewatering module generates a concentrated sludge flow rate of 9.6 $\mathrm{m}^3/\mathrm{day}$ and a sludge removal flow rate of 168.9 $\mathrm{m}^3/\mathrm{day}$. The anaerobic digester volume is split into two volume compartments, the liquid one with a volume of 3400 m^3, and a gaseous one with a volume of 300 m^3. Finally, the storage tank, whose aim is to store the rejected water to later feed the primary clarifier again, has a total volume of 160 m^3. When it is full, the rejected water is directly bypassed to the primary clarifier until the storage tank is emptied.

Default Control Approaches

As for the BSM1, the default control consist of a PI with anti-windup strategy, BSM2 default control approach aims to determine the K_{La} for each aerated tank. The main idea is to maintain the $S_{O,4}$ at the given set-point of 2 mg/L, but instead of managing only the $K_{La,4}$, the default control structure computes $K_{La,3}$, $K_{La,4}$, and $K_{La,5}$ (see Figure 3.5). BSM2 default control strategy also considers the constant addition of external carbon in the first anoxic tank at a flow rate of Q_{EC} 2 $\mathrm{m}^3/\mathrm{day}$. This is performed to ease the nitrification and denitrification processes involved in the pollutant reduction tasks. The default control strategy also considers two different Q_w, which are equal to: (i) 300 $\mathrm{m}^3/\mathrm{day}$ between days 0 and 182 and between days 364 and 546, while it equals to (ii) 450 for the rest days of a 609-day simulation [HS93, Ger14]. Taking all of this into account, $K_{La,4}$ is computed as follows when anti-windup is not considered:

$$K_{La,4}(s) = K_{S_{O,4}} \left[1 + \frac{1}{T_{i_{S_{O,4}}} \cdot s} \right] e_{S_{O,4}}(s) = 25 \left[1 + \frac{1}{1 \cdot 10^{-3} \cdot s} \right] e_{S_{O,4}}(s) \tag{3.13}$$

where $K_{S_{O,4}}$ corresponds to the gain of the PI controller, $T_{i_{S_{O,4}}}$ to its integral time and $e_{S_{O,4}}(s)$ to the error between the measured $S_{O,4}$ and its desired set-point. $K_{S_{O,4}}$ and $T_{i_{S_{O,4}}}$ equal to 25 and $1 \cdot 10^{-3}$ days^{-1}.

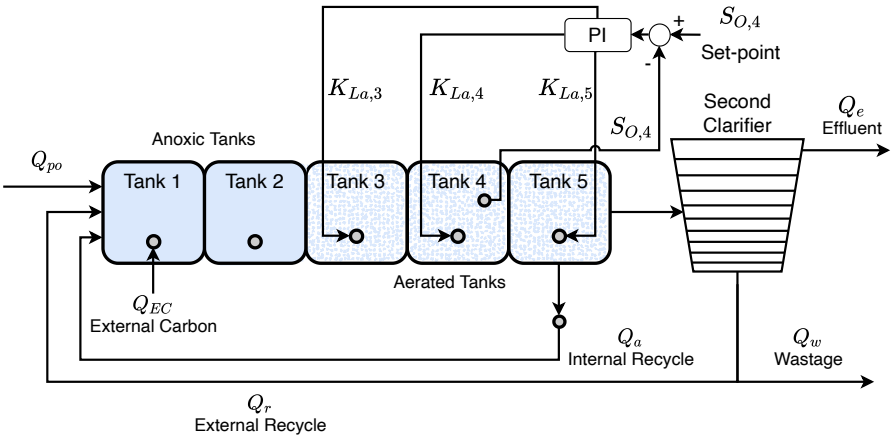

Figure 3.5: BSM2 default control strategy.

Then $K_{La,3}$ and $K_{La,5}$ are determined as:

$$K_{La,3}(s) = K_{La,4}(s) \qquad K_{La,5}(s) = 0.5 \cdot K_{La,4}(s) \tag{3.14}$$

Notwithstanding, BSM2 introduces a new control strategy which departs from the default structure. This new control strategy presents a hierarchical cascade control whose main aim is to compute again the $K_{La,3}$, $K_{La,4}$ and the $K_{La,5}$ (see Figure 3.6). The novelty is in the management of $K_{La,5}$ which is computed by means of a cascade structure overseeing the $S_{O,5}$. This structure considers two PI controllers devoted to maintaining the $S_{NH,5}$ at a given set-point of 1.5 mg/L modifying the $S_{O,5}$ set-point and therefore, the $K_{La,5}$ [Nop10]. The $S_{O,4}$ is managed by a third PI controller devoted to maintaining this concentration at a fix value of 2 mg/L. Moreover, the external carbon source considered in the first tank now equals to 1 $\mathrm{m}^3/\mathrm{day}$.

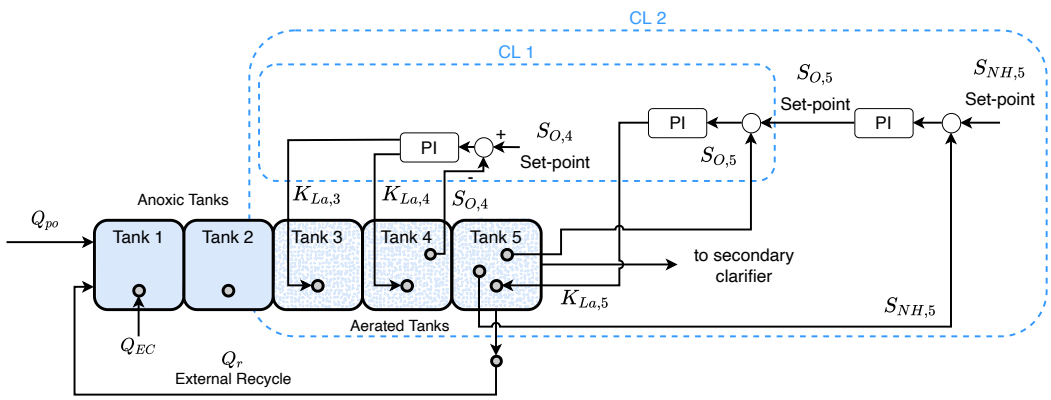

Figure 3.6: BSM2 cascade control strategy.

Simulation Protocol

BSM2 simulation protocol considers only a single profile showing the influent dynamics of a general purpose WWTP along 609 days. Although being a single file, the weather variations, such as rain and storm episodes as well as temperature changes in the WWTP environment, are still present in the influent profile. In that sense, the BSM2 simulation protocol establishes that the framework must be previously initialised by means of simulating at least a 200-day period of stabilisation in a closed-loop configuration. In this initialisation process constant values (see Table 7.4 in [Ger14, Section 7]) without noise in the measurements are considered. Then, the 609-day simulation can be carried out where only the last 364 days, one year, will be considered for evaluation purposes.

As in the BSM1 case, BSM2 framework also provides two types of simulations: (i) neglecting the effects of noise and non-idealities of the sensors, and (ii) considering their effects in the whole BSM2 performance. BSM2 considers the same sensors as BSM1 framework, i.e., the A and B_0 class of sensors. In this work, BSM2 is only considered in Chapter 4, and among all the BSM2 available measurements, only Q_{po}, the ammonium in the primary clarifier output ($S_{NH,po}$), the Q_a, the environmental temperature (T_{as}), the $S_{Ntot,e}$, and $S_{NH,e}$ in the effluent are considered. Table 3.3 depicts the values and classes of the BSM2 sensors considered in Chapter 4 of the thesis.

Evaluation Criteria

BSM2 performance is assessed from two different points of view: (i) the loop level performance evaluation, and (ii) the plant operation evaluation. As it is done in BSM1, the loop level performance is evaluated by means of the IAE and ISE. However, they are evaluated considering only the last 364 days of a 609-day simulation. In terms of the plant operation performance, BSM2 considers the same metrics as BSM1, i.e., the number and percentage of time that effluent limits are violated, the EQI, and the OCI.

Table 3.3: Parameters of the BSM2 sensors. Notice that the non-idealities of the different sensors are present in this table. Only those considered in this thesis are shown.

Measurement	Class of Sensor	Range of values	Introduced Delay
$K_{La,3}$	-	$0 - 360$ day^{-1}	4 minutes
$K_{La,4}$	-	$0 - 360$ day^{-1}	4 minutes
$K_{La,5}$	-	$0 - 360$ day^{-1}	4 minutes
Q_{po}	A	$0 - 100000$ m^3/day	1 minute
Q_a	A	$0 - 100000$ m^3/day	1 minute
$S_{NH,e}$	B_0	$0 - 20$ mg N/L	10 minutes
$S_{NH,po}$	B_0	$0 - 20$ mg N/L	10 minutes
$S_{NH,5}$	B_0	$0 - 20$ mg N/L	10 minutes
$S_{O,4}$	A	$0 - 10$ mg O/L	1 minute
$S_{O,5}$	A	$0 - 10$ mg O/L	1 minute
T_{as}	A	$5 - 25\ ^\circ C$	1 minute

Effluent limits are established for the $S_{Ntot,e}$, the COD, the $S_{NH,e}$, the $T_{SS,e}$ and the BOD_5. Their limits are depicted in Table 3.2.

EQI is adopted to determine the effluent quality of the BSM2 plant. As an effluent quality metric, the lower the index the higher the quality. In the case of BSM2, EQI is averaged along the last 364 days of the simulation, from $t_{i_{BSM2}} = 245th$ day to $t_{f_{BSM2}} = 609th$ day.

$$\begin{aligned} EQI = \frac{1}{1000 \cdot T} \int_{t_{i_{BSM2}}}^{t_{f_{BSM2}}} (B_{TSS} \cdot T_{SS}(t) + B_{COD} \cdot COD(t) + \\ + B_{NKj} \cdot NKj(t) + B_{S_{NO}} \cdot S_{NO}(t) + B_{BOD_5} \cdot BOD_5(t)) \cdot Q_e(t) dt \end{aligned} \tag{3.15}$$

where B_{TSS}, B_{COD}, B_{NKj}, $B_{S_{NO}}$, and B_{BOD_5} are weighting factors. They are equal to 2, 1, 30, 10, and 2, respectively. T here equals to 364 days [Cop02, Section 6].

OCI determines the costs related to the WWTP operation. It is calculated as the sum of the different consumed energies adding the methane production observed in the anaerobic digester and the heating energy of the BSM2 framework.

$$OCI = AE + PE + 3 \cdot SP + 3 \cdot EC + ME - 6 \cdot MET_{prod} + HE_{net} \tag{3.16}$$

where MET_{prod} is defined as the methane production of the anaerobic digester and HE_{net} as the heating energy. MET_{prod} is an economical benefit of the WWTP, for that reason it is considered as a negative value in the computation of OCI [Ger14, Section 6.3.2]. However, HE_{net} is defined as the energy required to heat the anaerobic digester as well as the heat obtained in the biogas generation of electricity [Ger14, Section 6].

AE is computed as:

$$AE = \frac{S_O^{sat}}{T \cdot 1.8 \cdot 1000} \int_{t_{i_{BSM2}}}^{t_{f_{BSM2}}} \sum_{i=1}^{5} V_i \cdot K_{La,i}(t) dt, \tag{3.17}$$

where S_O^{sat} is the saturation level of the dissolved oxygen and V_i the volume of the i-th reactor tank. Then, PE corresponds to:

$$\begin{aligned} PE = \frac{1}{T} \int_{t_{i_{BSM2}}}^{t_{f_{BSM2}}} (0.004 \cdot Q_{in}(t) + 0.008 \cdot Q_a(t) + 0.05 \cdot Q_w(t) + \\ + 0.075 \cdot Q_{pu}(t) + 0.06 \cdot Q_{tu}(t) + 0.004 \cdot Q_{do}(t))\, dt. \end{aligned} \tag{3.18}$$

where $Q_{pu}(t)$, $Q_{tu}(t)$, and $Q_{do}(t)$ are defined as the primary clarifier underflow, the thickener underflow, and the dewatering unit overflow, respectively.

Then, SP is computed as follows:

$$SP = \frac{1}{T} \cdot (T_{SS,a}(t_{f_{BSM2}}) - T_{SS,a}(t_{i_{BSM2}}) +$$

$$+ T_{SS,s}(t_{f_{BSM2}}) - T_{SS,s}(t_{i_{BSM2}}) + \tag{3.19}$$

$$+ 0.75 \cdot \int_{t_{i_{BSM2}}}^{t_{f_{BSM2}}} T_{SS_w} \cdot Q_w \cdot dt).$$

The consumption of EC and ME are computed as

$$EC = \frac{COD_{EC}}{T \cdot 1000} \int_{t_{i_{BSM2}}}^{t_{f_{BSM2}}} \left(\sum_{i=1}^{i=n} q_{EC,i} \right) dt \tag{3.20}$$

and

$$ME = \frac{24}{T} \int_{t_{i_{BSM2}}}^{t_{f_{BSM2}}} \sum_{i=1}^{n=5} (0.005 \cdot V_i) \cdot dt \tag{3.21}$$

for those tanks whose K_{La} is lower than 20 days^{-1} and 0 for those where K_{La} is equal to or higher than 20 days^{-1}.

3.2 Sensing Approaches

This section provides an insight of the current tendencies in sensing approaches applied in industrial domains. An overview of their main issues and the proposed techniques to tackle them will be assessed in the following lines.

Industrial control cannot be conceived without measurements or signals providing information about the industrial process being managed. Generally, these measurements and signals are obtained by means of conventional sensors such as the ones shown in Sections 3.1.1 and 3.1.2. Most of the time they are affected by noise and delays added by the same sensors. As a consequence, the control performance is degraded and therefore, the overall industrial performance compromised. Moreover, the adoption of sensors can become costly not only in the sense of expenses, but also in calibration processes. Another important point of industrial processes is related to the fact that their values can be unmeasurable. In other cases, the desired measurements are related to industrial processes which do not yield values in an online manner. Thus, they are only accessible after performing certain analyses [Ran13].

All these facts have motivated the adoption of soft-sensors as an option to: (i) infer measurements of unmeasurable processes, (ii) obtain offline measurements as though they are online, or (iii) to become a low-cost alternative to expensive hardware. This is achieved by means of predicting the measurements provided that soft-sensors use mathematical algorithms that approximates their behaviour towards real sensors [For05]. In such a context, the incursion of the Industry 4.0 paradigm is promoting the development of data-based approaches able to help in the management of industrial scenarios [Ust17, Section 1.2]. This is the case of the ANN-based soft-sensors, which have the particularity that they only require input and output measurements of the process for which they are designed [Yua18]. Their use is not new, for instance, ANNs had been designed to implement soft-sensors predicting the solar irradiance [Mel10, Bou18], the wind speed, and wind powers [Chi15, JL16, Cha17]. Their range of usage is even wider. ANN-based soft-sensors have been considered for different purposes: (i) detecting malfunctioning, anomalies or rare events [Che18, Coo19, The18], (ii) support the design of predictive control systems [Hua15], and (iii) predict and model certain components of the industrial environments [Lóp17].

The utmost interesting point of soft-sensors is related to its economical part. Their adoption as low-cost alternatives make the soft-sensors a suitable sensing approach. High benefits can be obtained, especially from those industries not making a profit from their final products. For that reason, they have been recently considered in scenarios such as WWTP environments. Most of their concentrations cannot be measured on-line. Instead, they are obtained from expensive and time-dependant laboratory analyses.

In such a context, ANN-based soft-sensors make the point since they can predict offline measurements as though they were on-line by means of properly designing and training the ANNs [Tor15]. For instance, in [Can16], MLPs have been considered to obtain on-line predictions of offline and hard-to-measure WWTP concentrations such as COD, T_{SS} and S_{Ntot}. These are predicted from on-line and easy-to-measure secondary variables such as the S_O, the water alkalinity, the S_{NH} and S_{NO}, among others. The MLP implementing the soft-sensor considers 70 input neurons, two hidden layers with 25 and 15 hidden neurons each and 3 outputs (see Figure 3.7). In [Han16], RNN have been considered to predict the WWTP sludge volume index. Related to the sludge bulking, i.e., the decrement of activated sludge, the sludge volume index has a deep impact on the performance of ASM. The main point is that kinetics describing the effects of the sludge bulking are difficult to model. Thus, RNNs are in charge of performing this task easing the prediction of the index. Other examples where ANNs are proposed to predict WWTP concentrations can be observed in [Ou15, Giw16, Hed16, Con18]. The common point between them is that an ANN-based soft-sensor can be easily obtained whenever measurements of the environment are available. They will be adopted to determine the ANN-based soft-sensor structure, which at the end corresponds to an algorithm easily generating hard-to-measure concentrations.

Related to WWTP scenarios, sewer systems are exploiting the power of ANN-based soft-sensors. They are crucial for WWTP industries since the objective of a sewer system is to collect the urban residual waters and transport them to the WWTP. This process is performed without too many complications since the sewer systems are designed considering the population of the city where they are implemented.

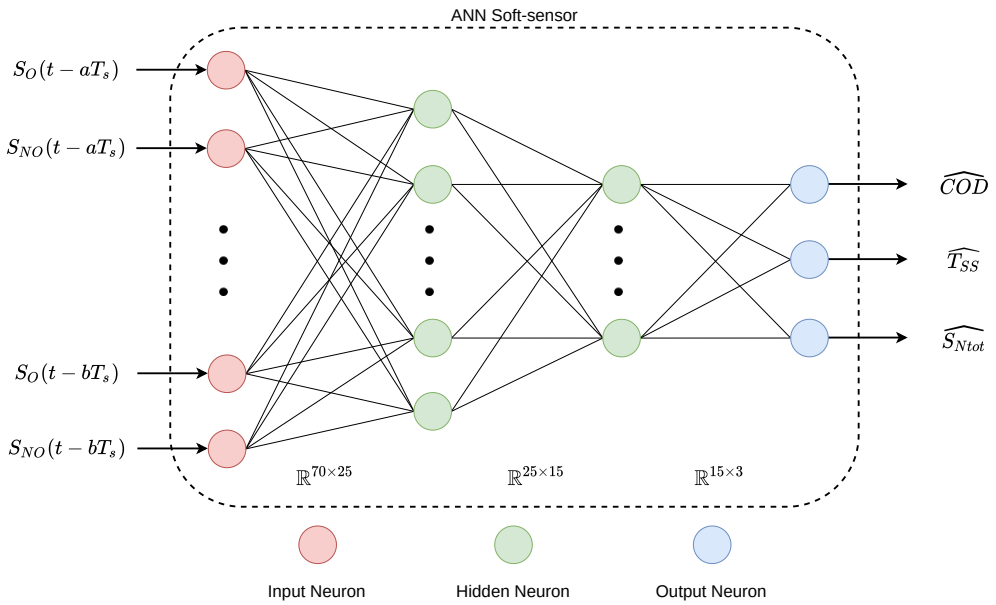

Figure 3.7: ANN-based soft-sensor proposed by Fernandez *et.al* in [Can16]. Notice that aT_s and bT_s represent different time lags of the input measurements.

Notwithstanding, several issues arise when extreme rainy and stormy events are produced. The amount of residual waters being transported by the sewerage increases in a sudden. This can entail the overflow of the sewer systems or even the bypass of untreated residual waters at the WWTP facilities.

ANN-based soft-sensors have arisen as a solution tackling these issues and therefore, avoiding the flooding derived problems. For instance, in [Zha18a], LSTM cells have been considered to model the hydraulic behaviour of sewer systems in Drammen, Norway. The sewerage feeds two WWTP plants of different dimensions, whose maximum flows equal to 1200 m^3/h and 4000 m^3/h, respectively. The smallest WWTP influent rate is forecasted by LSTMs. When its full capacity is predicted, the sewerage catchments are managed to share the residual waters and therefore, equally distribute the amount of residual waters entering in the WWTPs. Later, in [Zha18b], authors compare the behaviour of three ANN-based soft-sensors predicting the water level of a combined sewer overflow. Results have shown that LSTMs are the structure performing better. This is due to the LSTM modelling capacity of systems showing a strong temporal correlation [Gre17]. Finally, in [Zha18c], Zhang *et.al* implement the proposed LSTM-based soft-sensor in Drammen sewerage system to manage its flow rates and water levels. When a heavy rainfall is forecasted by the LSTM nets, the sewerage controller acts to share the water among all the pipes and therefore, avoid the WWTP overflow.

Nonetheless, soft-sensors have their own drawbacks, especially those based on ANNs. Industrial measurements are required to train the ANNs forming the soft-sensors. These measurements are obtained from industrial sensors providing continuous data flows in the form of time-series. The problem resides in the fact that industrial measurements, or even better said industrial time-series, are prone to show rare events. Such events are not likely to occur, however, highly valuable information can be obtained from

them. This low probability of occurrence entails that industrial time-series are generally unbalanced: certain ranges of values are overrepresented whereas others are sometimes unnoticeable [Río15].

This could be a critical issue whenever these measurements were considered as such to derive an ANN-based soft-sensor. Badly trained soft-sensors can lead to an undesired behaviour and prediction. Moreover, this is of utmost importance for soft-sensors acting over critical systems such as sewer and WWTP scenarios. This issue has been tackled in classification tasks by means of different data-preprocessing techniques such as subsampling and oversampling [Río15]. The former subsamples the dataset to equally represent the overrepresented and underrepresented data [Bud18]. The latter generates new synthetic data to achieve this equilibrium [He08]. Combinations of both techniques are proposed in the Synthetic Minority Over-sampling Technique (SMOTE) [Cha02]. It generates new synthetic data of the minor represented class. SMOTE considers an example, x_{minor}, of the minority class. Among the minority values, it adopts the k nearest samples in terms of the euclidean distance. Then, one example is randomly chosen, x_{rand}. Considering x_{minor} and x_{rand}, a new synthetic measurement is generated as $x_{new} = x_{minor} + \lambda \left[x_{rand} - x_{minor}\right]$, where λ is a random scalar between 0 and 1.

Nevertheless, these techniques cannot be adopted in regression tasks since they break the time-correlation among measurements. Some efforts have been performed to adapt these resampling techniques for regression purposes [Tor13, Tor15, NV17, Mun18]. However, due to the loss of the time-correlations, resampling techniques are not suitable for industrial measurements. Although this has been addressed in [Mon17], their solution is still not valid. They classify the measurements into bins subsampling the lowest representative. However, in the first classification the time-correlation is lost. Since this issue is of utmost importance, new approaches should be carried out to cope with it.

Another important issue related to ANN-based soft-sensors corresponds to the data scarcity problems shown by some industrial environments. If data is not available, the ANN implementing the soft-sensors cannot be properly trained. Nevertheless, TL techniques have arisen as a solution tackling this issue. In the industrial domain, TL techniques have been considered to alleviate problems observed in the design of soft-sensors, especially the data scarcity ones. For instance, in [Cur21], TL techniques are considered to implement an ANN-based soft-sensor which will be applied over a scenario showing severe data scarcity issues. To tackle them, the ANN-based structure will be trained in a scenario with enough measurements available and then transferred into the target domain.

As a summary, the adoption of ANN-based soft-sensors is experiencing a huge increase, especially in the industrial control domain. However, their usage in critical scenarios such as WWTP environments as well as the development of techniques to solve unbalanced data and data scarcity issues are still in its youth. For that reason, the adoption of ANN-based soft-sensors, and especially, the ones based on LSTM cells, must be widely explored. Regarding the data equilibrium and data scarcity issues, techniques dealing with the time-correlation of industrial measurement are to be proposed and assessed.

3.3 WWTP Control Approaches

WWTPs consist in critical industrial scenarios performing highly complex and non-linear pollutant reduction processes [LT16]. When they are not correctly performed, the amount of pollutant concentrations being spilled into natural water resources can be larger than allowed. This produces a harsh environment for the aquatic live and therefore, an environmental issue. It is here where the industrial control structures make the point. Not only are they considered to enable the correct behaviour of the nitrification and denitrification process but to avoid the exceed of pollutant limits. Thus, industrial control structures have been considered to fulfil a twofold objective:

- Maintain the required conditions for the nitrification and denitrification processes along time.
- Avoid the violation of pollutant limits in the WWTP effluent.

Traditionally, these structures consisted in conventional controllers, such as PI, MPC and FL. Generally, they are designed studying and analysing the systems to be controlled and then tuning the controller which fits best. Nevertheless, the appearance of ANNs is changing the industrial control paradigm. Their adoption is experiencing a huge growth. Moreover, their good performance in modelling non-linear and highly complex systems is paving the way to develop intelligent controllers. They only require input and output measurements of the process under control. For that reason, this section is devoted to providing the reader with a clear overview of the most common control structures in WWTP industries. Besides, an assessment of conventional controllers and their ANN-based supported versions is performed here.

3.3.1 PI Controllers

PI based control structures have been considered in WWTPs to assure the correct behaviour of the nitrification and denitrification processes and therefore, reduce the pollutant concentrations of the incoming waters [Ale08,Ger14,Nop10,FA09,FA11,Bar18]. In most of the cases, PIs are in charge of activating and deactivating the aeration pumps and recirculation flows of the WWTPs water line (see Figure 3.4). Prior to consider the PIs, their parameters have to be tuned, i.e., the integral time T_{PI} and the gain K_{PI}. For that purpose, the process under control needs to be approximated by either a first order system, a second order system, or state-space models [Oga10, Section 2.2]. These approximations relate the outputs of the process under control to its inputs. Therefore, it corresponds to a linear model telling how the outputs of the plant will be with respect to the actuation value of the PI structure.

Some examples of PI based structures being applied in WWTP scenarios are available in the literature. The basic one corresponds to the BSM1 default PI controller. As it has been stated in Section 3.1.1, it consists in two PIs devoted to maintaining the $S_{O,5}$ at a given set-point of 2 mg/L and the $S_{NO,2}$ at a given set-point of 1 mg/L.

Although BSM1 framework is managed by PIs, its control performance can be still improved. Being equal to 1.2813 days, $S_{Ntot,e}$ violations represent an 18.3036% of the BSM1 simulation time, i.e., 7 days. In terms of the $S_{NH,e}$, it is violated during 17.1131% of this time. From the environmental point of view, EQI and OCI equal to 6123.0182 Kg · pollutant units · day^{-1} and 16382.4027, respectively [Ale08, Appendix 3]. These results clearly show that the control actuation needs some modifications if the reduction of violations is desired.

With the extension proposed in the BSM2 framework, the default PI based structure consists in a unique PI. It is in charge of managing the $S_{O,4}$ by means of modifying $K_{La,3}$, $K_{La,4}$ and $K_{La,5}$ at the same time (see Figure 3.5). Results show that although improving the control performance with respect to BSM1, the number of violations increase at expense of reducing their duration. While in BSM1 there exist only 7 $S_{Ntot,e}$ violations, in BSM2 there are 32. However, they only represent violations during a 1.1819% of the BSM2 simulation time, i.e., during 4.3021 days. These numbers are reduced until 1.4896 days out of 364 and a 0.40923% of the simulation time when violations of $S_{NH,e}$ are assessed. BSM2 EQI and OCI values are equal to 5572.8572 Kg · pollutant units · day^{-1} and 9450.0324, respectively. As it is observed, the environmental metrics have been highly improved due to the new control strategy.

Seeking a higher improvement of the BSM2 control performance, Nopens *et.al* proposed the development of a hierarchical PI structure which manages the three aerated tanks accordingly to the set-point determined by an upper PI in charge of the $S_{NH,5}$ concentration [Nop10]. In doing so, this cascade control configuration aims to reduce the amount of $S_{NH,e}$ being spilled in the receiving waters. Results show that over 364 days, the $S_{NH,e}$ is only violated 0.8372 days, which means that the percentage of time S_{NH} is violated is reduced by an 80.54% with respect to the default BSM2 PI controller. This is also observed in terms of EQI and OCI metrics which are now equal to 5274 Kg · pollutant units · day^{-1} and 8052, respectively.

One actuation that is usually performed to decrease even more the number of violations, especially the $S_{Ntot,e}$ ones, corresponds to the addition of external carbon in the anoxic tanks [FA09]. Flores-Alsina *et.al* analyse these effects in one of the PI based structures shown in [FA09]. Authors proposed the application of two PIs in cascade to manage the $S_{O,4}$ and $S_{NH,5}$, and a PI to manage the addition of external carbon in the second biological reactor. As a result, at expense of increasing the violations of $S_{NH,e}$, the percentage of time that $S_{Ntot,e}$ is violated is reduced until a 0.8% of the BSM2 simulation time. Besides, authors proposed in [FA11] the addition of the emission of green-house gases in the computation of the control and environmental performance. Results show that $S_{Ntot,e}$ and $S_{NH,e}$ violations increased from 0.8% and 3.36% to 1.35% and 5.40%, respectively. EQI and OCI also show this increment: EQI is increased from 5376.1 to 5995 Kg · pollutant units · day^{-1} while OCI changed from 11346 to 13580, respectively.

As it is observed, violations of S_{NH} and S_{Ntot} have been reduced in most of the cases with respect to the BSM2 default PI structure. Nevertheless, they are still produced. By means of proposing more complex PI structures, Rojas *et.al* were able to achieve the total reduction of $S_{Ntot,e}$ violations at expense

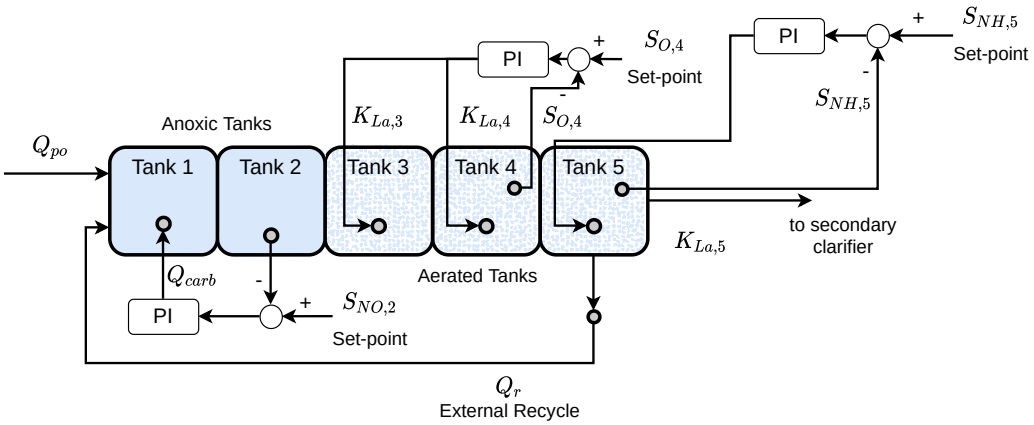

Figure 3.8: PI based control structure proposed by Barbu *et.al*. Notice that Q_{carb} denotes the external carbon source added in the first anoxic tank as stated in [Bar18].

of increasing the S_{NH} ones. This was achieved adopting a multivariate feedback tuning of different PI based structures [Roj12a]. As a result, OCI was extremely increased until a total value of 22986. Finally, Barbu *et.al* proposed four different PI based structures which sought the same objective, the reduction of effluent limits violations. In this case, the addition of external carbon resources has also been considered (see Figure 3.8). Results show better EQI and OCI values in comparison to [Roj12b]. Nevertheless, the complete reduction of $S_{Ntot,e}$ and $S_{NH,e}$ is not achieved. $S_{Ntot,e}$ was violated a 0.252% of the BSM2 simulation time whereas $S_{NH,e}$ was violated a 0.338%.

3.3.2 MPC and FLC controllers

MPC structures have been also widely considered to improve results obtained by PI based structures in the management of WWTP industries. Their adoption has been motivated since they can compute the control actuation of different industrial processes while respecting operational constraint [She08]. As its name suggests, MPC behaviour is based on twofold processes: (i) the optimization of the control problem by means of an optimization algorithm, and (ii) the adoption of a model to predict future outputs of the system so as to optimise the actuation signal. Thus, given the prediction (p) and control horizons (m), the MPC predicts the output sequences

$$\widehat{\mathbf{y}}(k+1|k), \widehat{\mathbf{y}}(k+2|k), \ldots, \widehat{\mathbf{y}}(k+p|k) \tag{3.22}$$

as a function of the obtained control moves:

$$\mathbf{\Delta u}(k), \mathbf{\Delta u}(k+1), \ldots, \mathbf{\Delta u}(k+m-1) \tag{3.23}$$

Then, the output sequence minimising a quadratic objective function by means of the optimization algorithm is considered as the MPC control signal [Mac02, Chapters 1 and 2]:

$$\begin{aligned} J = &\sum_{l=1}^{p} \left|\Gamma_{\mathbf{y}} \left[\widehat{\mathbf{y}}(k+l|k) - \mathbf{r}(k+l)\right]\right|^2 \\ &+ \sum_{l=1}^{m} \left|\Gamma_{\mathbf{\Delta u}} \left[\mathbf{\Delta u}(k+l-1)\right]\right|^2 \end{aligned} \tag{3.24}$$

where the prediction of a controlled output for a future instant $k+1$ performed at the instant k is denoted by $\widehat{\mathbf{y}}(k+l|k)$. $\Gamma_{\mathbf{y}}$ and $\Gamma_{\mathbf{\Delta u}}$ are the output and input rate weight matrices, respectively. Before performing the prediction process, the MPC structure requires a mathematical model relating the plant outputs to the actuation inputs. This mathematical model corresponds to a state-space linear model which approximates the operation of the process in the vicinity of a given working point:

$$\begin{aligned} \mathbf{x_{ss}}(k+1) &= \mathbf{A}\mathbf{x_{ss}}(k) + \mathbf{B}\mathbf{u}(k) \\ \mathbf{y_{ss}}(k) &= \mathbf{C}\mathbf{x_{ss}}(k) + \mathbf{D}\mathbf{u}(k) \end{aligned} \tag{3.25}$$

where $\mathbf{A}, \mathbf{B}, \mathbf{C}, \mathbf{D}$ are the state-space matrices, $\mathbf{x_{ss}}$ the state vector, $\mathbf{u}$ the controlled variable, and $\mathbf{y_{ss}}$ the output of the plant. Moreover, MPCs implement feed-forward control actions for those systems showing issues in tracking the controlled variables at the given set-points due to certain disturbances. This is the case of the $S_{NO,2}$ when BSM1 and BSM2 default control strategies are considered [Ger14]. Thus, the main objective of this feed-forward control is to manage the disturbances once they appear and just before their effects are observed in the output of the process.

In [She08], a multiple input multiple output MPC based structure was proposed to manage the BSM1 effluent concentrations, i.e., $S_{NH,e}$, $S_{Ntot,e}$, BOD_5, COD, and T_{SS}. Its main objective was to reduce the number of effluent violations, especially the $S_{NH,e}$ and $S_{Ntot,e}$. Two types of MPC configurations were considered: (i) without feed-forward control, and (ii) with feed-forward control. To achieve good results, authors had to tune the MPC structure reducing the set-point values of the effluent concentrations. For instance, $S_{Ntot,e}$ limit was fixed at a value of 14 mg/L instead of the usual 18 mg/L. Achieving the reduction of average concentrations, the MPC based structure still showed effluent violations in both configurations, i.e., with and without a feed-forward control [She08]. Besides, the lowering of effluent set-points entailed the increment of operational costs. Later, O'Brien *et.al* proposed the adoption of a MPC with feed-forward control to manage the dissolved oxygen concentrations of Lancaster's WWTP in England [O'B11]. The MPC was configured to consider the aeration powers as the managed variables and the dissolved oxygen values as the actuation signals. The MPC structure consisted again in a multiple input multiple output structure, however, it aimed to reduce the costs and not the effluent violations. Results provided in [O'B11] showed that a 20% of savings in the energy consumption was achieved.

Besides, the WWTP efficiency was increased a 25% with respect to not consider the proposed MPC. Similar approaches were proposed in [Rev17]. An economic oriented MPC was proposed to manage the control loops specified in the BSM1 framework. A reduction in the costs was achieved, but violations of effluent pollutants were still observed. OCI values were reduced at expense of observing $S_{NH,e}$ and $S_{Ntot,e}$ violations: 3.34% and 3.60% of the BSM1 simulation time, respectively.

Forming more complex control structures, MPCs have been complemented with FLCs [San15a, San15b]. The main characteristics of FLCs reside in the fact that they are interpretative controllers. Inputs of the controller are related to the outputs in a fuzzy way, i.e., the borders of the control function are not clearly defined [Bai06, Chapter 2]. Moreover, as depicted in Figure 3.9, they are formed by a set of different modules in charge of computing the control actuation. They consist in the fuzzifier, the inference engine, the fuzzy rule base and the defuzzifier. Their behaviour is based on the human expertise meaning that a good knowledge of the dynamics of the process under control is required. The FLC output is determined by words and sentences rather than mathematical expressions [Bai06, Chapter 3]. In that sense, the fuzzifier module is in charge of transforming the input values into linguistic ones thanks to the FLC membership functions [Bai06, Section 2.3]. Then, these linguistic values are treated in the fuzzy rule base, which consists in a set of if-then clauses. It is here where a huge knowledge of the process is required to determine the set of clauses. Then, the outputs of the if-then clauses according to the linguistic inputs are combined in the inference engine of the FL. These modules are operated by means of two different methods, the Mamdani and the Takagi-Sugeno [Mam76, Tak85]. Finally, the results of the engine are transformed into numerical values in the defuzzifier [Bai06, Chapter 3].

Two examples on the application of FLC correspond to [San15a] and [San15b]. The former considered the adoption of MPCs and FLCs to implement the management structure of the BSM1 framework. Santin *et.al* considered the structure proposed in [Nop10], but instead of PI controllers, they adopted MPC and FLCs. The two default BSM1 PI controllers were substituted by a MPC structure with two inputs, $S_{NO,2}$ and $S_{O,5}$, and two outputs, $K_{La,5}$ and Q_a. Its main aim was to improve the tracking performance of the $S_{O,5}$ and $S_{NO,2}$ set-points. A feed-forward action to avoid the effects of high disturbances in the $K_{La,5}$ and Q_a computation was also considered. The $S_{O,5}$ set-point was determined

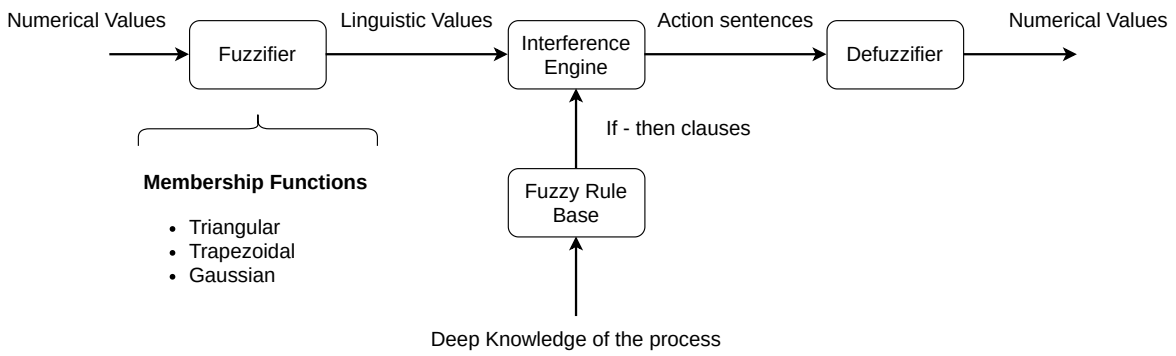

Figure 3.9: FLC architecture and behaviour.

by means of a higher control strategy to achieve a nitrification improvement. Implemented by means of FLCs, it determined the set-point according to the measured $S_{NH,5}$. Thus, when low $S_{NH,5}$ values were observed, the FL structure decreased the $S_{O,5}$ aiming to reduce the operational costs as well as the $S_{NO,2}$. On the other hand, when $S_{NH,5}$ was high, the FLC increased the $S_{O,5}$ to avoid peaks of $S_{NH,5}$.

Results showed, for instance, that EQI was reduced from 6123.0182 to 6048.31 Kg · pollutant units · day^{-1} when the PI structure was changed by the MPC. When the FLC was considered, it was even more reduced, from 6048.31 to 6047.95. In terms of OCI, it was increased from 16382.4027 to 16382.97. When the MPC was complemented with the FL, OCI was reduced until 16197.86. However, the effluent violations were not completely reduced, showing that some extra efforts in the WWTP control are required. That hierarchical structure based on MPC and FLCs presented in [San15a] was updated in [San15b]. The multiple input multiple output MPC was changed by three different MPCs which focused their efforts on controlling different variables. One MPC managed the $K_{La,5}$ and the Q_a actuation variables while the remaining ones managed the $K_{La,3}$ and $K_{La,4}$, respectively. Then, the dissolved oxygen considered by each MPC was determined as a function of the $S_{NH,5}$ by a FLC acting as a higher control structure.

Notwithstanding, the utmost interesting point of this work is placed in the adoption of extra FL structures devoted to reducing the $S_{Ntot,e}$ and $S_{NH,e}$ violations (see [San15b, Figure 7 and 8]). Their aim was to achieve the complete reduction of effluent violations at the same time that EQI and OCI were decreased. EQI and OCI were equal to 5862.03 Kg · pollutant units · day^{-1} and 16336.36, respectively, when the structure reducing the $S_{Ntot,e}$ violations was considered. In addition, violations of $S_{Ntot,e}$ were avoided at expense of observing $S_{NH,e}$ violations. They were equal to 16.66% of the BSM1 simulation time. Inversely, the total reduction of $S_{NH,e}$ violations was achieved when the structure reducing them was considered. In this case, $S_{Ntot,e}$ violations represented a 15.62% of the BSM1 simulation time. EQI and OCI equal to 5854.06 Kg · pollutant units · day^{-1} and 16307.26, respectively. Although representing a great improvement in terms of the reduction of violations, MPC + FLC structures were not able to completely avoid them. This clearly shows that more efforts can be done in the management of WWTPs.

Motivated by the appearance of the Industrial 4.0 paradigm, ANNs are being considered in the implementation of MPC and FLC based structures to tackle the reduction of violations. They are adopted to achieve a threefold objective: (i) the reduction of costs related to the deployment of expensive hardware sensors, (ii) the obtention of unmeasurable values, and (iii) the prediction of offline measurements [For05, Tra18, Nad18, Lan19]. In [Fos16], a RNN has been proposed to identify the input and output predictive models of the system under control. Then, this model is considered to tune a Dynamic Matrix Control based MPC.

Results have shown that the proposed structure can decrease in average the $S_{Ntot,e}$ violations but not the $S_{NH,e}$ ones. Instead of RNN, in [San16] two different control structures based on FFNN have been proposed to reduce $S_{NH,e}$ and $S_{Ntot,e}$ violations. Their main objective is to predict effluent violations of either $S_{NH,e}$ or $S_{Ntot,e}$. Depending on the prediction term, the control structures modify Q_a or Q_{ext} values. For instance, the ANN predicting $S_{Ntot,e}$ violations activates the addition of extra external

carbon in the anoxic tanks whilst the net predicting $S_{NH,e}$ violations activates the manipulation of Q_a. Results have shown that in this case, a complete reduction of $S_{NH,e}$ violations is achieved at expense of increasing the $S_{Ntot,e}$ ones. On the other hand, $S_{Ntot,e}$ violations can be reduced but not avoided at the same time that a reduction of $S_{NH,e}$ violations is obtained. Nevertheless, better results could be observed if RNN were considered instead of FFNN. This will be assessed in Chapter 4.

Other use-cases of ANNs as soft-sensors supporting the industrial management are shown in [Man17, Han18b, Sad18]. In [Man17], ANNs and fuzzy logic based techniques are considered to predict the amount of NKj. In [Han18b], a fuzzy neural network is proposed as part of an intelligent monitoring system devoted to forecasting in real time the total phosphorus and S_{NH} present in a WWTP. The main point is that reliable predictions can be obtained requiring only the WWTP measurements and the ANN-based structure. In [Sad18], ANNs, and especially Non-linear Autoregressive Exogeneous (NARX) models, have been proposed to implement a non-linear MPC controller whose set-points are computed by means of ANNs. Results show that a reduction in EQI and OCI values is achieved.

As it has been observed, ANNs are considered on most occasions as a powerful tool complementing conventional structures able to reduce the effluent quality and operational costs metrics. Nevertheless, these structures fail in the tasks of completely reducing the effluent violations. Great reductions have been obtained but at the expense of adding external sources that most of the times increase the operational costs. For that reason, low-cost solutions and industrial controllers are required to achieve better control performances as well as a reduction of costs. This is of the utmost importance in industrial scenarios where benefits are not obtained from the final product. This is where one of the efforts of this thesis will be focused on. A set of ANN-based solutions will be proposed to achieve an improvement in the WWTP effluent quality and a reduction of the operational costs.

3.3.3 IMC Controllers

Most of the times the PIs and PIDs considered in the management of WWTP environments are tuned by means of the Internal Model Controllers (IMCs) structures rather than by PID usual tuning processes. This is motivated by their structure, which derive the control actuation not from a given expression, but from the modelling of the process under control [Wan01, Yan02]. This is performed explicitly introducing the process under control $(P(s))$ in the control loop.

Its architecture, as depicted in Figure 3.10, considers two mathematical models: (i) the direct model of the process under control, $P_{dir}(s)$, and (ii) its inverse model, $P_{inv}(s)$. In that sense, the actuation signal, $u(t)$, enters at the same time in $P(s)$ and $P_{dir}(s)$. The former returns the real controlled signal $(y(t))$, while the later returns an estimation of it, $\widehat{y}(t)$. Notice that this estimation does not consider the effects related to the presence of disturbances, $d(t)$, entering in the plant or $P(s)$. Then, the mismatch between these outputs, $e'(t) = y(t) - \widehat{y}(t)$, is computed to be contrasted with the reference signal, $r(t)$. Understood as the reference modified by the mismatch, the resultant signal, $\tilde{y}(t)$, is then fed into the

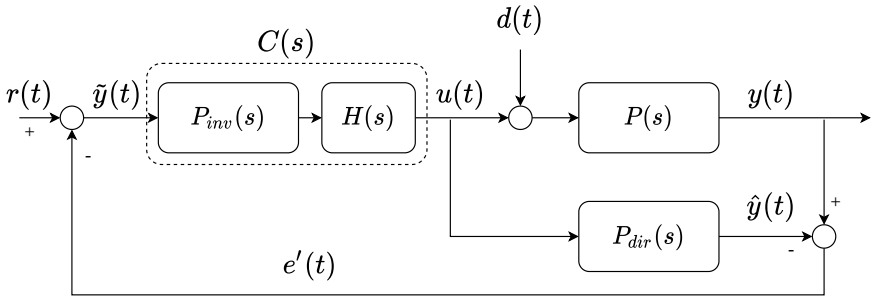

Figure 3.10: IMC architecture and behaviour.

controller itself, i.e., $C(s)$. It corresponds to the product between $P_{inv}(s)$ and a first-order low pass filter, $H(s)$. Its main aim is to manage the tolerance of $C(s)$, i.e., its behaviour when unmodelled dynamics, inversion uncertainties, etc., are present in the system under control [Roj12a]. As it is observed, the actuation of the controller is influenced by the mismatch between the real output and its estimation. Thus, the more accurate the $P_{dir}(s)$ and $P_{inv}(s)$, the better the control performance. All this makes the IMC a suitable structure for set-point tracking purposes.

Notwithstanding, the adoption of IMC structures is more related to the tuning of conventional PI and PID controllers rather than as a controller. By means of rearranging the elements of the IMC structure, an equivalent controller of the form

$$C_{eq} = \frac{C(s)}{1 - C(s) \cdot P_{dir}(s)} \tag{3.26}$$

can be derived. Then, PI, PID and high-order controllers can be derived by similarity of terms [Wan01, Yan02, Sha07, Qib13, Li19a]. For instance, in [Yan02], the IMC structure has been considered to determine the PID feedback controller for an open-loop unstable process. The same principle was adopted in [Sha07, Qib13]. In both cases, the IMC structure was again considered to derive PID controllers. The former was considered to tune a PID controller devoted to managing a second order delayed unstable process. The latter was considered to perform the same task. A PID controller to manage different plant configurations, i.e., different processes, was determined through the IMC configuration. In addition, the stability test of the derived PID is also performed in [Qib13]. Another example is shown in [Li19a], where a robust PID was derived following the IMC based tuning process.

In terms of the WWTP environment, the IMC structure has been also considered to derive conventional controllers managing elements of a WWTP. For instance, showing a 2.5% and a 13% of reduction of the overall costs of an WWTP scenario, two PI controllers have been derived in [Mac09] adopting the IMC structure. In [Vil18], an event-based IMC controller is proposed to derive a PI controller in charge of the $S_{O,5}$ and $S_{NO,2}$ concentrations of BSM1 framework. In other cases, however, the IMC structure has been considered as such. This is the case of [Vil11a, Roj16]. In [Vil11b], the IMC structure was considered to manage the $S_{O,5}$ concentration of the WWTP. Its performance was compared with an

analytical tuned controller and results showed that the latter was able to overcome the IMC structure. On the other hand, in [Roj16], an event-based IMC with a virtual reference feedback tuning approach is considered. Its main purpose was to manage the $S_{O,e}$ and the $S_{S,e}$. Later, in [Vil18], the event-based IMC was adopted to tune PI structures managing the BSM1 control loops, i.e., the $S_{NO,2}$ and the $S_{O,5}$. Results showed that such controllers where able to overcome the performance yielded by the default PI controllers for most of the cases.

One of the problems that arise corresponds to the necessity of accurate models of the process under control. As it has been previously stated, the better the accuracy, the better the performance. In that sense, $H(s)$ tries to mitigate this effect, but, as a low-pass filter, it can degrade the actuation signal at the expense of reducing the issues of inaccurate $P_{inv}(s)$ and $P_{dir}(s)$. Here is where the incursion and adoption of ANNs make sense. Their performance when modelling highly complex and non-linear relationships is promoting their adoption in the development of IMC controllers. Modelling the inverse and direct relationships of the process under control, the ANNs main objective is to increase the accuracy levels and therefore, obtain a better control performance. Notwithstanding, this entails that $P_{dir}(s)$ and $P_{inv}(s)$ do not consist in mathematical models any more. As a consequence, the IMC structure cannot be used as a tuning technique of conventional structures such as PI, PIDs or high-order controllers. When it is based on ANNs, it must be considered and adopted as a controller as such.

A first attempt was proposed in [Kan18], where an IMC implementing MLP networks as $P_{dir}(s)$ and $P_{inv}(s)$ was proposed to manage the illuminance of headquarter offices. The main idea there was to obtain the grade of illuminance through sensors and then consider this information and the outputs generated by each MLP to graduate the illuminance of each desk in the office. Potential energy savings were achieved since the illuminance was regulated as a function of the daylight. In numbers, the energy savings were placed around a 54% and a 40% in comparison to provide each light with the same intensity. Other examples consider the application of IMC structures based on ANNs to not only obtain a controller based on data, but also to achieve a control decoupled from the scenario where it is applied. This is the case of [Wan18], where an inverse system based on neural networks and an IMC configuration was considered to achieve the decoupling of an active front steering wheel of an autonomous vehicle. Results showed that a robust decoupled control system was obtained, especially for tracking the reference value of the given yaw angle of the steering wheel. In the line of decoupling the industrial control from its scenario, two conventional IMC structures were proposed to decouple the control of two interconnected thermal power systems [Kas18]. Results showed that good tracking and robust controllers were achieved at the same time they were decoupled from the strong coupling of the interconnected thermal plants.

All these results have shown that ANNs can be adopted as a power tool which can introduce the industrial control into a new era. Instead of deriving highly complex controllers, which sometimes involve a deep knowledge of the processes being managed, these controllers can be obtained by means of ANNs and data-based techniques. Nevertheless, one of the most important points is that ANNs as control systems are not excluding. They can live together with conventional structures or even complement them.

Chapter 4

Control Structures Enhancement Adopting ANN-based Solutions

ANNs have arisen as a new powerful tool able to model highly complex and non-linear processes. This is of the utmost importance for those scenarios, such as industrial environments, where processes like that are constantly present. This power has also motivated the adoption of ANN not only to model certain processes, but also to implement soft-sensors. Sensors representing a low-cost alternative to expensive hardware components. In this chapter, the adoption of ANNs, especially LSTM, to implement soft-sensors for a WWTP environment is assessed. Moreover, some of the most important issues related to industrial measurements are also tackled here. Finally, the proposed ANN-based soft-sensor is tested over the BSM2 framework to determine the improvement in terms of the WWTP effluent quality and overall costs indexes.

4.1 Introduction

As any other industrial scenarios, WWTPs environments rely on control structures whose main objective is to assure the correct behaviour of different processes. In that sense, WWTP control structures are mainly considered to maintain some concentrations under certain levels and to assure that pollutant levels are correctly reduced [Ale08]. This is the case of the MPC + FLC control structure presented in [San15b]. It consists in three MPCs and three FLCs structures deployed over BSM1 and devoted to reducing the $S_{Ntot,e}$ and $S_{NH,e}$ violations. The MPCs and one FLC implemented a hierarchical control in charge of managing the oxygen concentration in the three aerated tanks. However, the crucial point of the proposed control was placed in the remaining FLC structures. Their main aim was to avoid $S_{Ntot,e}$ and $S_{NH,e}$ violations by means of determining the addition of external carbon and recirculation flow rates. The former structure determines the amount of external carbon to add to the first reactor tank when $S_{Ntot,e}$ is prone to be violated, otherwise the OCI will be exponentially increased. On the other hand, the

second structure increases Q_a whenever S_{NH} at the input is high. When this rise is observed in the fifth tank, the FLC decreases the Q_a to preserve the WWTP retention time. Results show that there exists a trade-off between the reduction of $S_{Ntot,e}$ and $S_{NH,e}$ violations and their respective concentration values. To tackle this, some modifications have been performed in [San16].

These modifications consisted in the adoption of ANN-based structures to implement two different control structures. They consider MLP soft-sensors predicting the risk of violating $S_{NH,e}$ and $S_{Ntot,e}$ over the BSM2 framework, which entail two benefits: (i) the system will be provided with more predictive and reactive time to perform the desired actuations to prevent the violations, and (ii) the OCI will be reduced since the given actuations will only be applied when a real risk is forecasted. The MLPs purpose was to forecast the $S_{NH,e}$ and $S_{Ntot,e}$ violations in advance so as to have enough time to actuate over the plant. They were trained considering the behaviour of the WWTP structure for a whole year when control structures maintaining the $S_{NO,2}$ and $S_{O,5}$ set-points were applied. Besides, measurements considered in the training process correspond to the maximum and minimum concentration values. In this case, a hierarchical control structure based on MPC + FLCs and devoted to maintaining $S_{O,4}$ and $S_{O,5}$ at given set-points, 2 mg/L and 1 mg/L, respectively, is common for both control structures. They differ in the ANN-based soft-sensor structure. While the structure in charge of the $S_{Ntot,e}$ considers the ANN-based structure to feed a FL, the structure in charge of the $S_{NH,e}$ adopts the ANN-based structure as a selector of the control actuation (see Figure 4.1). Taking all this into account, when a risk of $S_{Ntot,e}$ is predicted, the FLC addressing the $S_{Ntot,e}$ violations computes the amount of carbon to add into the WWTP anoxic tank. On the other hand, when a $S_{NH,e}$ peak is forecasted, the ANN-based soft-sensor selects the control structure computing the Q_a needed to avoid the $S_{NH,e}$ violation. Nevertheless, results have shown that not all the violations are avoided neither eliminated. For instance, six $S_{NH,e}$ violations were predicted from which only 4 were real. The actuation achieved a 100% reduction. The problem is placed in the $S_{Ntot,e}$ actuation. There were 47 violations and only 43 were predicted by the MLP net. From these 43, only 34 were corrected. Hence, only a 72.34% were avoided. One of the reasons why this percentage is not equal to a 100% is related to the actuation time. As it is observed in the results presented in [San16], the amount of time considered in the prediction of $S_{Ntot,e}$ is not enough to assure a good actuation over this concentration. Thus, this has to be corrected to assure a 100% of violations avoided for both $S_{NH,e}$ and $S_{Ntot,e}$.

In such a context, a solution alleviating this problem consists in the development of an ANN-based soft-sensor system predicting the $S_{Ntot,e}$ and $S_{NH,e}$ concentrations. These predictions will feed existent control strategies with enough time in advance to actuate over possible violations to reduce them. Therefore, an improvement in the effluent quality indexes with low-cost tools is proposed. LSTM nets are proposed to implement the proposed ANN-based soft-sensor since they show a really good performance predicting certain values of sewerage systems. Besides, the non-linear behaviours and strong correlations in time of WWTP facilities make the LSTM nets the most suitable ANN. The proposed soft-sensor seeks a twofold objective: (i) predict $S_{Ntot,e}$ and $S_{NH,e}$ violations, and (ii) determine their amount. Two differ-

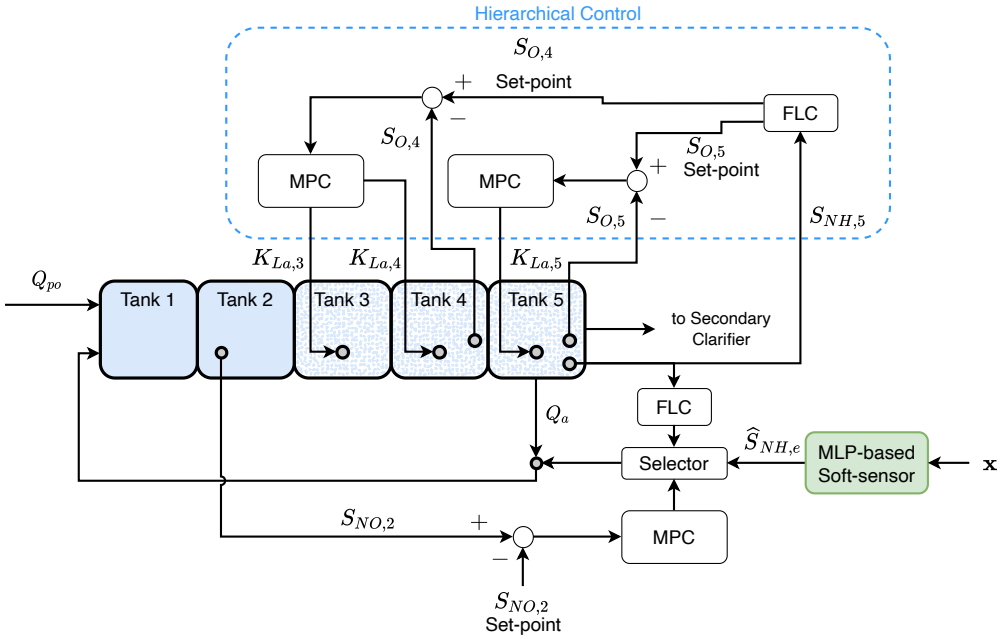

(a) Control structure aimed at avoiding $S_{NH,e}$ violations

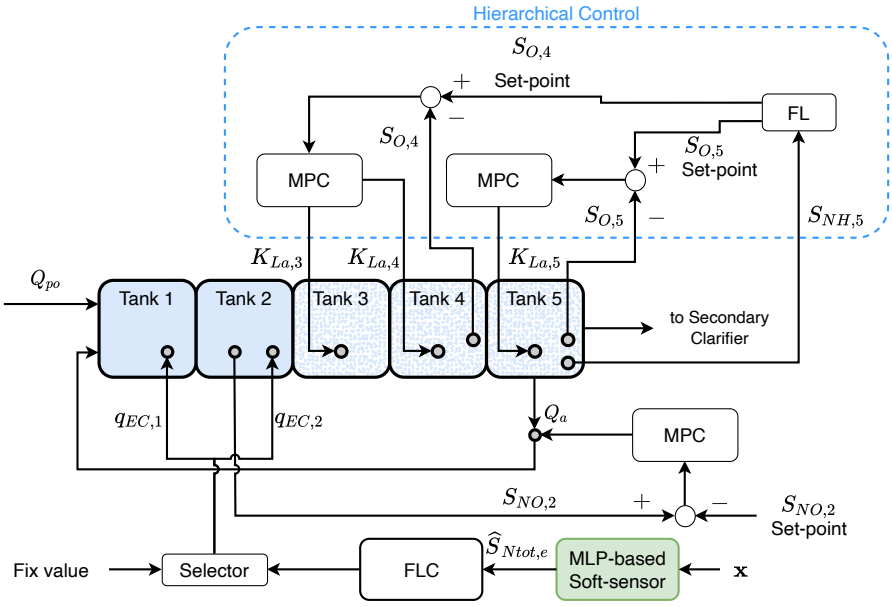

(b) Control structure aimed at avoiding $S_{Ntot,e}$ violations

Figure 4.1: Control structures proposed in [San16]. Notice that each structure adopted the MLP-based soft-sensor to predict either the $S_{NH,e}$ or the $S_{Ntot,e}$. The former considers it to predict the $S_{NH,e}$ violations and then select the control structure according to these values. The latter MLP-based structure is devoted to predicting the $S_{Ntot,e}$ values fed into the FLC controller. Blocks implementing MLP nets are depicted in green colour.

ent configurations are proposed to accomplish these two objectives. The former consists in the adoption of an ANN-based Alarm Detector while the latter adopts this detector and implements an ANN-based Operation Strategy. Moreover, the complete range of available measurements is adopted to properly train the LSTM net and therefore, to consider the complete dynamics of the WWTP scenario. Here, the scenario consists of the BSM2 framework with the hierarchical control structures defined in [San16]. Since the WWTP is already being managed, the proposed net has to be properly trained to avoid underfitting and overfitting problems related to the unbalanced data issues [Bud18]. This is tackled adopting the K-fold cross-validation technique to determine the best subset of data to train the net. Last but not least, the WWTP non-linear behaviour entails that superposition principles are not valid. Thus, strategies avoiding $S_{Ntot,e}$ and $S_{NH,e}$ violations cannot be evaluated separately. For that reason, the management of a WWTP scenario must be assessed as a whole, i.e., when both strategies are acting together.

In summary, the contributions of this chapter are:

- An assessment of LSTM cells implementing an ANN-based soft-sensor is provided.
- Overfitting and underfitting problems related to unbalanced data issues are tackled following the process explained in [Pis19d].
- Violations of $S_{NH,e}$ and $S_{Ntot,e}$ are predicted by the ANN-based soft-sensor.
- A new ANN-based operation strategy for WWTP facilities is derived.
- The effluent violations removal processes is improved as a result of the new ANN-based strategy.

This chapter is organised as follows: in Section 4.2 the Effluent Concentrations and Alarm Prediction System, which implements the ANN-based soft-sensor predicting $S_{Ntot,e}$ and $S_{NH,e}$ violations, is presented. Issues related to the unbalanced data problem are also assessed and tackled in this section. Section 4.3 describes the ANN-based operation strategy proposed to improve the effluent violation removal process. Finally, conclusions of this chapter are provided in Section 4.4. Notice that the work summarised in this chapter reflects the works presented in [Pis18, Pis19b, Pis19d, Pis19c, Pis19e].

4.2 Effluent Concentrations and Alarm Prediction

One of the main aims of control strategies is to avoid the violation of WWTP effluent concentrations. Not only because they are harmful for the environment, but also because a violation entails an increment on the WWTP overall costs due to the interposed fines [Eur91]. For that reason, solutions addressing the violation reduction without increasing the operational costs are welcomed.

This is the case of the proposed Effluent Concentrations and Alarm Prediction System (ECAPS), which for this occasion will be derived from measurements coming from the BSM2 framework. ECAPS

consists in an ANN-based soft-sensor system devoted to predicting the WWTP effluent concentrations and determining the occasions where a violation is likely to occur. Figure 4.2 depicts the structure of ECAPS which considers two subsystems: (i) the ANN-based soft-sensor, and (ii) the Alarm Generator. The former consists in an ANN-based soft-sensor which is formed by the Data Preprocessing and Effluent Prediction blocks. It predicts the WWTP effluent concentrations with enough time in advance to let the WWTP control structures actuate over possible violations. The Alarm Generator takes the ANN-based soft-sensor predictions and generates alarms whenever the effluent concentrations exceed the provided $S_{NH,e}$ and $S_{Ntot,e}$ thresholds, $\gamma_{S_{NH,e}}$ and $\gamma_{S_{Ntot,e}}$, respectively. They are configurable so as to determine the sensibility of the alarm detection. Among the BSM2 effluent concentration, only $S_{NH,e}$ and $S_{Ntot,e}$ are considered due to their effects to the environment: $S_{NH,e}$ is toxic for aquatic life whereas $S_{Ntot,e}$ increases the eutrophication likelihood and therefore, the proliferation of algae [San16].

4.2.1 Data Preprocessing Block

The Data Preprocessing block is in charge of gathering, sorting and standardising the input measurements considered by the ANN-based soft-sensors. In addition, some considerations must be taken into account in its implementation: the block must solve the input data heterogeneity as well as it has to preserve the information present in the time-correlation measurements. To achieve this, the proposed soft-sensor consists of three blocks performing each one of the aforementioned operations:

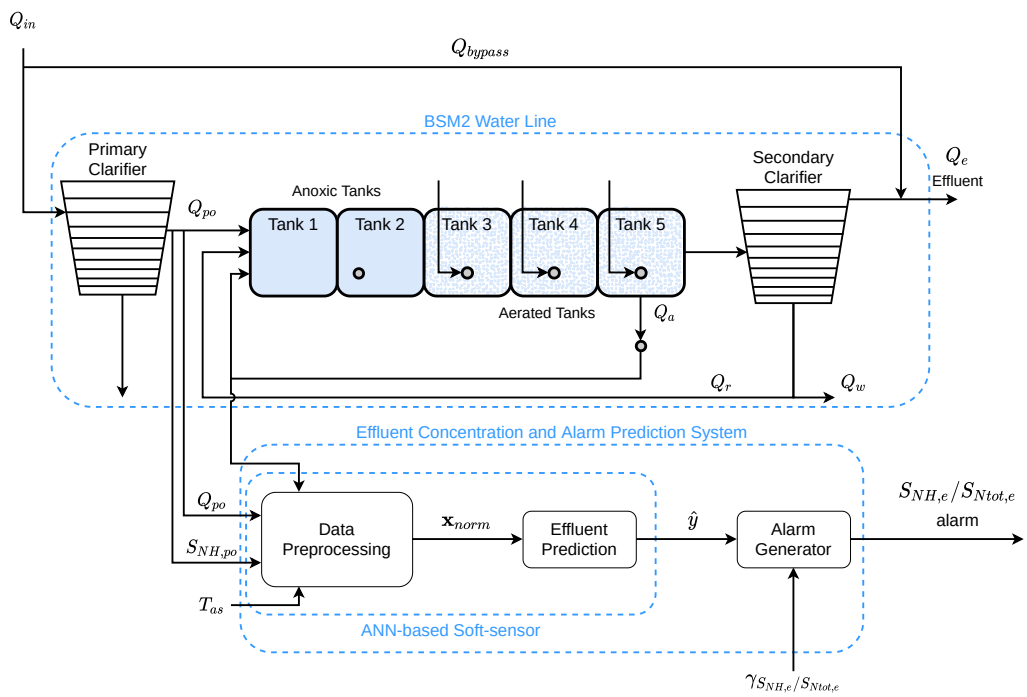

Figure 4.2: Effluent Concentration and Alarm Prediction System. Only the water line of BSM2 framework is depicted.

- **Gathering Block**: This block is in charge of gathering the different measurements from the BSM2 framework. Among all the available measurements, the proposed ANN-based soft-sensor only considers the Q_a, the influent flow rate after the primary clarifier (Q_{po}), the ammonium present at the same point ($S_{NH,po}$) and the T_{as}. These measurements are considered since they represent some of the influent, internal and effluent dynamics. Besides, they are strongly related to the nitrification and denitrification processes [Hen87, HS93, Hen00]. Q_{po} denotes the amount of water entering in the first biological reactor and therefore, it is directly related to the amount of pollutants to be processed by the WWTP. $S_{NH,po}$ has an important effect in the nitrification process yielding to an increment of the ammonium concentration in the effluent. T_{as} is considered due to their importance in the pollutant reduction processes. Q_a is only considered for those situations seeking the $S_{Ntot,e}$ reduction since it increases the amount of dissolved oxygen and sludge present in the first anoxic tank.

- **Feature Standardisation**: This block oversees the standardisation of the ANN-based soft-sensor input measurements. This process is required due to the highly heterogeneous input measurements. For instance, Q_{po} BSM2 sensor provides measurements in the range $0 - 100000\ \mathrm{m}^3/\mathrm{day}$ whilst this range equals to $0 - 20$ mg/L for the $S_{NH,po}$ (see Table 3.3). If no actions are performed, the heterogeneity can produce a very slow ANN training process or even the non-convergence of the ANN. For that reason, the Feature standardisation block performs the standardisation of measurements towards zero mean and unit variance set of measurements [Gar15, Section 3.4]:

$$\mathbf{x}_{norm} = \frac{\mathbf{x} - \mu_{\mathbf{x}}}{\sigma_{\mathbf{x}}} \tag{4.1}$$

  where $\mu_{\mathbf{x}}$ and $\sigma_{\mathbf{x}}$ are the mean and standard deviation of $\mathbf{x}$.

- **Sliding Window**: WWTPs are industries whose measurements present a strong correlation in time. Thus, valuable information can be extracted from these correlations. For that reason, a sliding window is proposed. It will sort the measurements, sampled every 15 minutes in time, preserving the given correlations. Its behaviour is determined by two parameters: the Window Length (WL) and the Prediction Horizon (PH). WL tells the amount of measurements that the sliding window has to store. It has to be high enough to preserve the correlation in time as well as some of the weather events such as rainy and stormy episodes. On the other hand, and determined by the WL, PH represents the amount of time between the last measurement and the current prediction. The point here is that the sum of WL and PH equals to the average hydraulic retention time (t_{hr}), $t_{hr} = PH + WL$. If the average hydraulic retention time of BSM2 ($t_{hr_{BSM2}}$) framework equals to 14 hours and a WL of 10 hours is considered, the PH will equal to 4 hours. This assures that the predicted effluent concentration is a product of the water currently going throughout the plant. Besides, the higher the WL, the better the prediction performance. This configuration can be changed to fulfil other operational policies. It is just a matter of correctly defining the behaviour of the sliding window. However, one has to be aware of the control strategies operational times. Here, 4 hours is

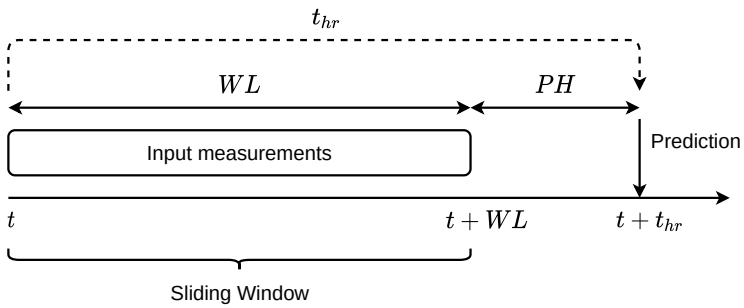

Figure 4.3: Sliding window considered in the ANN-based soft-sensor.

enough time to let the control strategies actuate and reduce the effluent violations. Notice that the sliding window follows a one-sample averaging time-window policy. This means that a prediction is provided whenever a new measurement is gathered. Figure 4.3 depicts the behaviour of the considered sliding window.

4.2.2 Effluent Prediction Block

The Effluent Prediction block goal is to perform the desired $S_{Ntot,e}$ and $S_{NH,e}$ predictions. It takes the standardise measurements and predicts the desired effluent concentrations. Therefore, the Effluent Prediction block consists in the core of the proposed ANN-based soft-sensor. LSTM cells have been considered to model the non-linear and highly complex biological and biochemical processes performed in WWTPs. Besides, the strong correlation in time shown by WWTP input and output measurements has motivated the adoption of such nets. Not only are LSTM cells able to model non-linear processes, but also to show a good prediction performance when dealing with measurements and data showing a high correlation in time, such as text or speeches [Goo16, Section 10.10] [Gre17].

In the case of this thesis, two stacked LSTMs have been considered as the base structure implementing the Effluent Prediction block. The input vector of standardised measurements ($\mathbf{x}_{norm}$) is firstly processed by the first LSTM cell. The output of this cell is then feed into the second cell to finally extract the information present in the time correlations. The output of this second cell is processed in a final output layer, which consists in a single output neuron and a linear activation function. Figure 4.4 depicts the structure of the Effluent Prediction block as well as the internal structure of the Data Preprocessing block.

Prediction Structures

ECAPS will be tested with measurements coming from three different control levels to compute its performance and suitability as an ANN-based soft-sensor. In order to generalise its behaviour, three different control configurations are considered:

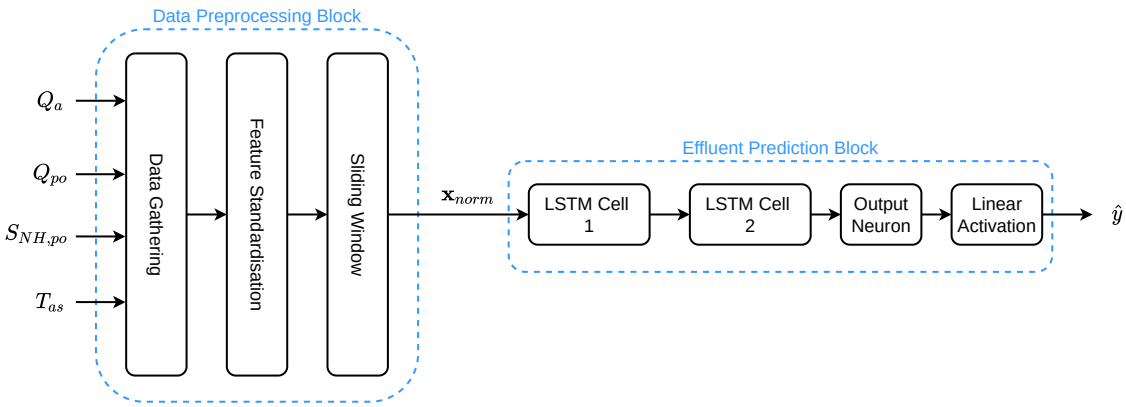

Figure 4.4: Data Preprocessing and Effluent Prediction block architecture. $\gamma_{S_{NH,e}/S_{Ntot,e}}$ denotes the $S_{NH,e}$ or the $S_{Ntot,e}$. $\widehat{y}$ corresponds to $S_{NH,e}$ or $S_{Ntot,e}$ prediction.

- **Open Loop configuration (OL)**: The OL configuration corresponds to a situation where the WWTP effluent is not being managed and therefore, no control strategies are considered. As its name states, it corresponds to an open loop configuration. Here, the number of effluent violations will be extreme. Figure 3.4 depicts the OL configuration of the BSM2 framework.

- **Default BSM2 Control (DC) strategy**: The DC strategy corresponds to the default BSM2 control strategy. It consists in a PI controller devoted to managing the oxygen transfer coefficients of the third, fourth and fifth reactor tanks. Its main goal is to assure a $S_{O,4}$ equal to 2 mg/L. The amount of external carbon added to the first tank ($q_{EC,1}$) is maintained at a fixed rate of 2 mg/L. This structure is shown in Figure 3.5.

- **Hierarchical Control (HC) strategy**: The HC strategy consists in the most complex strategy where ECAPS will be tested. It was proposed by Santin *et.al* in [San16]. They mainly considered the adoption of a hierarchical structure devoted to maintaining the S_O set-points at the desired values. This structure consists of two MPC controllers computing the $K_{La,3}$, $K_{La,4}$ and $K_{La,5}$, respectively. The former determines $K_{La,3}$ and $K_{La,4}$ as a function of $S_{O,4}$. The latter determines $K_{La,5}$ as a function of $S_{O,5}$. $S_{O,4}$ and $S_{O,5}$ set-points are computed by means of a FLC and $S_{NH,5}$ values. Moreover, two MLP structures were considered to predict the peaks of $S_{Ntot,e}$ and $S_{NH,e}$ concentrations, one for each pollutant. Here, these two MLP nets will be substituted by two LSTM cells. As it has been previously stated, the structure predicting the $S_{Ntot,e}$ feeds a FLC controller whereas the structure predicting the $S_{NH,e}$ determines the control strategy to adopt. Figure 4.1 depicts the two proposed control strategies. For more information regarding the HC strategies readers are referred to [San16].

ECAPS Effluent Prediction block is focused on predicting a unique effluent concentration. Thus, two prediction structures will be obtained per control configuration, one for predicting the $S_{NH,e}$ and another for the $S_{Ntot,e}$. In that sense, each prediction structure departs from the base structure shown

in Figure 4.4. They only differ in the LSTM hyperparameters, i.e., the number of hidden neurons per LSTM gate and the L2 regularisation value. These values are set according to the training process of the whole effluent prediction block. In the training process different configurations of hidden neurons per gate as well as L2 regularisation values are varied just to determine the configuration which fits better the WWTP behaviour [Ben12], i.e., the model hyperparameters have been computed by means of a grid search methodology. A total set of six prediction structures have been derived after performing the training process. Table 4.1 denotes the different control structures, their number of hidden neurons and the L2 regularisation value considered.

Training Process

The training process of the ECAPS Effluent Prediction block is one of the critical points of the proposed system. Since the endeavour of this block is to detect effluent violations, i.e., rare events, it has to be properly trained. Suppose the proposed system was incorrectly trained. A twofold situation could be observed. The soft-sensor could predict more effluent violations than the real observed ones. Consequently, more actuations on the effluent concentrations would be performed and therefore, the operational costs would increase. On the other hand, if violations were not predicted, no actuation would be performed. Thus, the cost would not be increased at expense of reducing the EQI and also polluting the receiving waters. This clearly show that a correct training of the ANN-based soft-sensor is required. In order to achieve this, huge amount of equilibrated measurements are required. For that reason, a whole simula-

Table 4.1: ECAPS Effluent Prediction Configuration. Two prediction configurations have been derived for each control strategy. For instance, the OL prediction configuration forecasting $S_{NH,e}$ values is denoted as OLPS-NH whereas the one in charge of $S_{Ntot,e}$ predictions is denoted as OLPS-NT. DCPS-NH, DCPS-NT, HCPS-NH and HCPS-NT denote the DC and HC configurations predicting the $S_{NH,e}$ and $S_{Ntot,e}$ violations, respectively.

OL Strategy			
Configuration	Output Concentration	Hidden Neurons per Gate	L2 regularisation value
OLPS-NH	$S_{NH,e}$	100	$1 \cdot 10^{-3}$
OLPS-NT	$S_{Ntot,e}$	125	$5 \cdot 10^{-3}$
DC Strategy			
Configuration	Output Concentration	Hidden Neurons per Gate	L2 regularisation value
DCPS-NH	$S_{NH,e}$	75	$1 \cdot 10^{-3}$
DCPS_NT	$S_{Ntot,e}$	100	$1 \cdot 10^{-3}$
HC Strategy			
Configuration	Output Concentration	Hidden Neurons per Gate	L2 regularisation value
HCPS-NH	$S_{NH,e}$	50	$1 \cdot 10^{-3}$
HCPS-NT	$S_{Ntot,e}$	40	$1 \cdot 10^{-3}$

tion of the BSM2 framework, i.e., 609 days of dynamic influent, has been performed for each control scenario. Three different datasets showing the BSM2 hydrochemical parameters are obtained when it considers the OL, DC and HC strategies. All of them with ideal sensors. Notwithstanding, unbalanced datasets are observed because most of the time, even there are effluent violations, the effluent concentrations are below the limits. From a statistical point of view, violations are "rare events". If this is not correctly tackled, the ANN will not learn how to model those situations producing effluent violations. Neither will it generalise. Figure 4.5 depicts the histograms for each one of the considered scenarios. Being the OL dataset the one much closer to the equilibrium, none of the datasets are balanced with respect to BSM2 effluent limits.

Here, the unbalanced issue has been tackled by means of the K-fold Cross Validation technique as further explained in [Pis19d]. Each dataset is divided into two subsets, an 85% of data to perform the K-Fold based training process and a 15% to finally test the different prediction structures. The 85% devoted to training the prediction structures is then split in 5 different folds (5-fold) to achieve the generally used 70-15-15% split of data. Here, the first 15% is left to test the final prediction structures whereas the remaining 85% (70% for training + 15% for testing purposes) is managed by the K-Fold process. The main goal of K-fold is to obtain 5 different prediction models per prediction structure. Each model will be derived considering 4 folds as training data and 1 fold as testing values. The key point is that the folds vary for each model. Therefore, at the end of the training process it can be assured that at least one of the models has been trained with a dataset as equilibrated as possible. This model will be then considered to implement the ECAPS effluent prediction structure. In that manner, the unbalanced data issues can be

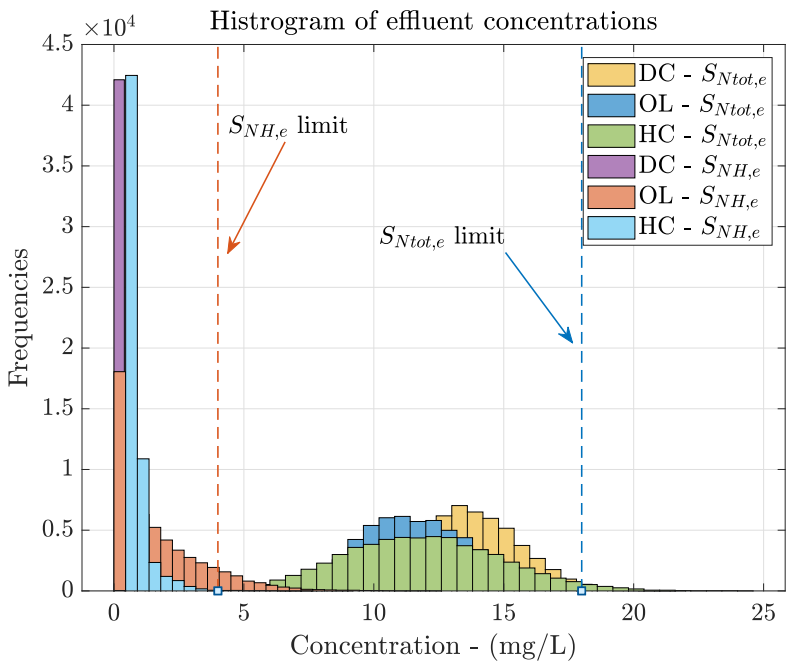

Figure 4.5: Histogram of effluent predictions. The three different control scenarios considered to train the ECAPS Effluent Prediction block are shown.

tackled without losing the time-dependence of measurements. Moreover, although K-fold splits the data in different subsets, it is respectful with the time correlation. The previous sliding window organises the measurements in time preserving the time-dependence. Moreover, the subsets considered in K-fold are divided in a way where training subsets represent consecutive measurements.

4.2.3 Alarm Generation block

The aim of the Alarm Generation block is to generate the alarm whenever the predicted effluent violations, $S_{NH,e}$ and $S_{Ntot,e}$ in this case, exceed the given thresholds, $\gamma_{S_{NH,e}}$ and $\gamma_{S_{Ntot,e}}$, respectively. These thresholds act as two degrees of freedom of the Alarm Generator block. They allow the plant operator to decide the sensitivity of the alarm generator, i.e., the level of trust for the predictions. If predictions are fully trusted, thresholds can be set to the effluent limits, i.e., 18 mg/L and 4 mg/L for $S_{Ntot,e}$ and $S_{NH,e}$, respectively. Otherwise, the thresholds can be decreased to be more cautious, i.e., detect more violations at the expense of generating alarms when violations are not really performed. This entails an improvement in terms of the probability of detection (P_d) and an increment of the probability of false alarm (P_{fa}) (generating an alarm when the effluent does not cause a violation). As a consequence, the overall costs will be increased since more actuations will be carried out when they are not necessary. P_{fa} and P_d are computed as

$$P_{fa} = P(\widehat{y} \geq \gamma_x | y < \gamma_x) \qquad P_d = P(\widehat{y} \geq \gamma_x | y \geq \gamma_x) \tag{4.2}$$

where $\widehat{y}$ here represents either the $S_{NH,e}$ or $S_{Ntot,e}$ predictions. γ_x denotes the threshold for the considered concentration. $P(x|y)$ corresponds to the conditional probability of x given y.

The Alarm Generator shows a trade-off between the alarm prediction accuracy and the overall costs. The lower the thresholds, the higher the number of false alarms and the higher the costs. In that sense, the Receiver Operating Characteristic (ROC) provides the comparative between the probability of detecting real alarms compared to the probability of generating false ones. Both of them as a function of the threshold values.

4.2.4 ECAPS Performance

ECAPS performance is computed considering data from BSM2 framework when OL, DC and HC control strategies are considered. For each strategy the prediction accuracy as well as the alarm generator performance is provided. The former is computed in terms of the RMSE, MAPE and R^2 metrics whereas the latter is computed in terms of the P_{fa} and P_d probabilities when $\gamma_{S_{NH,e}}$ = 4 mg/L and $\gamma_{S_{Ntot,e}}$ = 18 mg/L. Thus, the thresholds are chosen as the effluent limit values, but they may be lower. ROC curves are also provided. Results of the ECAPS performance for each control scenario are shown in Table 4.2.

Notice that ECAPS has not been still deployed over the BSM2 framework. It has been derived and tested considering only BSM2 measurements.

ANN-based Soft-sensor prediction performance

In terms of predictions, results clearly show that the proposed soft-sensor is able to perform good enough predictions of the pollutants of interest. If RMSE and MAPE values are considered, it can be clearly observed that the best behaviour is obtained when ECAPS is tested over the HC scenario. Its RMSE and MAPE values equal to 0.12 mg/L and 5.96%, respectively, when the HCPS-NH is adopted. If HCPS-NT is used instead, these values equal to 0.40 mg/L and 2.43%. On the other hand, the OL and DC performance experiences a degradation with respect to HC when $S_{NH,e}$ violations are forecasted. Incremented from 5.96% to 21.62% and 22.65%, MAPE values for OLPS-NH and DCPS-NH lead to the notion that very poor predictions are generated. However, RMSE values show that the experienced degradation is not as high as it seems. RMSE is increased by 0.16 mg/L and 0.03 mg/L when OLPS-NH and DCPS-NH are considered. In terms of the structures devoted to detecting $S_{Ntot,e}$ violations, no significant degradation is observed. MAPE values show that predictions errors are not high with respect to target $S_{Ntot,e}$ predictions. Being the OLPS-NT the structure yielding the lowest value, R^2 parameters show that all the ECAPS configurations correctly follow the tendency of the target concentrations.

From an operational point of view, the performance degradation is related to the variability of effluent concentrations. The largest peaks of $S_{NH,e}$ are obtained when the OL scenario is considered (see Figure 4.6). Moreover, this is the scenario showing the lowest number of $S_{Ntot,e}$ violations. Produced by the DC scenario control structures, the magnitude of $S_{NH,e}$ is reduced at the expense of increasing the vio-

Table 4.2: ECAPS performance. Notice that only results of the process yielding the best performance are shown. RMSE is measured in mg/L whereas MAPE is measured in %.

OL Scenario					
Configuration	RMSE	MAPE	R^2	P_{fa} (%)	P_d (%)
OLPS-NH	0.28	21.62	0.97	1.25	93.77
OLPS-NT	0.75	4.41	0.88	0.04	64.22
DC Scenario					
Configuration	RMSE	MAPE	R^2	P_{fa} (%)	P_d (%)
DCPS-NH	0.15	22.65	0.95	0.10	89.02
DCPS-NT	0.84	3.74	0.84	0.36	68.10
HC Scenario					
Configuration	RMSE	MAPE	R^2	P_{fa} (%)	P_d (%)
HCPS-NH	0.12	5.96	0.93	0.02	86.57
HCPS-NT	0.40	2.43	0.98	0.15	85.96

lations of $S_{Ntot,e}$. This is even more noticeable when HC control structures are adopted. The ammonium reduction achieved with the nitrification process and the HC control strategy increases the nitrates and therefore the total nitrogen amount. Figure 4.8 depicts this effect.

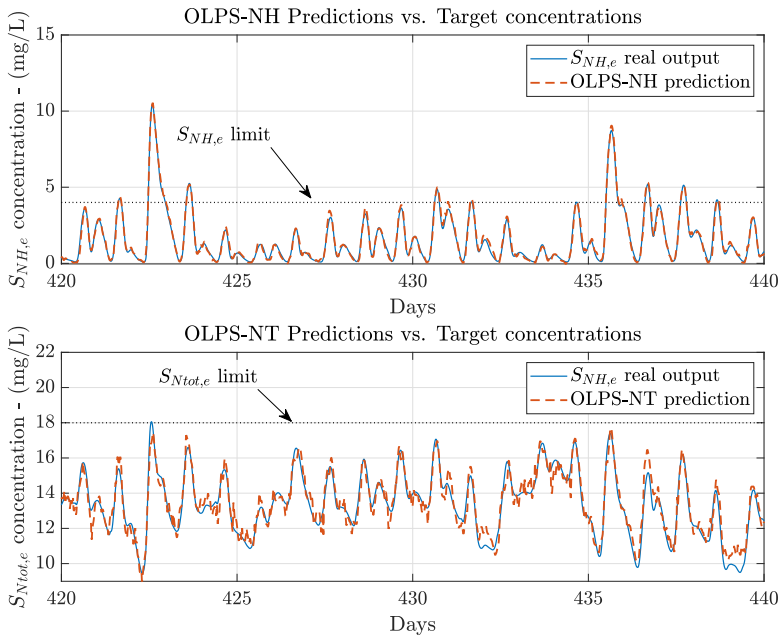

Figure 4.6: OL scenario prediction performance.

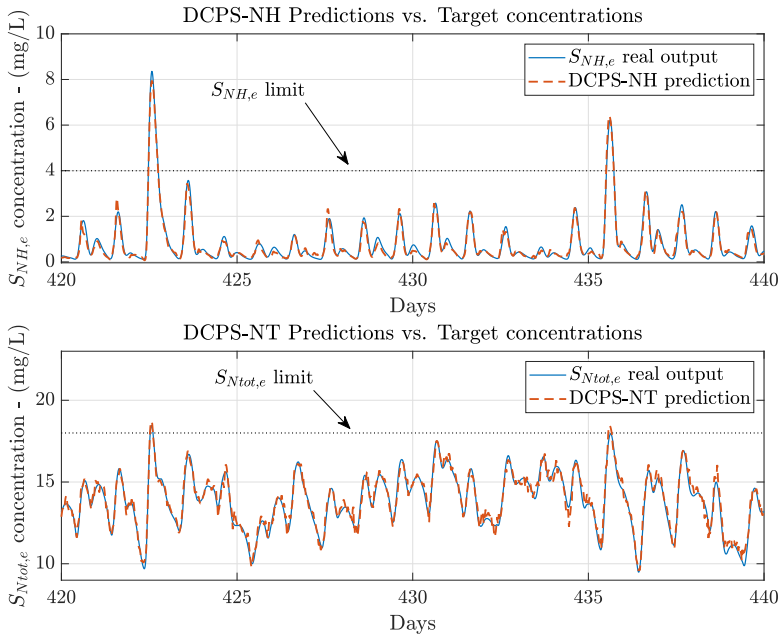

Figure 4.7: DC scenario prediction performance.

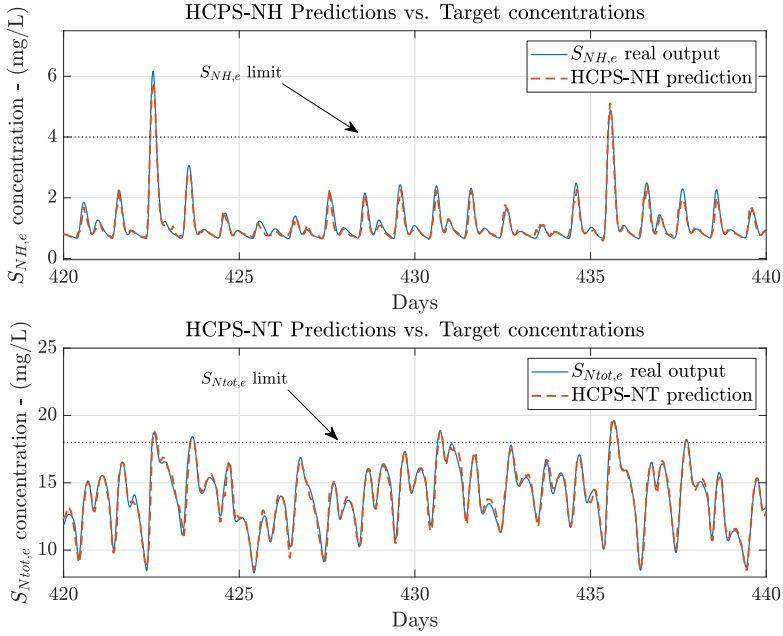

Figure 4.8: HC scenario prediction performance.

Alarm Generator performance

The Alarm Generator performance is also observed in Table 4.2. Probabilities of detection P_d and false alarm P_{fa} are computed according to $\gamma_{S_{NH,e}}$ = 4 mg/L and $\gamma_{S_{Ntot,e}}$ = 18 mg/L. Results show that leaving the thresholds as such entails a low P_d for most of the cases. Obtained when OLPS-NH structure is considered, the highest P_d equals to 93.77%. This means that most of the violations will be detected, however, some of them will be undetected. The situation is not better when other structures and scenarios are considered. For instance, in HC scenario, probabilities of detection equal to 86.57% and 85.96% for the HCPS-NH and HCPS-NT configurations, respectively. Similar P_d are obtained for the DCPS-NH. The highest issue is related to the P_d of structures predicting the $S_{Ntot,e}$. P_d for the OLPS-NT and DCPS-NT equal to 64.22% and 68.10%, which are very low values for the purpose of hazard prevention. In terms of the P_{fa}, all structures show low probabilities if $\gamma_{S_{NH,e}}$ and $\gamma_{S_{Ntot,e}}$ are equal to BSM2 effluent limits. Therefore, P_d probabilities have to be improved if ECAPS is devoted to predicting WWTP effluent violations.

This is performed by means of the ROC curves. Consisting in a tool relating P_d and P_{fa}, they are computed varying $\gamma_{S_{NH,e}}$ and $\gamma_{S_{Ntot,e}}$. ROC curves for OL, DC and HC scenarios are shown in Figure 4.9. They depict the behaviour of the Alarm Generator when its thresholds are varied. Figure 4.9e shows that a variation in the $\gamma_{S_{NH,e}}$ from 4 to 1 implies an increase not only in P_d but also in P_{fa}. Let's assume that $\gamma_{S_{NH,e}}$ is changed from 4 to 1. P_d will vary from 86.57% to 100% at expense of increasing P_{fa} from 0.02% to 18.38%. The same principle applies to the probability of detecting $S_{Ntot,e}$ violations. Changing the effluent threshold from 18 to 14 is translated into improving the probability of detection.

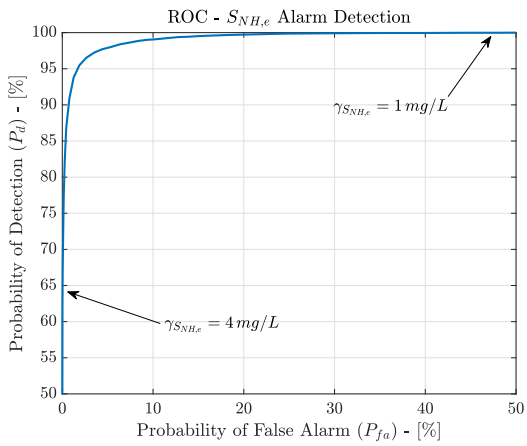

(a) ROC of OLPS-NH - AUC = 0.990

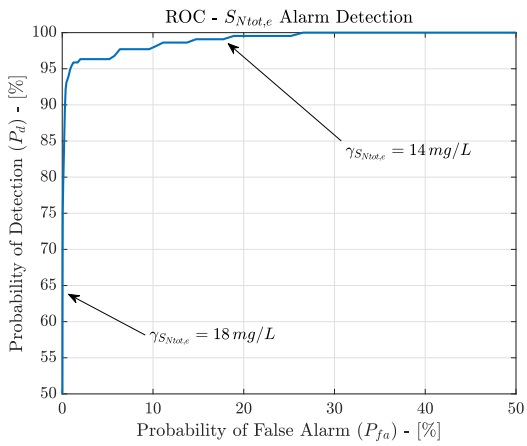

(b) ROC of OLPS-NT - AUC = 0.995

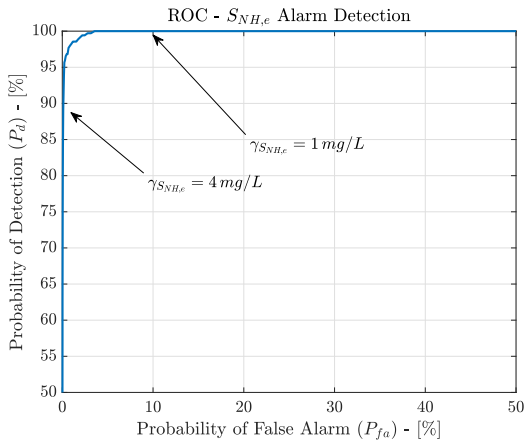

(c) ROC of DCPS-NH - AUC = 0.999

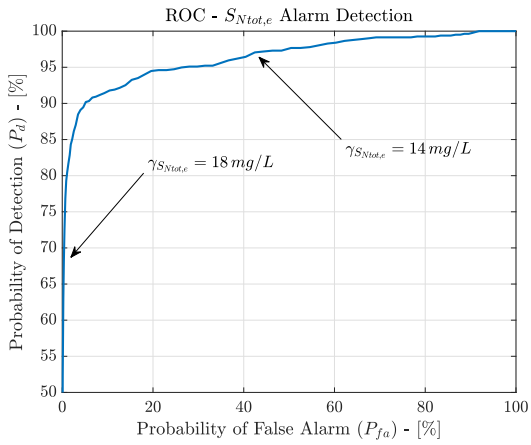

(d) ROC of DCPS-NT - AUC = 0.963

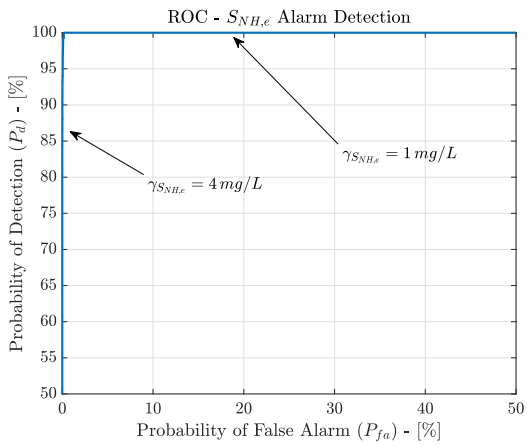

(e) ROC of HCPS-NH - AUC = 0.998

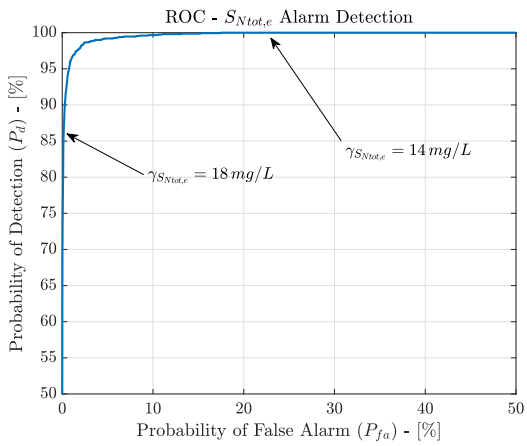

(f) ROC of HCPS-NT - AUC = 0.999

Figure 4.9: ROC Curves for OL, DC and HC scenarios.

For instance, OLPS-NH P_d is improved from 64.22% to 99.08%. Its P_{fa} is increased from 0.04% to 17.74%. However, the highest degradation in terms of P_{fa} is observed with the DCPS-NT configuration, where it is degraded from 0.36% to 42.65%. From an operational point of view, the modification of $\gamma_{S_{NH,e}}$ and $\gamma_{S_{Ntot,e}}$ entail that all future violations will be detected and therefore addressed by applying the correspondent control strategies. Nevertheless, the BSM2 overall costs will be increased needlessly due to the false positive violations. Thus, the operator of the plant has to deal with this trade-off: decide to detect all possible violations, even though false positives are also more likely to occur (the operational WWTP cost is increased), or assume some possible violations without increasing the operational cost.

Moreover, the Area Under the Curve (AUC) is computed as a metric complementing the P_d and P_{fa}. The closer to 1 the AUC, the better the performance. For instance, the OLPS-NH and OLPS-NT ROC curves yield AUCs around 0.990 and 0.995, respectively. These values are transformed into 0.999 and 0.963 for the DCPS-NH and DCPS-NT, respectively. In terms of the HC scenario, ROC curves provide AUC equal to 0.998 and 0.999 for the HCPS-NH and HCPS-NT configurations. Although P_{fa} is increased at expense of reducing the thresholds, ECAPS can still be adopted since the RoC curves show high AUC values.

4.3 ANN-based Operation Strategy

ECAPS performance when dealing with measurements from BSM2 framework has motivated their adoption as a complement of existent controllers. Until this section, ECAPS was neither deployed in BSM2 framework nor tested with control strategies. Thus, this section shows the benefits that can be obtained whenever ECAPS is considered as an extension of the work presented in Section 4.2. Here, a modified version of ECAPS without the Alarm Generator block directly feeding its predictions into control strategies is proposed and evaluated. This is performed by means of considering its interaction with control strategies managing the BSM2 framework.

It is also important to put into place the work contribution from the WWTP operation point of view. One of the appealing aspects of proposing ECAPS to support control structures is that it can be understood as an additional decision layer that can improve existing operation. Moreover, the performance improvement that it may provide with respect to existing approaches is also a key motivator. In that sense, ECAPS does not ask for changes in instrumentation nor in already existing control equipment, either software or hardware. Requiring measurements from usual control-loops, it allows the dissociation of pollutant concentrations predictions from the WWTP architecture. With them, ECAPS builds up operation decisions on the basis of predicted $S_{NH,e}$ and $S_{Ntot,e}$ violations. Thus, not only will the potential improvement provided by ECAPS reside on the reduction of effluent limit violations, but it also comes from its ease of deployment.

4.3.1 Control Strategy Enhancement

The proposed control strategy enhancement consists in the application of a modified version of ECAPS to support control strategies. Now, its Alarm Generator block is not needed any more since alarms will not be processed by the WWTPs operator. The ECAPS ANN-based soft sensor effluent predictions will be directly fed into the existent control strategies. In that sense, alarms will be directly managed by the existent control actuations without the intervention of the WWTP operator. $S_{NH,e}$ and $S_{Ntot,e}$ violations will be implicitly provided to the control strategy through the forecasted concentration value. This enhancement will provide a twofold benefit: (i) control strategies will actuate only when they are really necessary, and (ii) the actuations will be determined directly by the effluent predictions of the ANN-based soft-sensor.

Here, the ANN-based soft-sensor consists in the HCPS-NH and HCPS-NT configurations depending on the violations under consideration. As it is shown in Table 4.2, results show that these configurations are able to generate highly accurate predictions of ammonium and total nitrogen four hours in advance. The lowest RMSE equals to 0.12 mg/L and 0.40 mg/L for $S_{NH,e}$ and $S_{Ntot,e}$ predictions, respectively, when the soft-sensor is trained with the high-level control strategy data. In that sense, four different WWTP scenarios will be considered to determine the level of improvement that can be reached:

- **Default Scenario (DS)**: Non-predictive control scenario adopting the DC control configuration. It does not consider the ANN-based Soft-Sensor. It is worth remembering that carbon added to the first tank ($q_{EC,1}$) is maintained fix at a constant flow rate of 2 $\mathrm{m}^3/\mathrm{day}$.
- **Hierarchical Scenario (HS)**: Non-predictive control scenario which corresponds to the BSM2 control extension proposed by Nopens *et.al* [Nop10]. It is depicted in Figure 3.6. It does not consider the ANN-based Soft-Sensor. The amount of carbon added to the first tank ($q_{EC,1}$) is maintained fix at a constant flow rate of 1 $\mathrm{m}^3/\mathrm{day}$.
- **ANN-based Soft-Sensor $S_{NH,e}$ reduction scenario (ASS-NHRS)**: Predictive control scenario which is focused on reducing $S_{NH,e}$ violations varying the Q_a (Figure 4.1a). The MLP-based Soft-sensor is substituted by the HCPS-NH ANN-based soft-sensor configuration. In this case, carbon is only added when the control strategy actuates over the pollutant under control, therefore, costs derived from the addition of external carbon are directly related to the performance of the control strategy. Here, ECAPS ANN-based soft-sensor input variables differ from the ones considered in ECAPS system. $S_{NH,p}$, Q_{po} and T_{as} are maintained, however, the product between $S_{NH,p}$ and Q_{po} is considered due to its appearance in the mass-balance equations shown in [Hen87]. Q_a is discarded since this strategy modifies Q_a to reduce the amount of ammonium. The soft-sensor is calibrated to detect violations whenever $\gamma_{S_{NH,e}}$ exceeds 4 mg/L.
- **ANN-based Soft-Sensor $S_{Ntot,e}$ reduction scenario (ASS-NTRS)**: Predictive control scenario which is focused on reducing the total nitrogen violations (Figure 4.1b). The MLP-based Soft-

sensor is substituted by the HCPS-NT ANN-based soft-sensor configuration. External carbon is only added to tanks 1, 2 and 5 when the control strategy actuates over the pollutant under control. Consequently, costs derived from the addition of external carbon are directly related to the performance of the control strategy. The more violations detected, the more external carbon required. Thus, the minimisation of false violation detections is of utmost importance. ECAPS ANN-based soft-sensor inputs equal to the ones adopted in ECAPS. Besides, the product between $S_{NH,p}$ and Q_{po} is also considered. The soft-sensor has been calibrated to detect violations whenever $\gamma_{S_{Ntot,e}}$ exceeds 17 mg/L. Thus, more violations will be detected at the expense of allowing false positives.

4.3.2 Environmental Performance

BSM2 environmental performance is computed for the four different predictive control scenarios to determine the improvement achieved with the adoption of the ECAPS ANN-based soft-sensor. Results are shown in Table 4.3, where OCI, $S_{Ntot,e}$ and $S_{NH,e}$ violations are computed. They are compared to results presented in [Jep07] and [Nop10] to determine the improvement due to the increment in the control complexity. At first sight, it is clearly observed that the environmental performance depends on the variable under control, i.e., if the control structure is proposed to remove violations of $S_{NH,e}$ or $S_{Ntot,e}$. Results show that both structures, ASS-NHRS and ASS-NTRS, are able to totally remove the concentrations they are in charge of at the expense of allowing violations of the non-controlled pollutants.

Focusing on ASS-NHRS, one can observe that $S_{Ntot,e}$ violations have increased 1.57 percentage points with respect to DS control strategy. This effect is motivated by the fact that whenever a violation of $S_{NH,e}$ is predicted, the control strategy modifies the Q_a flow rate increasing the amount of sludge and dissolved oxygen in the anoxic tanks. Therefore, the nitrates concentrations are worsened increasing the levels and violations of total nitrogen [San16]. OCI is reduced a 37.2% since the control strategy is only applied when a violation is detected whilst it is continuously applied in DS and HS strategies. ASS-NHRS is also able to improve EQI reducing it a 3.30% with respect to DS motivated by the reduction of ammonium violations. Figure 4.10 shows the detection and reduction of a future $S_{NH,e}$ violation. Showing an offset of four hours with respect to predicted measurements, real ones depict the evolution of effluent concentrations in real time. For instance, the pollutant peak predicted at day 560.3 corresponds

Table 4.3: Environmental performance - DS, HS, ASS-NHRS and ASS-NTRS comparison. Effluent violation limits are measured in % of time that the limit is violated. $S_{Ntot,e}$ violation are not provided for results presented in [Nop10].

Scenario	EQI	OCI	$S_{Ntot,e}$ violation [%]	$S_{NH,e}$ violation [%]
DS [Jep07]	5577.97	9447.24	1.18	0.41
HS [Nop10]	5274	8052	N/A	0.23
ASS-NHRS	5394.11	5932.83	2.75	0
ASS-NTRS	5235.31	6547.21	0	0.14

to the peak measured at day 560.6 approximately.

In terms of ASS-NTRS, it is observed that $S_{Ntot,e}$ violations are completely removed. However, the $S_{NH,e}$ limit is violated a 0.14% of the BSM2 operational time. This percentage represents a reduction of violations equivalent to 0.27 and 0.09 percentage points with respect to DS and HS results, respectively. EQI measurement is also improved a 6.14%, a 2.94% and a 0.37% with respect to DS, ASS-NHRS and HS, respectively. Moreover, OCI is increased a 9.38% with respect to ASS-NHRS control strategy as it is shown in Table 4.3. Motivated by the predictions of violations, the control strategy adds external carbon to the first, second and fifth reactor tanks [San16]. In addition, if OCI is compared with DS and HS, it is observed that it has been reduced a 30.70% and an 18.69%, respectively. This is due to the fact that DS an HS are continuously adding carbon at a flow rate of 2 and 1 $\mathrm{m}^3/\mathrm{day}$ whilst ASS-NTRS does not. Finally, an example of a $S_{Ntot,e}$ violation removal process is shown in Figure 4.10 where a violation occurs at day 559.4 if the proposed predictive control is not adopted. In this case, the ECAPS ANN-based soft-sensor is able to predict it at day 559.2. Thus, the control strategy actuates achieving the reduction of $S_{Ntot,e}$ levels in the effluent avoiding the violation.

In terms of the number of violations, the same effect is observable for both structures, ASS-NHRS and ASS-NTRS. Their average and their standard deviation are shown in Table 4.4. For instance, $S_{Ntot,e}$

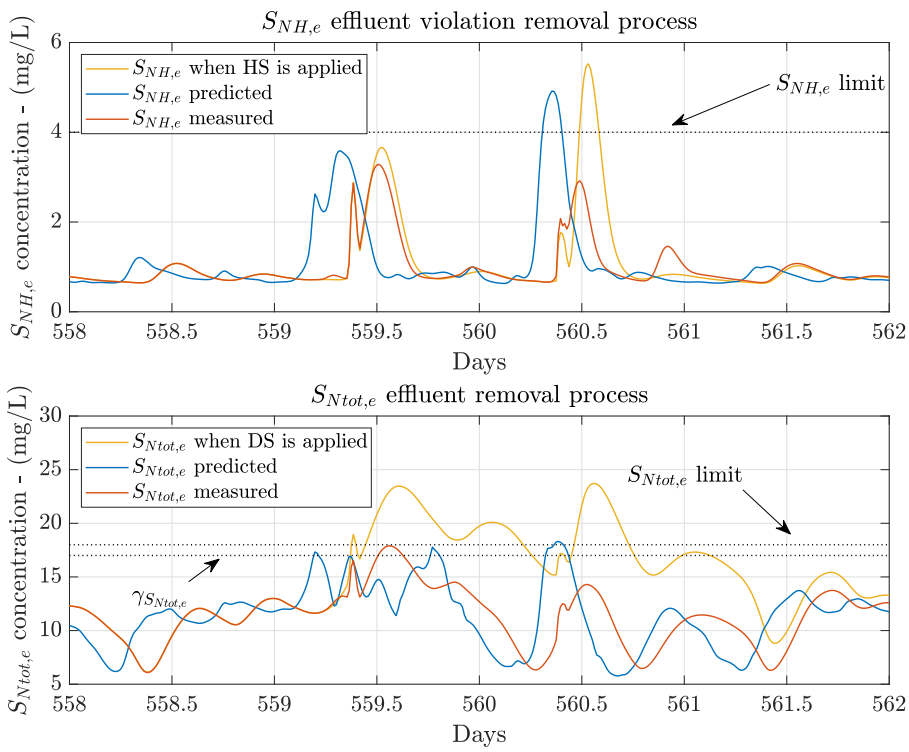

Figure 4.10: Effluent violations removal process. Both concentrations, when DS and HS scenarios are applied, are present to show that if no prediction is performed, $S_{NH,e}$ and $S_{Ntot,e}$ would incur into violations. $\gamma_{S_{Ntot,e}}$ = 17 mg/L.

Table 4.4: Number of violations, average of violation levels and standard deviation. Maximum violations, μ and σ are measured in mg/L.

$S_{Ntot,e}$ violations				
Strategy	Number	Maximum	μ	σ
DS [Jep07]	29	21.69	18.95	0.84
HS [Nop10]		N/A		
ASS-NHRS	49	23.47	19.62	1.31
ASS-NTRS		-		
$S_{NH,e}$ violations				
Strategy	Number	Maximum	μ	σ
DS [Jep07]	11	8.36	5.49	1.34
HS [Nop10]	4	6.16	5.63	0.56
ASS-NHRS		-		
ASS-NTRS	4	5.46	4.98	0.62

violations are completely removed in ASS-NTRS scenario. Nevertheless, they have been increased in the case of ASS-NHRS. In terms of $S_{NH,e}$, they have been removed in the case of ASS-NHRS and reduced from 11 to 4 in the case of ASS-NTRS. Furthermore, their maximum level has been significantly reduced from 8.36 in DS scenario to 5.46 in ASS-NTRS. As a summary, the adoption of the ECAPS ANN-based soft-sensor entails the improvement of the control strategies performance in terms of the percentage of time that concentrations under control are violated, the amount of violations and their maximum levels.

4.3.3 ASS-PRS Performance

As it is observed, ASS-NHRS and ASS-NTRS are able to control and correctly reduce the effluent violations of the concentration they have been designed for. However, violations of the non-controlled pollutant are sometimes increased degrading the EQI and OCI parameters. For instance, $S_{Ntot,e}$ concentration is increased when the $S_{NH,e}$ control actuation is applied. As a consequence of varying the Q_a to reduce $S_{NH,e}$ violations, the amounts of sludge and dissolved oxygen are increased in the anoxic tanks. This is translated into the rise of the concentrations of nitrates and total nitrogen [San16]. This example shows that some actuations controlling a unique pollutant concentration are counterproductive for the others. For that reason, a WWTP has to be observed as a whole system where control actuations have to be applied simultaneously. Following this point, the ANN-based Soft-sensor Pollutant Reduction Scenario (ASS-PRS) is proposed (see Figure 4.11). Unifying the ASS-NHRS and ASS-NTRS control strategies, its main aim is to reduce effluent peaks for $S_{NH,e}$ and $S_{Ntot,e}$ simultaneously. Predictions performed with the ANN-based soft-sensor will determine when the control strategies based on MPC and FLC have to be applied. In that manner, when the actuation over a pollutant increases the concentrations of the other, the control strategy will automatically reduce its concentration to avoid the limit violation. Notice that in this new control scenario, modifications of Q_a could produce an incorrect prediction of

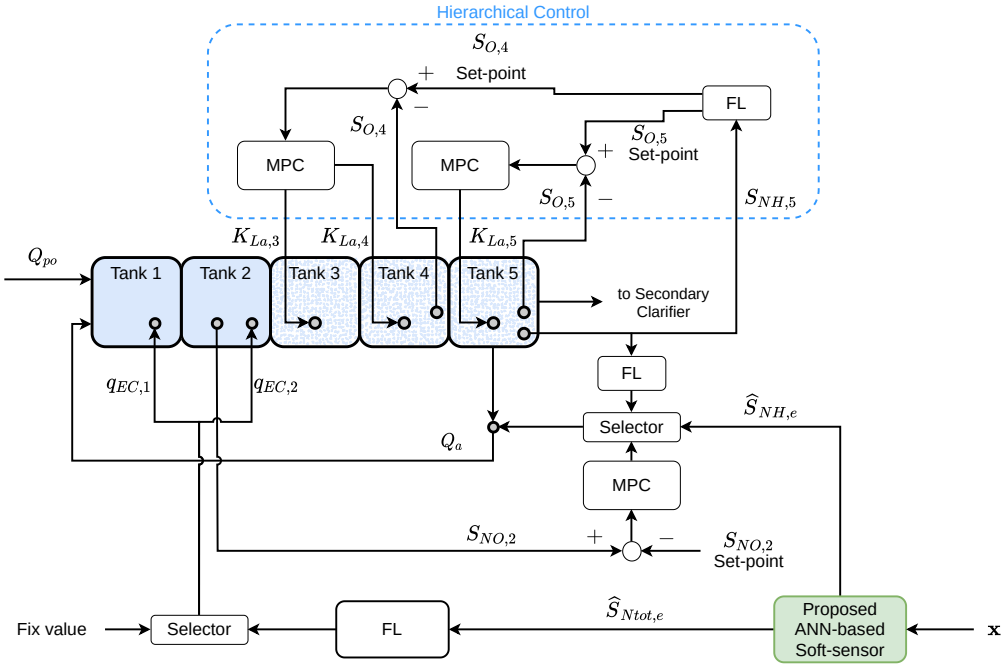

Figure 4.11: ASS-PRS Scenario.

$S_{Ntot,e}$ since it is acting as an input of the ECAPS ANN-based soft-sensor.

First, performance is computed without retraining the ECAPS ANN-based soft-sensor, i.e., without taking into account the Q_a modifications performed in the $S_{NH,e}$ violations removal process. Results in Table 4.5 show that a reduction of the number of violations is achieved. However, they are not completely removed with respect to DS: (i) $S_{Ntot,e}$ violations are reduced 1.1 percentage points, which represent violations during the 0.08% of the BSM2 simulation time, and (ii) $S_{NH,e}$ violations are reduced 0.396 percentage points, which are equal to violations during 0.014% of the same period of time. Violations cannot be completely removed because when varying Q_a, the levels of nitrate in the anoxic tanks are increased. This is translated into a trade-off between the $S_{NH,e}$ reduction and the levels of $S_{Ntot,e}$: when violations of $S_{NH,e}$ are reduced, the levels of $S_{Ntot,e}$ are increased and consequently the probability of observing violations (see Figure 4.12). Besides, the ECAPS ANN-based soft-sensor predicting $S_{Ntot,e}$ has not been trained considering these Q_a variations. Consequently, predictions of $S_{Ntot,e}$ are not accurate in those points where a violation of $S_{NH,e}$ is predicted.

Table 4.5: WWTP's performance - DS and ASS-PRS comparison

Scenario	EQI	OCI	$S_{Ntot,e}$ violation [%]	$S_{NH,e}$ violation [%]
DS [Jep07]	5577.97	9447.24	1.18	0.41
HS [Nop10]	5274	8052	N/A	0.23
ASS-PRS	5236.72	6633.73	0.08	0.014
ASS-PRS retrained	5218.76	6671.99	0.02	0.014

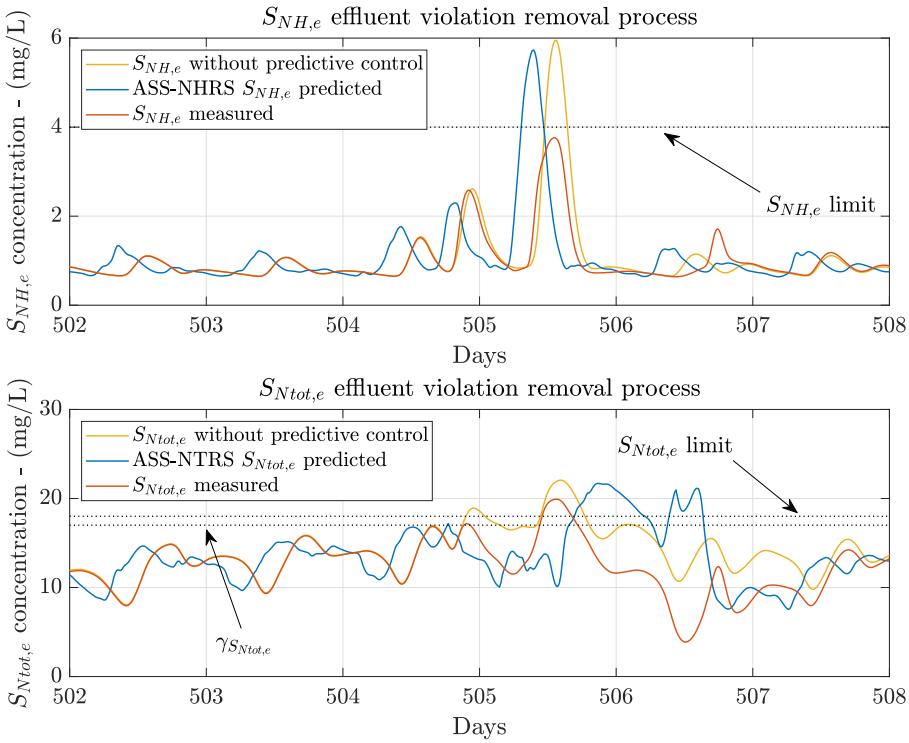

Figure 4.12: $S_{NH,e}$ violation predicted at day 505.4. Q_a will be modified to reduce the effluent peak before day 505.6. Consequently, $S_{Ntot,e}$ is badly predicted since the variations of Q_a have not been considered in the ANN-based soft-sensor training process.

To solve this, the soft-sensor is retrained when a whole year simulation is performed. Results in Table 4.5 show that the number of $S_{Ntot,e}$ violations is reduced a 75% when the ANN-based Soft-Sensor is retrained. $S_{NH,e}$ predictions do not vary since no action is performed on the considered input variables. In terms of EQI and OCI, the former is decreased a 0.34% whereas the latter is increased a 0.57% with respect to the situation where the ECAPS ANN-based soft-sensor is not retrained. Finally, if the performance of ASS-PRS is computed in terms of the percentage of operational time that an effluent is violated, an improvement of 98.31% in the reduction of $S_{Ntot,e}$ and a 96.58% for $S_{NH,e}$ with respect to DS scenario is achieved. It equals to a 99.27% for $S_{Ntot,e}$ and 90% for $S_{NH,e}$ in terms of ASS-NHRS and ASS-NTRS, respectively. Moreover, it is worth noting that, although the complete avoidance of violations is not achieved, they represent a low percentage of the BSM2 operational time. Equalling to a 0.014% of BSM2 simulation time, a unique violation of $S_{NH,e}$ is produced at day 410.5. $S_{Ntot,e}$ is violated two times, at days 384.4 and 560.5, which only represents a 0.02% of the BSM2 operational time. In such a context, Figure 4.13 and Figure 4.14 show the differences between the violations that occurred in ASS-NTRS, ASS-NHRS and ASS-PRS. In Figure 4.13, it is observed that violations performed in ASS-PRS scenario are much lower than those produced in ASS-NHRS. This is mainly motivated by the improve quality of the ANN-based soft-sensor predictions. Now, the violations reach $S_{Ntot,e}$ values of 18 mg/L and 18.12 mg/L at days 384.4 and 560.5, respectively.

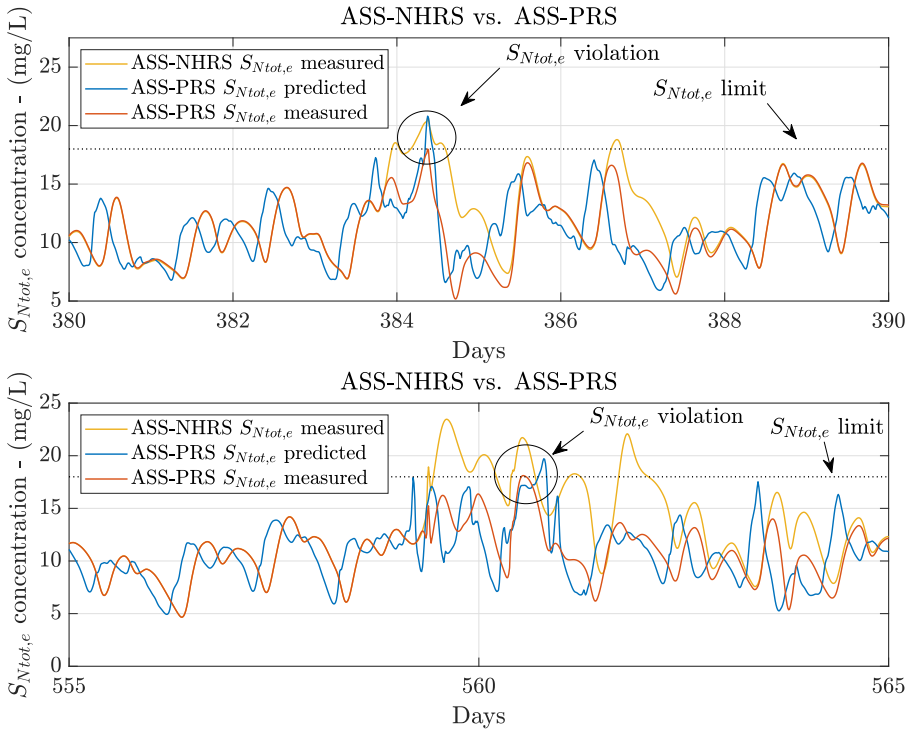

Figure 4.13: Comparative between violations produced in ASS-NHRS and ASS-PRS scenarios. Violations are highly reduced when ASS-PRS is considered. Moreover, violation levels are highly reduced.

On the other hand, Figure 4.14 compares the $S_{NH,e}$ violation obtained in ASS-PRS with the same violation performed in the ASS-NTRS scenario. In this case, both violations are produced because the level of ammonium reaches 4.177 mg/L. Both are produced by the actuation performed over $S_{Ntot,e}$ at day 410.5, where a violation of total nitrogen is predicted and reduced. This is clearly shown in Table 4.6, where the amount of violations has not changed from ASS-PRS to ASS-PRS retrained. The improvement here is shown in the average of violations and their maximum. For instance, ASS-PRS $S_{Ntot,e}$ maximum violation equals to 19.92 mg/L while in ASS-PRS retrained it has been reduced until 18.12 mg/L. Moreover, the average of violations (μ) has been reduced from 19.17 mg/L (ASS-PRS) to 18.06 mg/L (ASS-PRS retrained).

As a summary, the application of ASS-PRS scenario entails the reduction of the % of time that effluent concentrations are exceeding the BSM2 limits. Effluent violations are reduced between 0.216 and 0.396 percentage points for $S_{NH,e}$ and between 1.1 and 1.16 percentage points in the case of $S_{Ntot,e}$. The reduction of pollutant concentrations and the avoidance of violations also help in the improvement of the EQI metric: the lower the pollutant concentrations, the better the EQI. For instance, the ASS-PRS retrained scenario is the one showing the lowest pollutant concentrations and consequently the lowest EQI, 5218.76 Kg $\cdot$ pollutant units $\cdot$ day^{-1}. In terms of OCI, ASS-PRS scenario only adds external carbon when an effluent limit violation is predicted. Therefore, this is translated into an improvement (reduction)

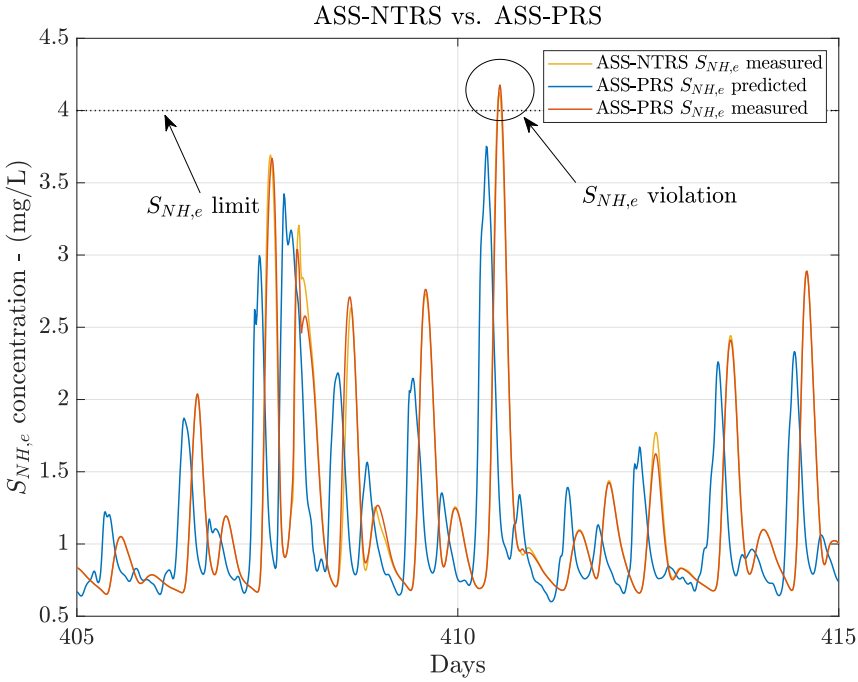

Figure 4.14: $S_{NH,e}$ unique violation produced at day 410.5. Notice that although the $S_{NH,e}$ violation, its level is not as high as it was before.

of the WWTP's OCI with respect to DS and HS control scenarios where its maximum improvement equals to a 29.78% with respect to DS.

Table 4.6: Number of violations, average of violation levels and standard deviation. Maximum violations, μ and σ are measured in mg/L.

$S_{Ntot,e}$ violations				
Strategy	Number	Maximum	μ	σ
DS [Jep07]	29	21.69	18.95	0.84
HS [Nop10]		N/A		
ASS-PRS	2	19.92	19.17	1.06
ASS-PRS retrained	2	18.12	18.06	0.08
$S_{NH,e}$ violations				
Strategy	Number	Maximum	μ	σ
DS [Jep07]	11	8.36	5.49	1.34
HS [Nop10]	4	6.16	5.63	0.56
ASS-PRS	1	4.13	4.13	-
ASS-PRS retrained	1	4.13	4.13	-

4.4 Chapter Conclusions

In this chapter the adoption of ANN-based soft-sensors in WWTP environments has been addressed. Based on LSTM cells, ECAPS system is proposed to achieve twofold objectives: (i) the prediction of WWTP effluent concentrations with a good enough accuracy, and (ii) the generation of alarms whenever an effluent limit is violated. For that purpose, ECAPS system consists in an ANN-based soft-sensor and an alarm generation block. The former is implemented with a data preprocessing and an effluent prediction block to predict effluent concentrations whilst the latter contrasts the predictions with the given limits. The data preprocessing block is devoted to gathering, standardising and sorting the measurements from the WWTP scenario. Implemented with LSTM cells, the effluent prediction block takes the measurements from the data preprocessing block and performs the effluent predictions. In that sense, LSTM cells have been trained considering the K-Fold cross-validation technique, not only to achieve a good generalisation of the predictive model, but also to tackle the unbalanced data issue usually observed at industrial scenarios. Finally, the performance of the proposed system has been assessed considering two operational cases, when the proposed system is considered to generate effluent violations alarms, and when its effluent predictions are considered to support WWTP operations.

Concerning the generation of alarms, results show that the proposed system is able to detect an 86.57% of $S_{NH,e}$ violations and an 85.96% of $S_{Ntot,e}$ ones when the WWTP is being managed by a hierarchical control structure. Besides, these accuracies can be improved at the expense of allowing false alarms. For instance, a 100% of $S_{Ntot,e}$ and $S_{NH,e}$ violations can be detected by lowering the effluent limits from 18 mg/L to 14 mg/L in the case of $S_{Ntot,e}$ and from 4 mg/L to 1 mg/L in the case of $S_{NH,e}$. Nevertheless, this entails the augmentation of false alarm probabilities from 0.02% to 18.38% and from 0.15% to 23.45% for the $S_{NH,e}$ and $S_{Ntot,e}$ alarms, respectively.

On the other hand, the complete reduction of effluent violations is achieved when ECAPS is applied to support existent controllers. It is able to generate predictions with enough time to let the control actuation reduce the effluent concentrations for which ECAPS has been designed for. Moreover, a new structure is proposed to manage effluent violations simultaneously. Results show that if nothing is performed, this new structure is able to reduce $S_{NH,e}$ violations but not the $S_{Ntot,e}$ ones. To achieve this, a retraining of the prediction structure is required. New results show that although a complete reduction of effluent violations is not accomplished, these are much lower than before. Representing a 0.02% and a 0.014%, there are still one violation of $S_{NH,e}$ and two violations of $S_{Ntot,e}$. The key point is that operational costs and effluent quality are improved with respect to different approaches from the literature considering such a low-cost ANN-based solution.

Chapter 5

ANNs in the Design of Industrial Controllers

One of the sectors where the power of ANNs can be highly exploited corresponds to the design of industrial controllers. ANNs have been considered to implement soft-sensors able to feed conventional controllers, but their adoption in industrial environments can go beyond. Thus, the adoption of ANNs to design and implement PI and IMC controllers is assessed in this chapter. As controllers relying on data, their performance depends on the quality of measurements and signals involved in the control process. Therefore, the assessment of these structures with ideal and non-ideal measurements is provided in this chapter as well.

5.1 Introduction

WWTP environments are characterised by their huge amount of control loops devoted to maintaining the operational conditions required to assure a correct pollutant reduction process. This is mainly performed by means of different control strategies such as PID, MPCs, FLCs or IMC control structures. The problem observed with these conventional controllers lie in the fact that they require a model which replicates the relationships between input and output measurements. Besides, most of the time, these relationships consist in non-linear relations which are difficult and tedious to model. This is where ANNs come in, since they are algorithms offering good performance when dealing with such kinds of relationships [Goo16, Chapter 6]. The first approach consists in the adoption of ANNs as elements whose predictions are adopted by conventional control structures. For instance, the solution proposed in [San15a] has been improved with the proposal defined in Chapter 4, where LSTM cells have been adopted to predict the WWTP effluent concentrations and determine when and which controller has to actuate. In other cases, neural networks have been considered to directly determine the optimal set-point values adopted by conventional controllers [Sad18] or to implement a Reinforcement Learning module performing the

same task [Olm18]. As observed, the power of ANNs is adopted to support conventional control structures. Thus, this raises the following question: can industrial controllers be based on data and ANNs?

Some works in the literature have tried to give an answer to it [Qia18, Vil18]. For instance, in [Qia18], an adaptive fuzzy neural network has been considered to track the optimal set-points of the dissolved oxygen in the WWTP fifth reactor tank and the nitrate-nitrogen in the second one. In [Vil18], two event-based IMC structures were implemented to later derive two PI structures devoted to managing the $S_{NO,2}$ and the $S_{O,5}$ WWTP concentrations. Despite their good behaviour and control performance, these strategies are based on mathematical models of the process under control and therefore, they rely on highly complex and non-linear processes. Here is where ANN-based methods can score the point. ANNs can be exploited to reduce the dependency on mathematical models. Indeed, the adoption of ANNs as part of control strategies is motivated by most of the key points of the Industry 4.0 paradigm [Ust17, Chapter 2]. New cloud technologies and the adoption of cyber-physical systems are two use-cases where the adoption of ANNs is a reality. Moreover, ANNs have arisen as new approaches able to offer a good control performance at the same time they increase the scalability and decoupling of the control strategy from highly complex mathematical models [Lan19, Che19, Hua20, Agu18, Wan18, Kas18]. In that sense, IMC structures are one of the control configurations which can benefit more from such kind of data-based methods. Instead of deriving conventional control structures from the IMC configuration, it can be directly implemented by means of ANNs. This yields into an easy implementation and good performance, especially in tracking purposes [Li19b]. For instance, in [Kan18] an ANN-based IMC controller is in charge of regulating and managing the lights and their intensity in an office environment. Results show that this structure can achieve potential energy savings around a 54% and a 40% with respect to the baseline situation where all the lights of the environment show the same intensity. Nonetheless, the control actuation not only will benefit from the power of ANNs, but also by the decoupling of the control actuation [Wan18, Kas18]. This is possible thanks to the IMC configuration. For instance, in [Wan18], an inverse system formed by static neural networks and an IMC structure are proposed to generate a decoupling control method for the active front steering and suspension subsystems of an autonomous vehicle. At the same time, in [Kas18], two IMC-based structures are proposed to develop the control of two interconnected thermal power systems, which present a strong coupling between them due to their interconnectivity. The good results as well as the decoupling achieved by the ANN-based IMC structure has motivated their implementation in the WWTP domain.

Taking all the aforementioned points into account, this chapter of the thesis is devoted to analysing the behaviour and issues that arise as a consequence of implementing ANN-based controllers able to track the desired set-points of the BSM1 $S_{O,5}$ control loop. The first approach consists in the development of two ANN-based PIs replicating the behaviour of the default BSM1 PI controllers. Later, ANNs are considered to implement an IMC structure. To achieve this, LSTM nets will be considered to implement the direct, $P_{dir}(s)$ and inverse models, $P_{inv}(s)$ of the IMC structure. Inversely from the ANN-based PI, the ANN-based IMC controller is implemented from scratch. For that reason, its stability must be ensured.

This is motivated by the fact that WWTP processes present unmodelled dynamics, uncertainties and non-linearities that could compromise the controller's stability [Li19a]. However, classical stability tests cannot be performed since the proposed ANN-based IMC controller only relies on data obtained from the real process. Therefore, a stability test based on the Empirical Transfer Function Estimation (ETFE) of the signals involved in the control process will be adopted [Roj12a]. The assessment of both ANN-based controllers will be performed considering two scenarios: (i) the ideal, and the (ii) real one. The appearance of non-idealities in real scenarios is inevitable and consequently, they must be considered. This is of utmost importance in structures which rely on measurements obtained from the environment. Since ANNs are one of them, one must be aware that these non-idealities could produce a drastic drop in the control performance of ANN-based controllers.

As a summary, the contributions of this chapter are:

- Data-driven methods are considered to model the highly complex and non-linear WWTP processes.
- Conventional PI controllers are substituted by ANN-based controllers, especially, ANN-based PIs and ANN-based IMCs.
- The stability analysis of the proposed structure is performed to determine if it is suitable to control the DO.
- The required knowledge of the process under control is reduced since the ANN-based structures only require input and output measurements either of the conventional controllers or the process under control. Besides, these measurements are easily obtained from the BSM1.

The rest of the chapter is structured as follows: in Section 5.2 the ANN-based PI structure design, implementation and performance over an ideal scenario is presented. Besides, the issues related to non-idealities of the measurements considered in the control process will be assessed here. In Section 5.3, the assessment of the ANN-based IMC is performed. Its prediction and control performance as well as its stability are computed for an ideal and a real environment. Finally, Section 5.4 concludes the chapter. This chapter encompasses the works presented in [Pis19a, Pis20c, Pis20b, Pis21d] and part of the work presented in [Pis20a, Pis21c].

5.2 ANN-based PI

The first approach consists in the assessment of ANNs as structures replicating the behaviour of the BSM1 default PI controllers. Therefore, two ANN-based PIs must be derived in order to manage the $S_{O,5}$ concentration in the DO control loop and the $S_{NO,2}$ one in the NO control loop. Hence, the two ANN-based PIs are:

- **DO ANN-based PI**: the first ANN-based PI controller corresponds to the DO ANN-based PI, which is derived from the PI managing the $S_{O,5}$ concentration.
- **NO ANN-based PI**: the second ANN-based PI corresponds to the NO ANN-based PI. It is derived from measurements of the default PI managing the $S_{NO,2}$.

Prior to their design and implementation, one could guess which ANN-based PI is prone to offer the best control performance. If the control behaviour of the default PI controllers is taken into account (see Figure 5.1), it can be observed that the best PI corresponds to the one managing the $S_{O,5}$, since it is able to maintain it at the desired value of 2 mg/L. On the other hand, the PI managing the $S_{NO,2}$ fails in its purpose of maintaining the desired set-point of 1 mg/L. Since the ANN are trained with measurements coming from the default control structures, the control performance of the ANN-based PIs will be similar to the default PI controllers. In other words, the better the conventional controller performance, the better the ANN-based one.

In that sense, it is worth remembering that BSM1 framework offers two kinds of simulations: (i) the ideal, and (ii) the real one. In the first case, the simulation of the WWTP behaviour is performed considering an ideal scenario where WWTP measurements are ideal. On the other hand, in a real simulation, the BSM1 framework considers real sensors, which return WWTP measurements corrupted with AWGN noise, $\omega_n \sim \mathcal{N}(0,1)$, and delays (see Section 3.1.1). For that reason, two different scenarios have been defined to assess the adoption of ANNs in the implementation of the ANN-based PI controllers:

- **Ideal Scenario**: The default PI controlling the BSM1 $S_{O,5}$ concentration is substituted by an ANN-based PI structure. Here, ideal sensors are considered.

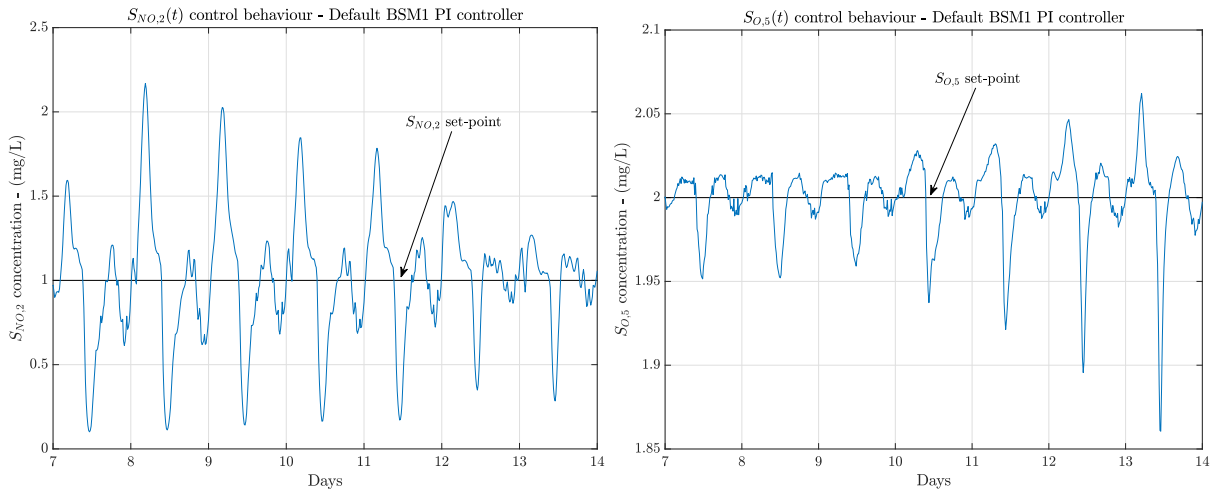

(a) $S_{NO,2}(t)$ Default BSM1 PI control performance.

(b) $S_{O,5}(t)$ Default BSM1 PI control performance.

Figure 5.1: Control performance when default BSM1 PI controllers are adopted. Notice that the worst performance is offered by the $S_{NO,2}(t)$ default PI controller.

- **Real Scenario**: This scenario considers the same ANN-based PI control strategy as in the ideal case. However, the sensors implemented here add noise and delays to the measurements. Thus, the ANNs trained with ideal data are no longer valid due to the non-linearities introduced by non-ideal sensors. This entails a new retraining process where the new non-ideal measurements are considered.

5.2.1 ANN-based Architectures

LSTM-based Architectures

The ANN-based PI controllers consider the ANN-based structure observed in Figure 5.2. This structure is obtained after performing a grid search methodology in the training process. The structure mainly consists in two LSTM cells devoted to extracting and obtaining information from the time correlation between the input and output measurements. In addition, each structure considers two MLP layers which transform the information provided by the LSTM cells into the desired outputs. Normalisation and Denormalisation stages are also considered in each structure in order to tackle the input measurements heterogeneity. The Normalisation stage is in charge of normalising the input data towards zero mean and unity variance, while the Denormalisation returns the outputs of the MLP nets into their natural range. These two stages are needed since the range of the measurements involved in the control loops could be quite different. For instance, the mean of $S_{O,5}$ and $K_{La,5}$ equal to 1.9752 and 144.68, respectively. In the case of the $S_{No,2}$ control loop, the mean values of the variables involved in the control are equal to 0.9937 and $2.1802 \cdot 10^4$ for the $S_{NO,2}$ and Q_a measurements. Thus, the DO ANN-based and NO ANN-based structures are as follows:

- **DO ANN-based PI**
  - Input measurements: the $S_{O,5}(t)$ and its desired set-point $S_{O,5_{set-point}}(t)$. Besides, the DO ANN-based net considers the Non-linear Autoregressive Exogenous principle (NARX) where the output predicted by the net will be considered as an extra input. This extra input provides the ANN-based structure with information about its performance in the prediction process [Bou18]. In this case, the extra input corresponds to the previously computed actuator signal, $K_{La,5}(t - t_s)$. t_s stands for the delay introduced in the NARX principle. It equals to the BSM1 sampling time, i.e., 15 minutes.
  - Normalisation Stage: stage devoted to normalising the input measurements towards zero mean and unity variance.
  - LSTM-based Net: main part of the ANN-based Controller. It consists of two LSTM cells with 100 and 50 hidden neurons per ANN managing each gate and two MLP layers with 50 and 25 hidden neurons, respectively.

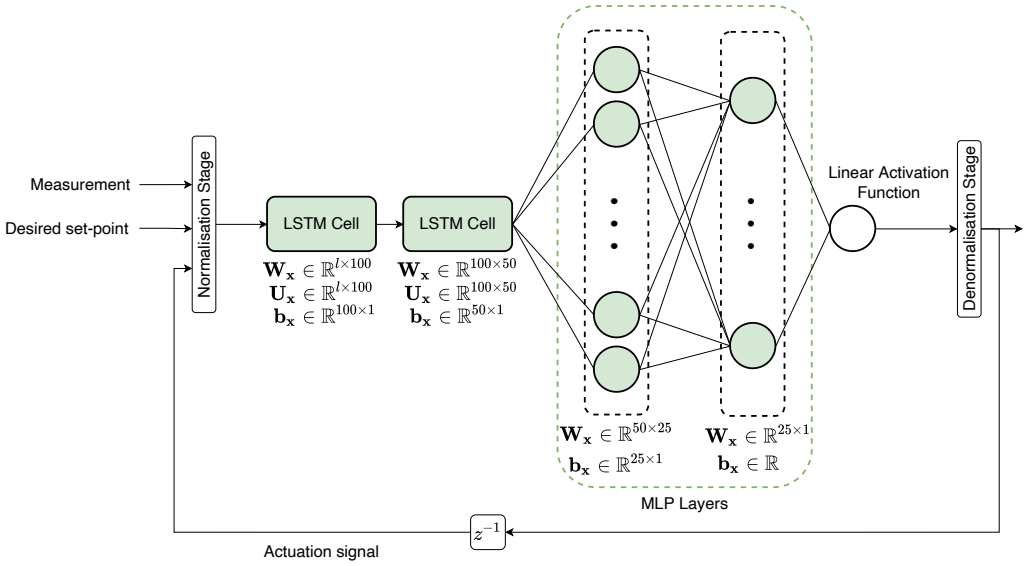

Figure 5.2: ANN-based PI structure. The different dimensions of the weights and biases involved in the ANN-based PI are depicted here. For instance, l corresponds to the number of inputs, which in this case is set to three measurements: the measured concentration of interest, $S_{O,5}(t)$ or $S_{NO,2}(t)$, its desired set-point, $S_{O,5_{set-point}}(t)$ or $S_{NO,2_{set-point}}(t)$, and the actuation variable, $K_{La,5}(t-t_s)$ or $Q_a(t-t_s)$.

- Denormalisation Stage: stage devoted to denormalising the actuation signal, i.e., the DO ANN-based output, towards its real range of values.
- Output: the actuation signal which corresponds to the oxygen transfer coefficient of the fifth reactor tank $(K_{La,5}(t))$.

- **NO ANN-based PI**
  - Input measurements: the $S_{NO,2}(t)$ and its desired set-point $S_{NO,2_{set-point}}(t)$. As it happens with the DO ANN-based PI, the NO ANN-based controller also considers the NARX principle. In this case, the extra input corresponds to the previously computed actuator signal, $Q_a(t-t_s)$.
  - Normalisation Stage: stage devoted to normalising the input measurements towards zero mean and unity variance.
  - LSTM-based Net: main part of the ANN-based Controller. It consists of two LSTM cells with 100 and 50 hidden neurons per ANN managing each gate and two MLP layers with 50 and 25 hidden neurons, respectively.
  - Denormalisation Stage: stage devoted to denormalising the actuation signal of the NO ANN-based output towards its real range of values.
  - Output: the actuation signal which corresponds to the WWTP $Q_a(t)$.

Training Process

The DO ANN-based PI and the NO ANN-based PI structures are obtained by means of a grid search method where different ANN-based structures are trained with the same set of measurements. The efforts of the grid search are focused on determining the number of LSTM cells, MLP layers, and hidden neurons per layer of the whole structure. Then, the LSTM structure offering the best prediction performance without committing overfitting is the one considered to implement the ANN-based PI.

As it is observed, the ANN-based PI structure is determined by the grid search process instead of finding the parameters characterising a conventional PI controller, that is, the $T_{i_{S_{O,5}}}$ and $T_{i_{Q_a}}$ and the proportional gains $K_{S_{O,5}}$ and K_{Q_a} [Vil12]. This means that a deep knowledge of the process under control is not required. Only pairs of input and output data of the existing default PI controllers are needed. These are obtained by means of simulating a complete year of uniformly distributed weather profiles to achieve a good control performance regardless of the weather conditions.

From all the available measurements in the form of time-series, the ANN-based PI controller input and output ones are determined accordingly to the control loop they manage: (i) $S_{O,5}(t)$, its desired set-point, $\left(S_{O,5_{set-point}}(t)\right)$, and $K_{La,5}(t)$ for the DO ANN-based PI, and (ii) $S_{NO,2}(t)$, its desired set-point $\left(S_{NO,2_{set-point}}(t)\right)$, and $Q_a(t)$ for the NO ANN-based PI. All of them are obtained from the BSM1 Simulink model.

In that sense, two datasets are considered to perform the grid search method: one obtained from the Ideal Scenario and the other from the Real one. Each dataset is split into two different subsets: 85% of the measurements to train and validate the different ANN-based PI configurations through K-Fold, and the remaining 15% to test the structures (see Figure 5.3). The grid search process is carried out adopting the Adam optimizer [Goo16, Sections 6.5 and 8.5.3] along 500 epochs. The initial learning rate value is

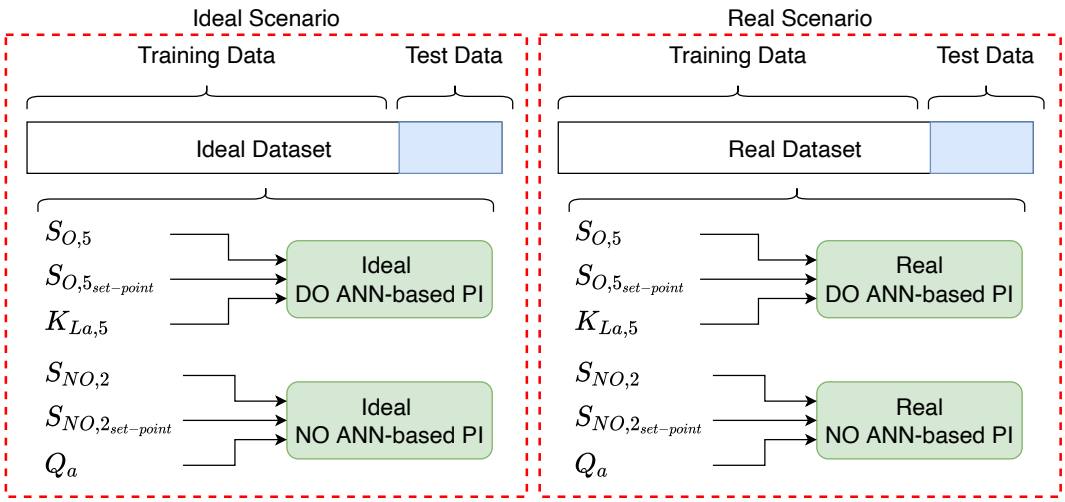

Figure 5.3: Data considered in the ANN-based PIs training process.

set to $1 \cdot 10^{-3}$, however, it is reduced along the process. In addition, LSTM nets are also known to suffer overfitting. To avoid this problem, the L2 parameter regularisation technique and early stopping methods are considered. The extra penalty of L2 is set to $5 \cdot 10^{-4}$. On the other hand, the patience of the early stopping technique is set to five epochs.

Prediction Performance

The prediction performance of both structures is computed in terms of the difference between the predicted actuation variables yielded by the ANN-based PI structures and the expected ones returned by the BSM1 default controllers. It is worth remembering that the DO ANN-based PI predicts the $K_{La,5}(t)$, whereas the NO one predicts the $Q_a(t)$. The RMSE, the MAPE, and the R^2 metrics are considered to determine the prediction behaviour of each ANN-based PI structure. Moreover, the training time t_{time} is provided to show the time lasted in the ANN's training process. Notice that all the prediction metrics are computed considering normalised values, except for the MAPE in order to avoid divisions by zero. In that sense, the results show that the proposed ANN-based structures are able to offer a good prediction performance for the Ideal Scenario (see Table 5.1). Both structures yield low RMSE and MAPE values as well as a R^2 nearly equal to 1. Their training time is not too high since in less than 2 minutes the structures are trained. In that sense, it is observed that the training process is more difficult for the NO ANN-based PI than to the DO ANN-based PI. In terms of the Real Scenario, however, the situation completely changes. Focusing on the DO ANN-based PI structure, it is observed that the RMSE is degraded from 0.026 to 0.251, the MAPE from 1.35% to 10.53% and the R^2 from 0.99 to 0.94. This change is also noticeable in terms of the NO ANN-based PI structure. Its RMSE is degraded from 0.048 to 0.229. Notwithstanding, the highest degradation is observed in the MAPE. Now it equals to 58.50%, which entails a degradation of 52.24 percentage points with respect to the Ideal Scenario. These degradations are produced because of the non-linearities introduced in the Real Scenario since they affect the measurements that are considered in the ANN-based PI training process. For that reason, the ANN-based PI controllers experience

Table 5.1: ANN-based PI architectures prediction performance. RMSE is measured in day^{-1} for the DO ANN-based PI and in $\mathrm{m}^3/\mathrm{day}$ for the NO ANN-based PI. MAPE is measured in %. The ANN's training time, t_{time}, is measured in seconds.

BSM1 Ideal Scenario				
Structure	RMSE	MAPE	R^2	t_{time}
DO ANN-based PI	0.026	1.35	0.99	69.91
NO ANN-based PI	0.048	6.26	0.99	98.60
BSM1 Real Scenario				
Structure	RMSE	MAPE	R^2	t_{time}
DO ANN-based PI	0.251	10.53	0.94	44.37
NO ANN-based PI	0.229	58.50	0.91	50.52

this degradation. Processes devoted to correcting the effects of these non-linearities are required so as to alleviate the issues related to them. In terms of the training time, it is reduced as a consequence of the noise effects. Since it corrupts the ideal measurements, the real minimum of the cost function is hidden and therefore, the optimization process ends in a local minima instead of the real one.

5.2.2 ANN-based PI Control Performance

The control performance of each ANN-based PI structure has been computed in terms of fix and variable set-points and the three weather profiles of the BSM1 framework. Fix set-points are considered since the default BSM1 control strategies consider them in order to assure that the nitrification and denitrification processes are correctly performed [HS93, Ale08]. They are set to 2 mg/L and 1 mg/L for the DO and NO control loops, respectively. Notwithstanding, variable set-points are the ones of most interest since most of the times the set-points are computed by means of other control strategies or are varied in order to optimise the pollutant reduction process [San15a, Olm18, Qia18, San19]. In this case, the variable $S_{O,5_{set-point}}(t)$ has been computed accordingly to the FLC adopted in [San15a], where the fuzzy controller is considered to determine the $S_{O,5_{set-point}}(t)$ generating the lower $S_{NH,5}(t)$.

DO ANN-based PI

Results of the DO ANN-based PI are shown in Table 5.2, where the first important effect that one can notice is that the control performance in the DO control loop, that is, in the management of $S_{O,5}(t)$, is even better than the control offered by the default PI when an ideal scenario is considered. This effect is motivated by two situations: (i) the fact that the DO ANN-based PI has been trained through the simulation of the control strategy when random variations in the set-point are provided, and (ii) the NARX principle which provides the ANN-based structure with information about the previous predicted outcomes. Thus, the ANN-based PI structure has learnt how to correct variations present either in the set-point, or in the measured concentration.

In terms of the IAE and ISE metrics, it is observed that they are improved with respect to the default PI control performance when a fixed set-point is considered. The IAE and ISE values are improved by around a 95.98% and a 99.84% in average with respect to the default PI controller, respectively. For instance, the highest IAE improvement is achieved when the stormy influent profile is simulated. The IAE offered by the default $S_{O,5}(t)$ PI controller is equivalent to 0.158, while it is reduced until 0.006 when the DO ANN-based PI is considered. This entails that the difference between the measured and the $S_{O,5}(t)$ controller is minimal. In terms of the ISE, the achieved improvements equal to 99.86%, 99.84% and 99.82% with respect to the default PI controller when the dry, rainy and stormy weathers are considered, respectively. However, the important results are the ones obtained with a variable set-point.

In such a context, the same effect is observed when a variable $S_{O,5_{set-point}}(t)$ is considered. In this case, the average improvement in terms of the IAE and ISE equals to 91.67% for the IAE and 97.77% for the ISE. Now, the highest improvement is achieved when the dry weather is considered: the IAE and the ISE are improved by 92.97% and 98.54% with respect to the default PI controller performance. This is motivated by the fact that rainy and stormy influents are derived from the dry weather where the rainy and stormy episodes are included. For that reason, the ANN-based structure has observed more often

Table 5.2: DO ANN-based PI control performance for the Ideal and Real BSM1 scenarios.

Fix set-point for the BSM1 Ideal Scenario						
	Influent Weather Profile					
	Dry		Rainy		Stormy	
Structure	IAE	ISE	IAE	ISE	IAE	ISE
DO Default BSM1 PI	0.148	0.007	0.143	0.007	0.158	0.007
DO ANN-based PI	0.006	0.001	0.006	0.001	0.006	0.001
Improvement [%]	95.95	99.86	95.80	99.84	96.20	99.82
Fix set-point for the BSM1 Real Scenario						
	Influent Weather Profile					
	Dry		Rainy		Stormy	
Structure	IAE	ISE	IAE	ISE	IAE	ISE
DO Default BSM1 PI	1.234	0.346	1.234	0.346	1.236	0.348
DO ANN-based PI	1.529	0.552	1.551	0.563	1.416	0.457
Improvement [%]	-23.91	-59.08	-25.77	-62.25	-14.47	-31.32
Variable set-point for the BSM1 Ideal Scenario						
	Influent Weather Profile					
	Dry		Rainy		Stormy	
Structure	IAE	ISE	IAE	ISE	IAE	ISE
DO Default BSM1 PI	0.185	0.016	0.155	0.014	0.206	0.020
DO ANN-based PI	0.013	$2.34 \cdot 10^{-4}$	0.016	$4.48 \cdot 10^{-4}$	0.016	$4.05 \cdot 10^{-4}$
Improvement [%]	92.97	98.54	89.68	96.80	92.00	97.98
Variable set-point for the BSM1 Real Scenario						
	Influent Weather Profile					
	Dry		Rainy		Stormy	
Structure	IAE	ISE	IAE	ISE	IAE	ISE
DO Default BSM1 PI	1.261	0.364	1.260	0.364	1.256	0.363
DO ANN-based PI	1.834	0.782	1.782	0.756	1.805	0.762
Improvement [%]	-45.52	-114.84	-41.43	-107.69	-43.60	-109.92

the effects of the PI controlling the $S_{O,5}(t)$ when dry episodes are observed rather than stormy or rainy ones. In addition, the control performance clearly shows that the DO ANN-based PI can be adopted as the main controller in the DO control loop.

When the Real Scenario is adopted, results clearly show that the DO ANN-based PI controller does not overcome the performance of the default PI structure. The IAE and ISE values have been highly increased regardless of the weather profile being simulated. This is produced since the performance of the ANN predictions is degraded too with respect to the Ideal Scenario. Consequently, a correct control performance cannot be ensured. Numerically, the control performance of the DO ANN-based PI is degraded to such a point that all the improvements with respect to the default PI structure are negative. For instance, the ISE of the DO ANN-based PI control performance is degraded a 114.84% when dry weather is considered. The DO ANN-based PI ISE equals to 0.782 whereas the same value is equivalent to 0.364 if the conventional PI is adopted. In that sense, Figure 5.4 shows the control performance of the DO ANN-based PI when it is configured to manage the Ideal and the Real Scenarios. As it is observed, in the ideal case the output of the controller is much closer to the given set-point of 2 mg/L than the default PI output. However, in the Real Scenario, the effect of noise is noticeable at a glance. Neither the PI nor the ANN-based PI are able to offer a proper control performance. This highlights the need to reduce the effects of the non-idealities.

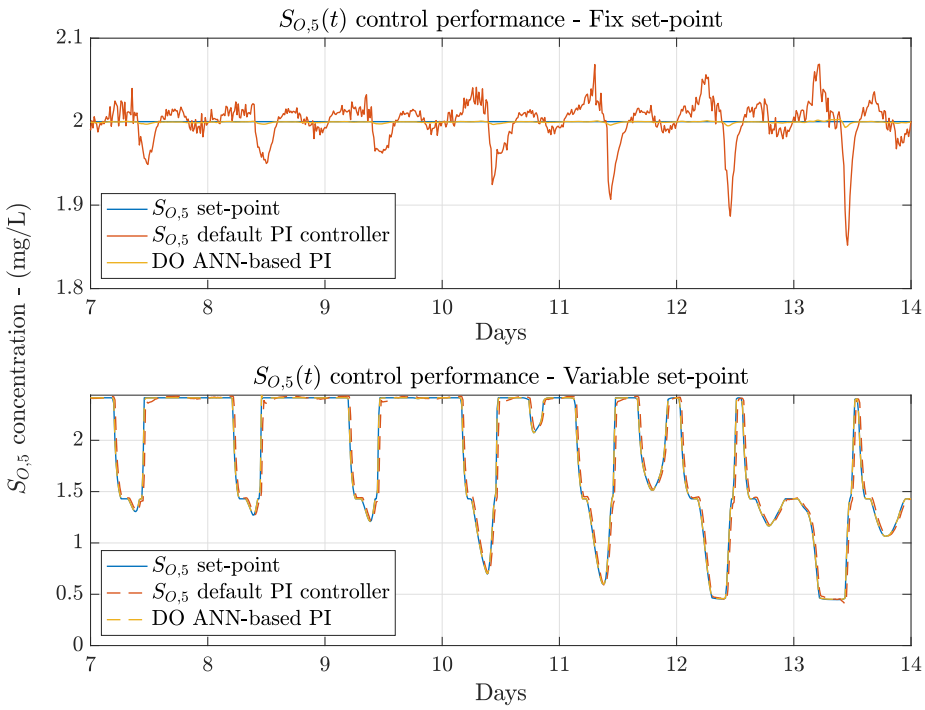

(a) DO ANN-based PI - Ideal Scenario

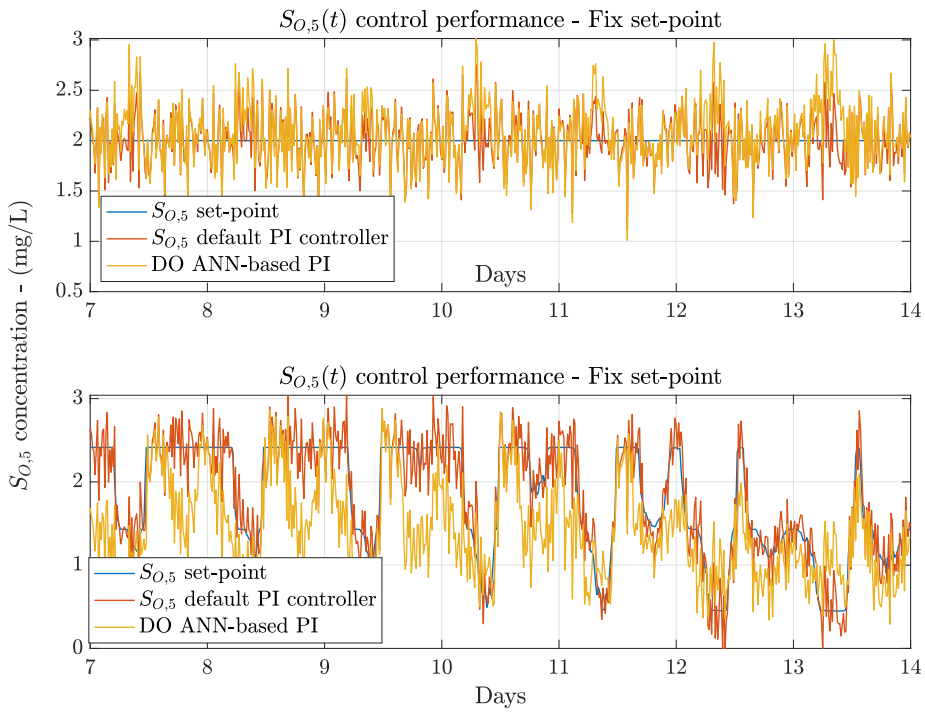

(b) DO ANN-based PI - Real Scenario

Figure 5.4: DO ANN-based PI control performance. Notice that when a fix set-point is considered the best performance is obtained for the DO ANN-based PI structure.

NO ANN-based PI

The control performance of the NO LSTM-based PI is shown in Table 5.3 where results for the Ideal and Real Scenario are shown. In terms of the Ideal Scenario, it is clearly observed at first sight that the IAE and ISE metrics are improved with respect to the default $S_{NO,2}$ PI controller. When a fix $S_{O,5_{set-point}}(t)$ is considered, the IAE and ISE values of the NO control loop are improved in average a 24.34% and a

Table 5.3: NO ANN-based PI control performance for the Ideal and Real BSM1 scenarios.

Fix set-point for the BSM1 Ideal Scenario						
	Influent Weather Profile					
	Dry		Rainy		Stormy	
Structure	IAE	ISE	IAE	ISE	IAE	ISE
NO Default BSM1 PI	1.594	0.691	1.922	0.951	1.874	0.997
NO ANN-based PI	1.302	0.486	1.399	0.542	1.360	0.543
Improvement [%]	18.32	29.67	27.21	43.01	27.43	45.54
Fix set-point for the BSM1 Real Scenario						
	Influent Weather Profile					
	Dry		Rainy		Stormy	
Structure	IAE	ISE	IAE	ISE	IAE	ISE
NO Default BSM1 PI	3.442	2.581	3.420	2.479	4.172	3.327
NO ANN-based PI	3.274	2.407	4.167	3.224	3.202	2.180
Improvement [%]	4.88	6.74	-21.84	-30.05	23.25	34.48
Variable set-point for the BSM1 Ideal Scenario						
	Influent Weather Profile					
	Dry		Rainy		Stormy	
Structure	IAE	ISE	IAE	ISE	IAE	ISE
NO Default BSM1 PI	1.792	0.858	2.132	1.089	1.884	0.989
NO ANN-based PI	1.266	0.464	1.574	0.662	1.372	0.557
Improvement [%]	29.35	45.92	26.17	39.21	27.18	43.68
Variable set-point for the BSM1 Real Scenario						
	Influent Weather Profile					
	Dry		Rainy		Stormy	
Structure	IAE	ISE	IAE	ISE	IAE	ISE
NO Default BSM1 PI	2.972	1.949	3.304	2.318	3.185	2.218
NO ANN-based PI	3.350	2.399	3.361	2.392	3.312	2.331
Improvement [%]	-12.72	-23.09	-1.73	-3.19	-3.99	-5.09

39.41%. Both with respect to the default PI managing the $S_{NO,2}$ concentration of the Ideal Scenario. The ISE improvement shows that the proposed NO ANN-based PI controller is able to reduce the highest errors between the measured $S_{NO,2}$ and its set-point. However, the control performance could be still improved. The best value is observed when the stormy weather is considered. There, the IAE goes from 1.874 to 1.360, whereas the ISE goes from 0.977 to 0.543. These values represent an improvement equal to a 27.43% and a 45.54% with respect to the default PI control metrics. Visually, one can observe that the $S_{NO,2}(t)$ control performance is slightly improved with respect to the default PI (see Figure 5.5). In this case, the peaks of $S_{NO,2}$ concentration are reduced, however, the desired set-point is not achieved.

When a variable $S_{O,5_{set-point}}(t)$ is considered, one can observe that the $S_{NO,2}(t)$ IAE and ISE metrics are improved a 27.56% and a 42.94% in average, with respect to the default BSM1 $S_{NO,2}(t)$ PI controller. In this case, the highest improvement is given when a dry influent profile is considered. This is motivated due to the fact that the ANN-based structures have been trained considering a whole year influent where dry episodes were the common weather. Taking this into account, the IAE and ISE correspond to 1.266 and 0.464, respectively. Notwithstanding, Figure 5.5 shows that neither the PI nor the NO ANN-based PIs are able to offer the desired behaviour. The best improvement is provided by the NO ANN-based PI when a fix $S_{O,5_{set-point}}(t)$ and a stormy weather are considered. In this case, the IAE is improved a 27.18% whilst this percentage is increased until a 43.68% for the ISE. When the Real Scenario is considered, the control performance drops. The highest degradation is given by the same structure when it is managing the rainy events. The IAE is degraded a 21.84% while the ISE is worsened a 30.05%. Notice that the degradation of the control performance when a variable $S_{O,5_{set-point}}(t)$ is adopted is not as high as for the fixed one. This is motivated by the fact that variable set-points are less vulnerable to the effects of noise.

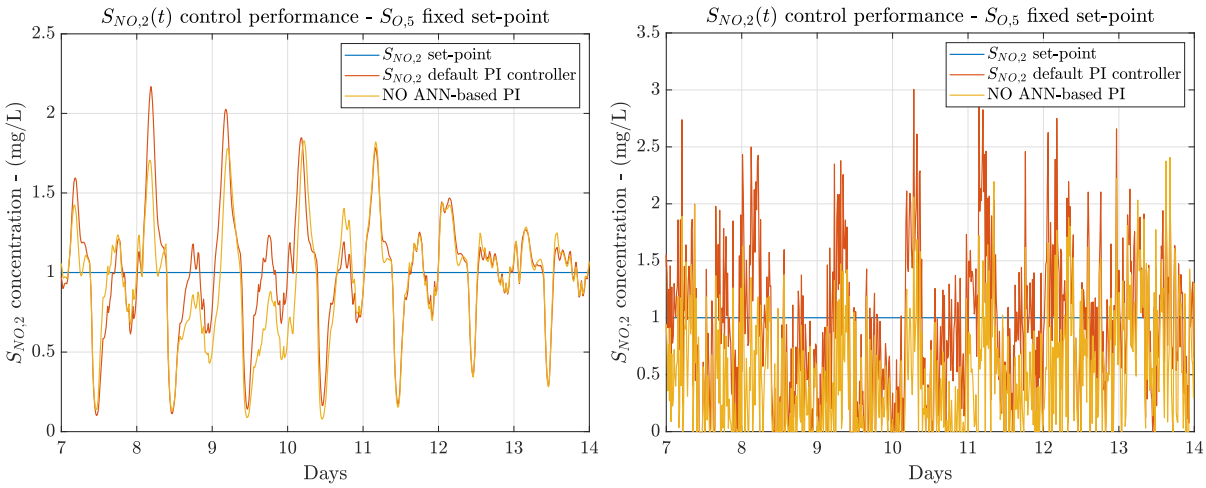

(a) NO ANN-based PI - Ideal Scenario

(b) NO ANN-based PI - Real Scenario

Figure 5.5: NO ANN-based PI control performance. Notice that the performance of the PI and the ANN-based PI controllers is deeply affected by the effects of non-idealities.

5.3 ANN-based IMC

The application of ANNs to replicate the behaviour of existent conventional controllers such as PIs has been assessed in the previous section. Nevertheless, the power of ANNs can be exploited even more. Here is where the IMC structure makes the point. They are characterised by offering a great performance when dealing with set-point tracking processes. Processes like the ones considered in the default control loops of the BSM1 framework [Vil18].

This is motivated by the implementation of the direct and inverse models of the process under control [Li19b]. Nevertheless, the performance of the IMC structure deeply relies on the accuracy of these models, which sometimes show highly complex and non-linear relationships [Vil18]. For that reason, in this section the adoption of an ANN-based IMC structure devoted to substituting the default PI controlling the $S_{O,5}$ concentration of the BSM1 framework is assessed. The adoption of such controller is motivated due to the ANNs ability to deal with non-linear processes as well as to their good performance in tracking tasks [Li19b, Vil18, Pis19a]. In that sense, the direct $(P_{dir}(s))$ and the inverse $(P_{inv}(s))$ models of the process under control are implemented by ANNs rather than highly complex mathematical models. Figure 5.6 depicts the conceptual idea of an ANN-based IMC. Therefore, if $ANN_d(\cdot)$ and $ANN_i(\cdot)$ are defined as the ANNs modelling $P_{dir}(s)$ and $P_{inv}(s)$, the actuation $(u(t))$ and the controlled $(y(t))$ signals of the IMC controller will be forecasted as follows:

$$\widehat{y}(t) = ANN_d\left(u(t)\right) \qquad u(t) = H(t) * ANN_i\left(\tilde{y}(t)\right) \tag{5.1}$$

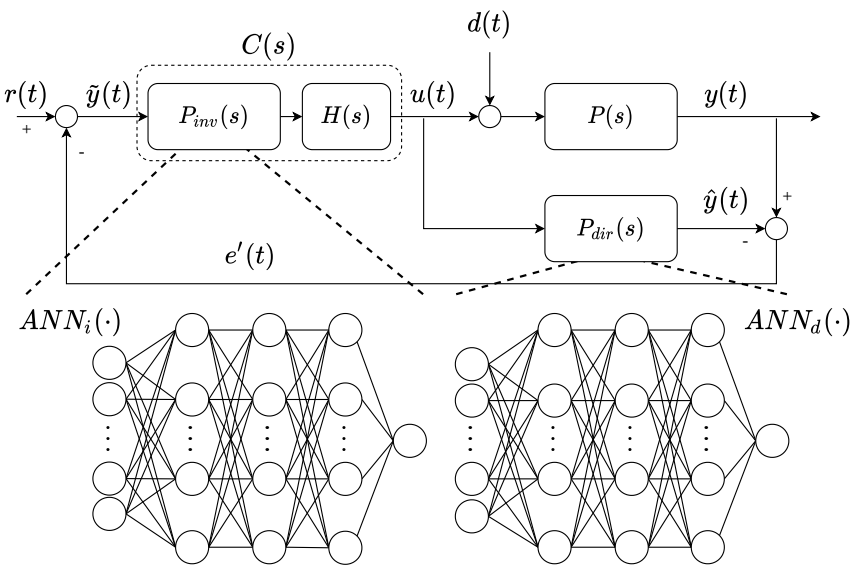

Figure 5.6: ANN-based Internal Model Controller. $r(t)$ corresponds to the reference signal, $e'(t)$ to the mismatch between the real process output and $P_{dir}(s)$ outcome, $\widehat{y}(t)$. $d(t)$ stands for the perturbations added to the process under control $P(s)$.

where $*$ denotes the convolution in time between the output of $ANN_i(\tilde{y}(s))$ and $H(s)$. Notice that $H(s)$ consists in a first-order filter whose transfer function is computed as follows:

$$H(s) = \frac{\omega_c}{s + \omega_c} \tag{5.2}$$

where ω_c denotes the filter's cut-off frequency. It is determined by means of the ETFE based stability test performed to the whole control strategy. Moreover, its main aim is to reduce the effects of non-desired behaviours such as non-linearities or non-invertible parts of the process under control [Li19b].

The main point of the ANN-based IMC controller is that it does not require a mathematical model of the process under control any more. Consequently, it becomes a purely data-driven approach. It completely relies on the pairs of input and output data considered in the ANNs training process. Thus, the more representative the measurements, the better the control performance. For that reason, it is important to gather measurements of the process under control in its open loop configuration with the minimum possible corruptions. In that sense, one must be careful with the ANNs and the data considered in their training process. ANNs trained with ideal measurements could be no longer valid because of the noise introduced by the non-ideal sensors. For instance, the ANN-based PI control performance drastically drops when non-ideal sensors are adopted. For that reason, the Ideal and Real Scenarios are adopted again to assess the sensitivity of the ANN-based IMC towards noise effects:

- **Ideal Scenario**: The default PI controlling the BSM1 $S_{O,5}$ concentration is substituted by the ANN-based IMC structure. Ideal measurements are considered in the ANNs training process.
- **Real Scenario**: This scenario considers the same ANN-based IMC control strategy as in the ideal case. However, the BSM1 sensors considered here add non-idealities to the measurements. As a consequence, the effects of these non-linearities are going to be observed in the ANN-based IMC control performance.

5.3.1 ANN-based Architectures

The ANN-based IMC controller is devoted to managing the BSM1 $S_{O,5}$ concentration. Since it fluctuates as a consequence of the highly complex and non-linear processes performed in the BSM1 fifth reactor tank, the adoption of ANNs is strongly recommended [Goo16, Chapter 6]. Among the different network topologies, $P_{dir}(s)$ and $P_{inv}(s)$ models can be implemented by means of MLP networks and LSTM cells. Nevertheless, LSTM cells are more suitable due to their good performance when dealing with time-series signals [Goo16, Chapter 10]. Indeed, concentrations and measurements involved in this control process can be understood as time-series signals. Besides, $S_{O,5}(t)$ does not only depend on the input concentrations currently entering in the tank. Its final concentration also depends on the oxygen concentration already present in the reactor. Taking all the aforementioned points into account, the adoption of LSTM cells as the ANNs to model $P_{inv}(s)$ and $P_{dir}(s)$ is utterly recommended [Gre17].

LSTM-based Architectures

Four architectures have been proposed, two of them dealing with ideal and two with non-ideal measurements. As it is observed in Figure 5.7, they follow the same structure: a data pre-processing stage where a Sliding Window and a Normalisation Layer are implemented, the LSTM cells themselves, a Linear Activation layer and a Denormalisation Layer. The architectures of the Ideal Scenario consider a unique

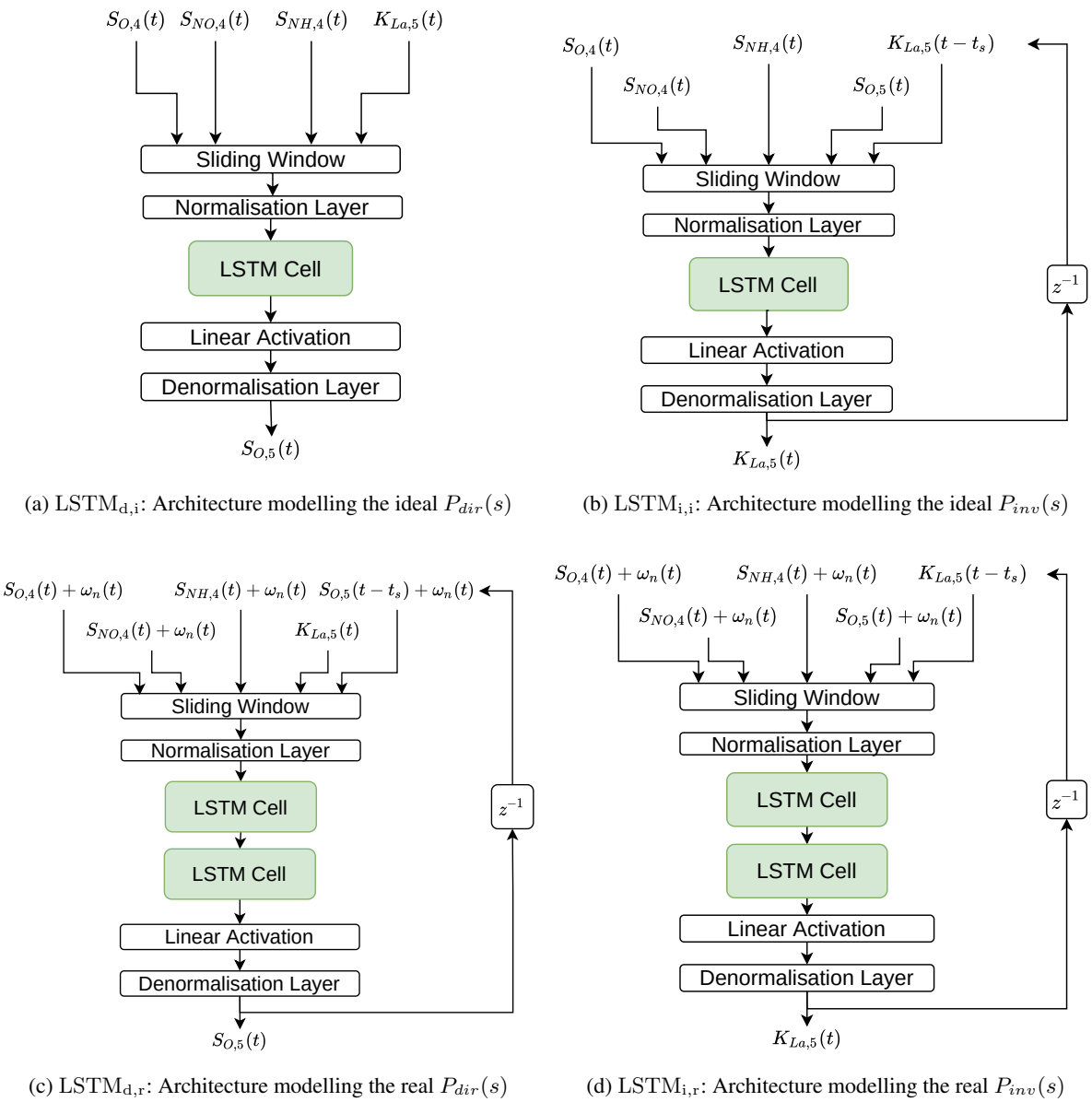

(a) $\mathrm{LSTM_{d,i}}$: Architecture modelling the ideal $P_{dir}(s)$

(b) $\mathrm{LSTM_{i,i}}$: Architecture modelling the ideal $P_{inv}(s)$

(c) $\mathrm{LSTM_{d,r}}$: Architecture modelling the real $P_{dir}(s)$

(d) $\mathrm{LSTM_{i,r}}$: Architecture modelling the real $P_{inv}(s)$

Figure 5.7: Architectures considered in the ANN-based IMC controller. $S_{O,4}(t)$, $S_{NO,4}(t)$ and $S_{NH,4}(t)$ are the oxygen, the nitrate-nitrogen and the ammonium concentrations in the fourth reactor tank. ω_n and t_s stands for the AWGN noise added by the non-ideal BSM1 sensors and the 15 minutes delay introduced by the delay block z^{-1}, respectively.

LSTM cell which is trained adopting ideal measurements. Instead, the two architectures of the real scenario consider two cells which are affected not only by the noise, but also by the delays introduced by the sensors (see Section 3.1.1).

The Sliding Window main purpose is to sort the values in time and therefore, preserve the information regarding the time-dependence of the input data. In this case, the WL equals to the lowest periodicity of the LSTM input signals. To determine it, the Fast Fourier Transform is applied instead of a heuristic method. In that manner, the lowest periodicity can be computed regardless of whether input signals are affected by noise or not: the highest input signal frequency component will determine the lowest periodicity and therefore, the minimum WL to consider. In our case, this periodicity is given by the ammonium concentration in the fourth tank, $S_{NH,4}(t)$, and equals to 4 hours. Lower window lengths would entail a poor training since not enough information from the input signals would be considered. On the other hand, if large window lengths are considered instead, there will be enough information to train the networks at expense of increasing their training time. More details can be observed in [Pis20c]. Notice that the PH of the sliding window is set to 15 minutes since the predicted actuation signal must be fed into the fifth reactor tank without delays. The Normalisation Layer is again in charge of reducing the heterogeneity of input data by means of normalising them towards zero mean and unit variance [Gar15]. The Denormalising Layer transforms the normalised values into their real range. Finally, a Linear Activation layer has been considered since the IMC structure is performing regression tasks [DS17, Chapter 1].

Input and Output Data

As it is observed in Figure 5.6, the input data of each LSTM vary according to the main purpose of the architecture. In that sense, structures modelling the direct relationship of the process under control will consider the actuation signal, $u(t)$, as an input and the controlled one, $y(t)$, as the output. On the other hand, the LSTMs modelling the inverse relationship forecast the actuation signal considering the controlled one. Notice that the actuation and controlled signals are the following ones:

- **Actuation Signal** $(u(t))$: the signal entering in the real plant and the IMC's direct model. Since the IMC is devoted to managing the $S_{O,5}(t)$, $u(t)$ corresponds to the $K_{La,5}(t)$.
- **Controlled Signal** $(y(t))$: it corresponds to the $S_{O,5}(t)$. The IMC aim is to maintain the $S_{O,5}$ concentration at the given set-point $(r(t))$ by means of modifying the $K_{La,5}(t)$.

Nonetheless, the inputs of the ANN are not limited to the actuation and control signals. More information can be provided to the ANN-based architectures in order to perform better predictions. In this case, signals and measurements from the effluent of the BSM1 fourth reactor tank are considered. Among the 15 possible measurements, only the $S_{O,4}(t)$, the $S_{NO,4}(t)$ and the $S_{NH,4}(t)$ concentrations are adopted to complement the actuation and controlled signals. These are selected considering the mutual information (MI) between the concentrations of the BSM1 fourth reactor tank and the controlled variable.

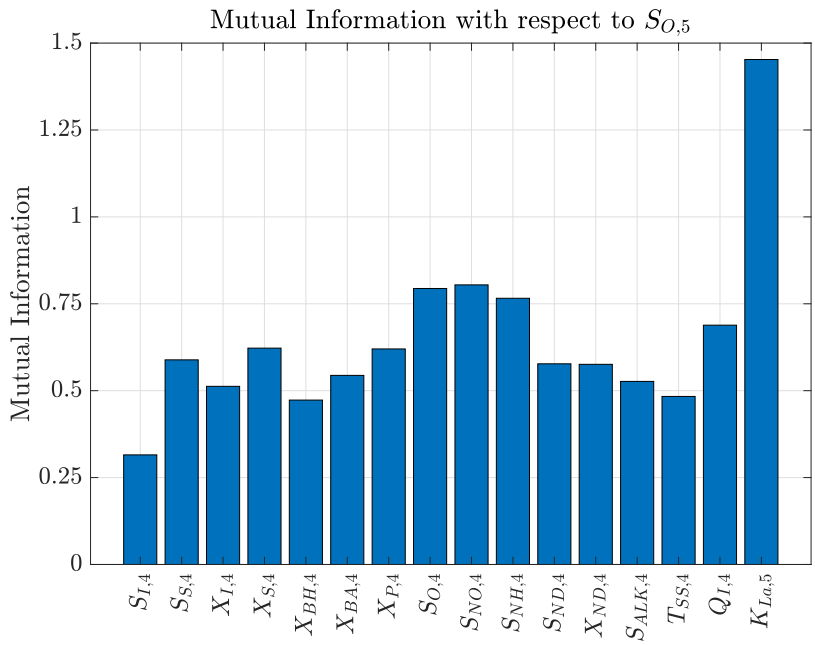

Figure 5.8: Mutual Information between ANN input data. The other concentrations correspond to the BSM1 influent concentrations: the soluble and particulate inert organic matter concentrations (S_I and X_I), the readily and slowly biodegradable substrate concentration (S_S and X_S), the active heterotrophic and autotrophic biomass concentration (X_{BH} and X_{BA}), the concentration of particulate products arising from biomass decay (X_P), the soluble and particulate biodegradable organic nitrogen concentration (S_{ND} and X_{ND}), the alkalinity (S_{ALK}) and the input flow rate (Q_i).

The ones showing the highest MI will be the ones considered as extra input data [Tra18, Bab15, Han15]. Results are shown in Figure 5.8. It is also important to notice that three of the four architectures consider the NARX principal. Therefore, a facilitation in the prediction of the current value is achieved. Furthermore, input data considered by the architectures dealing with non-ideal measurements consist in the aforementioned signals plus the noise added by the BSM1 real sensors. Taking this into account, it can be observed in Figures 5.7c and 5.7d, that $K_{La,5}(t)$ is not corrupted by ω_n. This is motivated by the fact that this value corresponds to an actuation parameter and not to a signal measured by a sensor.

Training Process

The internal structure of each LSTM cell in the architectures presented in Figure 5.7 are found adopting the grid search methodology. In such a context, the LSTM architectures are as follows:

- LSTM structure modelling P_{dir} model at the Ideal Scenario - $\mathrm{LSTM_{d,i}}$: considers a unique LSTM cell with 100 hidden neurons per ANN managing a gate.
- LSTM structure modelling P_{inv} model at the Ideal Scenario - $\mathrm{LSTM_{i,i}}$: considers a unique LSTM cell with 100 hidden neurons per ANN managing a gate. In this case, the architecture implements

the NARX principle, that is, the 15 minutes delayed $K_{La,5}(t - t_s)$ predicted value is considered as one input signal.

- LSTM structure modelling P_{dir} model at the Real Scenario - $\mathrm{LSTM_{d,r}}$: considers two stacked LSTM cells with 100 hidden neurons per ANN managing a gate. This architecture follows the NARX principle. Now, the predicted value and its delayed version correspond to the actuation signal, i.e., the $S_{O,5}(t)$ and $S_{O,5}(t - t_s)$, respectively.

- LSTM structure modelling P_{inv} model at the Real Scenario - $\mathrm{LSTM_{i,r}}$: considered two stacked LSTM cells with 100 hidden neurons per ANN managing a gate. The NARX principle is also considered. The predicted value corresponds to the $K_{La,5}(t)$.

All the architectures adopt a learning rate equal to $1 \cdot 10^{-3}$. They are obtained through the grid search adopting the BPTT algorithm with Adam optimizer [Goo16, Section 8.5.3]. Then, they are cross-validated by means of a 5 fold K-Fold method to fine-tune the regularisation parameters [Ber12, Ber18]. L2 extra-penalty and early stopping methods have been considered to overcome this effect [Goo16, Sections 7.1, 7.2 & 7.8]. In this case, L2 extra penalty has been set to $1 \cdot 10^{-3}$ for the $\mathrm{LSTM_{d,i}}$ and $\mathrm{LSTM_{i,i}}$ while it equals to $1 \cdot 10^{-4}$ for the $\mathrm{LSTM_{d,r}}$ and $\mathrm{LSTM_{i,r}}$. In terms of the epochs, 500 epochs are considered as a maximum.

Four datasets are considered to perform the hyperparameters tuning process: two of them obtained from the Ideal Scenario and two from the real one, that is, from BSM1 framework with non-ideal sensors. At each scenario, one dataset is considered to perform the grid-search process while the other is in charge of the cross-validation of the networks. The dataset devoted to cross-validating the architectures is split in two main parts: (i) an 85% of the data is considered to perform the cross-validation process; and (ii) the remaining 15% is leaved for testing purposes. In terms of the measurements, they correspond to the fifth reactor tank input and output concentrations observed during a year. To obtain them, a whole year simulation of different influent profiles is performed in Simulink. These profiles correspond to uniformly distributed dry, rainy and stormy weather influents. Measurements are gathered with a sampling frequency of $1.11 \cdot 10^{-3}$ Hz, or in other words, every 15 minutes.

Prediction Performance

Prediction results of the ANN-based IMC architectures are shown in Table 5.4, where the RMSE, the MAPE, the R^2 and the t_{time} are computed for the different architectures and scenarios. Notice that although LSTM cells have been considered to implement the ANN-based IMC, MLP nets and the Autoregressive Integrated Moving Average (ARIMA) method [Zha03, Cad16] are also considered for comparison purposes. From these three prediction approaches, only the ANNs can be implemented in the ANN-based IMC control structure: the IMC requires prediction approaches which predict the output

values from the input ones and vice-versa [Li19b]. On the other hand, the ARIMA model predicts the output measurements considering only the previous observed values [Cad16].

In terms of the Ideal Scenario and the direct relationship, $P_{dir}(s)$, the prediction approach offering the lowest performance corresponds to the $\mathrm{ARIMA_{d,i}}$ method. This is expected since ARIMA generates its model considering only the measurements of a certain variable. Thus, the model generation process becomes a harder task than in the case where more input information is provided (MLP and LSTM nets).

Table 5.4: ANN-based IMC architectures prediction performance. RMSE is measured in mg/L for the $P_{dir}(s)$ and in day^{-1} for the $P_{inv}(s)$ model. MAPE is measured in % and t_{time} in seconds. $\mathrm{ARIMA_{x,y}}$, $\mathrm{MLP_{x,y}}$ and $\mathrm{LSTM_{x,y}}$ stand for the ARIMA, the MLP and the LSTM prediction approaches for the x model (d - direct or i - inverse) and the y scenario (i - ideal or r - real), respectively.

BSM1 Ideal Scenario				
$P_{dir}(s)$ modelling				
Prediction Approach	RMSE	MAPE	R^2	t_{time}
$\mathrm{ARIMA_{d,i}}$	0.178	32.27	0.97	-
$\mathrm{MLP_{d,i}}$	0.050	3.72	0.98	44.69
$\mathrm{LSTM_{d,i}}$	0.030	0.84	0.99	45.16
Improvement [%]	40.00	77.42	1.01	-
$P_{inv}(s)$ modelling				
Prediction Approach	RMSE	MAPE	R^2	t_{time}
$\mathrm{ARIMA_{i,i}}$	0.053	5.01	0.97	-
$\mathrm{MLP_{i,i}}$	0.082	5.48	0.98	35.53
$\mathrm{LSTM_{i,i}}$	0.045	4.07	0.99	103.77
Improvement [%]	45.00	25.73	1.01	-
BSM1 Real Scenario				
$P_{dir}(s)$ modelling				
Prediction Approach	RMSE	MAPE	R^2	t_{time}
$\mathrm{ARIMA_{d,r}}$	0.374	282.09	0.86	-
$\mathrm{MLP_{d,r}}$	0.107	88.34	0.98	25.76
$\mathrm{LSTM_{d,r}}$	0.043	36.90	0.99	40.45
Improvement [%]	59.81	58.23	1.01	-
$P_{inv}(s)$ modelling				
Prediction Approach	RMSE	MAPE	R^2	t_{time}
$\mathrm{ARIMA_{i,r}}$	0.053	5.01	0.97	-
$\mathrm{MLP_{i,r}}$	0.291	38.40	0.92	21.14
$\mathrm{LSTM_{i,r}}$	0.101	15.85	0.99	42.93
Improvement [%]	65.29	58.72	7.07	-

For instance, the $\mathrm{MLP_{d,i}}$ net improves the RMSE and MAPE around a 71.91% and 88.47%, respectively, with respect to $\mathrm{ARIMA_{d,i}}$. Then, between $\mathrm{MLP_{d,i}}$ and $\mathrm{LSTM_{d,i}}$, the improvement for these metrics equal to a 40% and a 77.42%, respectively.

With respect to the inverse relationship of the process under control, $P_{inv}(s)$, and the Ideal Scenario, the lowest performance is given by the $\mathrm{MLP_{i,i}}$. As observed, the ARIMA method is able to overcome the MLP, however, it cannot be implemented in the ANN-based IMC structure by the aforementioned reasons. Nevertheless, $\mathrm{LSTM_{i,i}}$ improves not only the $\mathrm{MLP_{i,i}}$ results, but also the $\mathrm{ARIMA_{i,i}}$ ones. In this case, the improvement achieved by the $\mathrm{LSTM_{i,i}}$ with respect to the $\mathrm{MLP_{i,i}}$ corresponds to a 45% in terms of the RMSE, a 25.73% in terms of the MAPE and a 1.01% in terms of the R^2 metric. As observed, the MAPE improvement considerably differs between the direct and inverse relationships. This is directly related to the complexity of the processes being modelled since $P_{dir}(s)$ is less complex than $P_{inv}(s)$. This is also corroborated with the t_{time}. The time involved in the $\mathrm{LSTM_{d,i}}$ training process is much lower than the one involved to train the $\mathrm{LSTM_{i,i}}$. Finally, the results obtained here clearly show that LSTM cells are the prediction approach offering the best performance and therefore, the ones that should be considered to model the process under control. Moreover, their training time is not excessively high so as to decide not to use them.

Regarding the Real Scenario, results show that the performance of $\mathrm{ARIMA_{d,r}}$ has been degraded until it shows an RMSE three times bigger than in the ideal case ($\mathrm{ARIMA_{d,i}}$), a MAPE which equals to 282.09% and a R^2 of 0.86. MAPE results clearly show that ARIMA models cannot be considered not only by the aforementioned fact, but also by generating a model not able to deal with noisy signals. It is worth mentioning that $\mathrm{ARIMA_{i,r}}$, the model in charge of forecasting the actuation variable ($K_{La,5}$), is exactly equal to the ideal case. Being an actuation variable, it is not corrupted by noise since it is a value computed by the IMC. In terms of the MLP and LSTM structures, results show that the prediction performance is degraded with respect to the Ideal Scenario. This effect is expected since the nets have to model the process under control taking into account measurements corrupted by noise. For instance, the RMSE has increased from 0.030 mg/L to 0.043 mg/L and from 0.045 day^{-1} to 0.101 day^{-1} in the $\mathrm{LSTM_{d,r}}$ and $\mathrm{LSTM_{i,r}}$ architectures, respectively. This is translated into a degradation between a 30.23% and a 55.44% from the Ideal to the Real Scenario. If the performance is only compared in terms of the real one, the improvement of LSTMs with respect to the MLP equals to a 62.55% and a 58.48% in average for the RMSE and MAPE values, respectively. Analysing the MAPE, it is observed that it equals to a 15.85% and a 36.90% for the $\mathrm{LSTM_{i,r}}$ and the $\mathrm{LSTM_{d,r}}$, respectively. This shows that training the neural networks with noisy signals will entail the appearance of higher errors and therefore, an incorrect control behaviour.

5.3.2 ANN-based IMC stability

The stability of the proposed ANN-based IMC must be determined prior to proceed with its implementation and development. Such a controller is implemented with ANNs and therefore, it no longer relies on mathematical models. This entails that classical stability analyses cannot be applied. For that reason, the stability of the whole IMC structure will be computed adopting the ETFE strategy analysis defined in [Roj12a]. This test is mainly focused on the basis that neither mathematical models of the process under control, nor for the inverse or direct models are available. Thus, it estimates the transfer functions of the different elements involved in the ANN-based IMC [Lju99].

Empirical Transfer Function Estimation based Stability Test

ETFE considers that the frequency response of an arbitrarily system $(T(s))$, whose transfer function is unknown, can be inferred whenever pairs of input and output data $(u(t), y(t))$ are available. Thus, its frequency response is estimated as follows:

$$\widehat{T}(j\omega) = \frac{Y(j\omega)}{U(j\omega)} \tag{5.3}$$

where $U(j\omega)$ and $Y(j\omega)$ are the Fourier Transforms of input and output data, respectively. In such a context, the data-based stability test says that a system is stable if

$$\left|\widehat{P}_{dir}(j\omega)\widehat{C}(j\omega)l_m(\omega)\right| \leq 1, \tag{5.4}$$

where $\widehat{P}_{dir}(j\omega)$ and $\widehat{C}(j\omega)$ are the inferred frequency response of $P_{dir}(s)$ and $C(s) = P_{inv}(s)\cdot H(s)$, respectively. $1/|l_m(\omega)|$ stands for the multiplicative uncertainty bound which is defined as the stability limit of the system. Thus, if the product $\left|\widehat{P}(j\omega)\widehat{C}(j\omega)\right|$ is placed over $1/|l_m(\omega)|$ for a given frequency, ω, it means that the stability of the system cannot be assured for this frequency [Roj12a]. In this case, $l_m(\omega)$ is estimated as follows:

$$l_m(\omega) = \frac{|P_{mismatch}(j\omega)|}{|P_{dir}(j\omega)|} \tag{5.5}$$

where $|P_{mismatch}(j\omega)|$ is the frequency response inferred from the mismatch $e'(t)$ between the outputs of the process under control and the direct model when $u(t) = K_{La,5}(t)$:

$$P_{mismatch}\,(j\omega) = \frac{E\,(j\omega)}{U\,(j\omega)} \tag{5.6}$$

The frequency responses are inferred accordingly to their input and output measurements. Nevertheless, they must be obtained following an open-loop configuration, i.e., when the process of interest is not being controlled. Once the different frequency responses are inferred, the stability test is performed. For a given frequency, the ANN-based IMC will be stable whenever the criterion shown in (5.4) is accomplished. Otherwise, the robust stability of the system can be compromised for that frequency. Thus, after completing the test, those frequency ranges where the system is marginally stable will be determined. More details on the computation of the ETFE-based Stability Test can be observed in [Roj12a, Pis20b].

Low-pass IMC filter selection

Let's focus on $l_m(\omega)$, the inverse of the multiplicative uncertainty. Not allowing frequency components over it, this corresponds to the bound determining the stability of the system [Roj12a]. Since $P_{dir}(j\omega)$ and $C(j\omega)$ are the inverse of each other, the product between the two frequency responses should be 1 for all their components. Nevertheless, the stability of the ANN-based IMC cannot be assured for those frequency ranges where the product between frequency responses is placed over the multiplicative uncertainty bound. Here is where the adoption of $H(\omega_c)$ makes sense. Since it actuates over the actuation signal, it has an important role in the stability of the IMC controller. Its ω_c determines the range where the proposed ANN-based IMC is marginally stable. In other words, the decrement of ω_c entails a lowering of the number of frequencies where the ANN-based IMC stability is compromised. This is clearly observed in Figure 5.9 where 10 different configurations of ω_c are considered. As it is depicted, the IMC structure is marginally stable until $\omega = 1.6 \cdot 10^{-3}$ rad/s for the Ideal Scenario and $0.7 \cdot 10^{-3}$ rad/s for the real case. Notwithstanding, the reduction of ω_c increases this range at the expense of degrading the $P_{inv}(s)$

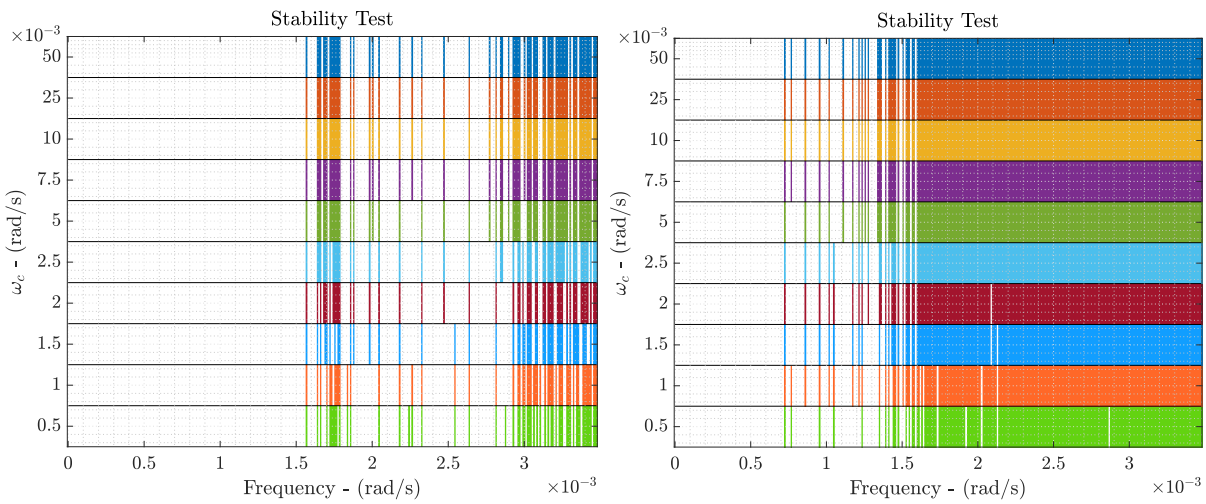

(a) ETFE-based stability for the Ideal Scenario

(b) ETFE-based stability for the Real Scenario

Figure 5.9: Stability test for the Ideal and Real Scenarios. Notice that coloured frequencies corresponds to those ω where the stability is compromised.

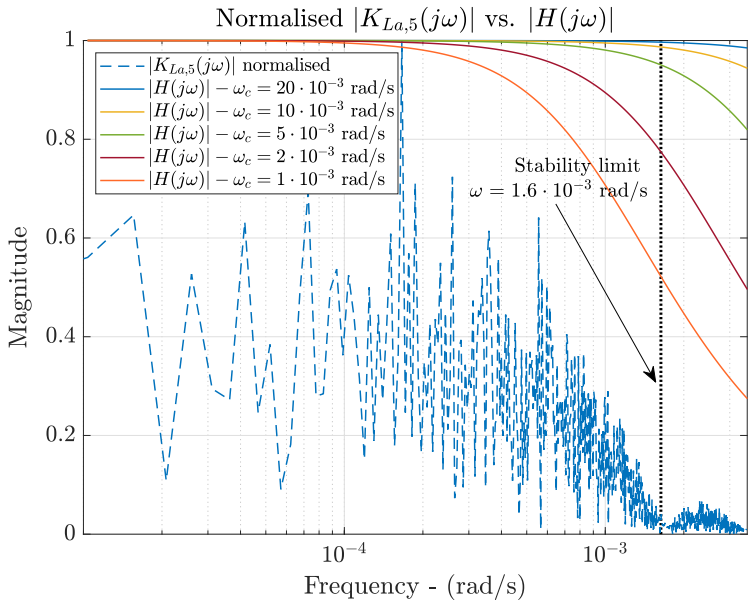

Figure 5.10: $|K_{La,5}(j\omega)|$ vs. $|H(j\omega)|$. Notice that the frequency response of $K_{La,5}(t)$ is normalised in order to place its maximum at a magnitude of 1.

predictions. In that sense, the highest frequency of the signals involved in the management process corresponds to the $K_{La,5}(t)$ on. It is placed just at $\omega = 1.5 \cdot 10^{-3}$ rad/s as depicted in Figure 5.10. Here it is observed that the lower the ω_c, the higher the filter attenuation at $\omega = 1.5 \cdot 10^{-3}$ rad/s. This entails a worsen in the control performance. Besides, it is shown that the stability of the ANN-based IMC for the Real Scenairo cannot be assured whatever ω_c is considered.

5.3.3 ANN-based IMC Control Performance

The ANN-based IMC performance is computed over the two previously mentioned scenarios: (i) the Ideal, and (ii) the Real one. In the ideal case, the default PI controlling the $S_{O,5}$ concentration of the BSM1 framework is substituted by the defined ANN-based IMC structure. On the other hand, the real scenario considers the same IMC control strategy as in the ideal case. Nevertheless, the sensors considered here add non-idealities to the different measurements that must be taken into account. Results are computed accordingly to the BSM1 simulation protocol (see Section 3.1.1) for both scenarios. Therefore, the controller performance is assessed in terms of the BSM1 IAE and ISE metrics. The three weather influents and a variable $S_{O,5_{set-point}}(t)$ (see Figure 5.11) are considered to determine the behaviour of the ANN-based IMC.

Ideal Scenario

Two tests are computed to determine the control performance of the proposed IMC structure. The first one is focused on determining the most suitable ω_c of $H(s)$. As it has been previously stated, when

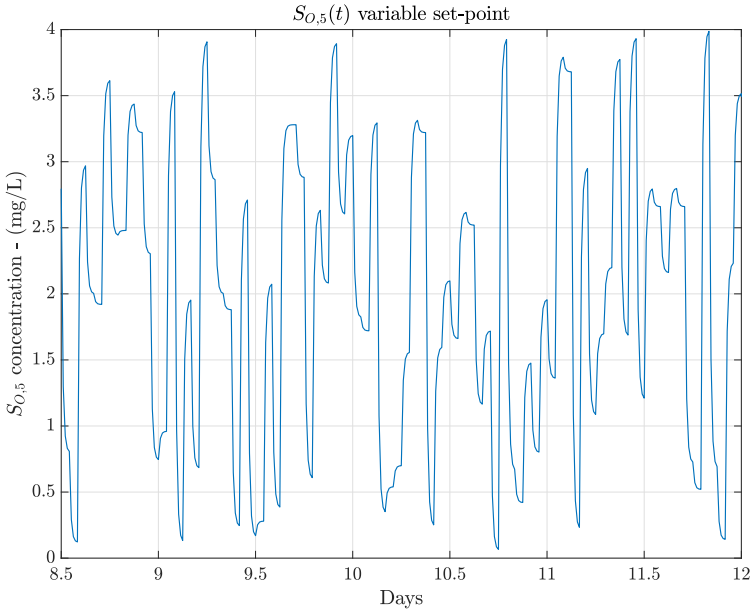

Figure 5.11: Variable set-point considered to compute the ANN-based IMC performance.

the cut-off frequency is decreased, the stability range of the ANN-based IMC is increased, however, the filter actuation will be higher and therefore, the control performance can be degraded. This is clearly depicted in Figure 5.12, where the control behaviour of the Ideal Scenario is computed for different configurations of ω_c. For each cut-off frequency, the IAE and ISE values are computed for the given set-point. As a result, the evolution of the IAE and ISE values is obtained and therefore, the optimal ω_c determined. As depicted in Figure 5.12, $\omega_c = 10 \cdot 10^{-3}$ rad/s is the optimal cut-off frequency offering

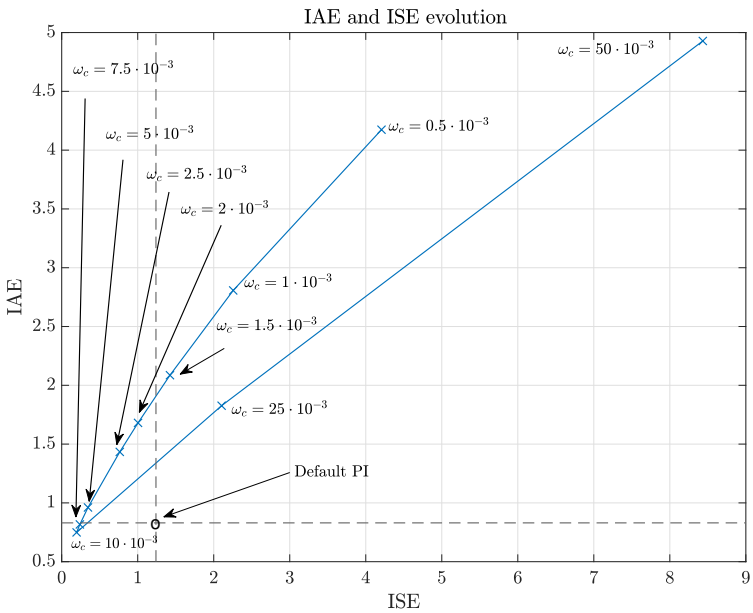

Figure 5.12: IAE and ISE evolution as a function of ω_c. The optimal ω_c equals to $10 \cdot 10^{-3}$ rad/s.

Table 5.5: ANN-based IMC control performance for the Ideal Scenario. Notice that a ω_c of $10 \cdot 10^{-3}$ rad/s is considered as the $H(s)$ cut-off frequency. Besides, dry, rainy and stormy weathers are considered.

ANN-based IMC for the Ideal Scenario						
	Influent Weather Profile					
	Dry		Rainy		Stormy	
Structure	IAE	ISE	IAE	ISE	IAE	ISE
Default BSM1 PI	1.235	0.827	1.227	0.826	1.265	0.851
ANN-based IMC	0.749	0.196	0.659	0.151	0.699	0.172
Improvement [%]	39.35	75.30	46.29	81.72	44.74	79.79

the lowest IAE = 0.75 and ISE = 0.20. Instead, if ω_c equals to $2.5 \cdot 10^{-3}$ rad/s, a worsening in the control performance is produced: IAE and ISE are increased around a 47.76% and 73.44%, respectively.

Finally, the last test is devoted to computing the control performance of the ANN-based IMC for the different weather profiles. Results are shown in Table 5.5. The proposed control is able to better track the given set-point than the default BSM1 PI controller does, independently of the considered weather. The IAE and ISE values are improved a 39.35% and a 75.30%, respectively when a dry influent is considered. These improvements resulted in a 46.29% and an 81.72% when the rainy weather profile is adopted instead. Similar values are also observed for the stormy episodes. In terms of the ANN-based IMC actuation, Figure 5.13 shows that it is able to compute the required amount of $K_{La,5}$ as a function of the measured $S_{O,5}$ and the desired set-point. For instance, when rain and storm episodes are produced, the amount of influent in the WWTP increases and therefore, the oxygen concentration in the reactor tanks

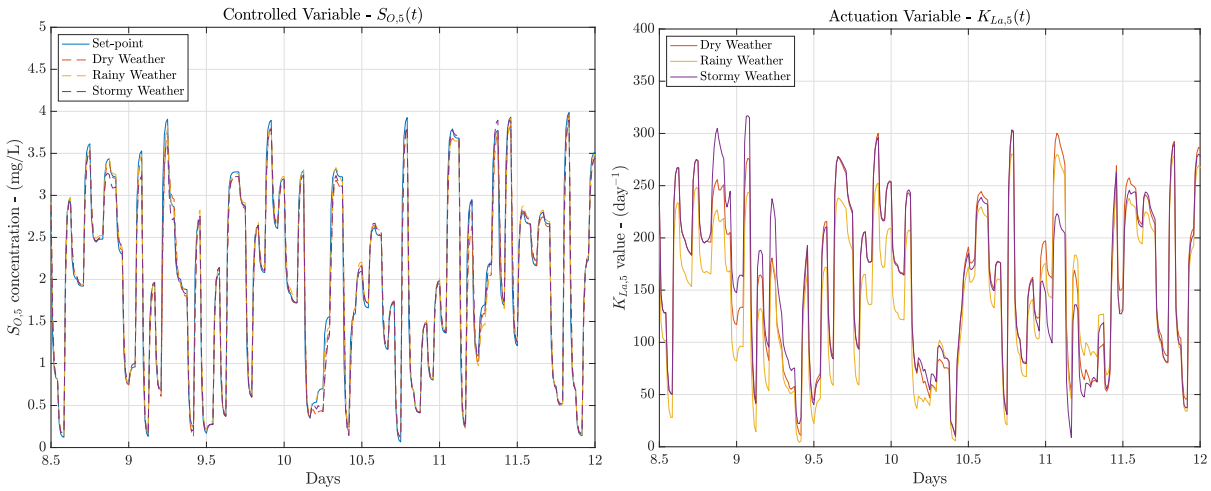

(a) Controlled Variable - $S_{O,5}(t)$ (b) Actuation Variable - $K_{La,5}(t)$

Figure 5.13: Control behaviour of the ANN-based IMC controller for the Ideal Scenario. Dry, rainy and stormy weathers are also considered. Notice that only those days where the behaviour of the ANN-based controller actuation varies are shown.

Table 5.6: ANN-based IMC control performance for the Real Scenario. Notice that a ω_c of $10 \cdot 10^{-3}$ rad/s is again considered as the $H(s)$ cut-off frequency.

ANN-based IMC for the Real Scenario						
	Influent Weather Profile					
	Dry		Rainy		Stormy	
Structure	IAE	ISE	IAE	ISE	IAE	ISE
PI	2.018	1.259	1.991	1.238	2.014	1.267
ANN-based IMC	1.909	0.847	1.888	0.818	1.900	0.828
Improvement [%]	5.40	32.72	5.17	33.93	5.66	34.65

decreases. Moreover, the control is able to add more oxygen in the fifth reactor tank when the $S_{O,5}(t)$ variable set-point requires that. As a summary, the ANN-based IMC controller, which is designed to track a given $S_{O,5}(t)$ variable set-point independently of the influent profile, is able to perform this task better than the default PI controller. Nevertheless, this performance corresponds to an ideal scenario where ideal BSM1 sensors are considered.

Real Scenario

In the Real Scenario, BSM1 real sensors are used instead of the ideal ones. Results of the ANN-based IMC are shown in Table 5.6. As it is observed, its control performance drops if the LSTM nets adopted in the Ideal Scenario are not modified accordingly to the new circumstances. For instance, their IAE and ISE metrics are now around 1.899 and 0.831, respectively, which represents an average increment in the IAE and ISE around a 63.03% and a 79.18% with respect to the Ideal Scenario (see Table 5.5). Moreover, if the difference between the ideal and the Real Scenario improvements is computed, it can be observed that they have been degraded around 38.05 and 45.17 percentage points, respectively. Moreover, the stability of the ANN-based IMC cannot be assured for frequencies over the $0.7 \cdot 10^{-3}$ rad/s as depicted in Figure 5.9b. In the supposition that the ANN-based IMC is considered to manage a real scenario, it could become unstable. Consequently, the correct behaviour of the BSM1 framework, could be compromised. For that reason, new approaches devoted to cleaning the noise-corrupted measurements are proposed in order to tackle the non-idealities and stability issues. Figure 5.14 depicts the effects of the noise.

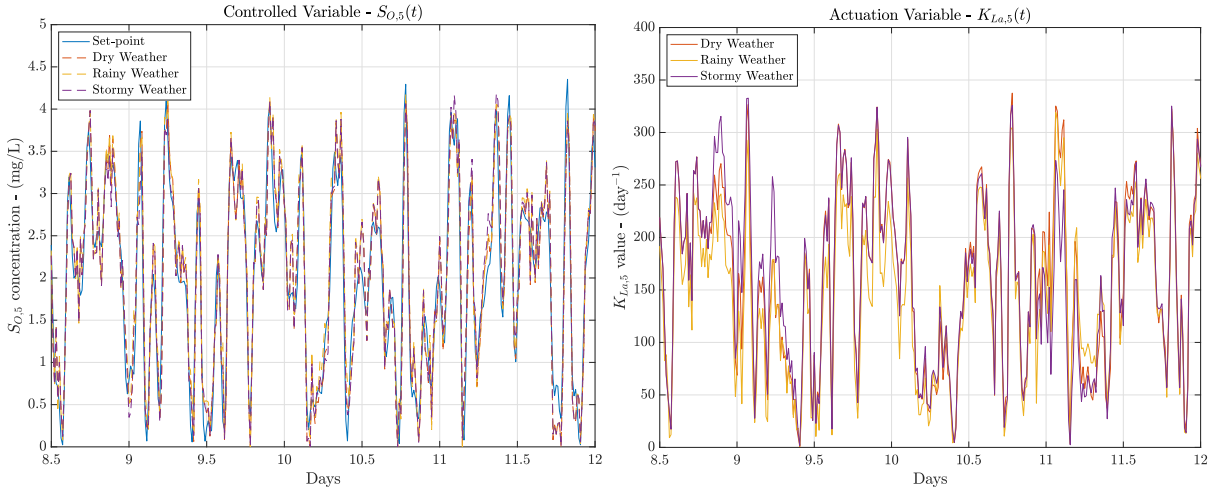

(a) Controlled Variable - $S_{O,5}(t)$

(b) Actuation Variable - $K_{La,5}(t)$

Figure 5.14: Control behaviour of the ANN-based IMC controller for the Real Scenario. Dry, rainy and stormy weathers are also considered. Notice that only those days where the behaviour of the ANN-based controller actuation varies are shown.

5.4 Chapter Conclusions

In this chapter the adoption of ANNs to implement industrial controllers managing the BSM1 control loops is assessed. Two different control structures are considered: (i) the conventional PI, and (ii) the IMC one. The main aim is to adopt ANNs to firstly implement an ANN-based PI controller and secondly an ANN-based IMC from scratch. In both cases the ideal and non-ideal configurations of the BSM1 sensors are considered. As a consequence, the assessment of the ANN-based control strategies provides an insight of their behaviour not only in terms of the control, but also in terms of their dependency on measurements.

Aiming to replicate the behaviour of the conventional BSM1 PI controllers, two ANN-based PI are obtained, one per BSM1 control loop. Both controllers adopt the same architecture, which follows the NARX principle. In addition, each structure is trained either considering the ideal measurements of the desired control loop, or the non-ideal ones. Thus, the prediction performance shows that the most accurate controllers are those trained with ideal measurements. Showing an RMSE equal to 0.026, the ANN-based PI in charge of the $S_{O,5}(t)$ control loop is the one offering the most accurate performance with respect to the conventional PI controller. In terms of the control behaviour, the same effects are observed. The best control performance is again provided by the ANN-based PI structure trained with ideal measurements. They achieve a good tracking process regardless of the weathers being simulated and the chosen set-point. For instance, the IAE and ISE metrics for a dry weather and a fix set-point equal to 0.006 and 0.001, respectively, for the ANN-based PI managing the $S_{O,5}(t)$. Nevertheless, this situation completely changes when non-ideal measurements are considered. The prediction performance

of the ANN-based PI structures drops as a consequence, mainly, of the AWGN noise introduced by the BSM1 sensors. In terms of the ANN-based PI managing the $S_{O,5}(t)$, the control behaviour for the fix and variable set-points is, in this case, degraded. The same is observed for the ANN-based PI managing the $S_{NO,2}(t)$. This shows that some efforts are required in order to reduce the effects of non-idealities in ANN-based PI structures.

The second approach introduced in this chapter consists in the adoption of ANNs to implement a controller from scratch instead of replicating the behaviour of a conventional one. To achieve this, the IMC structure is proposed. It is characterised by explicitly introducing the process under control in the control loop and by considering a direct and inverse model of the processes under control. This fact motivates the adoption of ANNs, especially LSTMs, to implement these models. As it is done with the ANN-based PI structure, the ANNs devoted to implementing the ANN-based IMC are trained considering ideal and real BSM1 measurements. Their prediction performance shows that these structures correctly model the inverse and direct relationships of the process under control. As a controller being modelled from scratch, its stability must be computed. This is performed by means of the ETFE-based stability analysis, which relies on data instead of mathematical expressions. Results show that the ANN-based IMC is stable in the Ideal Scenario, but this cannot be assured for the real one. This is corroborated with the control performance, where it is shown that the ANN-based IMC overcomes the performance offered by the conventional PI controller. In average, the IAE is improved a 43.46% while the improvement equals to 78.94% for the ISE. This paradigm changes when the Real Scenario is considered. Due to the non-idealities, the ANN-based IMC only improves in average the IAE and ISE a 5.41% and a 33.77%, respectively. Nonetheless, the stability of the controller is not assured.

All these results clearly show that ANNs can be adopted to implement controllers, either if a conventional structure is a priori available or if it is necessary to implement it from scratch. Results confirm that this is only possible when ideal measurements are considered. Otherwise, the stability of the controller cannot be assured as well as the control performance drastically drops. All this corroborates that when the Real Scenario is adopted, the need to reduce the effects of non-linearities added by noise is evident.

Chapter 6

ANNs as Non-linear Filters

The appearance of non-idealities in the signals involved in the control process entails a new challenge, especially if ANN-based structures are considered. Not only are the non-idealities degrading the controller performance, but also they can produce the instability of the process under control. For that reason, in this chapter the adoption of data-based approaches to correct and reduce the effects of these non-idealities is assessed. A new strategy based on ANNs is proposed to first clean the noise-corrupted signals and later to diminish the effects of the delays. Its analysis is performed at two levels: to improve the control performance of a conventional PI as well as of an ANN-based IMC.

6.1 Introduction

As it is shown in Chapter 5, the adoption of ANNs in the design and development of ANN-based controllers is possible and, in some cases, desirable. Notwithstanding, these kind of controllers are very sensible to non-idealities and perturbations introduced in the signals considered in the control process. The main perturbations that usually affect these signals are the noise and delays introduced by the non-ideal sensors placed over the industrial plants. The appearance of time-delays is inevitable and consequently, they must be corrected in order to avoid undesirable phenomena like undesired oscillations or the eventual instability of the control system [Red17, Hu19]. In terms of the noise, control strategies are characterised by the requirement of accurate control parameters and therefore, by the adoption of an accurate identification process. Thus, when noise is present in the measurements, the identification and proper control tuning process becomes a challenging task [Zha19]. As shown in Sections 5.2.2 and 5.3.3, the control performance of the proposed ANN-based PI and ANN-based IMC structures drops when such non-idealities are introduced in the control structure. Moreover, in the ANN-based IMC, the appearance of these non-idealities, especially the noise, decreases the range of frequencies where the controller is marginally stable. For that reason, solutions to alleviate these issues are proposed and assessed here.

Different denoising and delay correction approaches can be considered: (i) from the denoising filter-based solutions [Bua08, AlM14] to the data-based denoising techniques such as Principal Component Analysis (PCA) [Zho19] and Denoising Autoencoders (DAE) [Liu19a], and (ii) from forecasting algorithms and controllers to the application of ANNs [Tal17]. For instance, in [San19], a mix between optimised, highly tuned and data-based denoising approaches is proposed. It implements two stages, one to denoise the measurements and the other to correct the delays. The denoising process is performed adopting highly tuned low-pass filters whereas the delay correction process is done by means of ANNs. The main drawback there is that the complete structure has been designed and optimised to offer a good performance in a specific scenario: the filter-based solutions have been designed considering the type of signals as well as the type of sensors, whereas the ANNs correcting the delays are considering input and output pairs of data obtained from controlled structures. Thus, a high knowledge of the processes being controlled is required while the control solution may not be generalisable.

Taking all the aforementioned points into consideration, this chapter is devoted to showing and proposing a complete and easy tuning Data-based Control Enhancement Processing approach. Based on the structure proposed in [San19], the new proposed approach is purely based on data-driven methods, especially on ANNs. The point is that they are trained considering input and output data of the process being controlled. Thus, a deep knowledge of the process being managed is not required. It will be derived from the input and output measurements. Therefore, this new approach will achieve the reduction of the design process complexity and the increment of its scalability [Lan19, Hua20]. Besides, as a consequence of reducing the noise effects, the range where controllers are stable can be increased as well. To achieve this, the Data-based Control Enhancement Processing approach considers two different stages which can actuate separately depending on the non-linearity to tackle. The first stage consists in the data-based Denoising Stage, which is focused on the application of DAEs. Its main objective is to denoise the measurements involved in the control so as to treat them as ideal values. The second stage consists in the ANN-based Delay Correction, which is devoted to tackling the delays affecting the control and actuation signals. Since it is based on ANNs, this process is performed considering input and output data obtained from the environment's open-loop configurations. Therefore, the decoupling of the proposal from mathematical models and specific controllers is achieved. The proposed Data-based Control Enhancement Processing approach will correct the noise-corrupted and delayed measurements by means of the experience obtained from input and output data, neither requiring a highly complex tuning process, nor a deep knowledge of the processes being controlled. In order to assess the proposed approach, two different scenarios are considered. The first one consists in the scenario presented in [San19], where the Control Enhancement Processing approach is proposed to substitute the filtered-based denoising approach as well as the ANN-based delay correction of a control strategy being applied over BSM1. The second one consists in the ANN-based IMC presented in Section 5.3. Thus, the main aim is to reduce the effects of noise affecting the ANN-based IMC and therefore, increase its stability margin and improve its control performance.

As a summary, the contributions of this chapter are:

- A complete data-based solution is proposed to improve an existing control strategy. Its main objectives are the reduction of the design complexity as well as the increment of the solution scalability.
- Data-based methodologies and specially ANNs are considered as the main tools in the denoising process of measurements involved in the control process.
- ANNs in charge of correcting the delays introduced by the sensors and actuators will be trained with open-loop input and output data to assure the decoupling of the solution from the control topology.
- The stability margin of the ANN-based IMC structure is increased by means of ANNs, obtaining a much better control behaviour.

Finally, this chapter is structured as follows: in Section 6.2 the Data-based Control Enhancement Processing approach is presented and its main stages defined and analysed. Later, in Section 6.3, the application of the complete approach over a conventional PI structure is assessed. In Section 6.4, the same is performed to the ANN-based IMC, however, the efforts are focused on the most critical issue: the noise introduced by the BSM1 real sensors. Finally, Section 6.5 concludes the chapter. This chapter describes the works presented in [Pis19a,Pis20c,Pis20b] and part of the work presented in [Pis20a,Pis21b,Pis21c].

6.2 Data-based Control Enhancement Processing Approach

Measurements' original quality is one of the key factors that determines the operational and control performance of industrial controllers regardless they are data-driven or conventional approaches. Based on this, the proposed Data-based Control Enhancement approach will be directed towards a data-driven processing of the measurements and signals before they reach the controller. The main purpose is to minimise the effect of noise and delays, therefore allowing the controller to be as much transparent as possible to non-idealities effects. To achieve this the Data-based Control Enhancement Processing approach is proposed. It considers the data enhancement of the complete control process, i.e., from the sensor to the output of the actuator just before entering in the plant. Its main architecture is shown in Figure 6.1. As observed, it implements two main stages: (i) the Data-based Denoising Stage, and (ii) the ANN-based Delay Correction Stage.

Since both stages are based on ANNs, the Data-based Control Enhancement Processing approach can be implemented without requiring a deep knowledge of the system where it is going to be deployed. Only input and output pairs of measurements are required. They can be obtained following two manners according to the industrial scenario. If an open-loop configuration is considered, input and output measurements can be directly obtained from sensors and systems monitoring the processes, for instance, the

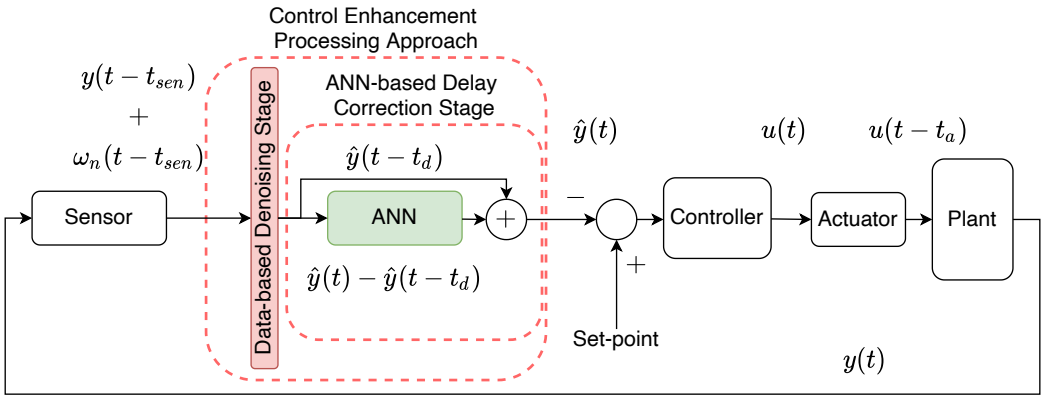

Figure 6.1: Data-based Control Enhancement Processing Approach. $u(t)$ is the actuation signal whereas $\widehat{y}(t)$ corresponds to the clean estimation of the controlled signal. t_{sen} and t_a are the delays introduced by the sensors and the actuator, respectively. t_d is the delay considered in the ANN-based Delay Correction Stage.

SCADA systems. In the case where the scenario is already being controlled, the effects of the considered control structure will be intrinsically present in the measurements. Therefore, the decoupling of the proposed approach from the control strategy will not be achieved.

Thus, focusing on the proposed architecture, the sensor determines the controlled, delayed and noise-corrupted variable, $y(t - t_{sen}) + \omega_n(t - t_{sen})$. Then, the noise effect is corrected by the Data-based Denoising stage, which estimates the ideal output from the input measurements, $y(t - t_{sen})$. Later, these estimations, which are still showing the delay effects, are treated in the ANN-based Delay Correction stage. It corrects the delays introduced by the non-ideal sensors estimating the non-delayed ideal value, i.e., the $\widehat{y}(t)$. Then, this output is compared to the given set-point and transformed into the corresponding actuation signal, $u(t)$. Notice that the actuator adds a delay equal to t_a, however, the forecasted measurements, $\widehat{y}(t) - \widehat{y}(t - t_d)$, as well as the actuation signal given by the PI controller have intrinsically considered this amount of time. Finally, the actuation signal entering in the plant, $u(t - t_a)$, equals to a non-delayed actuation signal with respect to the forecasted control one, $\widehat{y}(t)$.

As a summary, our Data-based Control Enhancement Processing approach achieves the improvement of a control strategy by means of (i) decreasing the design process complexity, and (ii) increasing its scalability [Lan19, Hua20]. Indeed, the complexity reduction is achieved since ANNs do not require a such precise adjustment to the scenario as usual filtering strategies do. In addition, the scalability is increased since ANNs can be applied in different industrial scenarios: the knowledge of the controlled scenario is directly derived by ANNs if they are trained with proper data [DS17, Chapters 1, 2, 5 and 17].

6.2.1 Data-based Denoising Stage

The Data-based Denoising stage is devoted to cleaning the noise-corrupted measurements. It can implement different denoising methods which have been applied in a great variety of fields, for instance, in the

image or the signal processing ones [Bua08, AlM14]. Some of them consist in the application of low-pass filters, wavelet transform and the application of certain estimations like the ones based on Least Means Squares [Sur18, Sam17]. However, the appearance of data-based denoising techniques promoted their adoption as denoising approaches as well. Their key point is that they only consider the data gathered from the scenario. This is the case for example of the PCA and DAEs:

- **Principal Component Analysis**: it is an algorithm adopted to reduce the dimensions of input data in linear problems by means of decomposing the input data into eigenvalues and eigenvectors. They will be considered later to map input data into a latent space with a lower dimension [Goo16, Chapter 14]. The same principle is applied when the PCA algorithm is considered as a denoising method. The noise-corrupted signals are decomposed into the signal and noise space. Thus, input values are mapped into the PCA latent space and then they are recovered considering only the eigenvalues of the signal space [Zho19]. However, although PCA can be adopted as a denoising method, its performance can be compromised due to the nature of the system: PCA has been conceived to work with linear systems while BSM1 framework replicates the behaviour of highly complex and non-linear processes [Cop02].

- **Denoising Autoencoder**: it is based on the application of Autoencoders, an ANN-based structure devoted to reducing the input dimensions of data [Goo16, Chapter 14]. The Autoencoder main aim is to replicate the input data in the output layer. Therefore, the idea of the DAE is to replicate the input data in the output of the net, but, reducing the amount of noise present in the measurements [Liu19a]. As a neural network structure, the DAE can be implemented considering different types of ANNs such as MLP, the usual structure, or more complex ones like LSTM cells [CJ16, Liu19b].

Since the proposed Data-based Control Enhancement Processing approach is going to be deployed over the BSM1 scenario, the adoption of DAEs is highly motivated [Goo16, Section 14.5].

Denoising Autoencoder Architectures

The DAE structure main aim is to take noise inputs and return clean versions of them. Its structure is characterised by its architecture. It considers two well-defined parts: (i) an encoder, and (ii) a decoder. The encoder is in charge of taking the m noise-corrupted measurements and map them into a latent space of dimensionality k, which not only extracts the characteristics of the input measurements, but also reduces their input dimensionality ($m > k$). The decoder part performs the inverse action, it takes the outputs of the latent space and transforms them into clean measurements with the same dimensionality as the inputs [Boq19]. The ANNs considered in the DAEs implementation depend on the type of measurements they are going to face to. In such a context, DAEs can be designed either considering MLP networks (see Figure 6.2) in those cases where the time correlation between measurements is not

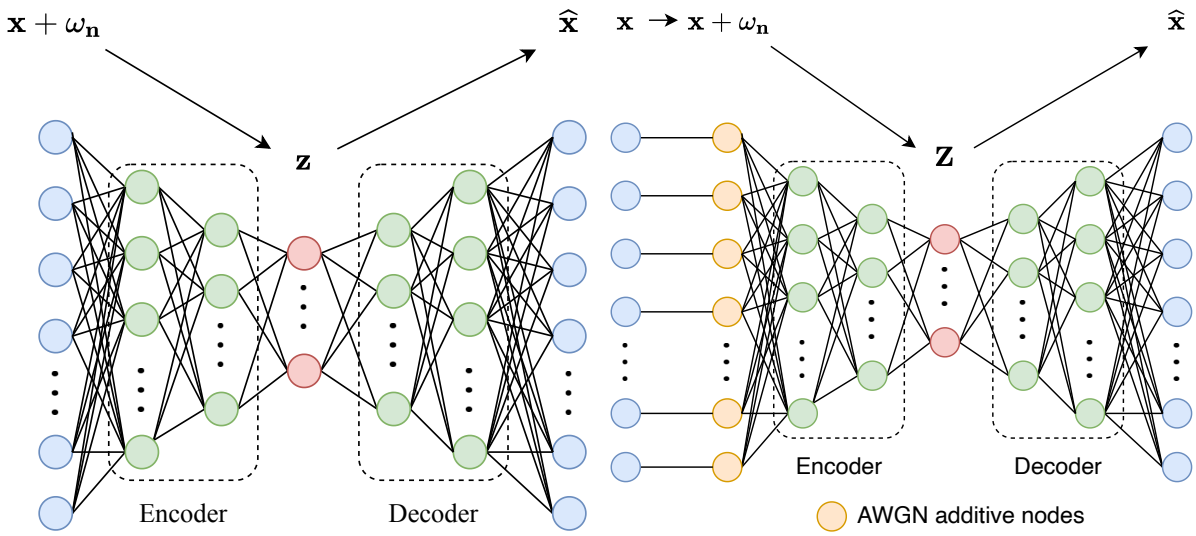

(a) DAE considering noise-corrupted and ideal measurements (b) DAE considering ideal measurements

Figure 6.2: DAE architectures. Notice that $\mathbf{x} \in \mathbb{R}^{m\times 1}$ corresponds to the input data of the DAE architecture. $\omega_\mathbf{n} \in \mathbb{R}^{m\times 1}$ stands for the noise corrupting $\mathbf{x}$. $\mathbf{z} \in \mathbb{R}^{k\times 1}$ corresponds to the compressed data which is represented in the k-dimensional latent space. Finally, $\hat{\mathbf{x}} \in \mathbb{R}^{m\times 1}$ is the denoised data vector.

so important [DS17, Chapter 5]. In those cases where the time correlation is predominant, MLPs with a Sliding Window or LSTM cells can be considered [Goo16, Chapter 10].

In terms of its training process, the DAE needs to be trained considering noise-corrupted measurements as input data and clean ones as the outputs. In such a context, two different architectures can be adopted depending on the available data. If noise-corrupted and clean measurements are available, the DAE architecture can be conceived as a neural network with different layers performing the encoding and decoding processes as depicted in Figure 6.2a. In the case where noise-corrupted information is not available, the DAE can be still considered if a noise layer is added to its structure. Figure 6.2b depicts this configuration. The noise distribution of the hidden nodes should equal to the noise added by the non-ideal sensors. For that reason, $\omega_n \sim \mathcal{N}(0, 1)$ is considered here since it is the noise distribution of the BSM1 non-ideal sensors.

6.2.2 ANN-based Delay Correction Stage

The Delay Correction Stage purpose is to correct the delay introduced not only by the sensors, but also by the actuator. This is performed by means of predicting the controlled variable. The predicting tool consists in a simple MLP network with two hidden layers (see Figure 6.3). The first one corresponds to a hidden layer with a sigmoid actuation function whilst the second corresponds to a hidden layer with a linear activation function [DS17, Chapter 1]. The sigmoid layer dimension SLd is determined by the designer while the linear layer dimension, $LLd = 1$, is fixed to 1 by default.

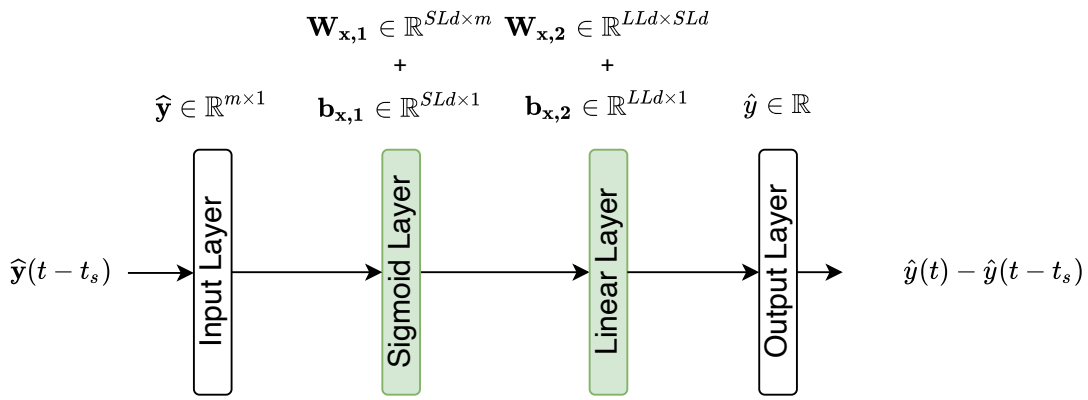

Figure 6.3: ANN-based Delay correction net. $\widehat{\mathbf{y}}$ corresponds to the vector of denoised measurements and $\widehat{y}$ corresponds to the controlled variable. $\mathbf{b_{x,i}}$ and $\mathbf{W_{x,i}}$ are the biases and weights of the i-th hidden layer, respectively. m is the number of variables considered in the ANN-based Delay Correction net. Hidden layers are green coloured while input and output layers are depicted in blue.

Here, the input data correspond to m denoised and delayed measurements which will be modified by the weights and biases of the sigmoid layer, $\mathbf{W_{x,1}} \in \mathbb{R}^{SLd\times m}$ and $\mathbf{b_{x,1}} \in \mathbb{R}^{SLd\times 1}$, respectively. The number of hidden neurons in this layer, which is defined by the designer, is equal to SLd. Then, the outputs of this hidden layer are modified by the linear layer, whose weights and biases are $\mathbf{W_{x,2}} \in \mathbb{R}^{LLd\times SLd}$ and $\mathbf{b_{x,2}} \in \mathbb{R}^{LLd\times 1}$, respectively. Finally, the output of the net corresponds to a prediction of the difference between the expected values of the controlled signal with the actuator delay correction, $\widehat{y}(t)$, and the delayed controlled signal $\widehat{y}(t-t_s)$. This is performed as such because the training process of the ANNs becomes less complex and therefore, the convergence point is reached before [San19]. The output of the whole ANN-based Delay Correction stage (see Figure 6.1) will be equal to $\widehat{y}(t)$. Then, the controller computes the actuation variable $u(t)$ accordingly to its input, $\widehat{y}(t)$. Finally, the signal obtained after the actuator, and therefore, the signal entering in the plant corresponds to $u(t-t_a)$, which is an estimation of the actuation signal derived from the ideal controlled variable.

In that sense, two different scenarios are considered to compute the performance of the proposed Data-based Control Enhancement Processing approach:

- **Denoised Conventional PI**: this scenario has been previously considered in [San19], where a classical denoising method, a moving average low-pass filter, is considered to clean the measurements involved in the control of BSM1's $S_{O,5}(t)$. However, the filter is able to reduce the noise effects at expense of adding extra delays. Not only this, the denoising performance can be still improved since it does not consider any kind of knowledge about the dynamics of noise affecting the measurements. This scenario is considered since the behaviour of the BSM1's default controller is already known, either when ideal or real measurements are considered. Thus, any improvement in the control performance achieved with the proposed Contron Enhancement Processing approach can be easily determined.

- **Denoised ANN-based IMC**: this scenario corresponds to the ANN-based IMC defined and implemented in Section 5.3. As it is previously shown, when the ANN-based IMC is dealing with noise-corrupted measurements, the control performance drastically drops. Moreover, its stability cannot be assured for the frequencies of the involved signals. Since the noise effects are the most critical and challenging non-idealities in the IMC structure, the Data-based Denoising stage of the proposed Data-based Control Enhancement approach is considered. By means of denoising the noise-corrupted signals, the improvement of the control performance and the widening of the marginal stability range is sought.

6.3 Denoised Conventional PI

The first scenario where the proposed Data-based Control Enhancement Processing approach is assessed corresponds to the one managed in [San19]. Thus, this section is devoted to assessing and determining the behaviour of the Data-based Control Enhancement approach to correct the non-idealities of measurements and therefore, improve the control performance of the conventional PI controller. To perform this assessment, the Data-based Denoising as well as the ANN-based Delay Correction stages will be evaluated separately.

6.3.1 Denoising Stage

In order to implement the Data-based Denoising Stage, two different MLP-based denoising architectures are considered. Although LSTM cells have been designed to work with time-correlated signals, MLP-based structures are considered for two reasons: their complexity is reduced with respect to LSTM cells, and they also show a good performance when dealing with WWTP measurements (see Chapter 5). Besides, the time correlation between measurements can be preserved by means of sliding windows, which not only sort the measurements in time, but also help in the denoising process.

In such a context, the two MLP-based structures consist in: (i) a MLP-based DAE, and (ii) a Dedicated MLP-based DAE, both considering a sliding window (see Figure 6.4). The MLP-based DAE corresponds to the structure shown in Figure 6.4a whereas the Dedicated MLP-based DAE approach is shown in Figure 6.4b. Both architectures have a common structure in charge of the data preprocessing tasks: the Sliding Window and the Normalisation layers. Here, the WL is determined through the process widely explained in [Pis20c], where it is shown that the minimum periodicity of input variables should be considered as the minimum length of the sliding window. Thus, it is set to 4 h. Then, the sorted measurements are normalised towards zero mean and unit variance in the Normalisation layer.

The denoising approaches of both architectures differ in the topology of the considered nets. The MLP-based DAE will take the vector of noise measurements sorted in time and normalised as the input data and will return a cleaned version of it (see Figure 6.4a). Here, the dimension of input and output

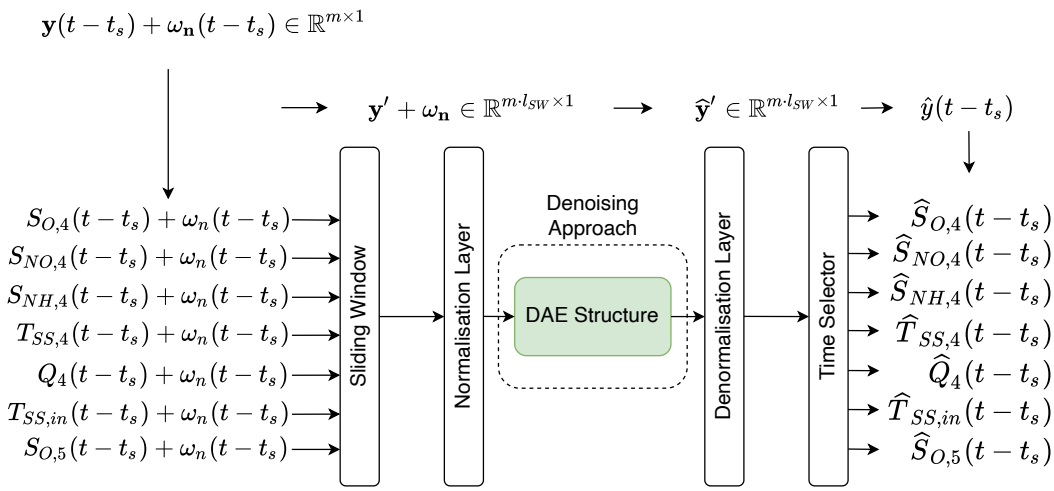

(a) MLP-based DAE

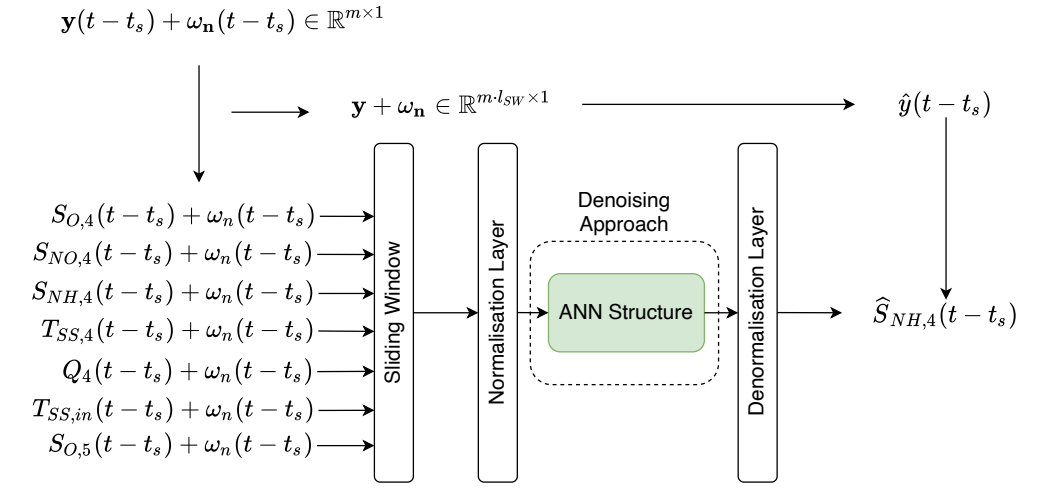

(b) Dedicated MLP-based DAE denoising the $S_{NH,4}(t)$ signal

Figure 6.4: MLP-based Denoising and Dedicated MLP-based Denoising Architectures. Notice that the main difference is placed after the denoising approach. The MLP-based DAE obtains a clean version of the measurements, i.e., a column vector of length $m \cdot l_{SW}$, where m represents the number of input measurements and l_{SW} the length of the sliding window. The Dedicated MLP-based DAE directly estimates a clean version of a unique measurement.

vectors are exactly equal, $\mathbb{R}^{m\cdot l_{SW}\times 1}$, where m and l_{SW} are the number of input variables and the length of the sliding window, respectively. Moreover, the input vector consists in noisy measurements whereas the output one consists in their clean version. Then, the clean measurements are denormalised in the Denormalisation layer and finally, only the last cleaned measurements per variable are selected in the Time Selector layer. Since this architecture replicates the input measurements, the outputs consist in all the measurements gathered by the sliding window. For that reason, the Time Selector layer is compulsory in order to select the desired measurements.

On the other hand, the denoising approach considered in the Dedicated MLP-based DAE structure (see Figure 6.4b) corresponds to a modified MLP-based DAE. It directly estimates a clean version of a unique variable rather than mapping the inputs into a latent space and then recover a clean version of them. In other words, it consist in an ANN predicting the denoised measurements.

Input Data & Training Process

In terms of the input measurements, both architectures consider inputs obtained from the mass balance equation of the $S_{O,5}$ concentration, its conversion rate and the biological processes described in [Hen87, San19]. These variables are:

- $S_{NH,4}$: the ammonium concentration present at the output of the BSM1's fourth reactor tank.
- $T_{SS,4}$: the total suspended solids at the output of the BSM1's fourth reactor tank.
- Q_4: the flow rate at the output of the BSM1's fourth reactor tank.
- $T_{SS,in}$: the total suspended solids at the input of the BSM1 model.
- $S_{O,5}$: the dissolved oxygen in the BSM1's fifth reactor tank

Extra variables are considered to complement the MLP-based Denoising architectures. They correspond to the $S_{O,4}$ and the $S_{NO,4}$. As shown in Section 5.3, they are two of the variables showing the highest mutual information with respect to the $S_{O,5}$ concentration [Han15, Pis19a, Pis19b].

A grid search methodology considering the BPTT algorithm and the Adam optimizer is considered to determine the MLPs' internal structures [Goo16, Sections 6.5 and 8.5.3] [Mai17, Ami20]. It is performed to compute the number of hidden layers and hidden neurons per layer of the two denoising approaches. Thus, results of the grid search show that the best architectures are:

- **MLP-based DAE**: DAE structure with two hidden layers as the encoder part, a hidden layer acting as the latent space and two hidden layers as the decoder. The two layers forming the encoder consider a total amount of 100 and 50 hidden neurons, respectively. The latent space considers 25 hidden neurons and the decoder layers consider 50 and 100 hidden neurons, respectively. Each hidden node implements a Rectified Linear Activation (ReLU) function except for the last hidden layer which implements a linear activation function in each node [DS17, Chapter 1].
- **Dedicated MLP-based DAE**: The Dedicated MLP-based DAE considers three hidden layers where the first one implements 100 hidden neurons whereas the last two 50 hidden nodes. Here, the last hidden layer corresponds to a unique node which implements the Linear activation function. The rest of nodes consider the ReLU function.

In both cases, an initial learning rate of $1 \cdot 10^{-3}$ and a total amount of 500 epochs are considered to perform the grid search. Overfitting issues are tackled by L2 and early stopping techniques. The L2 parameter is set to $1\dot{1}0^{-3}$ for the MLP-based DAE structure and $1 \cdot 10^{-4}$ for the Dedicated MLP-based DAE net. The early stopping patience is equal to 10.

The data required to perform the grid search process are generated in the BSM1 framework simulating twice a whole year of uniformly distributed BSM1 weather influents. Besides, ideal and real BSM1 sensors are considered. Consequently, four datasets are obtained in pairs: two for the Ideal Scenario and the other two for the real one. One pair of datasets, ideal + non-ideal data, are devoted to performing the grid search whilst the others are considered in the cross-validation process. Finally, each dataset has been divided into the usual 70-15-15 percentage distribution, where the first 85% of data are considered for training and validation purposes and the remaining 15% for testing ones.

Denoising Performance

The Data-based Denoising performance is shown in Table 6.1, where the results of the denoising structures are computed in terms of RMSE, MAPE, R^2 and t_{time}. The classical denoising approach, i.e., the moving average low-pass filter proposed in [San19], is also considered as a baseline showing the minimum available performance. One of the clearest points is that data-based methodologies overcome the performance offered by the moving average low-pass filter in terms of the RMSE. For instance, the MLP-based DAE improves the RMSE a 63.87%. This improvement is increased until an 87.32% and an 86.56% when the Dedicated MLP-based DAE is considered. Results also show that the best denoising approach corresponds to the Dedicated MLP-based DAEs, which are able to offer an average RMSE equal to 0.033, an average MAPE of 1.27% and a R^2 coefficient equal to 0.998.

It is worth noting here that the differences between the MLP-based DAE and the Dedicated MLP-based DAEs are motivated by their denoising efforts. For instance, the MLP-based DAE divides its efforts in denoising all the noise-corrupted measurements. On the other hand, the Dedicated MLP-based DAEs focus their efforts on estimating a clean version of just a unique concentration. Consequently, as many Dedicated MLP-based DAEs as signals and measurements involved in the control process are required. Moreover, it is appreciated in the t_{time} that the MLP-based DAE requires a total amount of 113.53 seconds while the Dedicated MLP-based DAEs highest training time equals to 62.25 s, nearly the half of the MLP-based DAE training time.

Although the MLP-based DAE is a similar approach to the Dedicated MLP-based DAEs and its performance shows low RMSE values, it has two critical points: the $S_{NH,4}(t)$ and the $S_{O,5}(t)$ MAPE values equal to 11.14% and 5.18%, respectively. Let's suppose that a real $S_{O,5}$ concentration equal to 2.5 mg/L is present in the WWTP fifth reactor tank. When it is measured, the value will be corrupted by noise and delayed by the sensor. To tackle this, the MLP-based DAE is considered, however, the range where the $S_{O,5}$ denoised measurement will be placed corresponds to $[2.37, 2.63]$, which is a wide range

Table 6.1: Data-based Denoising Stage performance. RMSE is measured in mg/L for all the measurements except for the Q_4, which is given in $\mathrm{m}^3/\mathrm{day}$. MAPE is measured in %. R^2 is a dimensionless metric.

Classical Filter Approach				
Variable	RMSE	MAPE	R^2	t_{time}
$S_{NH,4}$	0.203	14.65	0.96	-
$T_{SS,4}$	0.350	1.22	0.88	-
Q_4	0.215	4.75	0.97	-
$T_{SS,in}$	0.339	6.64	0.91	-
$S_{O,5}$	0.194	17.87	0.96	-
MLP-based DAE				
Variable	RMSE	MAPE	R^2	t_{time}
$S_{O,4}$	0.059	1.94	1.00	113.53
$S_{NO,4}$	0.078	1.29	0.99	113.53
$S_{NH,4}$	0.111	11.14	0.99	113.53
$T_{SS,4}$	0.127	0.46	0.98	113.53
Q_4	0.165	4.04	0.97	113.53
$T_{SS,in}$	0.085	2.07	0.99	113.53
$S_{O,5}$	0.034	5.18	1.00	113.53
Dedicated MLP-based DAE				
Variable	RMSE	MAPE	R^2	t_{time}
$S_{O,4}$	0.021	0.73	1.00	38.40
$S_{NO,4}$	0.030	1.00	1.00	43.04
$S_{NH,4}$	0.019	2.72	1.00	48.77
$T_{SS,4}$	0.043	0.39	0.99	41.71
Q_4	0.023	0.96	1.00	42.70
$T_{SS,in}$	0.024	0.97	1.00	49.80
$S_{O,5}$	0.016	2.15	1.00	62.25

and therefore, inaccurate. On the other hand, the moving average low-pass filter approach presents the same issue: its MAPE value is even higher, 17.87%. The solution therefore is to consider the Dedicated MLP-based DAE, whose MAPE value is equal to 2.15%. Thus, the range where the denoised $S_{O,5}$ measurement can be placed is drastically reduced until the $[2.45, 2.55]$ range. This will entail that the controller compares a more accurate $S_{O,5}$ measurement with the desired set-point. So, the lower the MAPE, the higher the accuracy, the better the denoising process and therefore, the better the control. In terms of R^2 metric, all the approaches are able to show a good correlation between denoised and ideal measurements.

All these facts motivate the adoption of the Dedicated MLP-based DAEs as the denoising approach of the Data-based Denoising Stage. Although one DAE is required per denoised measurement, their good performance is crucial to make the choice. Figure 6.5 depicts the denoising behaviour when the

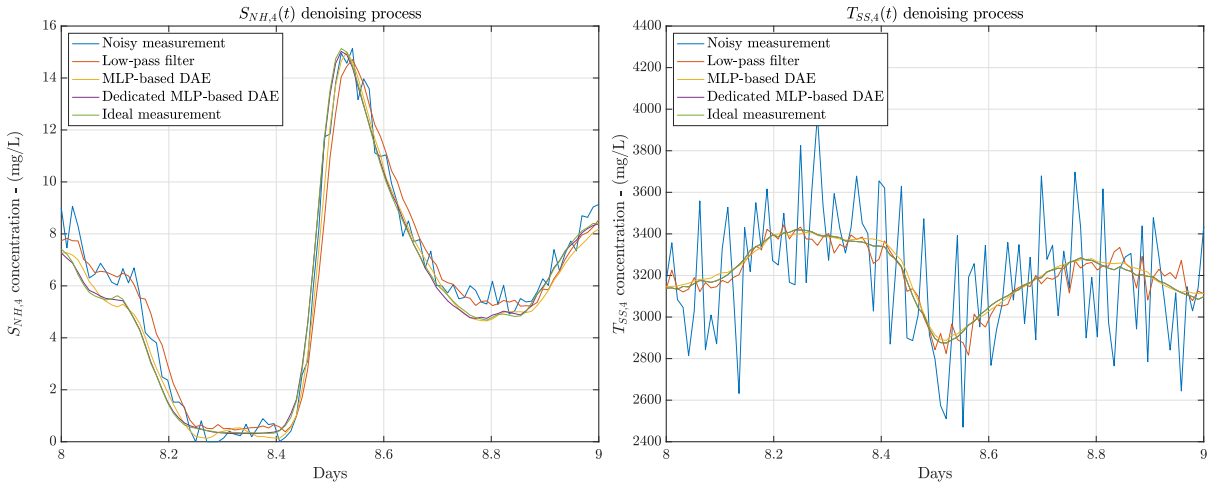

(a) $S_{NH,4}(t)$ denoising process.

(b) $T_{SS,4}(t)$ denoising process.

Figure 6.5: Denoising Process performed by the different approaches. Notice that the denoised $T_{SS,4}$ is not observed since it is hidden under the ideal measurement line.

different approaches are proposed to denoise the $S_{NH,4}$ and $T_{SS,4}$ concentrations. The worst performance if offered by the low-pass filter approach due to their implicit delay and low denoising accuracy. On the other hand, the best one corresponds to the Dedicated MLP-based DAEs which offer clean measurements practically identical to the ideal ones.

6.3.2 Delay Correction Stage

The ANN-based Delay Correction stage considers MLP networks whose main objective is to predict the difference between the cleaned measurement of the $S_{O,5}(t)$ sensor and the delayed $S_{O,5}$ concentration. In such a context, the concentration is even more delayed, t_d = 6 minutes so as to ensure that all the delays introduced by the non-ideal A sensors t_{sen} = 1 minute as well as by the delays of the actuator t_a = 4 min are corrected. In those cases where measurements from B_0 sensors are considered, the delay is nearly completely reduced since MLP networks will receive more information from type A sensors.

In that sense, the output of the whole ANN-based Delay Correction Stage (see Figure 6.1) equals to $\widehat{y}(t) = S_{O,5}(t)$. Then, the controller will compute the actuation variable accordingly to its input, $u(t) = K_{La,5}(t)$. For that reason, correcting the delay introduced in the controlled variable is of the utmost importance. A delayed measurement entails the computation of a delayed actuation and therefore, the estimation of an incorrect actuation variable. Moreover, the actuator also adds its own actuation delay. Thus, the signal obtained after the actuator, and therefore, the signal entering in the plant corresponds to $u(t - t_a) = K_{La,5}(t - t_a)$. For that reason, the actuation is provided to the plant with a little but affordable delay. Prior to achieve this behaviour, the ANN of the ANN-based Delay Correction stage has to be designed and trained accordingly to the considered input and output data.

Input Data & Training Process

Three different configurations of input and output data are considered. They have been selected according to the mass balance equations of $S_{O,5}(t)$, the type of control and the simulated weather profile. As a result, the three configurations are tested for the dry, rainy and stormy weathers (see Figure 3.3) when either a fixed, or a variable set-point is considered in the control strategy. Thus, these configurations are:

- **ANNconf1**: it considers the $S_{NH,4}(t)$, the $T_{SS,4}(t)$, the $Q_4(t)$, the $T_{SS,in}(t)$, the $K_{La,5}(t)$, the $S_{O,5}(t)$ and a storm flag which is enabled when $T_{SS,in}(t)$ is over 400 mg/L. This configuration is based on the one presented in [San19].
- **ANNconf2**: it considers the same inputs as ANNconf1, but the storm flag is changed by the readily biodegradable substrate in the fourth reactor tank, $S_s(t)$, which is measured with the soft-sensor proposed in [Ben07].
- **ANNconf3**: it considers the same inputs as the ANN-based denoising architectures adding the actuation variable of the $S_{O,5}$ control loop, i.e., the $K_{La,5}$.

Among the different variables, $T_{SS,in}(t)$, $S_{NO,4}(t)$ and $Q_4(t)$ are considered to detect the topology of weather since Q_4 values higher than 9.24×10^4 $\mathrm{m}^3/\mathrm{day}$ are observed when rainy and stormy events are produced (see Figure 3.3). In that sense, $T_{SS,in}(t)$ and $S_{NO,4}(t)$ determine when a stormy event is produced. This happens whenever $T_{SS,in}(t)$ values are placed over 400 mg/L or $S_{NO,4}(t)$ is below 5.5 mg/L (see Figure 6.6).

Each configuration has been trained considering the BSM1 open-loop configuration. This is performed to achieve the decoupling of the ANN-based Delay Correction stage from the considered con-

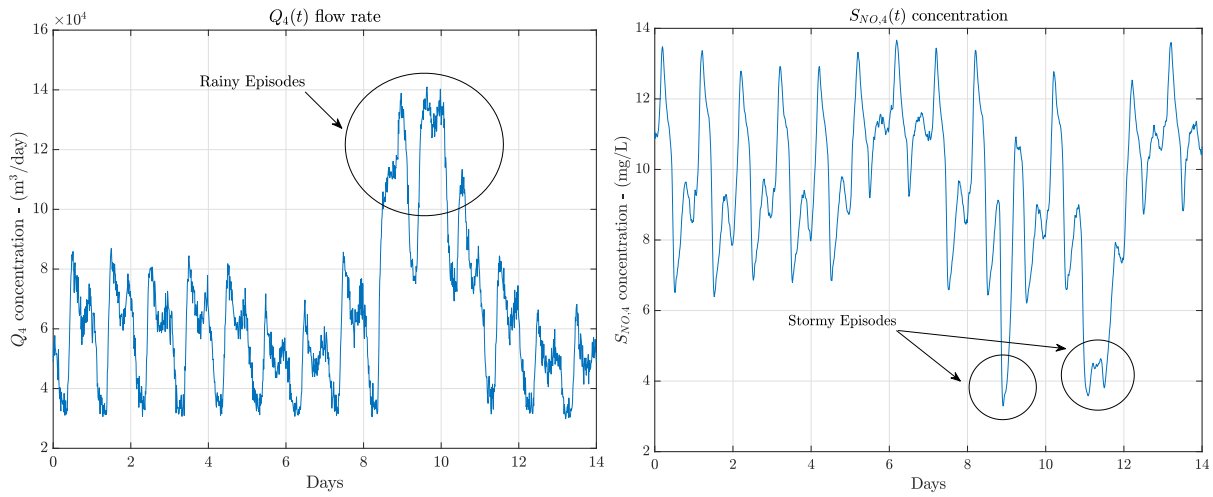

(a) $Q_4(t)$ flow rate showing the effects of rainy episodes

(b) $S_{NO,4}(t)$ concentration with two stormy episodes

Figure 6.6: Measurements and signals where the effects of rainy and stormy episodes are more noticeable.

troller. Moreover, this also decreases the design complexity of the whole structure since no controller is required to obtain the input and output data. For comparison purposes the different measurements are obtained performing the same pattern of simulations as in [San19]. This pattern corresponds to the simulation of 35 days of the WWTP behaviour. The first 21 days correspond to the simulation of a dry weather considering the following variations of $K_{La,5}(t)$: seven days between 45 and 245 days^{-1}, seven days between 5 and 355 days^{-1}, and seven days with a fixed $K_{La,5}(t)$ equal to 145 days^{-1}. The last 14 days correspond to the simulation of seven days of rainy and seven days of stormy weather profiles, respectively. Notice that ANNconf1 and ANNconf2 adopt the same input measurements or variables as the ones considered in ANN3 and ANN4 configurations of [San19]. Nevertheless, the nets considered here are trained considering only open-loop configurations.

Finally, the internal structure of the ANN considered in each configuration is as follows: the number of hidden neurons in the sigmoid layer of the MLP network is set to 20. A Bayesian regularisation algorithm is adopted to train the networks considering a maximum number of epochs equal to 1000 [Mac92]. Moreover, the cost function, $J(\theta)$, corresponds to the Mean Squared Error (MSE). Input and output pairs of data are again split in the following distribution: 70% for training and 15% for validation purposes and 15% for testing ones.

Delay Correction Performance

The training performance of the three configurations previously stated is shown in Table 6.2, where the training results are given in terms of the RMSE and the R^2 coefficient as well as in terms of the training and test datasets. The prediction performance is computed for the test dataset.

As it is observed, all the configurations are offering a good performance since their RMSE values are not higher than 0.03, their MAPE do not reach the 1% in any configuration and their R^2 coefficient is bigger than 0.94. However, ANNconf3 is overcoming the other two ANN configurations. It improves the RMSE, MAPE and R^2 of the ANNconf1 configuration in a 44.83%, $3 \cdot 10^{-4}$ percentage points and a 4.50%, respectively. Besides, the improvement of ANNconf3 when compared to the ANNconf2 equals to a 33.33% in the case of the RMSE, $3 \cdot 10^{-4}$ percentage points in terms of MAPE and a 2.25% in the case of the R^2.

Table 6.2: ANN Configurations Prediction Performance. RMSE is measured in mg/L, MAPE is measured in % and R^2 is a dimensionless metric.

ANN Configurations Training Performance			
ANN Configuration	RMSE	MAPE	R^2
ANNconf1	0.029	0.0013	0.94
ANNconf2	0.024	0.0013	0.96
ANNconf3	0.016	0.0010	0.98

6.3.3 Control Performance

After analysing the effects of the new proposed Data-based Denoising stage as well as the ANN-based Delay Correction process, the performance of the whole structure is computed. The data-based Denoising stage is implemented considering the Dedicated MLP-based DAEs. All the configurations proposed in the ANN-based Delay Correction stage are also considered. In addition, fox and variable set-points are simulated. The fix set-point equals to a $S_{O,5}$ concentration of 2 mg/L whilst the variable set-point is determined following the hierarchical control presented in [San15a]. Results are compared to the BSM1's default PI and the approach assessed in [San19].

Fix Set-point Control Performance

Results when a fix set-point is considered are shown in Table 6.3. It is clearly observed that the BSM1's default PI control strategy is the one yielding the worst performance. This is directly related to the noise effect introduced by the real sensors. On the other hand, the performance is improved in all terms when measurements are denoised and the delay corrected in the Control Enhancement Processing approach. The effects of both processes are directly observed in the IAE and ISE control metrics. The lowest IAE improvement, a 32.81%, is yielded by the ANNconf1 configuration when stormy weather is considered.

In terms of the ANN-based Delay Correction Stage configurations, the best performance is not always given by the same one. When dry and stormy weathers are considered, the designed and scenario-optimised strategy proposed in [San19] is the one offering the best results. This shows that the moving average low-pass filters and the BSM1's default PI controller are exhaustively designed to offer such a good behaviour. Notwithstanding, the proposals presented in this chapter does not differ too much from the best results. When dry weather is considered, the ANNconf2 configuration shows IAE and ISE values which are very close to the ones offered in [San19]: they are only degraded a 4.38% and a 6.66%. The same is observed when the stormy weather is considered. The IAE and ISE yielded by the ANNconf3 are degraded from 0.300 to 0.324 whereas ISE is increased from 0.022 to 0.024. In terms of the

Table 6.3: Control performance when a fix set-point is considered.

Control Performance for a fix set-point						
	Influent Weather Profile					
	Dry		Rainy		Stormy	
Configuration	IAE	ISE	IAE	ISE	IAE	ISE
Default PI	0.590	0.084	0.560	0.075	0.570	0.079
Approach in [San19]	0.240	0.014	0.350	0.026	0.300	0.022
ANNconf1	0.294	0.020	0.299	0.023	0.383	0.036
ANNconf2	0.251	0.015	0.335	0.025	0.380	0.032
ANNconf3	0.284	0.019	0.384	0.042	0.324	0.024

rainy weather, results show that all the proposed configurations are able to improve the best performance shown in [San19]. Now, the best ones are offered by the ANNconf1 and they correspond to a 14.57% in terms of the IAE and a 11.54% in terms of the ISE. This is related to the abilities of the ANNs in the modelling of non-linear behaviours and variations. Finally, in Figure 6.7 the performance of ANNconf1, ANNconf2 and ANNconf3 for the rainy weather is compared to the best performance in [San19]. As it is observed, all the structures are offering a good control behaviour since they maintain the $S_{O,5}(t)$ at the given set-point or at least at a very close value. Notice that changes in ANNconf1, ANNconf2 and ANNconf3 are produced by the daily variations of the influent profile.

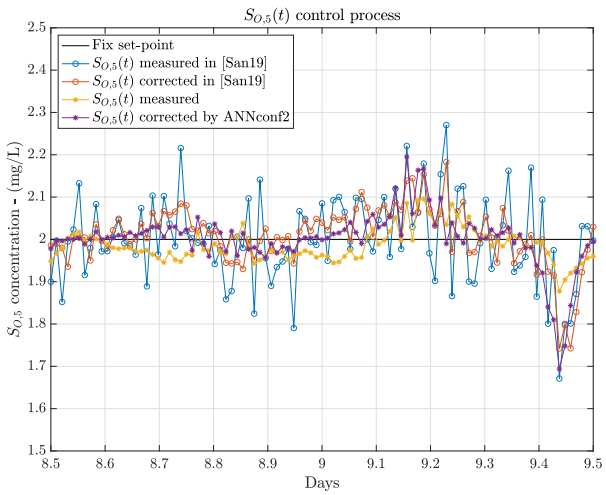

(a) Dry weather.

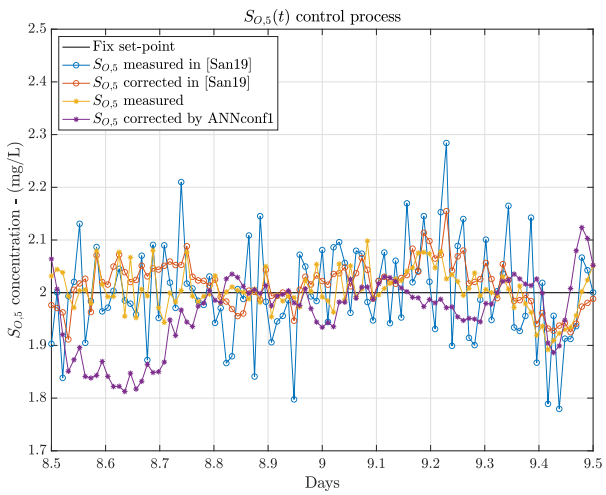

(b) Rainy weather.

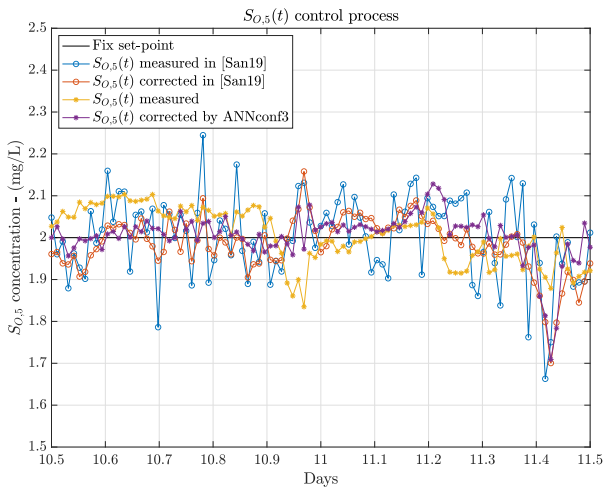

(c) Stormy weather.

Figure 6.7: Control process for the dry, rainy and stormy weathers and a fix set-point. Only the days where the effects of the weather events are predominant are shown. The performance is compared to the outputs given by the approach proposed in [San19].

Variable Set-point Control Performance

The performance of the whole system when a variable set-point is considered are shown in Table 6.4. The same effects as in the fix set-point are observed between the Default PI and the Default PI precedented either by a conventional delay correction approach or the Data-based Control Enhancement Processing one. However, the differences are not so big because effects of noise are lessened when variable set-points are considered [San19]. Now, the best improvement in terms of the IAE, a 41.05%, is offered by the ANNconf2 configuration when it is compared to the Default PI structure managing the dry weather.

When the performance of the proposed approaches is compared to the structure presented in [San19], the improvement is reduced, however, results are still better. The structure performing better in the case of the dry weather is the ANNconf2, which is able to offer IAE and ISE values equal to 0.336 and 0.035, respectively. This entails IAE and ISE improvements equivalent to a 13.84% and a 7.89%, respectively. In terms of the rainy and stormy weathers, the structure offering the best performance corresponds to the ANNconf3. This makes sense since this structure is the one considering not only the $T_{SS,in}$ concentration, but also the $S_{NO,4}$ one. Aforementioned, these two concentrations are the two where the effects of rainy and stormy episodes are more noticeable (see Figure 3.3). For instance, when the rainy weather is considered, this configuration is able to improve the IAE and ISE metrics from 0.482 to 0.364 and from 0.056 to 0.032, respectively. When the stormy weather is considered, the IAE and the ISE vary from 0.428 to 0.422 and from 0.046 to 0.040, respectively. The enhancement is reduced in this case since the variations of stormy weathers are not maintained in time like the rainy ones. Instead, they consist in high variations for a very short period of time. Similar variations to the dry profile are observed the rest of the time.

Figure 6.8 shows the control behaviour of the proposed approach when a dry weather is considered. The data-based Denoising stage adopts Dedicated MLP-based DAEs and the ANN-based Delay Correction Structure considers the best ANN configuration, i.e., the ANNconf2. Results of Default PI and the approach assessed in [San19] are also shown. As it is observed, the proposed approaches are the ones

Table 6.4: Control performance when a variable set-point is considered.

Control Performance for a variable set-point						
	Influent Weather Profile					
	Dry		Rainy		Stormy	
Configuration	IAE	ISE	IAE	ISE	IAE	ISE
Default PI	0.570	0.124	0.564	0.101	0.575	0.115
Approach in [San19]	0.390	0.038	0.482	0.056	0.428	0.046
ANNconf1	0.381	0.035	0.420	0.042	0.512	0.093
ANNconf2	0.336	0.035	0.381	0.034	0.473	0.052
ANNconf3	0.372	0.043	0.364	0.032	0.422	0.040

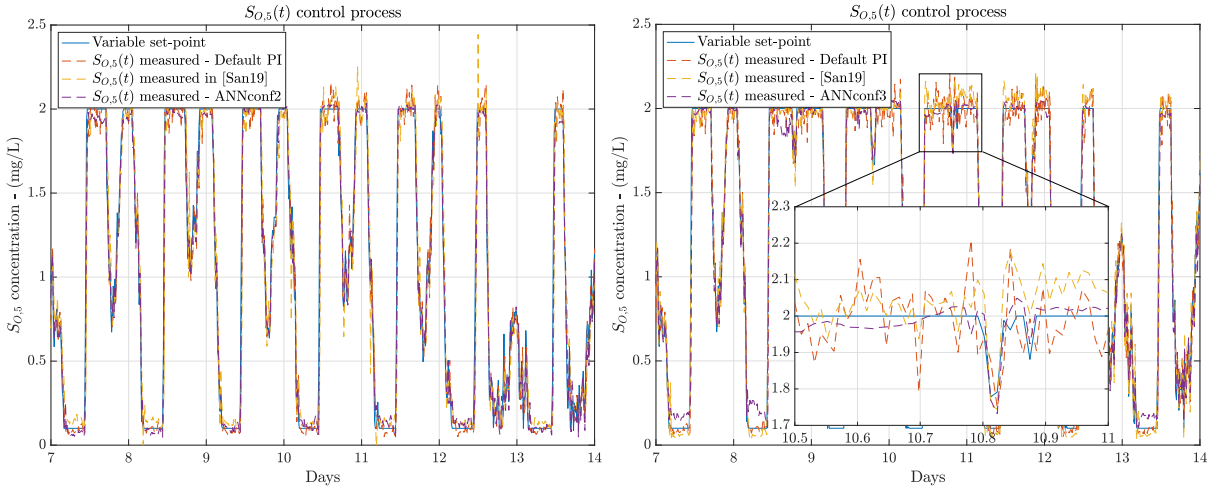

(a) Dry weather.

(b) Rainy weather.

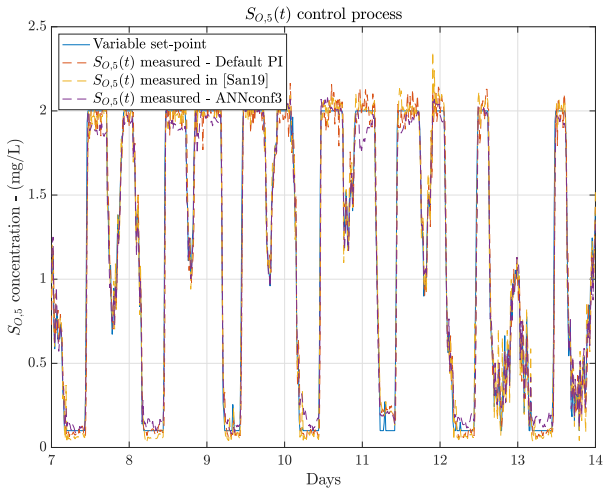

(c) Stormy weather.

Figure 6.8: Control process for the dry, rainy and stormy weathers and a variable set-point. Only the days where the effects of the weather events are predominant are shown. The performance is compared to the outputs given by the approach proposed in [San19].

performing better. When dry and rainy weathers are considered, the real $S_{O,5}$ concentrations obtained with the ANNconf2 and ANNconf3 are the ones closer to the variable set-point, i.e., the ones showing less oscillations as well as the ones showing no delays. Notice that there are some points where the $S_{O,5}(t)$ obtained is not as reliable as it should be (see the lowest values of the variable set-point in Figure 6.8). This effect is also observed when the stormy weather is considered. However, this is countered with the highest values of the set-point, where the proposed approach is making the point.

As a summary, the proposed Data-based Control Enhancement Processing approach is offering a good performance. Its efforts entail an improvement in the control performance of the BSM1's PI controller when it has to deal with non-ideal measurements. Notwithstanding, results have shown that the

performance could be improved even more. It is worth noting that until this point, the Data-based Control Enhancement approach is tested over the conventional PI. Therefore, the control performance of the whole BSM1 scenario is subjected to the best performance offered by the default PI. In that sense, other structures could provide a much better performance when dealing either with ideal or non-ideal measurements. Finally, more details on the implementation and results regarding the Data-based Control Enhancement Processing approach can be observed in [Pis21b].

6.4 Denoised ANN-based IMC structure

As it is stated in Section 5.3.3, the ANN-based IMC structure is implemented to manage the $S_{O,5}(t)$ control loop. Its behaviour overcomes the control performance of the BSM1's default PI controller when ideal measurements are considered. Nevertheless, when non-ideal effects are observed, the control performance of this approach drops even though it is able to offer a better performance than the default PI. For that reason, denoising and delay corrections are required so as to improve this performance. Since the ANN-based IMC controller is managing non-linear and highly complex processes, the application of the Data-based Control Enhancement Processing approach is more than suitable. Besides, it is observed that the degradation in the control performance of the ANN-based IMC is generally motivated by the effects of noise rather than the delays introduced by the sensors. This is due to the adoption of the sliding window, which mitigates most of the delay effects in the prediction of the IMC models. For that reason, this section is focused on the assessment of the Data-based Denoising stage as a denoising approach of the non-ideal measurements. Thus, the performance of Denoised ANN-based IMC structure will be computed in terms of the denoising accuracy, its stability and its control behaviour once the denoising approach is considered.

6.4.1 Denoising Autoencoder Architectures

Considered as a new layer, the Data-based Denoising stage is placed just before the sliding window of $\mathrm{LSTM_{i,i}}$ and $\mathrm{LSTM_{d,i}}$ architectures presented in Section 5.3. As depicted in Figure 6.9, it gathers measurements corrupted by noise to finally return their clean versions. In that manner, the $\mathrm{LSTM_{d,i}}$ and $\mathrm{LSTM_{i,i}}$ structures can be adopted instead of $\mathrm{LSTM_{d,r}}$ and $\mathrm{LSTM_{i,r}}$. Consequently, an increment of the range of marginal stability and an enhancement of the controller's performance is achieved.

Training Process

The DAE architectures implementing the Data-based Denoising stage are determined by means of a grid search where the number of hidden layers and hidden neurons as well as the learning rate value are determined. Two datasets are considered: the first one takes into account noise-corrupted data while the second one considers ideal measurements. Both datasets are generated considering a whole year

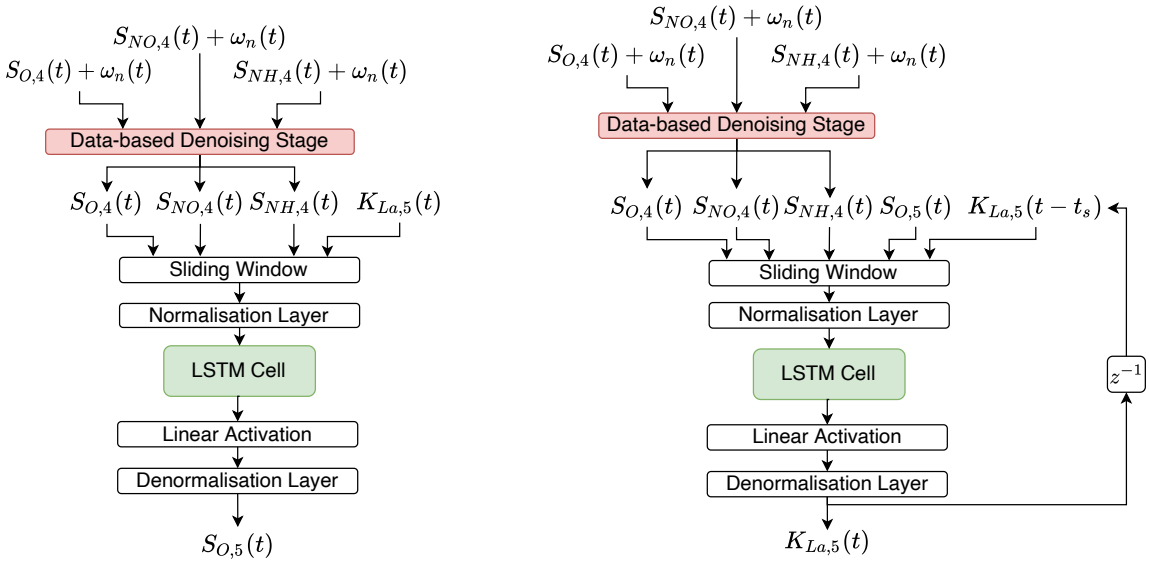

(a) Denoised $\mathrm{LSTM_{d,i}}$ architecture

(b) Denoised $\mathrm{LSTM_{i,i}}$ architecture

Figure 6.9: Data-based Denoising stage implemented over $\mathrm{LSTM_{d,i}}$ and $\mathrm{LSTM_{i,i}}$.

simulation of the BSM1 framework showing dry, rainy and stormy episodes uniformly distributed. As a result, the denoising stages derived from this process correspond to:

- **MLP-based DAE**: the encoder part considers two hidden layers. The former has 50 hidden neurons whereas the latter is halved, i.e., it considers 25. The latent space layer adopts 10 hidden neurons. Finally, the decoder implements the inverse distribution of the encoder, i.e., the first layer considers 25 hidden neurons while the last one has 50. The initial learning rate equals to $1 \cdot 10^{-3}$.
- **DMLP-SW**: MLP-based DAE implementing the sliding window with a WL of 4 hours. It replicates the internal structure of the MLP-based DAE.
- **LSTM-based DAE**: As in the case of the MLP-based DAE, the encoder and decoder parts have two layers. The encoder considers 50 and 25 hidden neurons per layer, respectively. The decoder layers have 25 and 50 hidden neurons. In this case, the learning rate is set to $5 \cdot 10^{-3}$.

The architectures are cross-validated adopting the dataset of ideal measurements where the 85% of data are adopted for training while the remaining 15% are considered for testing purposes. The regularisation techniques adopted in the training of the DAE architectures are the L2 extra penalty [Goo16, Section 7.1.1] and early stopping. It is also worth mentioning that depending on the measurements, a new regularisation technique can be applied. When the DAE is trained with ideal data, a noise layer is added to the DAE structures. Corresponding to a data augmentation strategy, the addition of noise to the input data is defined as a regularisation technique [Goo16, Section 7.4].

This noise layer has a multiplicative parameter, the noise factor, which determines the amount of noise introduced by the layer. This new parameter is set in the cross-validation process [Liu19b]. Thus, the L2 extra penalty and noise factor have been set to $1 \cdot 10^{-4}$ and 0.3 (30% of noise), respectively. This noise additive layer is not considered for testing purposes, therefore, the noise-corrupted dataset has to be taken into account while testing the ANN structure.

Denoising Performance

Results of the denoising approaches are shown in Table 6.5. The RMSE, the MAPE and the R^2 metrics are computed for the PCA, PCA-SW, the MLP-based DAE, DMLP-SW, and the LSTM-based DAE approaches. Their performance is assessed with and without a sliding window. As it is observed, the structure offering the best performance is the DMLP-SW. Its RMSE equals to 0.089 units, its MAPE to a 3.72% and its R^2 to 0.99. Besides, there are other approaches showing a good denoising accuracy. For instance, the LSTM-based DAE and the PCA-SW approaches offer RMSE values equal to 0.091 and 0.131 units, respectively. In percentage, these values correspond to a worsening of 2.20% and 32.06% with respect to the DMLP-SW approach. In terms of the MAPE and R^2, the worsening between the LSTM-SW and the PCA-SW with respect to the DMLP-SW is around 3.2 and 5.6 percentage points for the MAPE and 0.01 units for the R^2.

Among the denoising structures, the suitable approaches are those showing low MAPE values. Let's suppose a real sensor measuring a $S_{O,4}$ concentration equal to 2.3 mg/L. Ideally, it should correspond to 2 mg/L. To overcome this measurement error, one denoising approach is considered. If a simple MLP-based DAE is applied, the new value would be in the range $[1.74 - 2.27]$ mg/L. This entail that errors are still produced. Otherwise, the range of $S_{O,4}(t)$ would equal to $[1.93 - 2.07]$ when the DMLP-SW approach is adopted. For that reason, only those approaches showing MAPE values below a 10% are suitable. Moreover, if t_{time} is considered, it is observed that none of the ANN-based denoising approaches showing MAPE values below the 10% require a huge training time. The DMLP-SW structure requires 66.57 seconds whereas the LSTM-based DAE reduces this time until the 43.03 seconds. Notwithstanding, DMLP-SW shows a much lower MAPE. As a result, Figure 6.10 depicts the denoising process

Table 6.5: Denoising approaches accuracy. Each denoising approach is assessed by means of comparing the outputs of the approach with their ideal version. RMSE is measured in units, the MAPE equals to a %, the R^2 is dimensionless and t_{time} is measured in seconds. The terms succeeded by SW stand for the PCA and MLP denoising approaches considering a sliding window.

Denoising Approach	RMSE	MAPE	R^2	t_{time}
PCA	0.171	12.45	0.96	-
PCA-SW	0.131	9.31	0.98	-
MLP-based DAE	0.164	13.25	0.97	82.43
DMLP-SW	0.089	3.72	0.99	66.57
LSTM-based DAE	0.091	6.93	0.98	43.03

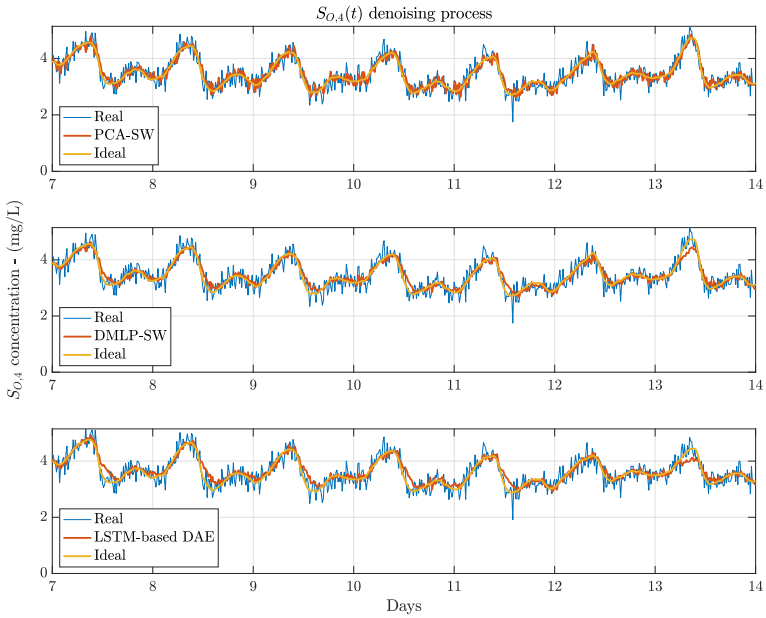

Figure 6.10: $S_{O,4}(t)$ denoising process. Notice that the best denoising performance is obtained when the DMLP-SW denoising approach is considered.

performed over $S_{O,4}(t)$ signals when the PCA-SW, DMLP-SW and LSTM-based DAE approaches are considered.

6.4.2 Denoised Control Performance

Before computing the control performance, the stability of the system is analysed. Figure 6.11 depicts the ETFE-based analysis for the PCA-SW, DMLP-SW and LSTM-based DAE. As shown, none of the different denoising approaches are able to ensure a robust stability below the $1.6 \cdot 10^{-3}$ rad/s, however, the stability margin is increased with respect to $\mathrm{LSTM_{d,r}}$ and $\mathrm{LSTM_{i,r}}$. For instance, the LSTM-based DAE increases the stability bandwidth from the $0.7 \cdot 10^{-3}$ rad/s until at least the $1.10 \cdot 10^{-3}$ rad/s when a $\omega_c = 10 \cdot 10^{-3}$ rad/s is chosen. When the DMLP-SW is considered, the ANN-based IMC becomes marginally stable until the $1.25 \cdot 10^{-3}$ rad/s. Furthermore, it only fails the ETFE-based stability test in three frequencies between that frequency and the $1.6 \cdot 10^{-3}$ rad/s. Neither the LSTM-based DAE, nor the PCA-SW can pass the stability test in more frequencies than the DMLP-SW does. For that reason, it is considered as the principal denoising approach.

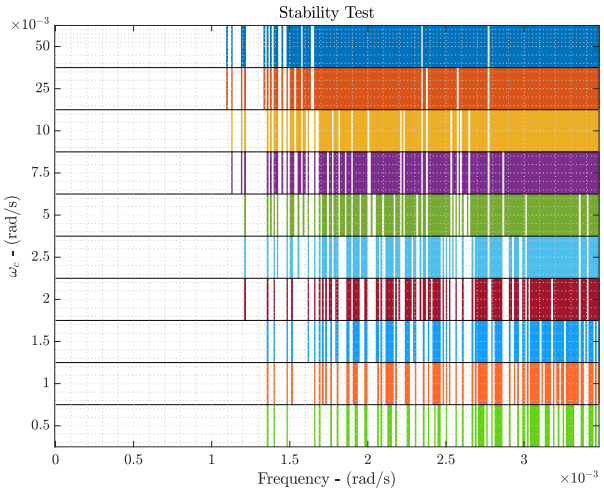

(a) PCA-SW stability test.

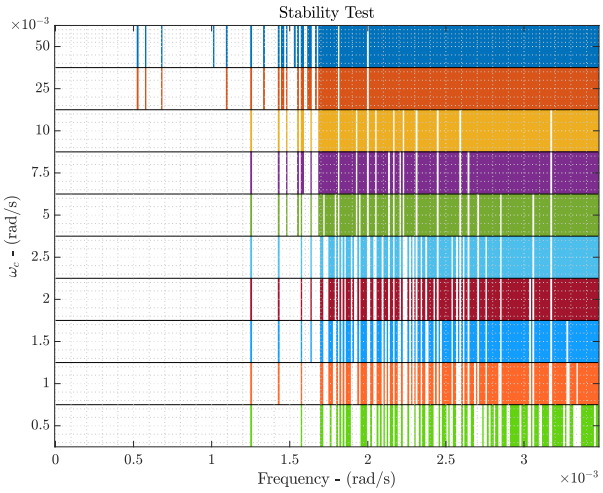

(b) DMLP-SW stability test.

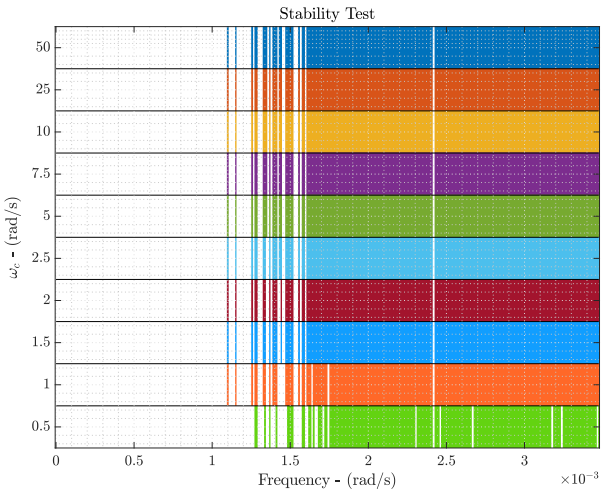

(c) LSTM-based DAE stability test.

Figure 6.11: ETFE-based stability analysis for the different denoising approaches. None of the analysed denoising structures ensure the stability below the $1.6 \cdot 10^{-3}$ rad/s. The greater stability range is provided by the DMLP-SW.

The control performance of the ANN-based IMC considering a denoising process is determined simulating the PCA-SW, DMLP-SW and LSTM-based DAE over the BSM1 framework. The denoising stages are implemented to operate over $\mathrm{LSTM_{d,i}}$ and $\mathrm{LSTM_{i,i}}$. Therefore, any improvement with respect to the results shown in Table 5.6 are directly related to the behaviour of the denoising approaches. In that sense, results of the whole system are shown in Table 6.6. In this case, the same variable set-point as the one considered in 5.3.3 is adopted. At first sight, it is observed that the ANN-based IMC with a denoising stage is able to overcome the results of the default PI dealing with non-ideal measurements. Among all the denoising structures, the one providing the best performance corresponds to the ANN-based IMC + DMLP-SW. It achieves an average improvement around a 21.25% for the IAE and a 54.64% for the

Table 6.6: ANN-based IMC + denoising stage control performance for the Real Scenario. Notice that a ω_c of $10 \cdot 10^{-3}$ rad/s is again considered as the $H(s)$ cut-off frequency.

Control Performance for a variable set-point						
	Influent Weather Profile					
	Dry		Rainy		Stormy	
Structure	IAE	ISE	IAE	ISE	IAE	ISE
PI	2.018	1.259	1.991	1.238	2.014	1.267
Ideal ANN-based IMC + Data-based Denoising stage						
PCA-SW	1.672	0.634	1.682	0.640	1.673	0.640
DMLP-SW	1.578	0.568	1.592	0.571	1.566	0.571
LSTM-based DAE	1.762	0.758	1.772	0.720	1.781	0.741

ISE. On the other hand, when the ANN-based IMC + the PCA-SW and the LSTM-based DAE, IAE and ISE values do not overcome the ANN-based IMC + DMLP-SW results. Figure 6.12 clearly shows that the ANN-based IMC + DMLP-SW approach is the one offering the most accurate tracking process. At this point, it it worth noting that, although their good denoising performance, DAEs are approaches with losses in the sense that they can reduce the noise of the signals at expense of recovering them with small variations [Goo16, Chapter 14] [Liu19a]. Consequently, part of the noise effect is still present in the predictions performed by $\mathrm{LSTM_{d,i}}$ and $\mathrm{LSTM_{i,i}}$. This entails the generation of $K_{La,5}(t)$ values which may differ from the ones required in the $S_{O,5}(t)$ tracking process.

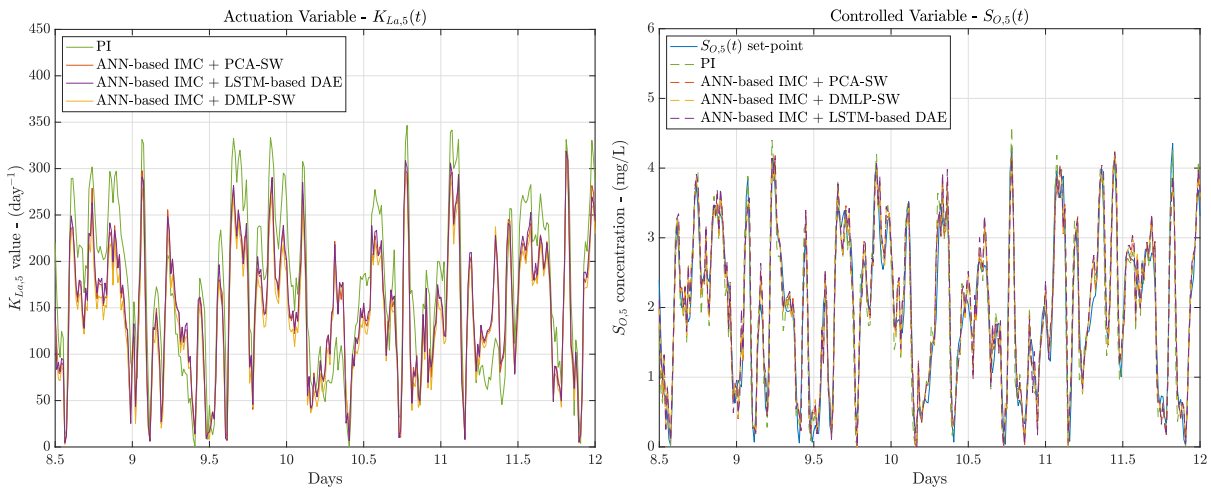

(a) Actuation Variable - $K_{La,5}(t)$.

(b) Controlled Variable - $S_{O,5}(t)$.

Figure 6.12: Tracking process of $S_{O,5}(t)$. The performance of the ANN-based IMC considering the PCA-SW, DMLP-SW and LSTM-based DAE is assessed. Notice that $S_{O,5}(t)$ is overlapped most of the time by the ANN-based IMC + DMLP-SW approach.

6.5 Chapter Conclusions

In this chapter the issues related to the appearance and consideration of non-idealities, especially effects corrupting the signals and measurements such as the noise and delays, are tackled. This is performed by means of a new data-based approach, the Data-based Control Enhancement Processing approach. It implements two differentiated stages: (i) the Data-based Denoising stage, and (ii) the ANN-based Delay Correction stage. The former is devoted to cleaning and treating the noise corrupted measurements and signals involved in the control strategy to finally return a clean version of them. On the other hand, the latter is mainly focused on correcting the delays introduced by the non-ideal sensors. Its performance is determined considering two different scenarios: the improvement of the BSM1's default PI controller managing the $S_{O,5}(t)$ and the improvement of the ANN-based IMC structure.

In the first case, the complete Data-based Control Enhancement Processing approach is considered. Its Denoising stage is implemented considering two possible configurations: a MLP-based DAE and a Dedicated MLP-based DAE. The first one corresponds to the usual DAE which considers as many outputs as inputs. On the other hand, the Dedicated MLP-based DAE focuses its efforts on estimating clean measurements of a unique concentration at the expense of requiring as many DAE structures as concentrations considered in the control process. Results show that the option performing better consists in the Dedicated MLP-based DAE. It yields the lowest RMSE and MAPE values when compared to the MLP-based DAE as well as to a classical low-pass filter denoising approach. In terms of the ANN-based Delay Correction stage, it has been implemented considering simple MLP-based structures devoted to computing the current denoised $S_{O,5}(t)$. The output of this stage is then feed into the BSM1's default PI. In that sense, three different ANN configurations are tasted to determine which input data must be considered in the delay correction. Results show that all the configurations are valid. Finally, the control performance of the BSM1's default PI when it is supported by the Data-based Control Enhancement Processing approach is computed. The behaviour of the default BSM1 PI is compared with conventional denoising and delay corrections proposed in the literature. In this case, it is observed that the proposed structure overcomes the conventional approaches for some of the BSM1 influent weathers, but not in all of them. Nevertheless, the difference with respect to the conventional structures is negligible.

The second scenario where the Data-based Control Enhancement Processing approach is considered consists in the ANN-based IMC presented in Chapter 5. As shown there, its performance and stability drastically dropped when non-ideal sensors were considered. For that reason, the proposed denoising approach is tested over this structure to determine if an improvement can be obtained. In this case, only the Data-based Denoising stage is considered since the most critical effects are those related to the noise. Here the stage is implemented by means of a MLP-based DAE considering a sliding window with a WL of 4 hours. Nevertheless, different approaches such as PCA and LSTM-based solutions are also assessed. In that sense, results show that the best denoising performance of the Data-based Denoising stage is obtained when the MLP-based DAE is considered. Showing a RMSE equal to 0.089 and a

MAPE to 3.72, its denoising performance allows the correction of nearly all the noise effects. This is corroborated computing the ANN-based IMC stability, where it is observed that the range of marginal stability is increased thanks to the Data-based Denoising stage. Finally, the control performance of the Denoised ANN-based IMC is determined. Results show that although the control performance does not reach the values obtained for the Ideal Scenario, the Data-based Denoising stage is achieving a significant improvement in the control behaviour with respect to the BSM1's default PI controller.

The results in both scenarios corroborate that the proposed Data-based Control Enhancement Processing approach can reduce the effects of noise and delays introduced by non-ideal sensors. Moreover, the fact that this approach completely relies on ANNs, motivates its adoption in an industrial environment such as the WWTP, where highly complex and non-linear processes are performed.

Chapter 7

Transfer Learning in the Industrial Control Domain

Until this point, ANNs have been adopted for different purposes such as elements supporting conventional control structures, as tools implementing PI and IMC controllers, or even to correct the non-linearities introduced by real sensors. However, the training of ANNs is not an easy and quick process to perform. Several aspects must be considered in the training process if a generalisable ANN is desired. For that reason, this chapter provides an insight of the application of TL techniques for a two-fold objective: (i) speed-up and ease the training process of ANNs, and (ii) provide a new design approach of ANN-based control structures based on the transference of ANNs. Concerning the last point, there is a crucial aspect that must be considered. Industrial environments tend to be critical and therefore, they cannot be uncontrolled, neither badly managed. For that reason, this chapter is also devoted to providing a new metric measuring the transferability of ANN-based structures so as to estimate the control performance before deploying them over the real industrial scenarios.

7.1 Introduction

As it has been assessed in the previous chapters, the power of ANNs is such that they can be considered to implement soft-sensors and data-based controllers as well as to correct non-idealities. Notwithstanding, ANNs present some drawbacks that must be considered [Sou16], especially if they are intended to actuate over industrial scenarios. One of the utmost importance is related to their training process. In it, the hyperparameters of each ANN are determined accordingly to the process for which it is designed. To achieve this, input and output data of the process being modelled are required. The problem raises when this cannot be assured for certain industrial environments showing data scarcity problems. Moreover, this training process can last hours or even days with respect to the network structure, the hyperparameters, and the amount of data [Ami20]. For that reason, TL has arisen as a method tackling these issues.

TL consists in a technique widely adopted in the image classification field, where it is considered to obtain ANN-based classifiers from a predesigned and pretrained structure in a source domain to later be transferred into an unseen target environment [Zhu21]. Then, these structures are retrained with images of a target domain in what is called a fine-tuning process [Sar18, Chapter 6]. This principal can be considered in the industrial environment, where their options can be widely exploited. For instance, TL techniques have been adopted to design and implement ANN-based soft-sensors in harsh environments showing a lack of measurements. Since this issue is critical for the development and training process of ANNs, TL can be considered to firstly design the desired soft-sensor in an environment without data scarcity problems, the source domain, to later transfer and retrain it in the environment suffering data scarcity issues, the target domain. This is the case of the work presented in [Cur21]. In there, LSTM-based soft-sensors are derived considering TL techniques. Their main objective is to obtain a first LSTM-based soft-sensor from a scenario where huge amounts of data are available to finally transfer it into a scenario presenting severe data scarcity issues.

In terms of the industrial control design, TL is an option that can be widely exploited. Instead of designing and tuning conventional controllers such as PI, MPC or FL, ANN-based control structures like the ones presented in Chapter 5 can be adopted. The main point is that a unique ANN-based structure is obtained for a given control loop and then transferred in the remaining ones rather than training and designing as many ANN-based controllers as conventional structures (see Figure 7.1). This is very useful in those industrial scenarios showing several control loops such as the petrochemical industry [Ran13, Mic14]. If TL is considered, efforts will be focused on designing and implementing a unique ANN-based controller instead of large numbers of conventional control structures. Then, the transference of the designed ANN-based controller is performed in the remaining control loops, where the ANNs will be fine-tuned to improve their performance. This entails that TL techniques are considered not only to obtain ANN structures performing well in a source model, but also to speed up the control design process.

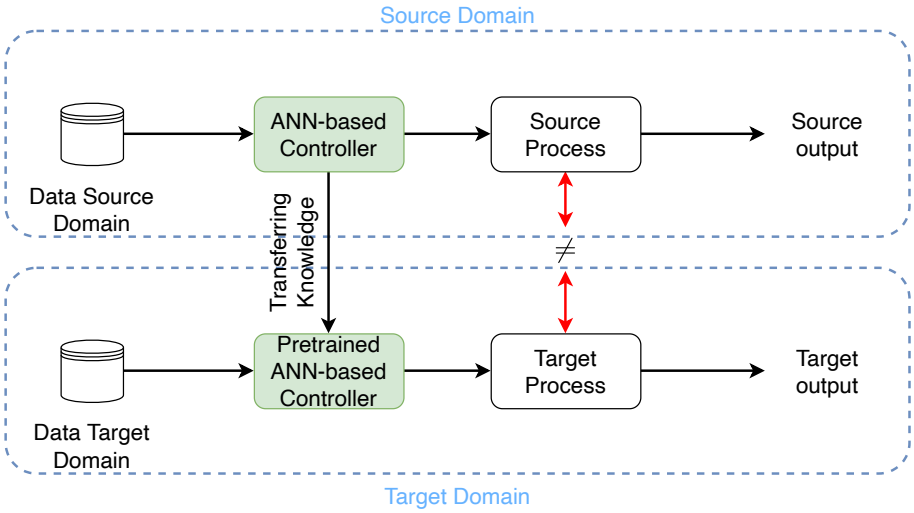

Figure 7.1: Transfer Learning performed between source and target environments.

Nevertheless, this process entails that the transferred structure has to be tested and retrained over the target environment. This fact represents a severe issue since most of the industrial environments are critical. In other words, TL is not always an option. On some occasions, the Negative Transfer can occur [Wan19]. This happens when a transferred ANN structure performs well in the source domain but really bad in the target one. For that reason, some efforts have been focused on generating and deriving certain metrics able to determine the transferability of ANN structures [Sou20, Sch21]. For instance, in [Sou20] some metrics have been assessed in their aim to determine the transferability of data to properly train a soil moisture predictor. The metric determines the benefit of choosing one or another sets of measurements. Other approaches determining the separability of classes have been proposed in [Sch21]. Nevertheless, the approaches presented in there are focused on measuring the transferability and separability of classification-oriented processes. In such a context, industrial control corresponds to a regression-oriented process since industrial measurements consist in temporal signals. The problem here relies in the fact that there exists a lack of metrics measuring the transferability of ANN structure performing such a kind of tasks.

For that reason, this chapter is devoted to assessing the adoption of TL techniques in the design and development of new industrial controllers. This is performance by means of the Transfer Learning-based Control Design whose main aim is to obtain an ANN-based controller in a source domain, the BSM1 DO control loop, and then transfer it into the target one, the BSM1 NO control loop. To perform this assessment, the ANN-based PIs proposed in Section 5.2 are considered, especially the DO ANN-based PI. Its performance shows that its transference into the NO control loop can be considered so as to achieve an improvement of the NO control loop behaviour. Once transferred, the adoption of fine-tuning processes is also evaluated to determine its effects. Last but not least, WWTP and therefore, the BSM1 framework, consist in critical environments which cannot actuate without supervision or freely. The consequences derived from these malfunctioning can produce really harmful problems to natural environments and water resources. For that reason, this chapter also assesses the ANN-based controller's transferability. The main objective is to provide the industrial control designer with a measurement of the ANN-based structure transfer suitability in order to determine if its behaviour would be correct or not in the target domain.

As a summary, the contributions of this chapter are:

- A new control design method is proposed to reduce the required knowledge of the process under control.
- A TL-based technique is proposed to speed up the implementation of the controllers managing the control loops of industrial environments.
- A fine-tuning process is carried out to ensure that the control performance of the control loop is improved with respect to the conventional BSM1's default PI controller.

- A new metric is derived to determine the suitability of transferring ANN-based controllers from one domain into a new one.

Finally, the remaining of this chapter is as follows: in Section 7.2, the Transfer Learning-based Control Design approach is presented and evaluated. Here, the transference of ANN-based controllers from the BSM1 DO control loop to the NO one and vice-versa is considered. Moreover, the fine-tuning of the ANN-based controller showing the best performance is performed in order to improve the control behaviour. In Section 7.3, the proposed Transfer Suitability Metric (TSM) is presented. Its application over different processes is assessed to corroborate its behaviour. Finally, the metric is evaluated over the BSM1 control loops. This will corroborate the results shown in Section 7.2. Finally, Section 7.4 concludes this chapter. It is based on the works presented in [Pis21c, Pis21a] and to be published in the proceedings of the ETFA 2022 conference.

7.2 Transfer Learning-based Control Design

The Transfer Learning-based Control Design approach is focused on designing and implementing ANN-based controllers. It consists in two stages: (i) the ANN-based controller derivation, where the design and training of an ANN-based structure is carried out, and (ii) the Control Knowledge Transfer approach, where the transfer of the controller's knowledge into the different industrial control loops is performed. The first stage is mainly based on designing an ANN able to manage the signals considered in the control of the industrial process. To achieve this, the proposed ANN-based controller predicts the corresponding actuation signal accordingly to its input measurements, that is, the measured value and its set-point. In the case of the BSM1 environment, the signals involved in the control loops are defined accordingly to the source control environment they come from:

- **DO control loop**: the controlled signal corresponds to $S_{O,5}(t)$ whilst the actuation one corresponds to $K_{La,5}(t)$.
- **NO control loop**: the controlled signal corresponds to $S_{NO,2}(t)$ whereas the actuation one corresponds to Q_a.

The ANN-based controller is implemented considering LSTM cells due to their good performance when dealing with time-series signals, such as the ones obtained from the BSM1 framework [Goo16, Section 10.10] [Ale08].

Then, the Control Knowledge Transfer approach is mainly focused on transferring the knowledge of the proposed controller into the other control loops. Once the source ANN-based controller is properly trained and its performance assessed, it can be transferred into the target domain. To perform this transference, the weights and biases of the ANN layers implementing the controller are maintained between

domains. Nevertheless, input and output measurements of the target domain may differ from the ones of the source domain. To tackle this, the layers of the ANN-based controller devoted to normalising and de-normalising the input and output data are modified in the Control Knowledge Transfer approach. This is performed so as to adapt the input and output measurements of the target domain to the ones considered in the training process. After this, the ANN-based controller can be finally transferred.

Once the knowledge of the ANN-based control structure is transferred, its control performance can be adjusted. This is performed by means of a fine-tuning process which consists in a retraining of the ANN-based structure replicating the conventional controller. However, this fine-tuning process is different from the processes carried out in the usual applications of transfer learning, that is, the development of image classifiers. There, the data considered to perform the fine-tuning process consist in a set of new images where the labels are intrinsically obtained from the original pictures. When talking about industrial processes, the situation completely changes. The new measurements as well as the knowledge about how to manage the corresponding loop have to be obtained from the control loop where the ANN-based controller is going to be transferred. For that reason, the new data is obtained after simulating the behaviour of the industrial process when a conventional controller is applied. Otherwise, the ANN-based controller will not be able to offer a good control performance.

In this case, the ANN-based controller, which is presented and widely assessed in Section 5.2, is considered as the baseline strategy to be transferred (see Figure 7.2). Thus, the objective is to design and transfer only an ANN-based controller instead of deriving as many ANN-based structures as control loops present in the BSM1 framework.

It is also important to notice that there is a requirement that has to be fulfilled: the Transfer Learning-based Control Design can only be applied among control loops sharing the same control objective, therefore it must be clearly defined. This is motivated by the fact that the ANN-based structure trained in the source control loop will learn how to generate an actuation signal whose objective is to perform a

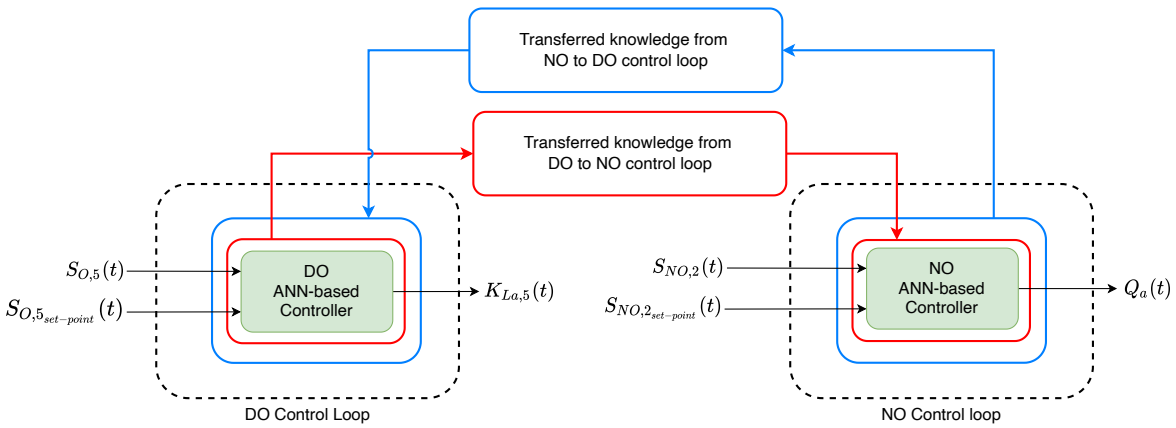

Figure 7.2: Graphical description of the Transfer Learning-based Control Design approach. Notice that DO refers to the BSM1 $S_{O,5}(t)$ control loop, whilst NO refers to the BSM1 $S_{NO,2}(t)$ one.

certain task, for instance, the tracking of a given set-point. Then, if it is going to be transferred, the target domain control purpose should be the same. Otherwise, the target structure would generate actuation signals which do not fulfil the control requirements. Here, the control objective is clear. DO and NO control loops are designed to track the given set-points regardless of the dynamics of the involved signals.

7.2.1 LSTM-based PIs

To assess the Transfer Learning-based Control Design approach, both DO and NO ANN-based PI controllers are considered. The two architectures consist in the:

- **DO ANN-based PI**: LSTM-based PI structure devoted to maintaining the $S_{O,5}$ concentration by means of modifying the $K_{La,5}(t)$. The LSTM structure considers two LSTM cells with 100 and 50 hidden neurons, respectively. Two feed-forward layers with 50 and 25 hidden neurons per layer are considered just after the two LSTM cells.
- **NO ANN-based PI**: LSTM-based PI structure devoted to maintaining the $S_{NO,2}$ concentration by means of modifying the $Q_a(t)$. It considered the NARX principle, thus, the inputs considered by the NO ANN-based PI consist in the $S_{NO,2}(t)$, its desired set-point $S_{NO,2_{set-point}}(t)$ and the previously observed actuation signal, $Q_a(t - t_s)$. In this case, the structure replicates the same structure as the DO ANN-based PI.

The performance of both structures is computed in terms of the prediction and control performance in Section 5.2. Results shown in Table 5.1 determine that both structures are offering a good prediction performance, i.e., they can replicate the outputs provided by the BSM1's default PIs for given inputs. Notice that only the ideal BSM1 scenario is considered here since the main aim of the chapter is to assess the transferability of the ANN-based PI structures. The best ANN-based PI controller is the DO ANN-based PI. Recapitulating its results, its average improvement with respect to the BSM1's default PI controllers equals to 95.98% in terms of the IAE and to 99.84% for the ISE. The average improvement of the NO ANN-based PI equals to 24.34% for the IAE and 34.21% for the ISE. Both cases when a fix set-point is considered. When a variable set-point is considered, these improvements equal to 91.55% and 97.77% for the DO ANN-based PI's IAE and ISE, and 27.57% and 42.94% for the NO ANN-based PI's IAE and ISE. Therefore, it is corroborated that the best ANN-based PI controller is the one in charge of the $S_{O,5}$ concentration.

7.2.2 Control Knowledge Transfer Approach

The Control Knowledge Transfer approach corresponds to the stage of the Transfer Learning-based Control Design devoted to transferring the knowledge of the ANN-based PI structures from one BSM1 con-

trol loop into the other. The adoption of this stage is motivated by the fact that the ease and speed-up of the controller design and implementation process is sought.

Two different TL approaches are considered to assess the transfer of the control knowledge between BSM1 control loops:

- **Transfer Learning from DO to NO**: The DO ANN-based PI structure is transferred directly from the DO to the NO BSM1 control loop. The ANN-based PI controller is trained to manage the $S_{O,5}$ concentration. Only the normalisation and denormalisation stages (see Figure 5.2) are adapted to the NO control loop measurements.
- **Transfer Learning from NO to DO**: The NO ANN-based PI structure is directly transferred from the NO to the DO BSM1 control loop without performing any change in the ANN's weights and biases. The unique change performed in this transfer approach corresponds to the normalisation and denormalisation stages (see Figure 5.2). They have been adapted to normalise and denormalise the measurements coming from the NO control loop instead of the DO control loop.

Transfer Learning from DO to NO

Results of the control performance of the DO ANN-based PI transferred into the NO control loop are shown in Table 7.1. They are computed in terms of the IAE and ISE metrics for a fix and a variable set-point. The fix set-points equal to the ones considered in the default BSM1 control loops, i.e., 2 mg/L for the $S_{O,5}(t)$ and 1 mg/L for the $S_{NO,2}$. In the case of the variable set-point, the hierarchical control proposed in [San15a] is considered. Notice that the variable set-point is only applied to the DO control loop. This decision is taken due to the complexity of the strategies. While the DO control loop directly relates the $S_{O,5}(t)$ variations to the modifications of $K_{La,5}(t)$, the $Q_a(t)$ variations do not have a direct effect on the $S_{NO,2}$ concentration.

At first sight, it is observed that the control performance of the DO control loop is much better than the NO one, either when the default BSM1 controllers, or the ANN-based PIs are considered. In that sense, the DO ANN-based PI and its transferred version into the NO control loop, the DO→NO ANN-based PI, improve the performance in all the cases. Results show that the control behaviour of the DO→NO ANN-based PI controller when it is managing a fix set-point in the NO control loop can be improved. In average, the IAE and ISE are improved a 36.25% and 53.57%, respectively. For instance, the highest improvement with respect to the BSM1 NO default PI structure is achieved when the stormy weather is considered. The IAE and ISE obtained in such a situation equal to 1.033 and 0.357, respectively, which in percentage values equal to an improvement of a 44.88% and a 63.46% for the IAE and ISE, respectively. However, this represents a reduction of the IAE and ISE improvement of 51.33 and 36.36 percentage points with respect to the one achieved when the DO ANN-based PI is managing the DO control loop. This is clearly motivated by the fact that this ANN-based controller is designed to offer the

best performance when managing the source control environment.

When a $S_{O,5}(t)$ variable set-point is chosen, the improvements achieved by the DO→NO ANN-based PI are reduced. Now, the highest improvement is obtained for the management of the dry weather. IAE and ISE values are enhanced with respect to the BSM1's $S_{NO,2}(t)$ default PI a 29.07% and a 41.38%, respectively. Moreover, the average improvement equals to a 26.19% and 37.27% for the IAE and ISE, respectively. Consequently, it is shown that the average improvement in terms of the IAE and ISE are degraded 10.06 and 16.30 percentage points with respect to the performance of the $S_{O,5}(t)$ fix set-point.

Table 7.1: Control Performance when transferring the DO ANN-based PI into the NO control loop.

Fix set-point - DO control loop						
	Influent Weather Profile					
	Dry		Rainy		Stormy	
Structure	IAE	ISE	IAE	ISE	IAE	ISE
DO Default BSM1 PI	0.148	0.007	0.143	0.007	0.158	0.007
DO ANN-based PI	0.006	$9.98{\cdot}10^{-6}$	0.006	$1.12{\cdot}10^{-5}$	0.006	$1.29{\cdot}10^{-5}$
Improvement [%]	95.95	99.86	95.80	99.84	96.20	99.82
Variable set-point - DO control loop						
	Influent Weather Profile					
	Dry		Rainy		Stormy	
DO Default BSM1 PI	0.185	0.016	0.155	0.014	0.206	0.020
DO ANN-based PI	0.013	$2.34{\cdot}10^{-4}$	0.016	$4.48{\cdot}10^{-4}$	0.016	$4.05{\cdot}10^{-4}$
Improvement [%]	92.97	98.54	84.68	96.80	92.23	97.98
Fix set-point - NO control loop						
	Influent Weather Profile					
	Dry		Rainy		Stormy	
Structure	IAE	ISE	IAE	ISE	IAE	ISE
NO Default BSM1 PI	1.594	0.691	1.922	0.951	1.874	0.977
DO→NO ANN-based PI	1.008	0.290	1.401	0.578	1.033	0.357
Improvement [%]	36.76	58.03	27.11	39.22	44.88	63.46
Variable set-point - NO control loop						
	Influent Weather Profile					
	Dry		Rainy		Stormy	
NO Default BSM1 PI	1.792	0.858	2.132	1.089	1.884	0.989
DO→NO ANN-based PI	1.271	0.503	1.672	0.758	1.358	0.593
Improvement [%]	29.07	41.38	21.58	30.39	27.92	40.04

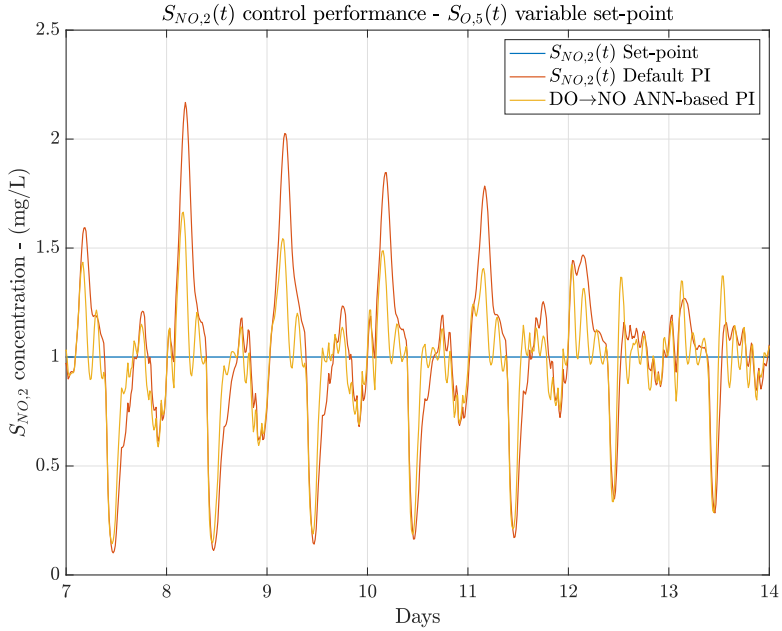

Figure 7.3: Control performance for the DO→NO ANN-based PI managing the $S_{NO,2}(t)$ control loop.

The performance of the DO→NO ANN-based PI is depicted in Figure 7.3. As it is shown, the NO control loop management could be still improved. Nevertheless, this performance shows that the DO ANN-based PI controller can be transferred into the NO BSM1 control loop. As a result, the default BSM1 performance would be improved, not only in terms of the DO control loop, but also in terms of the NO one. Moreover, results also corroborate the DO ANN-based PI can deal with fix and variable set-points whenever it is the control loop being managed. This entail a twofold benefit: (i) the DO ANN-based PI can manage both BSM1 control loops, and (ii) efforts are focused on deriving a unique ANN-based controller rather than two.

Transfer Learning from NO to DO

The control performance of the NO ANN-based PI is also computed to determine its behaviour when managing the NO control loop, its source domain, and its performance when managing the DO loop, its target domain. Results are shown in Table 7.2 where at first sight it is clearly observed that the IAE and ISE metrics are improved with respect to the default $S_{NO,2}(t)$ PI controller. When a $S_{O,5}(t)$ fix set-point is considered, the IAE of the NO control loop is improved in average a 24.32% while in terms of the ISE, the average improvement equals to a 39.03%. Both with respect to the default NO control loop PI controller. The ISE improvement shows that the proposed NO ANN-based PI controller is able to reduce the highest errors between the measured $S_{NO,2}(t)$ and its set-point. However, the control performance can be still improved since the IAE errors are still high. For instance, the best improvement is observed when the stormy weather is considered. There, the obtained IAE goes from 1.874 to 1.360, whereas the

ISE goes from 0.977 to 0.543. These values represent an improvement around a 27.43% and a 44.42% when the obtained IAE and ISE values are compared to the default PI control metrics. In terms of the $S_{O,5}(t)$ control performance, the transferred NO ANN-based PI, i.e., the NO→DO ANN-based PI, shows that the IAE performance is degraded instead of improved. For instance, when this controller is adopted, the IAE is increased from 0.148 to 0.158 when dry events are considered. This effect is motivated by the fact that the default PI of the NO control loop is not offering such a good control performance as does the default PI of the DO control loop. Thus, an important fact is observed: the control performance will not be improved if data from the NO control loop is considered to derive the NO→DO ANN-based PI.

Table 7.2: Control Performance when transferring the NO ANN-based PI into the DO control loop.

Fix set-point - NO control loop						
	Influent Weather Profile					
	Dry		Rainy		Stormy	
Structure	IAE	ISE	IAE	ISE	IAE	ISE
NO Default BSM1 PI	1.594	0.691	1.922	0.951	1.874	0.977
NO ANN-based PI	1.302	0.486	1.399	0.542	1.360	0.543
Improvement [%]	18.32	29.67	27.21	43.01	27.43	44.42
Variable set-point - NO control loop						
	Influent Weather Profile					
	Dry		Rainy		Stormy	
NO Default BSM1 PI	1.792	0.858	2.132	1.089	1.884	0.989
NO ANN-based PI	1.266	0.464	1.574	0.662	1.372	0.557
Improvement [%]	29.35	45.92	26.17	39.21	27.18	43.68
Fix set-point - DO control loop						
	Influent Weather Profile					
	Dry		Rainy		Stormy	
Structure	IAE	ISE	IAE	ISE	IAE	ISE
DO Default BSM1 PI	0.148	0.007	0.143	0.007	0.158	0.007
NO→DO ANN-based PI	0.158	0.004	0.146	0.004	0.160	0.004
Improvement [%]	-6.76	42.86	-2.10	42.86	-1.27	42.86
Variable set-point - DO control loop						
	Influent Weather Profile					
	Dry		Rainy		Stormy	
DO Default BSM1 PI	0.185	0.016	0.155	0.014	0.206	0.020
NO→DO ANN-based PI	0.288	0.030	0.239	0.022	0.385	0.049
Improvement [%]	-55.68	-87.50	-54.19	-57.14	-86.89	-145.00

Visually, Figure 7.4 depicts the control behaviour for the NO and DO control loops. As it is observed, the NO control loop performance is slightly improved with respect to the default PI. The peaks of $S_{NO,2}$ concentration are reduced, however, the desired set-point is not achieved. In terms of the DO control loop, the control performance is even slightly degraded with respect to the default PI controller. The measured $S_{O,5}(t)$ does not show variations as the default PI controller, however, there exists an offset which produces the IAE increment. For that reason, the ISE in terms of the $S_{O,5}(t)$ is reduced. It now equals to 0.004 in average instead of 0.007. Notice that ISE tells if there exists a huge difference between the measured and the desired concentration, whereas IAE tells if the difference is maintained over time.

When a variable set-point is considered, it is observed that the control performance is only improved in terms of the NO control loop. The IAE and ISE metrics are improved in average with respect to the default PI controller a 27.57% and 42.94%, respectively. In terms of the DO control loop performance, results show that the NO→DO ANN-based PI controller derived from the NO control loop and transferred into the DO one is not an option since the IAE and ISE metrics are degraded. For instance , they are nearly doubled with respect to the default PI controller when the stormy weather profile is simulated. This corroborates one of the main ideas stated in Chapter 5: the better the conventional control performance, the better the ANN-based one. Consequently, results show that training or implementing the NO ANN-based PI is not a suitable option.

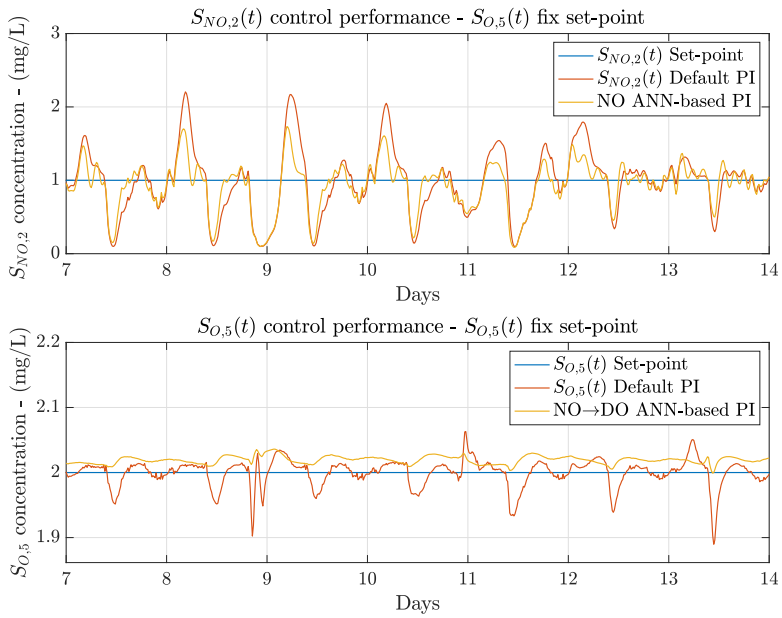

Figure 7.4: Control performance for the NO and DO control loops when the stormy weather is considered. The NO→DO ANN-based PI managing the DO control loop is derived from the NO control loop and transferred into the DO one.

7.2.3 Improving the Transfer Learning performance

Once the control performance of the DO and NO ANN-based PI controllers is computed it is clearly observed that the DO ANN-based PI is the controller offering the best control performance in both control loops. Nevertheless, its control behaviour can be improved. For that reason, it is fine-tuned in the Fine-Tuning process. In this case, the DO ANN-based PI is transferred from the DO control loop to the NO one. Then, a fine-tuning process is performed to adapt its behaviour to the target domain dynamics. In that sense, information about how to control and manage the $S_{NO,2}$ concentration is provided to the DO ANN-based PI. Therefore, the fine-tuned DO ANN-based PI (FTDO ANN-based PI) will be able to provide a better control performance in terms of the $S_{NO,2}(t)$ management process.

In terms of the three TL classes, the FTDO ANN-based PI is derived considering an inductive transfer learning task: data from the source domain, the DO control loop, is considered to firstly obtain the DO ANN-based PI structure. Then it is fine-tuned with data coming from the PI controlling the target domain, the NO control loop. In other words, the default $S_{NO,2}(t)$ PI controller whose performance is observed in Figure 5.1a is considered to perform the fine-tuning process of the DO ANN-based PI controller. Thus, the FTDO ANN-based PI will know how to correctly manage the desired variable, but adapted to the NO control loop. This clearly shows that an existing controller managing the target control loop might be compulsory to obtain the measurements considered in the fine-tuning process. Otherwise, no measurements would be available. This differs from traditional and conventional TL applications, where labelled data are intrinsically available.

The main point here is that in the fine-tuning process not all the layers of the DO ANN-based PI controller will be retrained with measurements of the target domain: the weights of the two LSTM cells are blocked whilst the weights and biases of the two MLP layers (see Figure 5.2) are modified in the fine-tuning process. Measurements of the target domain are again obtained by performing a whole year simulation of the BSM1 behaviour when the three weather profiles, dry, rainy, and stormy, are uniformly distributed. The weights and biases of the two retrained MLP layers are obtained considering the same training parameters as in the case of the DO ANN-based PI training process: initial learning rate equals to $1 \cdot 10^{-3}$, the weight decay equals to $5 \cdot 10^{-4}$ and the early patience is set to 5 epochs (see Section 5.2).

FTDO ANN-based PI Prediction Performance

After performing the fine-tuning process, the prediction performance of the FTDO LSTM-based PI equals to a RMSE of 0.095 mg/L, a MAPE of 6.24% and a R^2 of 0.991. Its t_{time} equals to 20.27 seconds. If these values are contrasted to the ones provided in 5.1, it is observed that prediction performance is degraded with respect to the DO and NO ANN-based PI controllers. This degradation is the consequence of focusing the efforts of the ANN-based PI controller on learning how to correctly manage the $S_{O,5}$ and $S_{NO,2}$ concentrations rather than a unique one.

In terms of the t_{time}, it equals to 20.27 seconds, which means that the time spent in the fine-tuning process is largely reduced with respect to training the ANN-based structure from scratch. This effect is motivated by the information already present in the ANN-based structures, that is, the weights and biases of the blocked LSTM cells. This measurement corroborates that TL techniques can be adopted to simplify and speed up the control design process. Let's suppose that instead of transferring the knowledge of the DO ANN-based PI into the NO control loop and performing a fine-tuning process, it is decided to control each loop with its corresponding ANN-based PI structure. As it is observed in Table 5.1, the amount of time devoted to training the networks correspond to 69.91 and 98.60 seconds for the DO and NO control loops, respectively. This yields a total training time of 168.51 seconds. Although this time is affordable, if the DO ANN-based PI is transferred into the NO control loop, only 69.91 seconds plus the time spent in the fine-tuning process, no more than 21 seconds, is required. Thus, the total amount of time invested in the design process equals to 90.18 seconds, which represents a reduction of 78.33 seconds with respect to training two individual nets. In addition, it is important to notice that BSM1 framework only considers two control loops. Therefore, this reduction of time will be even higher in those situations where the number of control loops to design is larger. In that sense, an estimation of the training time reduction can be performed. Supposing that the training time of the baseline ANN-based PIs (from scratch) correspond to $t_{time_{bs}}$ and that the time spent in the fine-tuning process on average equals to $t_{time_{ft}}$, the reduction of time (Δt) provided by the proposed approach can be computed as:

$$\Delta t = N \cdot t_{time_{bs}} - [t_{time_{bs}} + (N-1) \cdot t_{time_{ft}}] = (N-1)[t_{time_{bs}} - t_{time_{ft}}], \tag{7.1}$$

where $t_{time_{ft}} \ll t_{time_{bs}}$. N equals to the number of control loops where the baseline ANN-based PI is the transfer. As it is observed, the higher the number of control loops to design, the higher the reduction of time and the higher the benefit of the proposed methodology.

This methodology can also be applied in those situations where the control of a new WWTP scenario has to be designed. In such a context, the new control structure can be derived by transferring the knowledge of the control structure of an already controlled WWTP environment. This would involve an even higher reduction of the complexity and time required in the development of the control strategy.

FTDO ANN-based PI Control Performance

In terms of the control performance, results of the FTDO ANN-based PI are shown in Table 7.3, where the IAE and ISE values are computed for the different weather profiles and the fix and variable set-points. It is worth noticing that $S_{NO,2}(t)$ is now managed by the FTDO ANN-based PI, whereas the $S_{O,5}$ concentration is managed by the DO ANN-based PI. Since the management of each concentration has effects on the other, the performance for $S_{O,5}(t)$ and $S_{NO,2}(t)$ is computed again. The behaviour of the default PIs is provided for comparison purposes.

Table 7.3: Control Performance when transferring and fine-tuning the DO ANN-based PI into the NO control loop.

Fix set-point - DO control loop						
	Influent Weather Profile					
	Dry		Rainy		Stormy	
Structure	IAE	ISE	IAE	ISE	IAE	ISE
DO Default BSM1 PI	0.148	0.007	0.143	0.007	0.158	0.007
DO ANN-based PI	0.004	$5.12{\cdot}10^{-6}$	0.008	$2.43{\cdot}10^{-5}$	0.006	$1.76{\cdot}10^{-5}$
Improvement [%]	97.30	99.93	94.41	99.65	96.20	99.75
Variable set-point - DO control loop						
	Influent Weather Profile					
	Dry		Rainy		Stormy	
DO Default BSM1 PI	0.185	0.016	0.155	0.014	0.206	0.020
DO ANN-based PI	0.013	$1.99{\cdot}10^{-4}$	0.017	$3.91{\cdot}10^{-4}$	0.017	$3.72{\cdot}10^{-4}$
Improvement [%]	92.97	98.76	89.03	97.21	91.75	98.14
Fix set-point - NO control loop						
	Influent Weather Profile					
	Dry		Rainy		Stormy	
Structure	IAE	ISE	IAE	ISE	IAE	ISE
NO Default BSM1 PI	1.594	0.691	1.922	0.951	1.874	0.977
FTDO ANN-based PI	0.091	0.002	1.150	0.625	0.357	0.151
Improvement [%]	94.29	99.71	40.17	34.28	80.95	84.54
Variable set-point - NO control loop						
	Influent Weather Profile					
	Dry		Rainy		Stormy	
NO Default BSM1 PI	1.792	0.858	2.132	1.089	1.884	0.989
FTDO ANN-based PI	0.129	0.004	0.643	0.261	0.324	0.122
Improvement [%]	92.80	99.53	69.84	76.03	82.80	98.14

When a fixed set-point is considered, it is observed that the control performance is hugely improved not only in terms of the $S_{O,5}(t)$, but also in terms of the $S_{NO,2}(t)$. The improvement of the DO control loop with respect to the default PI controller is translated into an average reduction of the IAE around a 95.94% and a 99.78% in the case of the ISE. Thereby, this is translated in a better tracking process of the $S_{O,5}(t)$ and consequently, a better management of this concentration. In terms of the NO control loop, one can observe that IAE and ISE are hugely improved as well. However, there is an exception with the rainy weather. In this case, the $S_{NO,2}$ IAE and ISE are only improved a 40.17% and a 34.28%,

respectively. This is because the rainy weather profile shows two large perturbations during days 9 and 11. Besides, the fine-tuning process is performed with measurements obtained from the $S_{NO,2}(t)$ default PI controller when a whole year of uniformly distributed weathers is simulated. Thus, this entails that most of the knowledge provided to the DO ANN-based PI consists in the control actuations to manage the $S_{NO,2}$ concentration when the dry weather is considered (remember that rainy and stormy weathers are equal to the dry weather except for the two rainy and the two stormy episodes). On average, the NO control loop IAE and ISE are reduced by 71.80% and 72.84% with respect to the default $S_{NO,2}(t)$ PI control performance. The greatest improvement is observed when the dry weather is considered. The IAE is reduced from 1.594 to 0.091, whereas the ISE is decreased from 0.691 to 0.002 (see Figure 7.5).

Results for a variable set-point show the same tendency as the fix set-point ones. The IAE and ISE metrics have been improved for all the weather profiles. Again, the most important results are the ones corresponding to the FTDO ANN-based PI, which is the controller whose control performance improvement is sought with the fine-tuning process. In that sense, the highest improvement is now observed when the dry weather is simulated. Equalling to an improvement of 92.80%, the IAE has been decreased from 1.792 to 0.129. In terms of the ISE, it is decreased from 0.858 to 0.004, which represent an improvement of a 99.53%. It is important to notice that the lowest control performance is obtained when the rainy weather is considered: the IAE deceases from 2.132 to 0.643 while the ISE is reduced from 1.089 to 0.261. Although these improvements are not so high as the ones achieved with the dry weather, they are still much better than the performance obtained when the fine-tuning process is not carried out, i.e., with

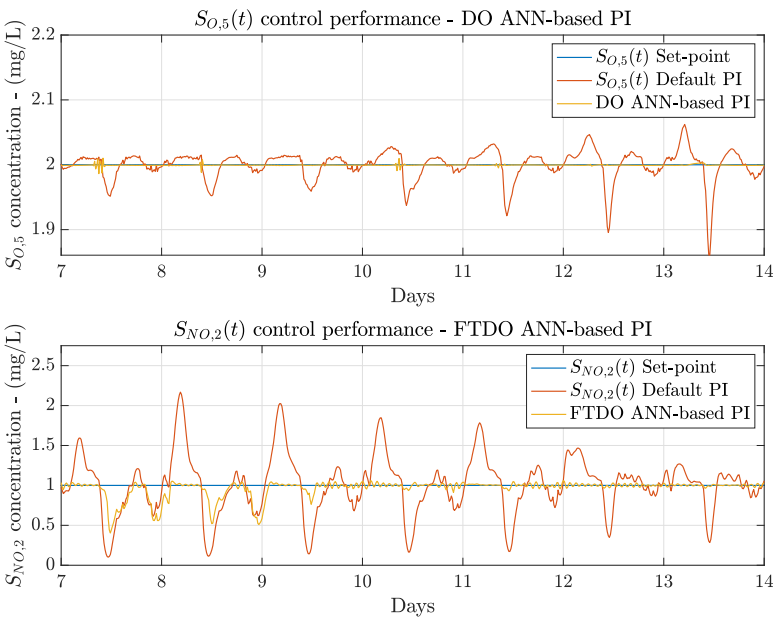

Figure 7.5: Control performance for the NO and DO control loops and a $S_{O,5}(t)$ fix set-point. Dry weather is considered. The FTDO ANN-based PI managing the NO loop is transferred from the DO control loop and fined-tuned with data from the target control loop.

respect to the results of Table 7.1. For instance, the IAE and iSE are improved a 69.84% and a 76.03%, both with respect to the default $S_{NO,2}$ PI. Finally, the average IAE improvement represents an increase of 55.62 and 54.24 percentage points with respect to the improvements achieved in the transference from DO to NO and from NO to DO, respectively. In terms of the ISE, these increments equal to 51.72 and 46.05 percentage points, respectively.

Visually, it is observed in Figure 7.6 that the $S_{NO,2}(t)$ desired value of 1 mg/L is obtained at the same time the $S_{O,5}(t)$ variable set-point is correctly tracked. In addition, the rainy episodes are plotted to show that the FTDO ANN-based PI controller requires some more knowledge to finally learn how to manage these events.

As a summary, the control performance is improved in all terms regardless of the set-point topology and the weather profiles. This entails that the best option to design or improve a control strategy of an industrial plant, and especially a WWTP, is to obtain a first baseline controller, the DO ANN-based PI, and then transfer its knowledge to the rest of control loops. The main point is to design the baseline controller with data coming from the controller performing better. In the case assessed here, this controller corresponds to the BSM1's $S_{O,5}$ default PI. Then, the derived DO ANN-based PI is transferred into the remaining control loops and fine-tuned with data coming from controllers actuating in the target domain. Moreover, this approach entail that control loops can be designed without requiring a high knowledge of the different processes carried out in the plant. Only input and output measurements of a control strategy performing well are required. Another benefit is placed on the speed-up of the control design process.

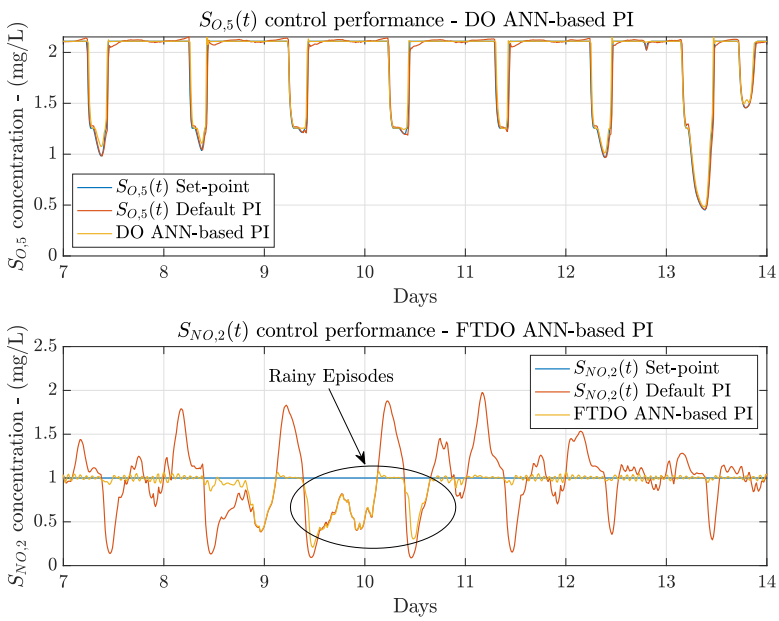

Figure 7.6: Control performance for the NO and DO control loops and a $S_{O,5}(t)$ variable set-point. Rainy weathers are considered. The FTDO ANN-based PI managing the NO loop is transferred from the DO control loop and fined-tuned with data from the NO one.

Thus, the higher the number of control loops, the higher the benefit offered with this design approach. Here, this benefit is not widely exploded since only the transference of the ANN-based PIs between two control loops is performed. However, this approach can be adopted in other scenarios where the number of control loops is largely higher than the ones managed here.

7.3 Measuring the Transfer Learning Suitability

The adoption of TL techniques in the design of control strategies entails a benefit for the industrial scenario for which a new controller is being designed. The key point is that the control structures of a full plant can be obtained from a unique ANN-based controller which would be transferred into all the control loops conforming the industrial environment under control. This has been assessed in Section 7.2, where the adoption of the Transfer Learning-based Control Design approach is proposed to derive ANN-based controllers to manage the $S_{NO,2}(t)$ control loop of the BSM1 framework.

The problem here lies in the fact that the control performance of the control loop where the ANN-based controller is being transferred to, the target scenario, is computed once the controller is already managing it. This fact can entail several issues if effects such as Negative Transfer are not considered [Wan19], especially in critical industrial scenarios which cannot be uncontrolled or badly managed. Thus, there exists a necessity of providing some kind of metrics or measurements determining if an ANN-based controller can be transferred into a new control loop. In that manner, one could determine if the control behaviour would be good enough before deploying the ANN-based structure over the real industrial domain. For that reason, this section is devoted to proposing the Transfer Suitability Metric (TSM). The main objective of TSM is to determine if an ANN-based structure is suitable to be transferred into a target domain from a source one before really deploying it. In that sense, issues related to Negative Transfer effects can be avoided. This is assessed in this section, where the TSM is computed over the BSM1 so as to determine the transferability of the DO and NO ANN-based PIs between the DO and NO control loops and vice-versa.

7.3.1 Transfer Suitability Metric

TSM is proposed to measure the suitability of transferring an ANN-based control strategy from a source control environment to a target one. Similar approaches have been proposed in other fields where classification tasks are carried out. For instance, the evolution of the separability between images as they are being processes by an ANN is assessed in [Sch21]. Results show that the proposed metric is able to numerically determine this feature, however, industrial controllers are in charge of forecasting the actuation signal rather than in performing classification tasks. Thus, if this metric was to be considered, an infinitesimal division should be performed and therefore, the sense of the metric would be lost. In [Sou20] a first attempt to measure the transferability for regression processes has been performed. However, the

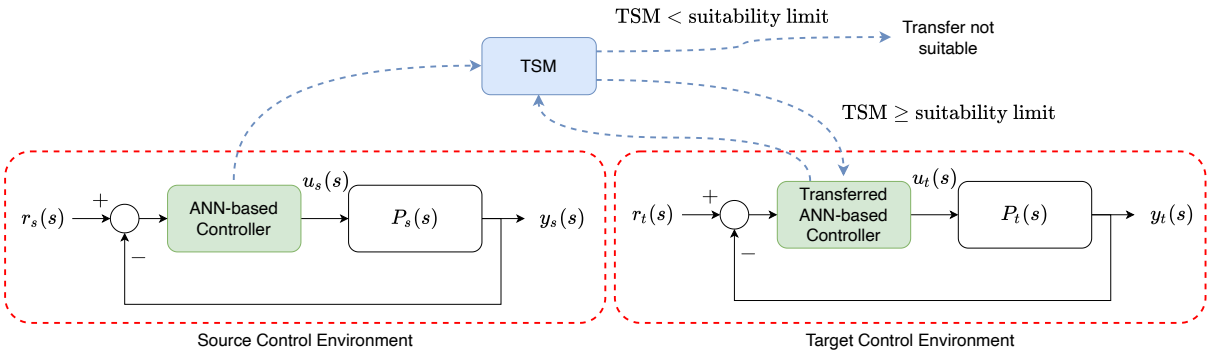

Figure 7.7: TSM computed over two control environments. Rainy weathers are considered. $r_s(s)$, $u_s(s)$ and $y_s(s)$ stand for the reference, the actuation and the controlled signals of the source environment. The same applies for $r_t(s)$, $u_t(s)$ and $y_t(s)$, which refer to the target environment.

objective of the proposed metric was to determine if data can be transferred so as to train a given ANN. Nevertheless, the metric is applied over incoming data and not over the evolution of data after being processed by the ANN structure. For that reason, the TSM metric is proposed. Instead of measuring the separability of measurements, or the transferability of data, it computes the similarity between source and target industrial domains and therefore, the transferability of the ANN-based control structure (see Figure 7.7).

The transferability of the ANN-based controller is computed following the premise that the more similar the processes performed by the ANN-based controller, the similar the industrial scenarios. For that reason, the evolution of input data through the different layers of the ANN-based controller is obtained, not only from the source domain, but also from the target one. In that sense, if the outputs of the layers of the controller for the source domain are similar to the outputs for the layers of target one, it can be said that both domains are similar and therefore, the ANN-based controller could be transferred.

TSM Formulation

TSM determines the similarity between the source and target domains. Since the main objective is to compute this similarity between domains so as to know if an ANN-based controller is transferable, it is computed for each one of the layers forming the ANN-based controller being transferred. Nevertheless, the layers of the ANN-based controller may differ in their internal structure, and therefore, in the number of hidden nodes. For instance, if the ANN-based PI controller of Figure 5.2 is considered, one can observe that the number of hidden neurons per LSTM gate differs between the first and the second layer. Even more, a change of ANN topology is performed from the second to the third layer. For that reason, there exists a necessity of scaling the outputs of each ANN layer to the same dimension and therefore, ensure a fair comparison among the whole ANN-based structure.

Among the different scaling approaches available in the literature, the Multidimensional Scaling (MDS) algorithm is considered [Car98]. This is motivated by the fact that MDS algorithm is able to reduce the dimensions of the data taking into account the relations among measurements, which is vital when dealing with industrial data. Other approaches such as PCA, are more focused on the dimensions themself than in the relations between measurements [Hou13]. Thus, approaches like PCA may not ensure that relationships among data are maintained.

To determine the behaviour of the MDS algorithm let's consider an ANN-based controller which is designed to manage a source domain. The outputs for the i-th layer equal to $\mathbf{X}_i \in \mathbb{R}^{N_R \times N_C}$, where N_R and N_C stand for the dimension of the i-th layer and N_C to the amount of time that input data is considered. Then, input measurements from the target domain are obtained and passed through this ANN-based control structure to determine if the process performed to the incoming data is similar or not. Consequently, the outputs for the same i-th layer of the ANN-based structure now consist in $\mathbf{Y}_i \in \mathbb{R}^{N_R \times N_C}$. Thus, each row of $\mathbf{X}$ and $\mathbf{Y}$ represents the evolution of a hidden node along the amount of time defined by the input measurements.

Suppose that both outputs correspond to the ones shown in Figures 7.8a and 7.8c. As it is observed, it is difficult to extract some features from these outputs: (i) the amount of dimensions for the i-th layer is huge, and (ii) no relationship can be established among dimensions, neither between domains. For that reason the MDS algorithm is applied with the objective of scaling each layer to a 2-dimensional layer. Now, the new matrices of outputs correspond to $\mathbf{X}'_i$ and $\mathbf{Y}'_i$:

$$\begin{aligned} \mathbf{X}_i \in \mathbb{R}^{N_R \times N_C} \quad & \xrightarrow{MDS} \quad \mathbf{X'}_i \in \mathbb{R}^{2 \times N_C} \\ \mathbf{Y}_i \in \mathbb{R}^{N_R \times N_C} \quad & \xrightarrow{MDS} \quad \mathbf{Y'}_i \in \mathbb{R}^{2 \times N_C} \end{aligned} \tag{7.2}$$

These matrices are a reduced and scaled representation of the real outputs of the i-th layer. The key point is that the time-instants are left as such so as to preserve the time evolution of the layer. Moreover, the reduction towards a 2-dimensional matrix is considered in order to ensure a visual interpretation of the outputs (see Figures 7.8b and 7.8d).

As it is observed, the 2-dimensional outputs can be easily interpreted. Moreover, some similarities between outputs can be appreciated. Therefore, the autocorrelation of the source domain output and the cross-correlation between the source and target domains outputs, both after perming the MDS, are considered in order to determine the similarity between domains [Sou20]. This is motivated by their adoption in the signal processing domain as a computation of the similarity between two different signals. In this case, the autocorrelation and cross-correlation compare the temporal evolution of $\mathbf{X'}_i$ and $\mathbf{Y'}_i$:

$$\begin{aligned} \mathbf{r}_{x'_{i,j}} &= E\left\{\mathbf{x'}_{i,j} \cdot \mathbf{x'}^*_{i,j}\right\} \\ \mathbf{r}_{x'y'_{i,j}} &= E\left\{\mathbf{x'}_{i,j} \cdot \mathbf{y'}^*_{i,j}\right\} \end{aligned} \tag{7.3}$$

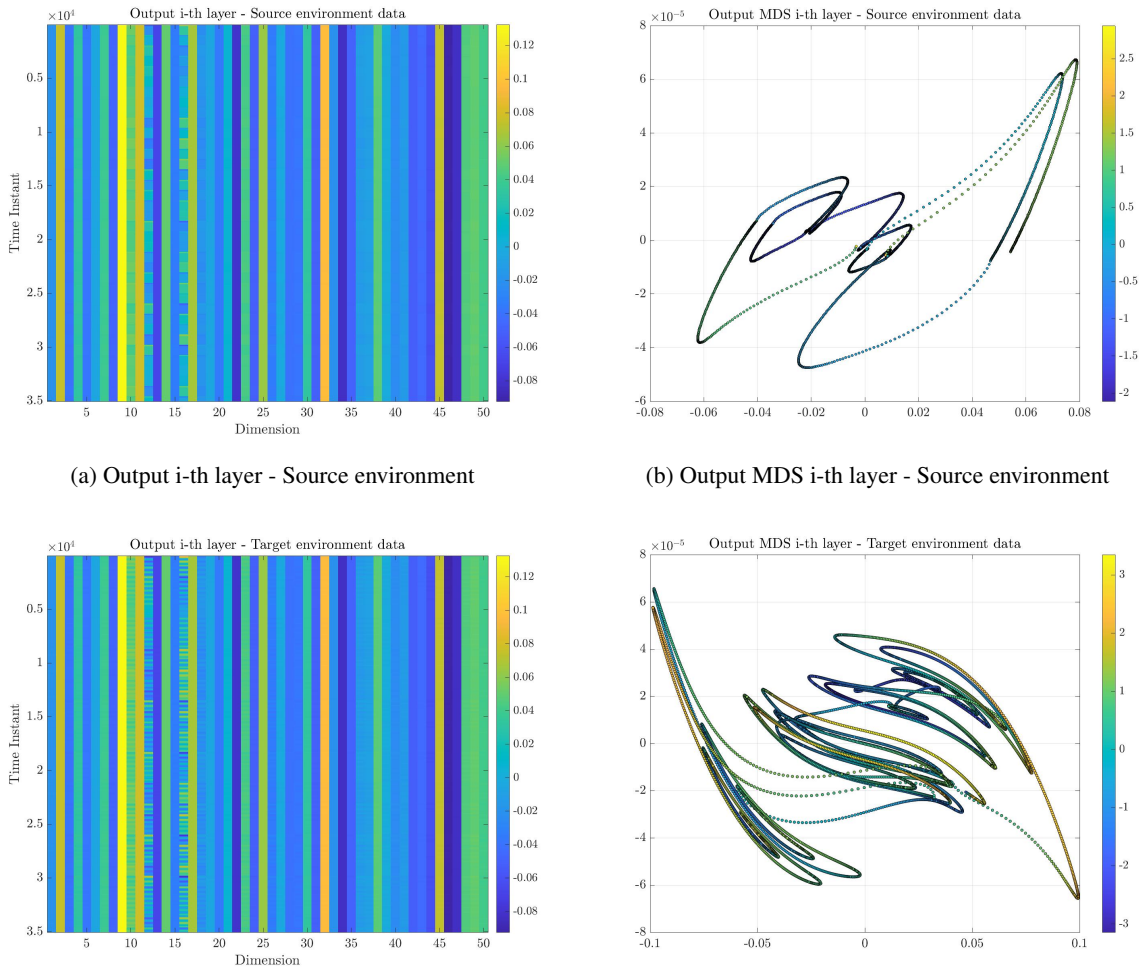

(a) Output i-th layer - Source environment

(b) Output MDS i-th layer - Source environment

(c) Output i-th layer - Target environment

(d) Output MDS i-th layer - Target environment

Figure 7.8: Output i-th layer before and after applying MDS algorithm.

where $\mathbf{r}_{x'_{i,j}}, \mathbf{r}_{x'y'_{i,j}} \in \mathbb{R}^{1\times(2N_C-1)}$ are the autocorrelation and cross-correlation vectors of the j-th row of $\mathbf{X'}_i$ and $\mathbf{Y'}_i$.

To compute the TSM, the autocorrelation is computed for the source domain since it corresponds to the environment for which the ANN-based control structure is designed. The cross-correlation matrix consists in the correlation values between outputs of the ANN-based controller when it is dealing with measurements from the source and target domain, respectively. Moreover, the maximum values of the autocorrelation and cross-correlation may vary as a function of the involved signals. Thus, if they are compared, results can show a huge difference between correlations even though environments are really similar. To tackle this, the normalised autocorrelation and cross-correlation matrices, $\mathbf{R}_{x'_i}$ and $\mathbf{R}_{x'y'_i}$, are considered. They yield measurements between 0 and 1, which ease the comparison between matrices. The normalised autocorrelation and cross-correlation matrices are computed as follows:

$$\mathbf{R}_{x'_i} = \begin{bmatrix} \frac{1}{\max(\mathbf{r}_{x'_{i,j=1}})} \cdot \mathbf{r}_{x'_{i,j=1}} \\ \frac{1}{\max(\mathbf{r}_{x'_{i,j=2}})} \cdot \mathbf{r}_{x'_{i,j=2}} \end{bmatrix} \tag{7.4}$$

$$\mathbf{R}_{x'y'_i} = \begin{bmatrix} \frac{1}{\sqrt{\max(\mathbf{r}_{x'_{i,j=1}})\max(\mathbf{r}_{x'y'_{i,j=1}})}} \cdot \mathbf{r}_{x'y'_{i,j=1}} \\ \frac{1}{\sqrt{\max(\mathbf{r}_{x'_{i,j=2}})\max(\mathbf{r}_{x'y'_{i,j=2}})}} \cdot \mathbf{r}_{x'y'_{i,j=2}} \end{bmatrix} \tag{7.5}$$

Finally, the TSM for the i-th layer of the ANN-based controller is computed to give a sense of distance between domains, the closer the source and target domains, the higher the TSM, and therefore, the higher the transfer suitability. To achieve that, each value of the normalised autocorrelation is compared to its counterpart in the cross-correlation matrix. Figure 7.9 depicts the process perform in the TSM computation for the i-th layer of the ANN-based controller. Taking all this into account, the TSM is computed as follows:

$$\text{TSM}_i = 1 - \sqrt{\frac{1}{2 \cdot (2N_c - 1)} \sum_{j=1}^{2} \sum_{k=1}^{2N_c-1} \left(\left[\mathbf{R}_{x'_i}\right]_{j,k} - \left[\mathbf{R}_{x'y'_i}\right]_{j,k} \right)^2} \tag{7.6}$$

Its values are placed in the range $[0, 1]$. Since it is computed considering the squared differences between the autocorrelation and cross-correlation matrices, TSM values equal to 1 entail maximum similarity between outputs of the ANN-based controller and therefore, maximum transfer suitability for the given layer. On the other hand, 0 means no similarity at all.

Nevertheless, a limit has to be established so as to classify the ANN-based structure as transferable or not. In that sense, and after defining the TSM expression, two scenarios which totally differ between them are considered to determine it. The source domain returns a matrix full of ones for the i-th layer, $\mathbf{1} \in \mathbb{R}^{10\times10}$. On the other hand, the output of the target domain's i-th layer consists in a matrix plenty of zeros, $\mathbf{0} \in \mathbb{R}^{10\times10}$. The resulting autocorrelation matrix of the source domain, $\mathbf{R}_{x'_i} = \mathbf{R}_{\mathbf{1}_i}$, presents its maximum value for the central lag. Resulting in a null matrix, the cross-correlation one, $\mathbf{R}_{x'y'_i} = \mathbf{R}_{\mathbf{0}}$, determines that both environments are not at all similar. This is corroborated by the TSM value, which for this example equals to TSM $= 0.4062$, a value placed far from 1. For this chapter, the limit of transfer suitability of the ANN-based controller is heuristically established at TSM ≥ 0.7.

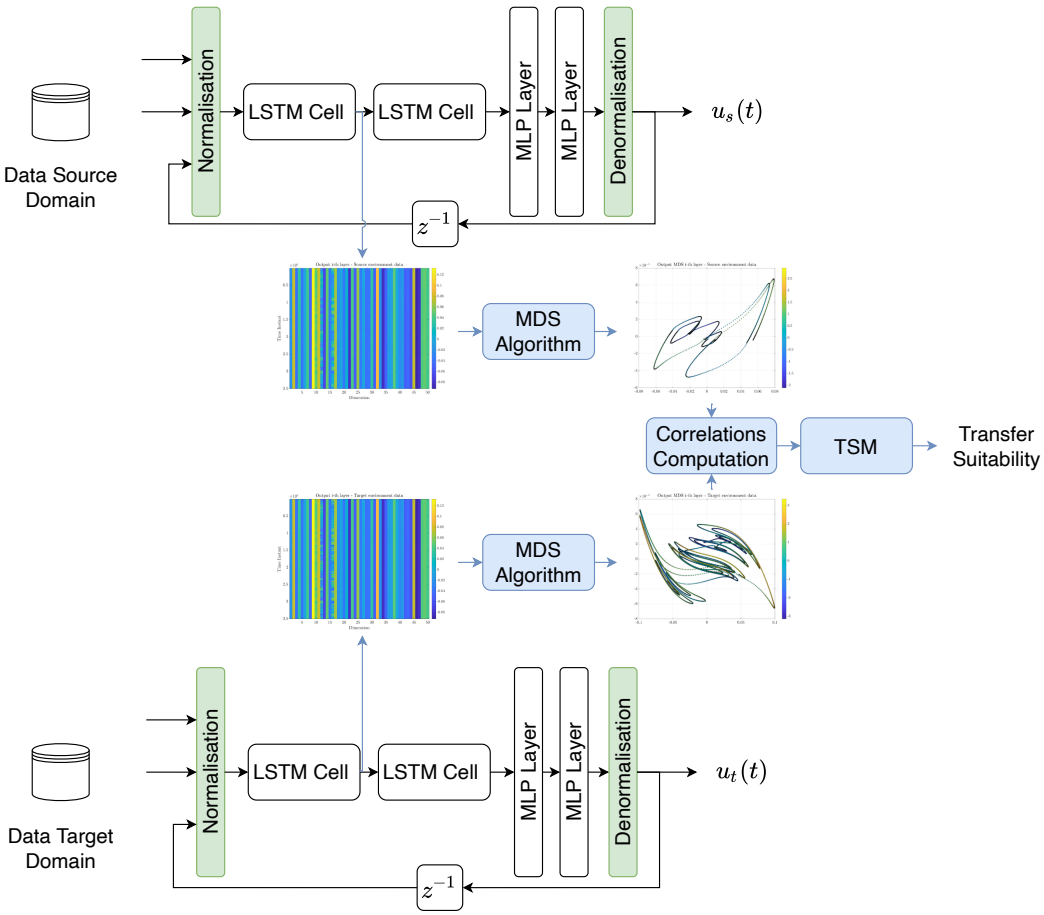

Figure 7.9: TSM schematic. As it is observed, the process performed for each of the outputs of the i-th layer of the ANN-based controller is depicted.

TSM Behaviour

Prior to applying the TSM metric between the BSM1 control loops, its behaviour is assessed adopting three different environments described by their transfer functions. The main objective is to compute the transfer suitability of the ANN-based PI managing the source environment in order to transfer it into the two target domains. In that sense, the source domain is defined as a First Order Plus Dead-Time (FOPDT) process, $P_1(s)$. It has been defined in [Kur19] as:

$$P_1(s) = \frac{1.4}{1.2s + 1} \cdot e^{-0.4s} \tag{7.7}$$

Moreover, the conventional PID, on which the ANN-based PI to be transferred is based on, is also defined in [Kur19]:

$$u_1(s) = 1.0217 \cdot \left[\left(1 + \frac{1}{1.3331s} \right) \cdot e_1(s) + \frac{0.1048s}{0.01048s + 1} \cdot y_1(s) \right] \tag{7.8}$$

where $u_1(s)$ is the actuation signal generated by the PID controller, $e_1(s)$ the error between the reference signal, $r_1(s)$, and the output of the process under control, $y_1(s)$. Thus, $e_1(s) = r_1(s) - y_1(s)$.

An ANN-based PI of the same form as the one shown in Figure 5.2 is derived to replicate the behaviour of (7.8). Since it is devoted to substituting the conventional PID, its inputs consist in $r_1(t)$ and $y_1(t)$ plus the previously predicted actuation signal, i.e., $u_1(t - t_s)$. In addition, the structure also incorporates the Normalisation and Denormalisation layers so as to scale and descale the inputs towards a zero mean and unity variance distribution. A variable set-point is considered in its training process. The prediction performance of the ANN-based PI returns a RMSE equal to 0.012, a MAPE of 0.25% and R^2 equivalent to 0.99. In terms of the control performance, results show that the conventional PID returns an IAE and an ISE equal to 17.113 and 7.007, respectively, when a variable set-point is considered. The ANN-based PI offers an IAE and ISE equal to 18.646 and 7.047, respectively. Therefore, these values show that the ANN-based PI nearly replicates the conventional PID (see Figure 7.10). If a unitary fix set-point is considered instead, the PID returns an IAE equal to $8.4742 \cdot 10^{-4}$ and an ISE equal to $2.8727 \cdot 10^{-7}$. On the other hand, the ANN-based PI returns IAE and ISE values equal to 0.5349 and $7.9928 \cdot 10^{-4}$, respectively. These values corroborate that the ANN structure can be adopted as a controller for $P_1(s)$. Furthermore, the fact of being based on ANNs makes the ANN-based controller a structure easy to be replicated and transferred among control loops.

This controller is then analysed to be transferred into the target environments, which consist in two Second Order Plus Dead-Time (SOPDT) systems. They have been proposed and analysed in [Kur20]:

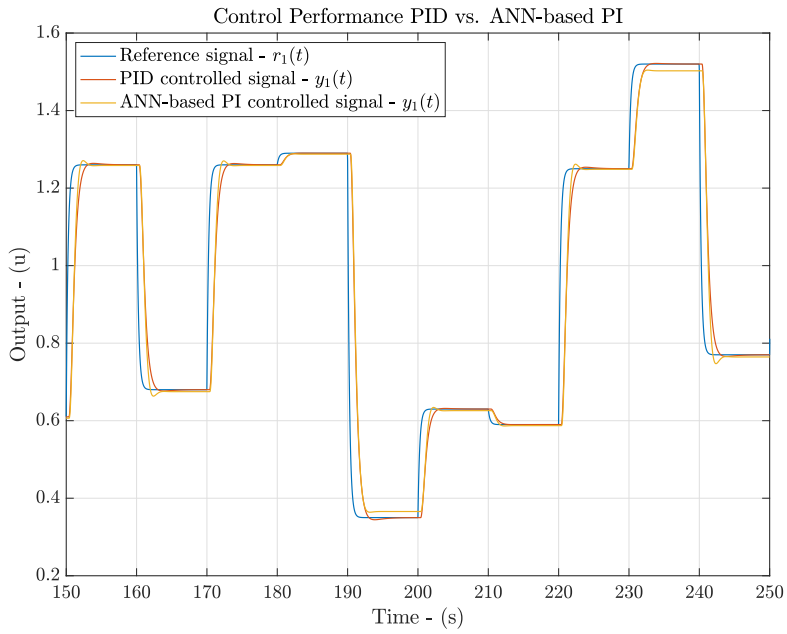

Figure 7.10: PID vs. ANN-based PI control performance when a variable set-point is considered.

$$P_2(s) = \frac{1}{s+1.5918} \cdot \frac{1.11}{s+0.6282} \cdot e^{-0.420s} \qquad P_3(s) = \frac{3.3120}{s^2+0.5280s+1.44} \cdot e^{-0.310s} \tag{7.9}$$

The key point here is that $P_2(s)$ consists in an overdamped SOPDT system whereas $P_3(s)$ consists in a SOPDT showing resonant phenomenon at a frequency of ω = 1.14 rad/s (see Figure 7.11). Besides, it is also observed that among these systems, $P_1(s)$ dynamics are more similar to $P_2(s)$ than $P_3(s)$. Therefore, one could say that the proposed ANN-based PI would be transferable from the source domain to $P_2(s)$, but not to $P_3(s)$.

Since the idea of TSM is to compute the transferability without deploying the ANN-based PI in the Real Scenario, the target processes are identified by means of the 123c identification technique [Alf21]. In that manner, the real situation is emulated, where information of the target environments must be obtained either by approximated models, or by digital twins if they are available. Digital twins can be understood as digital replicas of real systems. Thus, any change in the digital twin is to be observed in the Real Scenario if produced there [Gri17, Bos16]. In that sense, the models are identified by Double Pole Plus Dead-Time (DPPDT) systems. As a result, the identified models correspond to $P_{2m}(s)$ and $P_{3m}(s)$:

$$P_{2m}(s) = \frac{1.11}{(1.1410s+1)^2} \cdot e^{-0.3240s} \qquad P_{3m}(s) = \frac{2.30}{(0.3468s+1)^2} \cdot e^{-1.3040s} \tag{7.10}$$

Consequently, the information regarding the transient mode of $P_3(s)$ is not contemplated in the

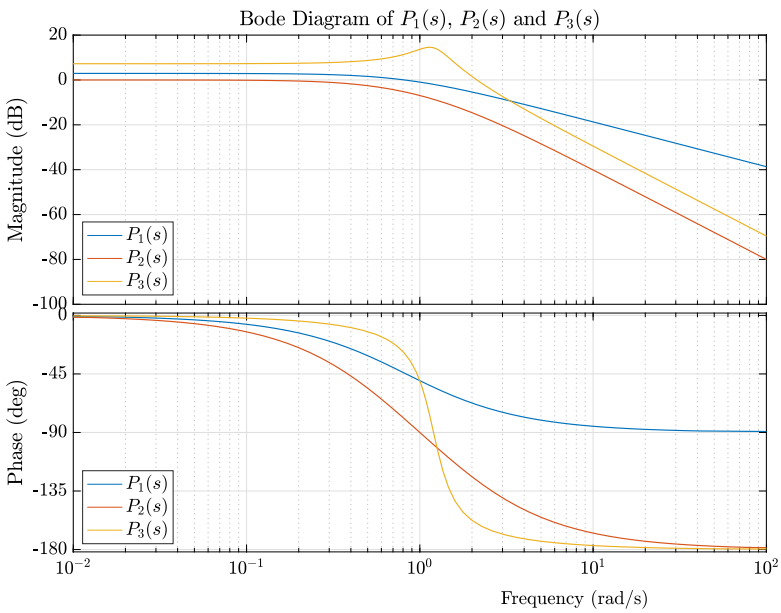

Figure 7.11: Bode diagrams of $P_1(s)$, $P_2(s)$ and $P_3(s)$.

identified models (see Figure 7.12). Notwithstanding, the proposed metric can compute the transferability of the system regardless of this information. In the real world, this would correspond to the linearisation of a non-lineal process, where part of the information of the process' dynamics would be lost.

Once the identified models are obtained, new input and output measurements of the process in a closed-loop configuration are considered, i.e., the ANN-based PI is deployed over $P_{2m}(s)$ and $P_{3m}(s)$ instead of the real $P_2(s)$ and $P_3(s)$. Fix and variable set-points are considered. In terms of the variable set-point, it is the same as the one adopted in $P_1(s)$ in order to assure a fair comparison and avoid biased results. In this case, TSM is computed for each layer of the ANN-based PI when it is managing both identified models. Results are shown in Table 7.4. Concerning the fix set-point, it can be observed that the transference from $P_1(s)$ to $P_{2m}(s)$ is classified as suitable since all the TSM values are placed over the suitability limit which is set to 0.7. In average, they equal to 0.9067. The highest TSM is provided by the first MLP layer, whose TSM equals to 0.9345. The lowest TSM offered by the layers of the ANN-based PI corresponds to the outputs of the input later, which returns a TSM equal to 0.8803. In terms of the transference of the ANN-based PI from $P_1(s)$ to $P_{3m}(s)$, results show that the transfer suitability is compromised. This is because all the TSM values are placed below and in the vicinity of the suitability limit. Besides, the average TSM of the ANN-based PI being transferred into $P_{3m}(s)$ equals to 0.6279, which is below the suitability limit. Therefore, the ANN-based controller should not be transferred even though there are some layers which return TSM values in the vicinity of this limit.

Results concerning the simulation of a variable set-point show that the transference of $P_1(s)$ into $P_2(s)$ is suitable since the TSM for all the ANN-based PI layers are showing values really close to 1. In

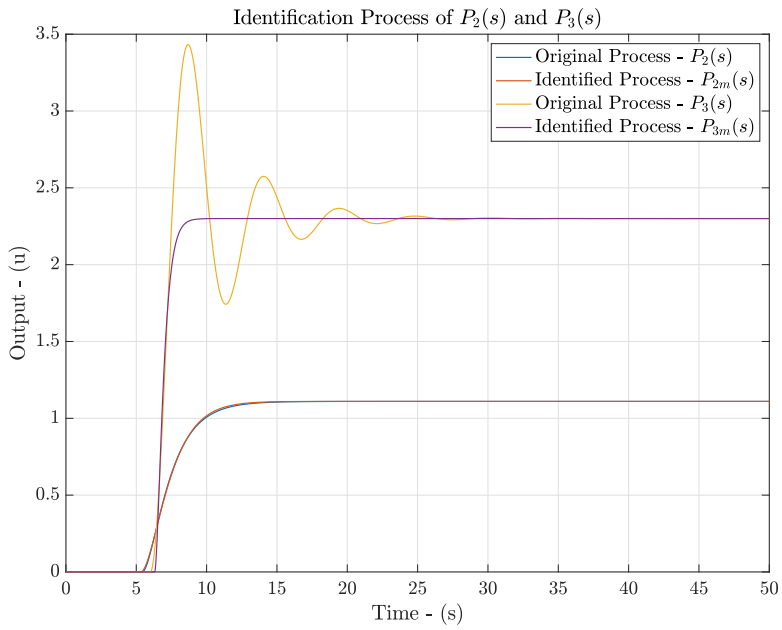

Figure 7.12: Comparative between the original processes and their identifications.

Table 7.4: TSM of the ANN-based PI being transferred from $P_1(s)$ into $P_{2m}(s)$ and $P_{3m}(s)$.

Transfer Suitability Metric of the ANN-based PI				
	Fix Set-point		Variable Set-point	
Layer	$P_1(s) \rightarrow P_{2m}(s)$	$P_1(s) \rightarrow P_{3m}(s)$	$P_1(s) \rightarrow P_{2m}(s)$	$P_1(s) \rightarrow P_{3m}(s)$
Input	0.8803	0.6954	0.9739	0.7873
1st LSTM cell	0.9003	0.7357	0.9718	0.6889
2nd LSTM cell	0.9334	0.6084	0.9717	0.6857
1st MLP layer	0.9345	0.6289	0.9721	0.6450
2nd MLP layer	0.8850	0.4713	0.9867	0.5909
Average	0.9067	0.6279	0.9752	0.6796

average, the TSM values equal to 0.9752, being the 2nd MLP layer the one offering the closest vale to 1. However, the lowest TSM value provided by the ANN-based PI layers is equivalent to 0.9717, which is observed in the second LSTM cell. On the other hand, the transference of the ANN-based PI from $P_1(s)$ into $P_{3m}(s)$ is not suitable since none of the TSM values are placed over the suitability limit. In that sense, the highest TSM is provided at the input layer and equals to 0.7873. The lowest one is observed at the output of the second MLP layer and it equals to 0.5909.

Finally, these values are corroborated with the deployment of the ANN-based PI over the real processes, i.e., over $P_2(s)$ and $P_3(s)$. As a result, Figure 7.13 depicts the control behaviour of the ANN-based PI when it manages $P_2(s)$ and $P_3(s)$. As it is observed, the final performance of the ANN-based PI when it is transferred into $P_2(s)$ and $P_3(s)$ follows the same tendency as the performance for $P_{2m}(s)$ and $P_{3m}(s)$. Therefore, the ANN-based PI is only transferable into $P_2(s)$ since all the $P_{2m}(s)$ TSM values, and its average, is placed over the suitability limit. On the other hand, when it is transferred into $P_3(s)$, the instability of the system is observed.

All these results corroborate the behaviour and the idea of TSM. It can be used as a metric measuring the suitability of transferring an ANN-based controller from a source controlled environment into a non-controlled one. Whenever the metric in general is placed over the suitability limit, the ANN-based structure can be transferred, otherwise, this is not an option.

7.3.2 TSM Applied Over the BSM1

Having proposed and assessed the TSM metric, it is applied over the BSM1 framework. Instead of identifying the $S_{O,5}(t)$ and $S_{NO,2}(t)$ processes, the BSM1 framework is adopted as a digital twin of a general purpose WWTP. In that sense, the main aim is to determine the transferability of the ANN-based PI proposed and analysed in Section 5.2.2. The control behaviour of the transferred versions is assessed in Section 7.2, where it is observed that the transference of the DO ANN-based PI from the DO control loop into the NO one is the best option. Therefore, this subsection is devoted to corroborating the results

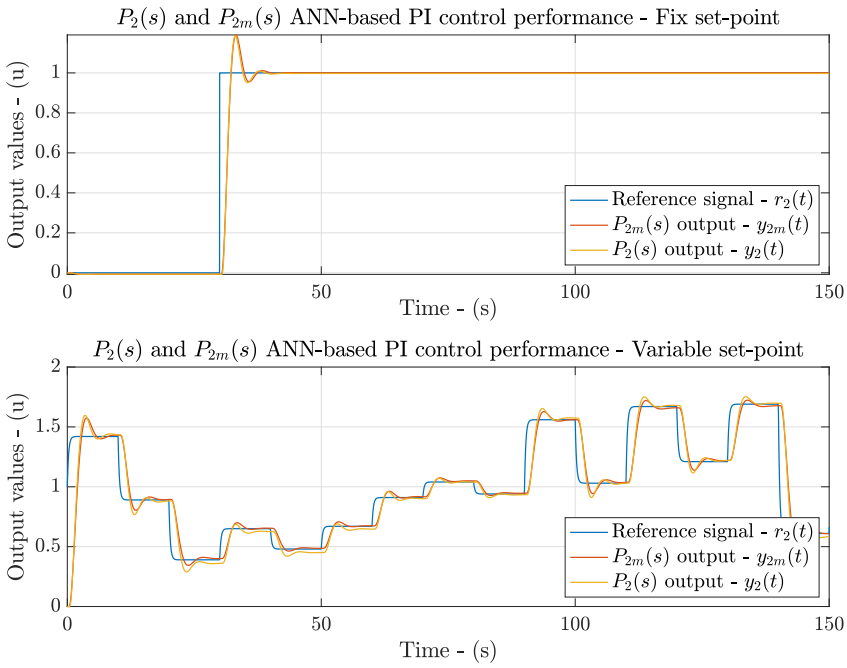

(a) $P_2(s)$ and $P_{2m}(s)$ control behaviour.

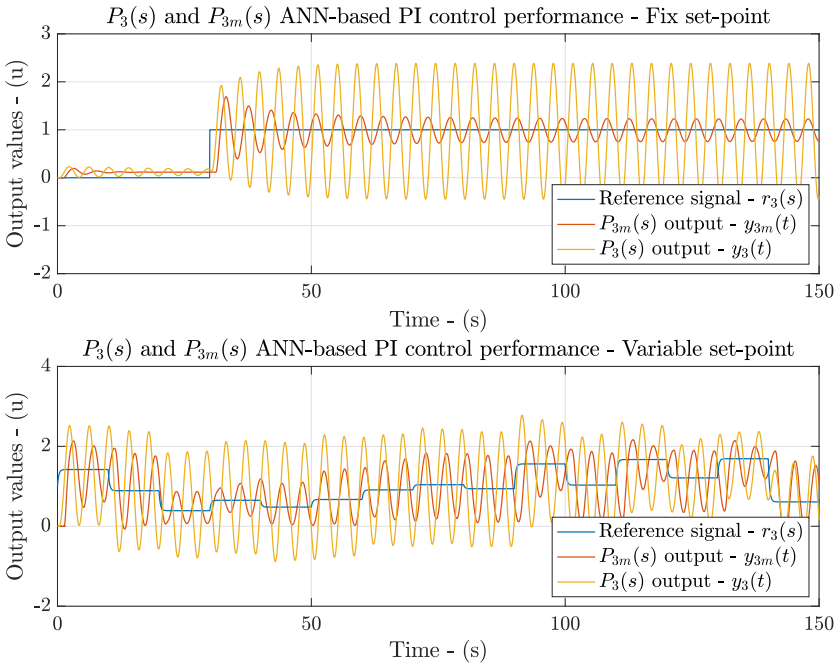

(b) $P_3(s)$ and $P_{3m}(s)$ control behaviour.

Figure 7.13: Control behaviour for the real, $P_2(s)$ and $P_3(s)$, and the identified processes $P_{2m}(s)$ and $P_{3m}(s)$.

provided before.

In that manner, a numerical value would be provided to reinforce the election of the DO ANN-based PI as the controller to be transferred without resorting to its analysis once it is deployed in the real WWTP target environment. Two different tests are considered in the computation of the TSM, where measurement from the source and the target environment are obtained from its deployment over the BSM1 scenario. It is worth noting that BSM1 is considered here as a WWTP digital twin. Thus, any modification or adjustment performed over BSM1 would produce the same effect on the real WWTP.

Taking this into account, TSM is computed for the DO→NO and the NO→DO ANN-based PIs.

- **DO→NO ANN-based PI**: ANN-based PI transferred from the DO control loop managing the $S_{O,5}(t)$ to the NO control loop. The main aim is to manage the $S_{NO,2}(t)$ without resorting to a new design of the ANN-based PI.
- **NO→DO ANN-based PI**: ANN-based PI transferred from the NO control loop managing the $S_{NO,2}(t)$ to the DO control loop. The main aim is to manage the $S_{O,5}(t)$ without resorting to a new design of the ANN-based PI.

To determine the TSM, a complete year of the BSM1 behaviour is simulated instead of the 14 days of BSM1 behaviour. In addition, the new weather profile including dry, rainy and stormy influents uniformly distributed is also considered to obtain the behaviour of the ANN-based PI regardless of the influent profile. Results are shown in Table 7.5. As it is observed, all the layers of the ANN-based PI structure return TSM values over the suitability limit. Notwithstanding, the situation which makes the difference corresponds to the transference of the ANN-based PI from the DO to the NO control domain. In this case, the highest TSM value corresponds to the one obtained at the output of the 1st LSTM layer and equals to 0.9274. The lowest one, and therefore, the closest to the suitability limit corresponds to the input layer, which returns a value equal to 0.8930. In average, the TSM value is equivalent to 0.9194, showing that the transference from DO to NO control loops is more than suitable.

In terms of the ANN-based PI's transference from the NO to the DO control loop, the TSM metric also shows that each layer is transferable since none of the values are placed below the suitability metric. For instance, the average TSM equals to 0.8421. However, the outputs provided by the Input layer and the 1st LSTM cell are close to it. Thus, this entails that the transference from the NO control loop towards the DO one may it be possible, but, a good performance cannot be ensured. The aforementioned results corroborate the control performance observed in Section 7.2. As it has been shown there, the DO→NO ANN-based PI is able to improve the NO Default BSM1 PI a 36.25% in terms of the IAE whereas this improvement equals to a 53.57% for the ISE, both when a fix set-point is considered (see Table 7.1). If TSM is taken into account, its average value equals to 0.9194. This entails that the higher the TSM, the more suitable the transference and the better the performance of the transferred ANN-based controller. Similar improvements are obtained for a variable set-point, where the average improvements

of the IAE and ISE are equal to 26.19% and 37.27%, respectively. These improvements can be increased until much higher percentages if a fine-tuning process is carried out (see Table 7.3). On the other hand, results in Table 7.2 clearly shows that the IAE is not improved, but degraded. The average degradation equals to -3.38. Indeed, if the TSM values are considered, it is clearly observed that the vicinity of the TSM to the suitability metric is the cause of this degradation. Moreover, if a variable $S_{O,5}$ set-point is considered rather than a fix one, the degradation of the IAE and ISE is even higher. Clearly stating that the transference of the NO ANN-based PI to manage the DO control loop is not an option.

7.4 Chapter Conclusions

In this chapter the adoption of TL to design and implement ANN-based controllers is assessed. The idea is to design an ANN-based controller in a source domain to later transfer it into the target one. In that manner, the design of the control structures can be sped up in the sense that there is neither a necessity to design a new ANN structure, nor to train it from scratch. Moreover, the complexity of designing a control structure can be reduced either. For instance, scenarios showing severe data scarcity issues could benefit from the transference of an ANN-based controller since it would be previously trained in an environment with enough data. As a consequence of the transference, however, the control performance at the target environment can be affected. For that reason, a fine-tuning process is also proposed to finally adapt the behaviour of the ANN-based structure to the new domain. Here, this has been analysed by means of transferring the ANN-based PI controllers from the BSM1 control loop managing the $S_{O,5}$ concentration to the one managing the $S_{NO,2}$, and vice-versa. Results show that the transference of the ANN-based PI managing the $S_{O,5}$ into the control loop in charge of $S_{NO,2}$ overcomes the performance provided by the default BSM1 PI controllers. For instance, the IAE and the ISE are improved a 36.25% and a 53.57% with respect to the default BSM1 PI controller. Results also determine that the transference in the other direction does not provide such good results. For instance, the IAE is degraded instead of improved. In addition, despite its good performance, the ANN-based PI transferred into the $S_{NO,2}$ control loop is

Table 7.5: TSM applied over the BSM1 control loops. Notice that TSM is only computed for the DO and NO control loops when a fix set-point is considered. $S_{O,5}$ has to be maintained at 2 mg/L while the $S_{NO,2}$ at 1 mg/L.

Transfer Suitability Metric of the ANN-based PI over BSM1 control loops.		
Layer	DO → NO	NO → DO
Input	0.8930	0.7320
1st LSTM cell	0.9274	0.7718
2nd LSTM cell	0.9144	0.8910
1st MLP layer	0.9144	0.8910
2nd MLP layer	0.9148	0.9246
Average	0.9194	0.8421

fine-tuned so as to adapt its behaviour to the target scenario. Results of this fine-tuning process, which is much quicker than training an ANN-based controller from scratch, show that the IAE and ISE values of the $S_{NO,2}$ management can be improved at most a 94.24% and a 99.71%, respectively.

Notwithstanding, the adoption of TL techniques to derive new ANN-based controllers has an important drawback regarding its deployment. ANN-based controllers cannot be transferred from the source domain into the target one without knowing that it would be able to correctly manage the new environment. This is crucial in most of the critical industrial environments. For that reason, in this chapter the TSM metric is proposed. The objective of this metric is to determine if an ANN-based structure can be deployed over a target domain or not. Based on the comparison between the autocorrelation and cross-correlation matrices of the ANN-based controller's layers, TSM returns the similarity value between zero and one. The closer to one the higher the similarity between the source and target domain. Thus, this feature is exploited to determine if the ANN-based structure is transferable or not. Here, the assessment of TSM is performed by means of simulating three processes: one FOPDT, one SOPDT and one SOPDT with resonant nodes. An ANN-based PI designed for managing the FOPDT is analysed so as to be transferred to manage the two SOPDT. TSM is computed to determine the transfer suitability. Results show that the proposed ANN-based PI can only be transferred into the SOPDT while the transference is not recommended for the SOPDT with resonant nodes. The control performance of the ANN-based PI managing the two SOPDT processes is also computed in order to corroborate the information provided by the TSM. The transferred ANN-based controller is able to correctly manage the SOPDT whereas it becomes unstable when controlling the SOPDT with resonant nodes. Finally, TSM is applied over the BSM1 framework, and therefore, over the transference of an ANN-based PI from the $S_{O,5}$ to the $S_{NO,2}$ control loops. TSM values corroborate the control performance obtained before. The transference is suitable from the $S_{O,5}$ to the $S_{NO,2}$ control loops whereas it cannot be ensured for the inverse direction, i.e., from the $S_{NO,2}$ to the $S_{O,5}$. These results clearly shows that the closer to one the TSM, the higher the transferability and the better the control performance in the target domain. This paves the way to a new form of designing and implementing control structures, and what it is more important, to exploit powerful tools such as ANNs.

Chapter 8

General Conclusions and Future Work

In this PhD dissertation the application of Deep Learning techniques to support and improve conventional industrial controllers is assessed The efforts of this thesis have been mainly focused on the adoption of ANNs over WWTPs, and especially, over their control loops in order to tackle some of the most important issues. By means of the power of ANNs, the complete behaviour of a WWTP infrastructure has been improved. The first approach has corresponded to the adoption of ANNs so as to support the operative of conventional industrial controllers. Forecasting WWTP effluent values, ANNs have provided conventional control structures with information regarding the pollutant levels in the WWTP's effluent. In that sense, conventional structures will have more time to actuate over these concentrations and therefore, achieve a higher reduction of effluent pollutants. Later, the adoption of ANN-based structures implementing control strategies has been proposed. The power of ANNs is such that control performance of these new controllers overcomes the one given by conventional control structures. However, non-idealities introduced by sensors of the WWTP plant (delays and noise) produce a drastic drop in the control behaviour of these new controllers. This has been tackled by means of ANN-based denoising and delay correction strategies, which not only are able to reduce the effects of such non-idealities, but also to reduce the required knowledge of the environment. Having assessed these applications, the dissertation ends with the adoption of TL techniques to design and implement industrial controllers as well as with the derivation of a new transfer suitability measuring approach.

8.1 Conclusions

First, in Chapter 1, the main motivations and the outline of this thesis are presented. Moreover, the contributions derived from the realisation of this thesis have been presented in this chapter as well.

In Chapters 2 and 3, the background on which this thesis is based on has been presented. First, an overview on ANNs and their main topologies has been provided. Moreover, TL concepts are also provided. Second, BSM1 and BSM2 are presented since they correspond to the two frameworks where the

application of ANNs is assessed. Third, a brief introduction to sensing approaches and the adoption of ANN-based Soft-sensors in industrial environments has been provided. Finally, the evolution of conventional industrial controllers over WWTP scenarios towards the adoption of ANN in control structures has been analysed.

In Chapter 4, the adoption of ANNs as elements supporting conventional controllers has been proposed. In there, the ability of LSTM cells in modelling highly complex and non-linear processes is firstly exploited to obtain a predictor of effluent violations (exceed of pollutant limits), especially of $S_{Ntot,e}$ and $S_{NH,e}$ concentrations. Results have shown that a good prediction performance is obtained and therefore, useful information for the operability of the WWTP plant can be provided. In that sense, the predictions returned by the proposed LSTM architectures are fed into conventional controllers so as to let them actuate in advance over pollutant levels willing to cause an effluent violation. Results have shown that this information is of the utmost utility since nearly a complete reduction of pollutant violations is observed. Since the reduction of $S_{Ntot,e}$ levels increases the $S_{NH,e}$ ones, the complete reduction has not been achieved. Nevertheless, the amount of effluent violations have been reduced until three: a unique violation of $S_{NH,e}$ representing a 0.014%, and two violations of $S_{Ntot,e}$ representing only a 0.02%, both with respect to the BSM2 simulation time. In all the cases, the violations do not represent more than a 3.25% of the maximum allowed value in the case of the $S_{NH,e}$ and a 0.67% in the case of $S_{Ntot,e}$.

In Chapter 5, ANNs have been considered to directly implement the control structures of WWTP control loops. Two control architectures have been proposed, an ANN-based PI replicating the default BSM1 PI behaviour and an ANN-based IMC. The former has been devoted to managing either the $S_{NO,2}$ or the $S_{O,5}$ concentrations, while the latter has been in charge of managing only the $S_{O,5}$. In both cases, results have shown that ANN-based control structures are not only able to replicate the conventional control behaviour, but also to overcome their performance. For instance, the ANN-based PI managing the $S_{O,5}$ improves in average the conventional PI around a 96.24%. The same tendency is observed in the case of the ANN-based IMC. By means of modelling the direct and inverse relationships of the process under control, this structure is able to improve the conventional PI performance a 61.20%. As a controller being derived from scratch, the stability of the ANN-based IMC must be determined. Performed by means of data-based techniques, the stability test results have determined that the controller is marginally stable for the whole operability range of frequencies. Finally, the effects of non-idealities introduced by real sensors are assessed. A drop in the control performance of both structures is observed.

In Chapter 6, a new denoising and delay correction approach is presented to tackle the issues caused by non-idealities. This new approach consists in two stages, the denoising and the delay correction one. The former has been implemented by means of DAE, ANN-based structures in charge of returning clean versions of the noise-corrupted input data. The delay correction stage consists in an ANN devoted to predicting the difference between the current real output measurement and the one really measured by the plant's sensor. Both stages have been analysed separately, firstly to tackle the ANN-based PI's drop of performance and secondly, to improve the ANN-based IMC control behaviour. Results have shown

that the denoising stage is able to provide clean measurements from the noise-corrupted ones meanwhile the delay correction stage succeeds in its purpose. In terms of the control behaviour, it has been observed that the ANN-based PI as well as the ANN-based IMC behaviours have been improved with respect to their performance when dealing with non-ideal measurements.

Finally, in Chapter 7, a new ANN-based control design approach based on TL techniques is proposed. Not only is it devoted to designing new control strategies, but also it aims to speed up the design and training process. The main idea is to derive an ANN-based controller in a source environment to later transfer it into a target one. In that manner, new control structures can be obtained from a principal one without resorting to their designing and training from scratch. This approach has been tested over the BSM1 scenario, where an ANN-based PI controller managing the $S_{O,5}$ control loop is transferred into the $S_{NO,2}$ and vice-versa. Moreover, the application of a fine-tuning process is also performed so as to finally adapt the behaviour of the transferred ANN-based controller to the target environment's dynamics and features. Results have shown that the transference of ANN-based controllers form a source to a target domain is possible. For instance, the control behaviour of the ANN-based PI transferred into the $S_{NO,2}$ control loop has been able to improve the results of the conventional PI control structures. Nevertheless, the transferability of ANNs, and especially those actuating as industrial controllers, cannot be performed without ensuring the correct behaviour of the controller before deploying it in the target environment. For that reason, a new metric, the TSM, has been proposed with the intention of measuring the transfer suitability of ANN-based controllers. Placed in the range [0,1], TSM's results determine if an ANN-based control structure is suitable to be transferred and therefore, offer a good control performance. Results of its application over the BSM1 framework have corroborated that the closer to one, the more transferable the ANN-based controller and the better the initial performance.

8.2 Future Work

The work presented in this thesis can be extended as follows:

- Validate all the results obtained by simulations in a real WWTP environment, where non-ideal measurements and other non-idealities are present.
- Use of the effluent predictions to design MPC controllers that base the prediction on the LSTM models.
- Propose the adoption of Reinforcement Learning techniques as a way of managing WWTP environments rather than addressing the creation of ANN-based controllers as it has been done.
- Consider the TL based control design approach to derive controllers from well-known and easy to access industrial environments to later deploy them in critical and also harmful environments.

- Apply all the proposed systems and processes, not only on other and more complex WWTP scenarios, but also in other industrial environments.

Moreover, there are some aspects derived from the work presented in each chapter that remains as future work:

- In Chapter 4, the design and implementation of ANN-based controllers can be addressed in order to substitute the conventional ones and therefore, try to completely avoid the violations of $S_{NH,e}$ and $S_{Ntot,e}$ concentrations.
- In Chapter 5, a possibly extension consists in the development of ANN-based controllers which are trained following the Reinforcement Learning principles. In that manner, the ANN-based controller could adapt its behaviour while it is already managing the WWTP plant. Thus, a change in the dynamics of the process under control could be automatically tackled without requiring huge efforts.
- In Chapter 6, the noise and delay correction can be performed at the sensors level rather than at the control loop one. In that manner, the scalability of the noise and delay correction approach would be hugely increased since it will not be specific to the control objective, but to the sensor.
- In Chapter 7, the adoption of TL techniques and especially the development of the TSM metric is performed over existent control loops, i.e., control structures where a conventional controller is available. In that sense, the adaptation of the transfer approach and the proposed metric to work with data from open loop configurations should be addressed. Therefore, the adoption of the TSM will become even more useful.

References

[Agu18] R. Aguilar, J. Torres, C. Martín, "Aprendizaje automático en la identificación de sistemas. un caso de estudio en la predicción de la generación eléctrica de un parque eólico", *Revista Iberoamericana de Automática e Informática.*, Vol. 16, nº 1, pags. 114–127, 2018.

[Ale08] J. Alex, L. Benedetti, J. Copp, K. V. Gernaey, U. Jeppsson, I. Nopens, M. N. Pons, L. Rieger, C. Rosen, J. P. Steyer, P. Vanrolleghem, "Benchmark simulation model no. 1 (BSM1)", Tech. rep., Department of Industrial Electrical Engineering and Automation, Lund University, 2008.

[Alf21] Alfaro, Víctor M and Vilanova, Ramon, "Control of high-order processes: repeated-pole plus dead-time models' identification", *International Journal of Control*, pags. 1–11, 2021.

[AlM14] M. AlMahamdy, H. B. Riley, "Performance study of different denoising methods for ECG signals", *Procedia Computer Science*, Vol. 37, pags. 325–332, 2014.

[Ami20] M. A. Amirabadi, M. H. Kahaei, S. A. Nezamalhosseini, "Novel suboptimal approaches for hyperparameter tuning of deep neural network [under the shelf of optical communication]", *Physical Communication*, Vol. 41, pags. 101057, 2020.

[Bab15] M. S. Babel, G. B. Badgujar, V. R. Shinde, "Using the mutual information technique to select explanatory variables in artificial neural networks for rainfall forecasting", *Meteorological Applications*, Vol. 22, nº 3, pags. 610–616, 2015.

[Bai06] Y. Bai, H. Zhuang, D. Wang, *Advanced fuzzy logic technologies in industrial applications*, Springer: London, England, 2006.

[Bar18] M. Barbu, I. Santin, R. Vilanova, "Applying Control Actions for Water Line and Sludge Line to Increase Wastewater Treatment Plant Performance", *Industrial and Engineering Chemistry Research*, Vol. 57, nº 16, pags. 5630–5638, 2018.

[Ben07] F. Benazzi, K. V. Gernaey, U. Jeppsson, R. Katebi, "On-line estimation and detection of abnormal substrate concentrations in WWTPs using a software sensor: a benchmark study", *Environmental Technology*, Vol. 28, nº 8, pags. 871–882, 2007.

[Ben12] Y. Bengio, *Practical Recommendations for Gradient-Based Training of Deep Architectures*, pags. 437–478, Springer Berlin Heidelberg, Berlin, Heidelberg, 2012.

[Ber12] C. Bergmeir, J. M. Benítez, "On the use of cross-validation for time series predictor evaluation", *Information Sciences*, Vol. 191, pags. 192–213, 2012.

[Ber18] C. Bergmeir, R. J. Hyndman, B. Koo, "A note on the validity of cross-validation for evaluating autoregressive time series prediction", *Computational Statistics & Data Analysis*, Vol. 120, 2018.

[Boq19] G. Boquet, J. L. Vicario, A. Morell, J. Serrano, "Missing Data in Traffic Estimation: A Variational Autoencoder Imputation Method", *ICASSP 2019-2019 IEEE International Conference on Acoustics, Speech and Signal Processing (ICASSP)*, pags. 2882–2886, IEEE, 2019.

[Bos16] S. Boschert, R. Rosen, "Digital twin—the simulation aspect", *Mechatronic Futures*, pags. 59–74, Springer, 2016.

[Bou18] Z. Boussaada, O. Curea, A. Remaci, H. Camblong, N. Mrabet Bellaaj, "A nonlinear autoregressive exogenous (NARX) neural network model for the prediction of the daily direct solar radiation", *Energies*, Vol. 11, nº 3, pags. 620, 2018.

[Bua08] A. Buades, B. Coll, J.-M. Morel, "Nonlocal image and movie denoising", *International Journal of Computer Vision*, Vol. 76, nº 2, pags. 123–139, 2008.

[Bud18] M. Buda, A. Maki, M. A. Mazurowski, "A systematic study of the class imbalance problem in convolutional neural networks", *Neural Networks*, Vol. 106, 2018.

[Cad16] E. Cadenas, W. Rivera, R. Campos-Amezcua, C. Heard, "Wind speed prediction using a univariate ARIMA model and a multivariate NARX model", *Energies*, Vol. 9, nº 2, pags. 109, 2016.

[Can16] J. F. de Canete, P. del Saz-Orozco, R. Baratti, M. Mulas, A. Ruano, A. Garcia-Cerezo, "Soft-sensing estimation of plant effluent concentrations in a biological wastewater treatment plant using an optimal neural network", *Expert Systems with Applications*, Vol. 63, pags. 8–19, 2016.

[Car98] J. D. Carroll, P. Arabie, "Multidimensional scaling", *Measurement, Judgment and Decision Making*, pags. 179–250, 1998.

[Cha02] N. V. Chawla, K. W. Bowyer, L. O. Hall, W. P. Kegelmeyer, "SMOTE (Synthetic Minority Over-Sampling Technique)", *Journal of Artificial Intelligence Research*, Vol. 16, 2002.

[Cha17] G. W. Chang, H. J. Lu, Y. R. Chang, Y. D. Lee, "An improved neural network-based approach for short-term wind speed and power forecast", *Renewable Energy*, Vol. 105, pags. 301–311, 2017.

[Che18] M. Cheng, Q. Li, J. Lv, W. Liu, J. Wang, "Multi-scale LSTM model for BGP anomaly classification", *IEEE Transactions on Services Computing*, 2018.

[Che19] T. Chen, S. Barbarossa, X. Wang, G. B. Giannakis, Z.-L. Zhang, "Learning and management for internet of things: Accounting for adaptivity and scalability", *Proceedings of the IEEE*, Vol. 107, nº 4, pags. 778–796, 2019.

[Chi15] H. Chitsaz, N. Amjady, H. Zareipour, "Wind power forecast using wavelet neural network trained by improved Clonal selection algorithm", *Energy Conversion and Management*, Vol. 89, pags. 588–598, 2015.

[CJ16] M. Coto-Jiménez, J. Goddard-Close, F. Martínez-Licona, "Improving automatic speech recognition containing additive noise using deep denoising autoencoders of LSTM networks", *International Conference on Speech and Computer*, pags. 354–361, Springer, 2016.

[Con18] Q. Cong, W. Yu, "Integrated soft sensor with wavelet neural network and adaptive weighted fusion for water quality estimation in wastewater treatment process", *Measurement*, Vol. 124, pags. 436–446, 2018.

[Coo19] A. A. Cook, G. Mısırlı, Z. Fan, "Anomaly detection for IoT time-series data: A survey", *IEEE Internet of Things Journal*, Vol. 7, nº 7, pags. 6481–6494, 2019.

[Cop02] J. B. Copp, *The cost simulation benchmark: Description and Simulator Manual (cost action 624 and action 682)*, Office for Official Publications of the European Union: Luxembourg, 2002.

[Cur21] F. Curreri, L. Patanè, M. G. Xibilia, "RNN-and LSTM-Based Soft Sensors Transferability for an Industrial Process", *Sensors*, Vol. 21, nº 3, pags. 823, 2021.

[Der20] Dereli, Recep Kaan and Giberti, Matteo and Liu, Qipeng and Flynn, Damian and Casey, Eoin, "Benchmarking leachate co-treatment strategies in municipal wastewater treatment plants under dynamic conditions and energy prices", *Journal of Environmental Management*, Vol. 260, pags. 110129, 2020.

[DS17] I. N. Da Silva, D. H. Spatti, R. A. Flauzino, L. H. B. Liboni, S. F. dos Reis Alves, *Artificial neural networks*, Springer International Publishing: Cham, Switzerland, 2017.

[Eur91] European Commission, "Council Directive 91/271/EEC of 21 May 1991 concerning urban waste water treatment", *Journal of the European Communities*, Vol. 34, 1991.

[FA09] X. Flores-Alsina, J. Comas, I. R. Roda, M. Poch, K. V. Gernaey, U. Jeppsson, "Evaluation of plant-wide WWTP control strategies including the effects of filamentous bulking sludge", *Water Science and Technology*, Vol. 60, nº 8, pags. 2093–2103, 2009.

[FA11] X. Flores-Alsina, L. Corominas, L. Snip, P. A. Vanrolleghem, "Including greenhouse gas emissions during benchmarking of wastewater treatment plant control strategies", *Water Research*, Vol. 45, nº 16, pags. 4700–4710, 2011.

[For05] L. Fortuna, S. Graziani, M. G. Xibilia, "Soft sensors for product quality monitoring in debutanizer distillation columns", *Control Engineering Practice*, Vol. 13, nº 4, pags. 499–508, 2005.

[Fos16] C. Foscoliano, S. Del Vigo, M. Mulas, S. Tronci, "Predictive control of an activated sludge process for long term operation", *Chemical Engineering Journal*, Vol. 304, pags. 1031–1044, 2016.

[Gar15] S. García, J. Luengo, F. Herrera, *Data preprocessing in data mining*, Springer, 2015.

[Ger14] K. V. Gernaey, U. Jeppsson, *Benchmarking of control strategies for wastewater treatment plants*, IWA publishing: London, UK, 2014.

[Giw16] A. Giwa, S. Daer, I. Ahmed, P. R. Marpu, S. W. Hasan, "Experimental investigation and artificial neural networks ANNs modeling of electrically-enhanced membrane bioreactor for wastewater treatment", *Journal of Water Process Engineering*, Vol. 11, pags. 88–97, 2016.

[Goo16] I. Goodfellow, Y. Bengio, A. Courville, *Deep Learning*, MIT Press: Cambridge, MA, USA, 2016.

[Gre17] K. Greff, R. K. Srivastava, J. Koutnik, B. R. Steunebrink, J. Schmidhuber, "LSTM: A Search Space Odyssey", *IEEE Transactions on Neural Networks and Learning Systems*, Vol. 28, nº 10, pags. 2222–2232, oct 2017.

[Gri17] M. Grieves, J. Vickers, "Digital twin: Mitigating unpredictable, undesirable emergent behavior in complex systems", *Transdisciplinary Perspectives on Complex Systems*, pags. 85–113, Springer, 2017.

[Han15] M. Han, W. Ren, X. Liu, "Joint mutual information-based input variable selection for multivariate time series modeling", *Engineering Applications of Artificial Intelligence*, Vol. 37, pags. 250–257, 2015.

[Han16] H.-G. Han, Y. Li, Y.-N. Guo, J.-F. Qiao, "A soft computing method to predict sludge volume index based on a recurrent self-organizing neural network", *Applied Soft Computing*, Vol. 38, pags. 477–486, 2016.

[Han18a] H. G. Han, L. Zhang, H. X. Liu, J. F. Qiao, "Multiobjective design of fuzzy neural network controller for wastewater treatment process", *Applied Soft Computing Journal*, Vol. 67, pags. 467–478, jun 2018.

[Han18b] H. Han, S. Zhu, J. Qiao, M. Guo, "Data-driven intelligent monitoring system for key variables in wastewater treatment process", *Chinese Journal of Chemical Engineering*, Vol. 26, nº 10, pags. 2093–2101, 2018.

[Han20] T. Han, C. Liu, W. Yang, D. Jiang, "Deep transfer network with joint distribution adaptation: A new intelligent fault diagnosis framework for industry application", *ISA Transactions*, Vol. 97, pags. 269–281, 2020.

[He08] H. He, Y. Bai, E. A. Garcia, S. Li, "ADASYN: Adaptive Synthetic Sampling Approach for Imbalanced Learning", *IEEE International Joint Conference on Neural Networks*, 2008.

[Hed16] S. Heddam, H. Lamda, S. Filali, "Predicting effluent biochemical oxygen demand in a wastewater treatment plant using generalized regression neural network based approach: a comparative study", *Environmental Processes*, Vol. 3, nº 1, pags. 153–165, 2016.

[Hen87] M. Henze, L. Grady Jr, W. Gujer, G. V. R. Marais, T. Matsuo, "Activated Sludge Model No 1", *IAWPRC Scientific and Technical Reports*, Vol. 29, 01 1987.

[Hen00] M. Henze, W. Gujer, T. Mino, M. C. M. van Loosdrecht, *Activated sludge models ASM1, ASM2, ASM2d and ASM3*, IWA Publishing: London, UK, 2000.

[Hou13] M. C. Hout, M. H. Papesh, S. D. Goldinger, "Multidimensional scaling", *Wiley Interdisciplinary Reviews: Cognitive Science*, Vol. 4, nº 1, pags. 93–103, 2013.

[HS93] B. Halling-Sørensen, S. E. Jorgensen, *The removal of nitrogen compounds from wastewater*, Elsevier: Amsterdam, The Netherlands, 1993.

[Hu19] J. Hu, H. Zhang, X. Yu, H. Liu, D. Chen, "Design of sliding-mode-based control for nonlinear systems with mixed-delays and packet losses under uncertain missing probability", *IEEE Transactions on Systems, Man, and Cybernetics: Systems*, 2019.

[Hua15] H. Huang, L. Chen, E. Hu, "A neural network-based multi-zone modelling approach for predictive control system design in commercial buildings", *Energy and Buildings*, Vol. 97, pags. 86–97, 2015.

[Hua20] N.-S. Huang, Y.-C. Chen, J. C. Larsen, P. Manoonpong, "AHEAD: Automatic holistic energy-aware design methodology for MLP neural network hardware generation in proactive BMI edge devices", *Energies*, Vol. 13, nº 9, pags. 2180, 2020.

[Isl12] S. Islam, J. Keung, K. Lee, A. Liu, "Empirical prediction models for adaptive resource provisioning in the cloud", *Future Generation Computer Systems*, Vol. 28, nº 1, pags. 155–162, 2012.

[Jep07] U. Jeppsson, M. N. Pons, I. Nopens, J. Alex, J. B. Copp, K. V. Gernaey, C. Rosen, J. P. Steyer, P. A. Vanrolleghem, "Benchmark simulation model no 2: general protocol and exploratory case studies", *Water Science & Technology*, Vol. 56, nº 8, oct 2007.

[JL16] F. Jaramillo-Lopez, G. Kenne, F. Lamnabhi-Lagarrigue, "A novel online training neural network-based algorithm for wind speed estimation and adaptive control of PMSG wind turbine system for maximum power extraction", *Renewable Energy*, Vol. 86, pags. 38–48, 2016.

[Kan18] N. K. Kandasamy, G. Karunagaran, C. Spanos, K. J. Tseng, B.-H. Soong, "Smart lighting system using ANN-IMC for personalized lighting control and daylight harvesting", *Building and Environment*, Vol. 139, pags. 170–180, 2018.

[Kas18] I. Kasireddy, A. W. Nasir, A. K. Singh, "IMC based Controller Design for Automatic Generation Control of Multi Area Power System via Simplified Decoupling", *International Journal of Control, Automation and Systems*, Vol. 16, nº 3, pags. 994–1010, Jun 2018.

[Kur19] R. Kurokawa, T. Sato, R. Vilanova, Y. Konishi, "Discrete-time first-order plus dead-time model-reference trade-off PID control design", *Applied Sciences*, Vol. 9, nº 16, pags. 3220, 2019.

[Kur20] R. Kurokawa, T. Sato, R. Vilanova, Y. Konishi, "Design of optimal PID control with a sensitivity function for resonance phenomenon-involved second-order plus dead-time system", *Journal of the Frankling Institute*, Vol. 357, nº 7, pags. 4187–4211, 2020.

[Lan19] N. Lanzetti, Y. Z. Lian, A. Cortinovis, L. Dominguez, M. Mercangöz, C. Jones, "Recurrent neural network based MPC for process industries", *2019 18th European Control Conference (ECC)*, pags. 1005–1010, IEEE, 2019.

[Li19a] P. Li, G. Zhu, "Robust internal model control of servo motor based on sliding mode control approach", *ISA Transactions*, Vol. 93, pags. 199–208, 2019.

[Li19b] P. Li, G. Zhu, "Robust internal model control of servo motor based on sliding mode control approach", *ISA Transactions*, 2019.

[Liu19a] P. Liu, P. Zheng, Z. Chen, "Deep learning with stacked denoising auto-encoder for short-term electric load forecasting", *Energies*, Vol. 12, nº 12, pags. 2445, 2019.

[Liu19b] P. Liu, P. Zheng, Z. Chen, "Deep learning with stacked denoising auto-encoder for short-term electric load forecasting", *Energies*, Vol. 12, nº 12, pags. 2445, 2019.

[Lju99] L. Ljung, *System Identification, Theory for the User*, Pretince Hall, 2nd ed., 1999.

[Lóp17] M. E. López, E. R. Rene, Z. Boger, M. C. Veiga, C. Kennes, "Modelling the removal of volatile pollutants under transient conditions in a two-stage bioreactor using artificial neural networks", *Journal of Hazardous Materials*, Vol. 324, pags. 100–109, 2017.

[LT16] Y. Lorenzo-Toja, I. Vázquez-Rowe, M. J. Amores, M. Termes-Rifé, D. Marín-Navarro, M. T. Moreira, G. Feijoo, "Benchmarking wastewater treatment plants under an eco-efficiency perspective", *Science of the Total Environment*, Vol. 566, pags. 468–479, 2016.

[Mac92] D. J. C. MacKay, "Bayesian interpolation", *Neural Computation*, Vol. 4, nº 3, pags. 415–447, 1992.

[Mac02] J. M. Maciejowski, *Predictive control: with constraints*, Pearson education: Harlow, England, 2002.

[Mac09] V. C. Machado, D. Gabriel, J. Lafuente, J. A. Baeza, "Cost and effluent quality controllers design based on the relative gain array for a nutrient removal wwtp", *Water Research*, Vol. 43, nº 20, pags. 5129–5141, 2009.

[Mai17] E. Maiorino, F. M. Bianchi, L. Livi, A. Rizzi, A. Sadeghian, "Data-driven detrending of nonstationary fractal time series with echo state networks", *Information Sciences*, Vol. 382, pags. 359–373, 2017.

[Mam76] Mamdani, Ebrahim H, "Advances in the linguistic synthesis of fuzzy controllers", *International Journal of Man-Machine Studies*, Vol. 8, nº 6, pags. 669–678, 1976.

[Man17] D. S. Manu, A. K. Thalla, "Artificial intelligence models for predicting the performance of biological wastewater treatment plant in the removal of Kjeldahl Nitrogen from wastewater", *Applied Water Science*, Vol. 7, nº 7, pags. 3783–3791, 2017.

[Mel10] A. Mellit, A. M. Pavan, "A 24-h forecast of solar irradiance using artificial neural network: Application for performance prediction of a grid-connected PV plant at Trieste, Italy", *Solar Energy*, Vol. 84, nº 5, pags. 807–821, 2010.

[Mic14] M. Miccio, B. Cosenza, "Control of a distillation column by type-2 and type-1 fuzzy logic PID controllers", *Journal of Process Control*, Vol. 24, nº 5, pags. 475–484, 2014.

[Mon17] N. Moniz, P. Branco, L. Torgo, "Resampling strategies for imbalanced time series forecasting", *International Journal of Data Science and Analytics*, Vol. 3, 2017.

[Mun18] M. Munir, S. A. Siddiqui, A. Dengel, S. Ahmed, "DeepAnT: A deep learning approach for unsupervised anomaly detection in time series", *IEEE Access*, Vol. 7, pags. 1991–2005, 2018.

[Nad18] A. A. Nadiri, S. Shokri, F. T.-C. Tsai, A. A. Moghaddam, "Prediction of effluent quality parameters of a wastewater treatment plant using a supervised committee fuzzy logic model", *Journal of Cleaner Production*, Vol. 180, pags. 539–549, 2018.

[Nop10] I. Nopens, L. Benedetti, U. Jeppsson, M. N. Pons, J. Alex, J. B. Copp, K. V. Gernaey, C. Rosen, J. P. Steyer, P. A. Vanrolleghem, "Benchmark Simulation Model No 2: finalisation of plant layout and default control strategy", *Water Science and Technology*, Vol. 62, nº 9, pags. 1967–1974, 2010.

[NV17] S. Naduvil-Vadukootu, R. A. Angryk, P. Riley, "Evaluating preprocessing strategies for time series prediction using deep learning architectures", *The Thirtieth International Flairs Conference*, 2017.

[O'B11] M. O'Brien, J. Mack, B. Lennox, D. Lovett, A. Wall, "Model predictive control of an activated sludge process: A case study", *Control Engineering Practice*, Vol. 19, nº 1, pags. 54–61, 2011.

[Oga10] K. Ogata, *Modern control engineering*, Prentice hall: New Jersey, USA, 2010.

[Olm18] F. Hernández-del Olmo, E. Gaudioso, R. Dormido, N. Duro, "Tackling the start-up of a reinforcement learning agent for the control of wastewater treatment plants", *Knowledge-based Systems*, Vol. 144, pags. 9–15, 2018.

[Ou15] H. S. Ou, C. H. Wei, H. Z. Wu, C. H. Mo, B. Y. He, "Sequential dynamic artificial neural network modeling of a full-scale coking wastewater treatment plant with fluidized bed reactors", *Environmental Science and Pollution Research*, Vol. 22, nº 20, pags. 15910–15919, 2015.

[Pis18] I. Pisa, I. Santin, J. L. Vicario, A. Morell, R. Vilanova, "A Recurrent Neural Network for Wastewater Treatment Plant effluents prediction", *Proc. XXXIX Jornadas de Automatica 2018*, Badajoz, Spain, Sept. 2018.

[Pis19a] I. Pisa, A. Morell, J. L. Vicario, R. Vilanova, "ANN-based Internal Model Control strategy applied in the WWTP industry", *Proc. 24th IEEE International Conference on Emerging Technologies and Factory Automation (ETFA)*, 2019.

[Pis19b] I. Pisa, I. Santín, A. Morell, J. L. Vicario, R. Vilanova, "LSTM based Wastewater Treatment Plants operation strategies for effluent quality improvement", *IEEE Access*, Vol. 7, nº 1, pags. 159773–159786, 2019.

[Pis19c] I. Pisa, I. Santín, J. L. Vicario, A. Morell, R. Vilanova, "ANN-based soft sensor to predict effluent violations in wastewater treatment plants", *Sensors*, Vol. 19, nº 6, pags. 1280, 2019.

[Pis19d] I. Pisa, I. Santín, J. L. Vicario, A. Morell, R. Vilanova, "Data preprocessing for ANN-based industrial time-series forecasting with imbalanced data", *2019 27th European Signal Processing Conference (EUSIPCO)*, pags. 1–5, IEEE, 2019.

[Pis19e] I. Pisa, R. Vilanova, I. Santin, J. L. Vicario, A. Morell, "Artificial Neural Networks Application to Support Plant Operation in the Wastewater Industry", L. M. Camarinha-Matos, R. Almeida, J. Oliveira (eds.), *Technological Innovation for Industry and Service Systems. DoCEIS 2019. IFIP Advances in Information and Communication Technology*, Vol. 553, Springer: Cham, 2019.

[Pis20a] I. Pisa, A. Morell, J. L. Vicario, R. Vilanova, "Denoising Autoencoders and LSTM-Based Artificial Neural Networks Data Processing for Its Application to Internal Model Control in

Industrial Environments—The Wastewater Treatment Plant Control Case", *Sensors*, Vol. 20, nº 13, pags. 3743, 2020.

[Pis20b] I. Pisa, A. Morell, J. L. Vicario, R. Vilanova, "LSTM-based IMC approach applied in Wastewater Treatment Plants: performance and stability analysis", *IFAC-PapersOnLine*, Vol. 53, nº 2, pags. 16569–16574, 2020.

[Pis20c] I. Pisa, A. Morell, R. Vilanova, J. L. Vicario, "Noisy Signals in Wastewater Treatment Plants data-driven control: Spectral Analysis approach for the design of ANN-IMC controllers", *2020 IEEE Conference on Industrial Cyberphysical Systems (ICPS)*, Vol. 1, pags. 320–325, IEEE, 2020.

[Pis21a] I. Pisa, A. Morell, J. L. Vicario, R. Vilanova, "Transfer Learning Approach for the Design of Basic Control Loops in Wastewater Treatment Plants", *Proc. 26th IEEE International Conference on Emerging Technologies and Factory Automation (ETFA)*, 2021.

[Pis21b] I. Pisa, A. Morell, R. Vilanova, J. L. Vicario, "Industrial Control under Non-Ideal Measurements: Data-Based Signal Processing as an Alternative to Controller Retuning", *Sensors*, Vol. 21, nº 4, pags. 1237, 2021.

[Pis21c] I. Pisa, A. Morell, R. Vilanova, J. L. Vicario, "Transfer Learning in Wastewater Treatment Plant Control Design: From Conventional to Long Short-Term Memory-Based Controllers", *Sensors*, Vol. 21, nº 18, pags. 6315, 2021.

[Pis21d] I. Pisa, R. Vilanova, I. Santin, J. L. Vicario, A. Morell, "LSTM based Plug-and-Play controller for Dissolved Oxygen Control in Wastewater Treatment", *Proc. IWA Digital World Water Congress (IWA DWWC2021)*, May 2021.

[Pis22] I. Pisa, A. Morell, J. L. Vicario, R. Vilanova, "Transfer Learning Suitability Metric for ANN-based Industrial Controllers", *to be published in Proc. 27th IEEE International Conference on Emerging Technologies and Factory Automation (ETFA)*, 2022.

[Qia18] J.-F. Qiao, Y. Hou, L. Zhang, H.-G. Han, "Adaptive fuzzy neural network control of wastewater treatment process with multiobjective operation", *Neurocomputing*, Vol. 275, pags. 383–393, 2018.

[Qib13] J. Qibing, L. Qie, W. Qi, T. Yuqi, W. Yuanfei, "Pid controller design based on the time domain information of robust imc controller using maximum sensitivity", *Chinese Journal of Chemical Engineering*, Vol. 21, nº 5, pags. 529–536, 2013.

[Ran13] A. Rani, V. Singh, J. R. P. Gupta, "Development of soft sensor for neural network based control of distillation column", *ISA Transactions*, Vol. 52, nº 3, pags. 438–449, 2013.

[Red17] H. Redjimi, J. K. Tar, "On the effects of time-delay on precision degradation in fixed point transformation-based adaptive control", *2017 IEEE 30th Neumann Colloquium (NC)*, pags. 000125–000130, IEEE, 2017.

[Rev17] S. Revollar, P. Vega, R. Vilanova, M. Francisco, "Optimal control of wastewater treatment plants using economic-oriented model predictive dynamic strategies", *Applied Sciences*, Vol. 7, nº 8, pags. 813, 2017.

[Río15] S. del Río, J. M. Benítez, F. Herrera, "Analysis of Data Preprocessing Increasing the Oversampling Ratio for Extremely Imbalanced Big Data Classification", *Trustcom/BigDataSE/ISPA*, 2015.

[Roj12a] J. Rojas, R. Vilanova, "Data-driven based IMC control", *International Journal of Innovative Computing, Information and Control*, Vol. 8, nº 3, pags. 1557–1574, 2012.

[Roj12b] J. D. Rojas, X. Flores-Alsina, U. Jeppsson, R. Vilanova, "Application of multivariate virtual reference feedback tuning for wastewater treatment plant control", *Control Engineering Practice*, Vol. 20, nº 5, pags. 499–510, 2012.

[Roj16] J. D. Rojas, O. Arrieta, M. Meneses, R. Vilanova, "Data-driven control of the activated sludge process: Imc plus feedforward approach", *Internationl Journal of Computers Communications & Control*, Vol. 11, nº 4, pags. 522–537, 2016.

[Saa14] Saagi, Ramesh and Flores-Alsina, X and Fu, G and Benedetti, L and Gernaey, KV and Jeppsson, Ulf and Butler, D, "Benchmarking integrated control strategies using an extended BSM2 platform", *13th International Conference on Urban Drainage*, 2014.

[Sad18] M. Sadeghassadi, C. J. B. Macnab, B. Gopaluni, D. Westwick, "Application of neural networks for optimal-setpoint design and MPC control in biological wastewater treatment", *Computer Chemical Engineering*, Vol. 115, pags. 150–160, 2018.

[Sam17] R. Sameni, "Online filtering using piecewise smoothness priors: Application to normal and abnormal electrocardiogram denoising", *Signal Processing*, Vol. 133, pags. 52–63, 2017.

[San15a] I. Santin, C. Pedret, R. Vilanova, "Applying variable dissolved oxygen set point in a two level hierarchical control structure to a wastewater treatment process", *Journal of Process Control*, Vol. 28, pags. 40–55, 2015.

[San15b] I. Santin, C. Pedret, R. Vilanova, "Fuzzy control and model predictive control configurations for effluent violations removal in wastewater treatment plants", *Industrial & Engineering Chemistry Research*, Vol. 54, nº 10, pags. 2763–2775, 2015.

[San16] I. Santín, C. Pedret, R. Vilanova, M. Meneses, "Advanced decision control system for effluent violations removal in wastewater treatment plants", *Control Engineering Practice*, Vol. 49, nº 2, 2016.

[San19] I. Santín, M. Barbu, C. Pedret, R. Vilanova, "Dissolved Oxygen Control in Biological Wastewater Treatments with Non-Ideal Sensors and Actuators", *Industrial & Engineering Chemistry Research*, Vol. 58, nº 45, pags. 20639–20654, 2019.

[Sar18] D. Sarkar, R. Bali, T. Ghosh, *Hands-On Transfer Learning with Python: Implement advanced deep learning and neural network models using TensorFlow and Keras*, Packt Publishing Ltd: Birmingham, UK, 2018.

[Sch21] A. Schilling, A. Maier, R. Gerum, C. Metzner, P. Krauss, "Quantifying the separability of data classes in neural networks", *Neural Networks*, Vol. 139, pags. 278–293, 2021.

[Sha07] M. Shamsuzzoha, M. Lee, "Imc- pid controller design for improved disturbance rejection of time-delayed processes", *Industrial & Engineering Chemistry Research*, Vol. 46, nº 7, pags. 2077–2091, 2007.

[She08] W. Shen, X. Chen, J. P. Corriou, "Application of model predictive control to the BSM1 benchmark of wastewater treatment process", *Computers and Chemical Engineering*, Vol. 32, nº 12, pags. 2849–2856, dec 2008.

[Sou16] F. A. A. Souza, R. Araújo, J. Mendes, "Review of soft sensor methods for regression applications", *Chemometrics and Intelligent Laboratory Systems*, Vol. 152, pags. 69–79, 2016.

[Sou20] R. Souissi, A. Al Bitar, M. Zribi, "Accuracy and transferability of artificial neural networks in predicting in situ root-zone soil moisture for various regions across the globe", *Water*, Vol. 12, nº 11, pags. 3109, 2020.

[Sur18] S. Suresh, S. Lal, C. Chen, T. Celik, "Multispectral satellite image denoising via adaptive cuckoo search-based Wiener filter", *IEEE Transactions on Geoscience and Remote Sensing*, Vol. 56, nº 8, pags. 4334–4345, 2018.

[Tak85] Takagi, Tomohiro and Sugeno, Michio, "Fuzzy identification of systems and its applications to modeling and control", *IEEE transactions on systems, man, and cybernetics*, pags. 116–132, 1985.

[Tak91] I. Takács, G. G. Patry, D. Nolasco, "A dynamic model of the clarification-thickening process", *Water Research*, Vol. 25, nº 10, pags. 1263–1271, 1991.

[Tal17] M. K. Talkhoncheh, M. Shahrokhi, M. R. Askari, "Observer-based adaptive neural network controller for uncertain nonlinear systems with unknown control directions subject to input time delay and saturation", *Information Sciences*, Vol. 418, pags. 717–737, 2017.

[The18] S. N. Thennadil, M. Dewar, C. Herdsman, A. Nordon, E. Becker, "Automated weighted outlier detection technique for multivariate data", *Control Engineering Practice*, Vol. 70, 2018.

[Tor13] L. Torgo, R. P. Ribeiro, B. Pfahringer, P. Branco, "SMOTE for regression", *Portuguese Conference on Artificial Intelligence*, 2013.

[Tor15] L. Torgo, P. Branco, R. P. Ribeiro, B. Pfahringer, "Resampling strategies for regression", *Expert Systems*, Vol. 32, 2015.

[Tra18] N. Tran, T. Nguyen, B. M. Nguyen, G. Nguyen, "A multivariate fuzzy time series resource forecast model for clouds using LSTM and data correlation analysis", *Procedia Computer Science*, Vol. 126, pags. 636–645, 2018.

[Ust17] A. Ustundag, E. Cevikcan, *Industry 4.0: managing the digital transformation*, Springer: Cham, Switzerland, 2017.

[Vil11a] R. Vilanova, V. M. Alfaro, "Control PID robusto: Una visión panorámica", *Revista Iberoamericana de Automática e Informática Industrial RIAI*, Vol. 8, nº 3, pags. 141–158, 2011.

[Vil11b] R. Vilanova, M. R. Katebi, N. Wahab, "N-removal on wastewater treatment plants: A process control approach", *Journal of Water Resource and Protection*, Vol. 2011, nº 3, pags. 1–11, 2011.

[Vil12] R. Vilanova, A. Visioli, *PID Control in the Third Millennium - Lessons Learned and News Approaches*, Springer, 2012.

[Vil18] R. Vilanova, I. Santin, C. Pedret, M. Barbu, "Event-based control for dissolved oxygen and nitrogen in wastewater treatment plants", *2018 22nd International Conference on System Theory, Control and Computing (ICSTCC)*, pags. 212–217, IEEE, 2018.

[Wan01] Q.-G. Wang, C. C. Hang, X.-P. Yang, "Single-loop controller design via imc principles", *Automatica*, Vol. 37, nº 12, pags. 2041–2048, 2001.

[Wan18] C. Wang, W. Zhao, Z. Luan, Q. Gao, K. Deng, "Decoupling control of vehicle chassis system based on neural network inverse system", *Mechanical Systems and Signal Processing*, Vol. 106, pags. 176–197, 2018.

[Wan19] Z. Wang, Z. Dai, B. Póczos, J. Carbonell, "Characterizing and avoiding negative transfer", *Proceedings of the IEEE/CVF Conference on Computer Vision and Pattern Recognition*, pags. 11293–11302, 2019.

[Wol17] M. Wollschlaeger, T. Sauter, J. Jasperneite, "The future of industrial communication: Automation networks in the era of the internet of things and industry 4.0", *IEEE Industrial Electronics Magazine*, Vol. 11, 2017.

[Yan95] P. Y. Yang, Z. Zhang, "Nitrification and denitrification in the wastewater treatment system", *Traditional Technology for Environmental Conservation and Sustainable development in the asian-pacific region*, pags. 145–158, 1995.

[Yan02] X.-P. Yang, Q.-G. Wang, C. Hang, C. Lin, "Imc-based control system design for unstable processes", *Industrial & Engineering Chemistry Research*, Vol. 41, nº 17, pags. 4288–4294, 2002.

[Yua18] X. Yuan, B. Huang, Y. Wang, C. Yang, W. Gui, "Deep learning-based feature representation and its application for soft sensor modeling with variable-wise weighted SAE", *IEEE Transactions on Industrial Informatics*, Vol. 14, nº 7, pags. 3235–3243, 2018.

[Zha03] G. P. Zhang, "Time series forecasting using a hybrid ARIMA and neural network model", *Neurocomputing*, Vol. 50, pags. 159–175, 2003.

[Zha18a] D. Zhang, E. S. Hølland, G. Lindholm, H. Ratnaweera, "Hydraulic modeling and deep learning based flow forecasting for optimizing inter catchment wastewater transfer", *Journal of Hydrology*, Vol. 567, pags. 792–802, 2018.

[Zha18b] D. Zhang, G. Lindholm, H. Ratnaweera, "Use long short-term memory to enhance Internet of Things for combined sewer overflow monitoring", *Journal of Hydrology*, Vol. 556, pags. 409–418, 2018.

[Zha18c] D. Zhang, N. Martinez, G. Lindholm, H. Ratnaweera, "Manage sewer in-line storage control using hydraulic model and recurrent neural network", *Water Resources Management*, Vol. 32, nº 6, pags. 2079–2098, 2018.

[Zha19] X. Zhang, J. Ji, J. Xu, "Parameter identification of time-delayed nonlinear systems: An integrated method with adaptive noise correction", *Journal of the Franklin Institute*, Vol. 356, nº 11, pags. 5858–5880, 2019.

[Zho19] K. Zhou, M. Li, Y. Li, M. Xie, Y. Huang, "An Improved Denoising Method for Partial Discharge Signals Contaminated by White Noise Based on Adaptive Short-Time Singular Value Decomposition", *Energies*, Vol. 12, nº 18, pags. 3465, 2019.

[Zhu21] F. Zhuang, Z. Qi, K. Duan, D. Xi, Y. Zhu, H. Zhu, H. Xiong, Q. He, "A Comprehensive Survey on Transfer Learning", *Proceedings of the IEEE*, Vol. 109, nº 1, pags. 43–76, 2021.